AD-775 306

ANGEL CLUTTER AND THE ASR AIR TRAFFIC CONTROL RADAR. VOLUME II. APPENDICES

J. R. Barry, et al

Johns Hopkins University

Prepared for:

Federal Aviation Administration

February 1973

REPORT NO. FAA-RD-73-158, II

ANGEL CLUTTER AND THE ASR AIR TRAFFIC CONTROL RADAR

VOLUME II APPENDICES

FEBRUARY 1973
FINAL REPORT

PREPARED FOR

DEPARTMENT OF TRANSPORTATION
FEDERAL AVIATION ADMINISTRATION
SYSTEMS RESEARCH & DEVELOPMENT SERVICE
WASHINGTON, D.C. 20590

Technical Report Documentation Page

1. Report No.	2. Government Accession No.	3. Recipient's Catalog No.
FAA-RD-73-158, II		

4. Title and Subtitle	5. Report Date
Angel Clutter and the ASR Air Traffic Control Radar	February 1973
	6. Performing Organization Code: APL/JHU
7. Author(s) J. R. Barry, B. K. Carter, R. J. Erdahl, R. L. Harris, J. T. Miller, G. D. Smith, R. M. Barnes	8. Performing Organization Report No.: MSO-F-195
9. Performing Organization Name and Address The Johns Hopkins University Applied Physics Laboratory 8621 Georgia Avenue Silver Spring, Maryland 20910	10. Work Unit No. (TRAIS): 19509 11. Contract or Grant No.: DOT-FA72WA-2705
12. Sponsoring Agency Name and Address Department of Transportation Federal Aviation Administration Systems Research and Development Service Washington, D. C. 20590	13. Type of Report and Period Covered: October 1971 - February 1973 14. Sponsoring Agency Code

15. Supplementary Notes

This report is issued in two volumes. Volume I contains the summary and conclusions (Chapter 1) and the study results (Chapters 2-4). Volume II (Appendices) contains supporting data and analyses.

16. Abstract

The goal of this study was to identify angel clutter reduction techniques which were cost-effective for the existing ASR-4,5, and 6 radars. This report identifies a combination of techniques which can be implemented without major radar re-design and which improves the ASR surveillance capability. These techniques were developed by thorough analysis of ASR video and track radar data gathered during the Spring 1972 bird migrations at Milwaukee's General Mitchell Airport. The proposed angel clutter reduction (ACR) features operate on the three major differences observed between angel and aircraft signal characteristics: signal strength, pulse-to-pulse amplitude fluctuations, and velocity. These ACR features were chosen because they provide the highest level of effectiveness consistent with timely implementation and a reasonable degree of radar modification.

Chapter 1 summarizes all results. Chapter 2 discusses the impact of angel clutter on air traffic control operations. Chapter 3 describes angel and aircraft characteristics measured during the Milwaukee tests and compares them with previously-published information. Chapter 4 describes the recommended ACR system in detail. The Appendices provide a description of the field test instrumentation and supporting data and analyses.

17. Key Words	18. Distribution Statement
Angel Clutter, Bird Clutter, Airport Surveillance Radar, Angel Clutter Reduction, Video Signal Processing, Pattern Recognizers, Air Traffic Control	Document is available to the public through the National Technical Information Service, Springfield, Virginia 22151

19. Security Classif. (of this report)	20. Security Classif. (of this page)	21. No. of Pages	22. Price
Unclassified	Unclassified	256	$6.50

Form DOT F 1700.7 (8-72)

PREFACE

This study report contains the results obtained to date on the Angel Clutter Reduction Techniques Program conducted by the Applied Physics Laboratory, Johns Hopkins University, for the Federal Aviation Administration under Task II of Contract No. DOT-FA-72WA-2705, issued on 8 October 1971.

The report includes the results published during the initial phase of effort in three interim reports (May, July, and August 1972) and the results of an extension phase which investigated the feasibility of applying pattern recognition techniques developed by Bendix Communications Division to reduce ASR Angel Clutter. Mr. O. E. McIntire of ARD-200 was the FAA Technical Representative for this effort. The support of Mr. K. E. Coonley of ARD-200, Mr. C. Chapman and others of the National Aviation Facilities Experimental Center (NAFEC), and of the FAA personnel at General Mitchell Field, Milwaukee, is gratefully acknowledged.

This study report is organized into two volumes. Volume I contains the Study Results. Chapter 1, Summary and Conclusions, contains all significant results and a recommended course of action leading to realization of an operational angel clutter reduction capability. Chapter 2 discusses the angel clutter problem, its sources, and its effect on air traffic control operations. Chapter 3 identifies differences in ASR signal return characteristics for angels and aircraft which were measured at Milwaukee airport during the spring bird migration period. Chapter 4 describes angel clutter reduction techniques which can exploit these differences in a manner which is cost effective for the ASR-4, 5 and 6 radars.

Volume II contains five appendices providing a summary of field test operations, supporting data, supporting analyses, a discussion of pattern recognition techniques and hardware design data for the suggested angel clutter reduction techniques.

INDEX

VOLUME I - STUDY RESULTS

VOLUME II - APPENDICES

APPENDIX A

FIELD TEST OPERATIONS

APPENDIX A-1

ANGEL CLUTTER TEST INSTRUMENTATION AT MILWAUKEE

Instrumentation Requirements

The overall objectives for both the Radar/Beacon Multisensor Tracking study and the Angel Clutter Characteristics study undertaken by the Applied Physics Laboratory (APL) for the FAA, presented similar instrumentation requirements. Each required mobile radar recording and processing equipments which could be located at designated FAA field test sites. The field installation of the instrumentation required interfacing with operational ASR systems on an operationally safe and non-interfering basis.

Specific data requirements for the Angel Clutter Characteristics study necessitated the simultaneous recording of normal and MTI radar information at an operational ASR site, and digital radar processing facilities for on and off-line data collection, formatted and recorded in a manner which was compatible with the available laboratory digital data reduction facilities. Additionally, a source of precision target position measurement was required to permit a determination of angel clutter range, bearing, altitude, motion and velocity. Clutter position information was also required in a form which was compatible with digital processing. A pictorial diagram of the angel clutter field test instrumentation installation is presented in Figure A-1.

Instrumentation Description

Applied Physics Laboratory experience in the research and development phases of U. S. Navy search and fire control radar system programs, and the recent laboratory development of the U. S. Navy Detector/Tracker Set AN/SYS-1 target information processing system was instrumental in the rapid design and construction of a mobile Data Acquisition Module for use in FAA field testing. The major components of the module are shown in Figure A-2. The module is designed to accept analog ASR radar video with separate input lines

FIGURE A-1 MILWAUKEE TEST INSTRUMENTATION

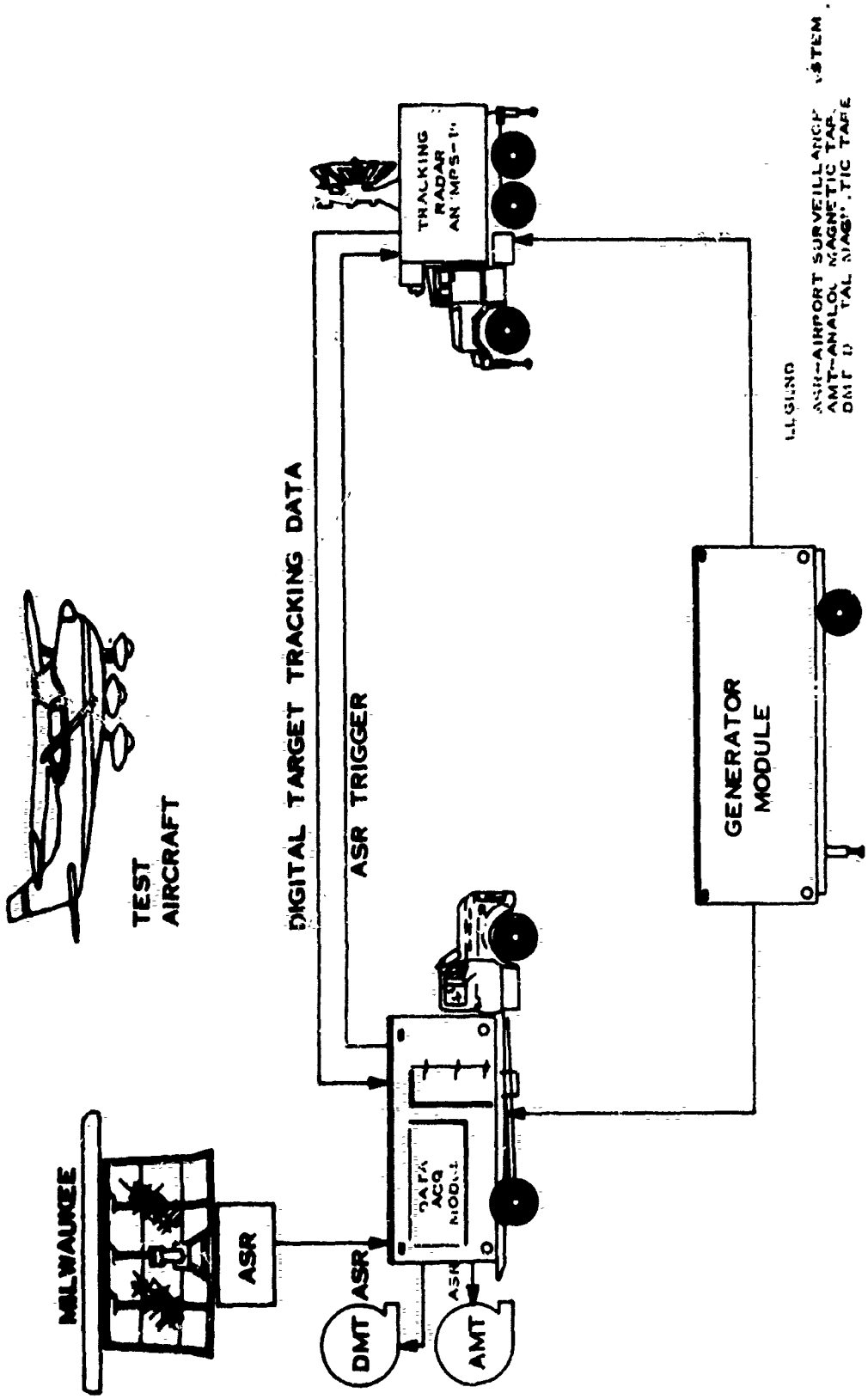

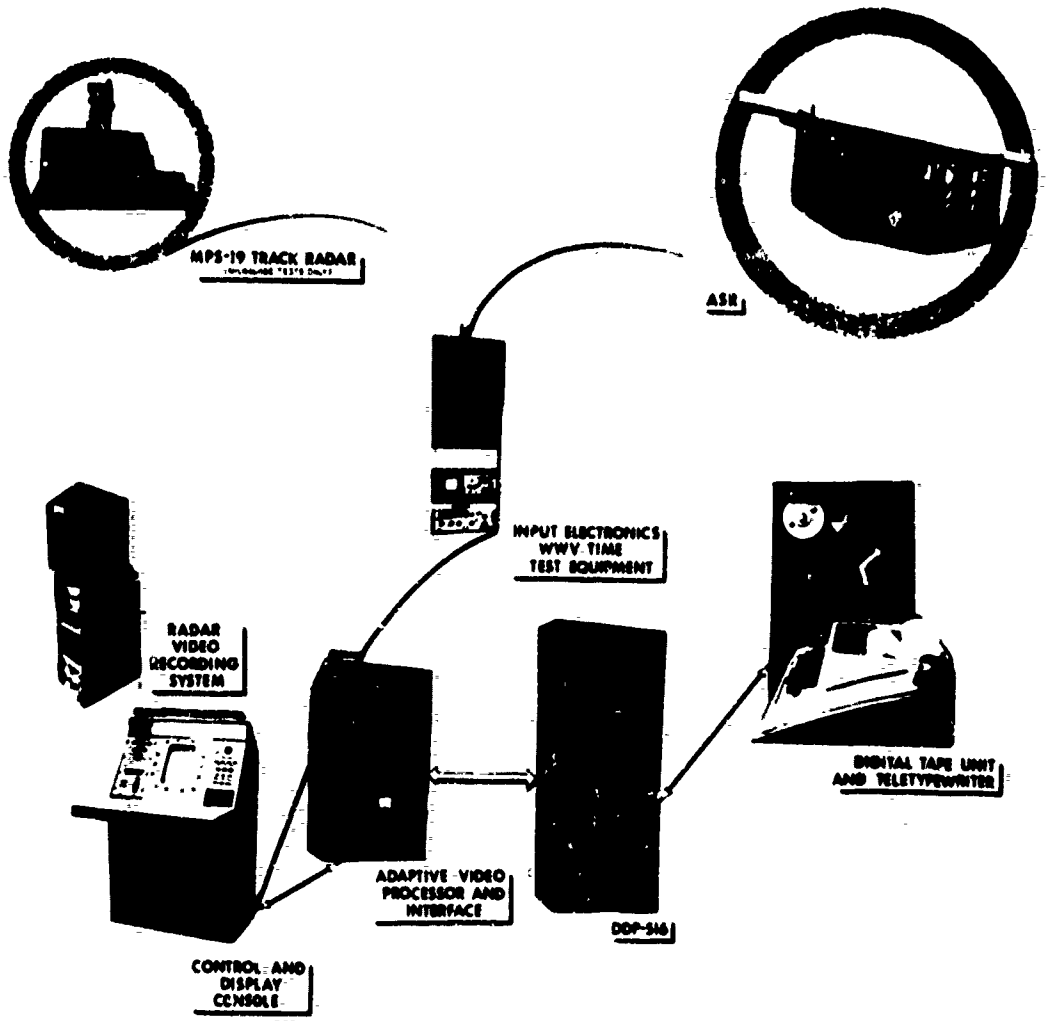

DATA ACQUISITION MODULE EQUIPMENT

FIGURE A–2

for normal, MTI and beacon video, triggers, azimuth 1X synchro, and APG (Azimuth Pulse Generator) pulses, each with appropriate isolation. These inputs may be recorded directly on an analog Radar Video Recording System (RAVIR) or processed by a radar digitizer (referred to as the Adaptive Video Processor in the AN/SYS-1 system) and recorded in digital form on magnatic tape. The off-line mode of the equipment allows the replay or previously recorded analog video tapes into the digitizer for processing and digital recording. A Display and Control Console allows an operator to view normal, MTI or beacon video, processed video in the form of fixed, moving and tentative tracks and/or tracking radar positions. Ancillary equipments in the module include a WWV receiver and Time Code Generator, VHF communication transceiver, a Teletypewriter and electronic test equipment. These equipments are installed in a truck mounted, climate controlled 8 x 16 foot van. The Data Acquisition Module, AN/MPS-19 Tracking Radar and Generator van were located at General Mitchell Field, Milwaukee, Wisconsin during the Angel Clutter Characteristics testing.

In addition to the instrumentation provided, a Cessna 172, single engine aircraft was employed for the collection of typical light aircraft radar data. These data were collected under the same conditions as the angel clutter data.

Test Coordination and Instrumentation Control

Data collection was coordinated by a Test Conductor positioned at the Data Acquisition Module Display and Control Console. An intercom link with the MPS-19 Tracking Radar permitted voice designation to ASR detected targets of interest. Television monitors in the MPS-19 and at the Display and Control Console provided a visual display of the target being tracked by the tracking radar. This information was obtained from a television camera which was attached to the MPS-19 antenna and boresited with the radar beam. (Aircraft targets were

generally clearly visible on the television system, however, the limited power of the system precluded visual observation of angel clutter being tracked). During controlled aircraft data collection, the Test Conductor directed the aircraft runs via the VHF communication facilities provided in the Data Acquisition Module.

Angel Clutter Test Instrumentation, Detailed Description

Data Acquisition Module

The Data Acquisition Module is a mobile and highly versatile instrumentation van which provides the facilities for the recording/reproduction and display of analog radar data; the digital processing and recording of radar data with target returns categorized as fixed or moving and providing specific information such as video amplitudes, hit counts, run lengths, etc. A special mode of operation allows the collection of data in a finite volume of space with discrete measurements of video surrounding a designated point, e.g., clutter surrounding an aircraft target, the distribution of video in a thunder cell, the distribution of discrete targets in a flock of birds, etc. These unique processing and recording facilities are supported by subsystems and equipment necessary for remote all-weather operation.

A pictorial diagram of the Data Acquisition Module was shown in Figure A-2. The major components of the module are discussed in the following paragraphs.

RAVIR is a wideband radar signal recording system which was designed and developed by the Applied Physics Laboratory for use by the U. S. Navy as a radar training device. Seven magnetic tape recording channels are available with interchangeable input signal conditioning units. This flexibility allows the simultaneous recording of normal video, MTI video, raw defruited beacon video, radar triggers, APG pulses, 1X synchro and timing.

APPENDIX A-1

A listing of RAVIR recording parameters is provided in Table A-1.

TABLE A-1 RAVIR RECORDING PARAMETERS

General Tape Recorder Characteristics	
Parallel Channels	7
Frequency Response (3 dB)	400 Hz to 1.5 MHz
Record Time	24 min.
Tape Speed	120 inches/sec.
Tape Speed Error (Short Term)	± 0.1% max.
Dynamic Skew (adj. channels)	± 0.3 micro sec.
Signal-Noise Ratio	23 dB max.
Crosstalk	20 dB min.
RAVIR Accuracy	
Bearing	± 0.5 degrees
Range	1%
Output Trigger Delay	0.25 microsec max.
Frequency Response	DC to 1.5 MHz

During radar signal processing, the normal and MTI video signals are multiplexed to allow MTI video utilization out to a manually-selected transition range and normal video beyond that range. The result of this video selection is directed to the Target Information Processing System (TIPS) which contains the Adaptive Video Processor (AVP). The AVP employed in the module was designed for a high level of effectiveness in a land environment and in rain clutter. The processor samples the video amplitude in the ten range cells (each cell being equal to the pulsewidth of 0.833 usec) preceding and ten cells succeeding the cell being tested for the presence of a target. These twenty cells are summed to determine a mean clutter level. The cell being tested is compared to this average

level and if the test cell exceeds the level by a specified factor, a target is declared present. The data storage is advanced by one cell and the process is repeated. Thus, the output of this portion of the digitizer is a string of ones and zeroes, where the ones indicate the existence of a possible target and the occurrence in time indicates the range. This string of data is then stored in a serial delay line which is segmented so that each segment corresponds to the binary data obtained from one azimuth dwell. Nineteen such azimuth strings are stored and at each range cell the output of all nineteen are sampled. If at least m out of the nineteen (n) bits are one, then a target "hit" is declared. This process is referred to as azimuth correlation or "sliding window correlation". The output of this correlator is used to transfer the range of the detection into the data converter which formats data for the digital data processor.

In addition to processing all targets as indicated above, it is possible to collect concentrated data about a single target of interest, referred to as a "hooked" target. When a specific target is designated (by the Test Conductor), the digital data processor generates a grid about the target and requests the amplitude of the radar returns for all cells within the grid from the digitizer. The grid consists of twenty cells in range and twenty azimuth positions, although they need not be adjacent azimuth dwells. These samples are converted to 5 bits of amplitude data and loaded into the digital processor. The characteristics of the digitizer are listed in Table A-2.

TABLE A-2

ADAPTIVE VIDEO PROCESSOR (DIGITIZER)
CHARACTERISTICS

Delay Line Length	20τ (τ = 0.8 microsec)
Delay Line Spacing	$\tau/2$ or τ
Signal Tap	10τ
Average	estimate of rms noise
Azimuth Correlation Length (n)	variable, 1-19 ($n \geq m$)
Minimum Required Azimuth Hits (m)	variable, 1-19

In addition to the features described above, a constant false alarm loop is incorporated around the signal detection threshold to maintain a constant false alarm rate (CFAR), as averaged over each azimuth position. The desired false alarm can be manually set at 0.5%, 1.0%, 5.0%, 10%, or 20%. A wide pulse discriminator (WPD) is also incorporated following the threshold detector. Basically, the assumption is that an aircraft could be detected in two adjacent range cells, but due to the length of aircraft and the allowable minimum spacing, aircraft detections cannot occur in three or more adjacent range cells. In strong clutter, however, this condition is possible. Consequently, the WPD inhibits detections when three or more consecutive range cells experience detections. The WPD can be manually bypassed, if desired.

The Data Converter is an interface unit between the AVP and the digital data processor, and between the radar and the processor. It contains the range counter for specifying the location of potential targets. The least significant bit of this counter corresponds to approximately 1/16 of a nautical mile. (In the data collect mode (hooked target) the range of the grid points are specified to about 1/64 of a nautical mile). Angle measurements to an accuracy of 0.022 degrees are converted to the appropriate format and loaded into the digital data processor when the AVP azimuth correlator declares a hit.

The Digital Data Processor is a Honeywell DDP-516R computer. The inputs to the processor are the hits as declared by the AVP azimuth correlator, MPS-19 tracking radar and timing data. Typically, twenty to forty successive hits in azimuth would be received via the AVP from a large aircraft target. The processor shows this as one target and distinguishes between adjacent targets by the absence of at least twelve hits in azimuth. For the hit group assigned to a single target, the position halfway between the first and last hits (centroid) is defined as the target center. A detailed description of the process involved in the establishment of target files, classification of targets, modification of target classifications, and criteria for dropping tracks, etc. is beyond the scope of this description. In general, however, new hits which do not correlate with existing tracks are established as new tentative tracks. Depending upon the number of successive detections, the number of misses and the computed velocities, these new tentative targets are promoted to tentative, firm, or fixed tracks. As tracks develop further, the classifications may change and some tracks may be dropped if insufficient detections occur.

Once each complete ASR antenna rotation the processor dumps the contents of all track files onto magnetic tape along with a real-time reading which has been received from the module time code generator.

Table A-3 lists the significant characteristics of the data processor.

TABLE A-3

DDP-516R DIGITAL DATA PROCESSOR
CHARACTERISTICS

Memory Size	8K words
Word Length	16 bits
Memory Cycle Time	1 microsec
Direct Memory Access Channels	3
Add/Subtract Time	2 microsec
Divide Time	11 microsec
Multiply Time	6 microsec

The Control and Display Console serves as the primary means for monitoring the performance of the digitizer and digital data processor. Using a PPI type display, the operator may select analog normal/MTI video from the ASR in real-time or RAVIR playback video, or he may select processed video with the appropriate symbology for tentative, firm and fixed tracks, and/or a track symbol indicating the tracking position of the MPS-19 radar. An azimuth display and range rings are also available. The track ball feature of the console allows the operator to "hook" a target of interest to place the system in the data collect mode previously described. The "hooked track" feature at the console is primarily employed during system calibration and test, or when the module is operated at remote locations. The "hooked track" is initiated by positioning video cross hairs over the target of interest with a track ball, thereby positioning the data collect matrix. Depressing a thumb operated switch activates the data collect mode.

The MPS-19 was selected as the instrumentation tracking radar due to the near identical characteristics to the ASR series characteristics. These are listed in Table A-4.

TABLE A-4

RADAR CHARACTERISTICS

	ASR	MPS-19
Frequency	2700-2900 MHz	2700-2900 MHz
Peak Power	400 kW	137 kW - 250 kW
PRR	1200 pps	300-2000 pps, adjustable
Pulsewidth	0.833 μs	0.8 μs
Antenna Beamwidth Az.	1.5°	3.0°
El.	30°	3.0°
Antenna Gain	34 dB	34 dB
IF Bandwidth	2 MHz	2 MHz

An analog to digital converter was fabricated and installed in the MPS-19 to allow direct tracking data input to the Data Acquisition Module Data Processor. The tracking radar was also instrumented for the recording of the AGC voltage to permit the determination of target size.

APPENDIX A-2

SUMMARY OF MILWAUKEE DATA COLLECTION OPERATIONS

The Milwaukee field operations were conducted April 12-20 and May 10-12, 1972. The instrumentation consisted of the Data Acquisition Module, the AN/MPS-19 Track Radar Module, and a 150 KW generator van previously described in Appendix A-1.

In addition to the recorded data described below, observations were made and local reports were collected on weather and bird activity.

ASR Radar Video Data

ASR normal and MTI video was recorded on the Radar Video Recording System (RAVIR) installed in the Data Acquisition Module. It was also used in the off-line mode to generate digital magnetic tapes via the Target Information Processing System (TIPS) portion of the Data Acquisition Module.

The TIPS was used to process and record several types of data which would be required in subsequent reconstruction of the Milwaukee radar environment. These included angel clutter, land and lake clutter, light to moderate rain clutter, heavy weather cell clutter, specific aircraft track histories and the Milwaukee ASR environment under various traffic conditions

A high speed data collect mode was employed primarily in the collection of angel clutter data. In this mode, system tracking of all ASR targets is suspended and replaced by an expanded data collect mode wherein the data collect matrix center is positioned by the target track coordinates of the Track Radar Module This enables the measurement and recording of the position and amplitude of all radar returns within the matrix area.

A low speed data collect mode was utilized primarily in the accumulation of ASR track histories. These histories were recorded during various terminal traffic conditions and in various weather and AP clutter conditions.

Track Radar Module Data

The AN/MPS-19 Track Radar Module contained in addition to the tracking radar, a television monitor and recording system, a strip chart recorder used to record radar automatic gain control (AGC) voltages, and an analog SONY recorder used to record track radar video.

The bore-sited TV system was intended as a means of identifying bird angels in track. However, this was ineffective due to a combination of darkness and excessive range for visual detection, even though a high-power lens was used.

During angel or aircraft tracking, the A/D converter track radar outputs were transmitted to the Data Acquisition Module in the high speed data collect mode. Track range, azimuth, and elevation were recorded every 0.4 seconds, and the eight bit (255 level) radar video or AGC level was recorded for every radar pulse. To avoid interference with the ASR, the track radar transmissions were synchronized with the ASR pulse repetition frequency (PRF). Continual use of the ASR stagger led to variations in track radar output power because of uneven modulator charging times; hence the MPS-19 PRF was reduced to approximately 575 Hz and was maintained in synchronism with every other ASR transmit pulse.

Data Library

Table A-4 provides a summary of all Milwaukee digital and analog data tapes collected. Table A-5 provides a detailed listing by date and time of the data collected.

TABLE A-4

Tape Library Summary

	Digital Tapes	RAVIR Tapes	SONY Tapes	*AGC (Analog)
ASR Environment	14	0	0	0
System Calibration	4	2	2	4
AP Track Factory	5	3	0	0
AP MPS-19 Tracks	10	9	4	9
Total No. of Tapes	33	14	6	13
Total Minutes (Approx)	700	330	420	450

* A strip chart recording of MPS-19 receiver AGC was made during all runs when this radar was used

TABLE A-5

DATA LISTING ANGEL CLUTTER REDUCTION TESTS

RUN #	DATE	TIME		DATA SPEED		DIGITAL TAPE #	RAVIR TAPE #	SONY TAPE #	ANALOG AGC	REMARKS
		START	END	N/S	H/S					
1	4/12	1658	1715	X		1	NO	NO	NO	MKE CLUTTER-JAMMING-WEATHER CELLS
2	4/12	1715	1730	X		1	NO	NO	NO	MTI RESIDUE-HEAVY WEATHER CELLS
3	4/12	1743	1749	X		2	NO	NO	NO	TEST TARGET IN RAIN (MTI)
4	4/12	1752	1803	X		2	NO	NO	NO	TEST TARGET IN RAIN (MTI)
5	4/12	1810	1823	X		2	NO	NO	NO	TEST TARGET IN RAIN (NORMAL)
6	4/13	1859	1905		X	3	NO	NO	NO	MOVING TARGET (NORMAL)
7	4/13	1910	1918		X	3	NO	NO	NO	MOVING TARGET(MTI)
8	4/13	1927	1929		X	3	NO	NO	NO	FIXED TARGET (NORMAL) MPS-19 TRACK
9	4/13	1931	1946		X	3	NO	NO	NO	FIXED TARGET (NORMAL) MPS-19 TRACK
10	4/13	1951	1952		X	3	NO	NO	NO	FIXED TARGET (MTI) MPS-19 TRACK
11	4/13	1953	2001		X	3	NO	NO	NO	FIXED TARGET (MTI)MPS-19 TRACK
12	4/14	0557	0611		X	4	NO	NO	NO	FIXED TARGET (MTI) MPS-19 TRACK
13	4/14	0621	0625		X	5	1	NO	YES	AP(POSSIBLE BIRDS)-MPS-19 TRACK
14	4/14	0627	0629		X	5	1	NO	YES	AP(POSSIBLE BIRDS-MPS-19 TRACK
15	4/14	0642	0646		X	5	1	NO	YES	AP-MPS-19-A/C TRACK THRU POSSIBLE BIRDS
16	4/14	1714	1718		X	6	NO	NO	NO	MOVING TARGET (NORMAL) MPS-19 TRACK
17	4/14	1721	1728		X	6	NO	NO	NO	MOVING TARGET (NORMAL) MPS-19 TRACK
18	4/14	1732	1740		X	6	NO	NO	NO	MOVING TARGET (MTI) MPS-19 TRACK
19	4/14	1750	1805		X	7	NO	NO	NO	FIXED TARGET (MTI) MPS-19 TRACK

DATA LISTING

ANGEL CLUTTER REDUCTION TESTS (cont'd.)

RUN #	DATE	TIME		DATA SPEED		DIGITAL TAPE #	RAVIR TAPE #	SONY TAPE #	ANALOG AGC	REMARKS
		START	END	M/S	H/S					
20	4/14	1827	1849	X		8	NO	NO	NO	TEST TARGET (IN MTI) RESIDUE
21	4/14	1851	1911	X		8	NO	NO	NO	TEST TARGET IN NORMAL NOISE
22	4/15	2044	2104	X		9	NO	NO	NO	TEST TARGET IN NORMAL LAKE CLUTTER
23	4/15	2122	2145		X	10	1	1	YES	AP(Probable Birds)-MPS-19 TRACK
24	4/15	2158	2229		X	11	2	1	YES	AP(Probable Birds)-MPS-19 TRACK
25	4/17	0548	0622		X	12	3/4	2	YES	AP-MPS-19 TRACK
26	4/17	?	?	X		13	NO	NO	NO	AP-TRACK HISTORY
27	4/17	1845	1910		X	14	4/5	2	YES	AP-MPS-19-TRACK
28	4/17	1921	1952		X	15	5	2/3	YES	AP-MPS-19 TRACK
29	4/18	0601	0630		X	16	5/6	3	YES	AP-MPS-19-TRACK
30	4/18	0651	0744		X	17	6	3	YES	AP-MPS-19 TRACK
31	4/20	1049	1109	X		18	7	NO	NO	HEAVY AP(Probable Weather) - NORMAL DATA COLLECT
32	4/20	1209	1225		X	19	8	3	YES	HEAVY AP (Probable Weather) - MPS TRACL
33	4/20	1344	?	X		20	8	NO	NO	HEAVY AP-(Probable Weather) - TRACK HISTORY
34	4/20	1635	1655		X	21	9	3	YES	SYSTEM CALIB. MPS-19 TRACK-LIGHT A/C
35	4/20	1745	1825		X	22	10	4	YES	SYSTEM CALIB.-MPS-19 TRACK-LIGHT A/C

DATA LISTING

ANGEL CLUTTER REDUCTION TESTS (cont'd.)

RUN#	DATE	TIME		DATA SPEED		DIGITAL TAPE #	RAVIR TAPE #	SONY TAPE #	ANALOG AGC	REMARKS
		START	END	N/S	H/S					
36	5/10	1150	1220	X		23	NO	NO	NO	DATA COLLECT-KNOWN A/C(3 TRACKS)
37	5/10	1354	1424	X		24	NO	NO	NO	DATA COLLECT-KNOWN A/C(3 TRACKS)
38	5/11	1452	1520	X		25	NO	NO	NO	DATA COLLECT-CONTROLLED LIGHT A/C
39	5/11	1541	1606	X		26	NO	NO	NO	DATA COLLECT-CONTROLLED LIGHT A/C
40	5/11	1614	1701	X		27	NO	NO	NO	DATA CP::ECT-CONTROLLED LIGHT A/C
41	5/11	1712	1733	X		28	NO	NO	NO	DATA COLLECT-CONTROLLED A/C(1 TRACK)
42	5/12	0631	0659	X		29	11	NO	NO	MODERATE AP(POSSIBLE BIRDS-NORMAL - MPS-19 ELEV. PHOTOS
43	5/12	0710	0729	X		30	12	NO	NO	MODERATE AP-(POSSIBLE BIRDS)-NORMAL DATA COLLECT WITH TEST TARGET
44	5/12	0746	0838		X	31	13/14	5	YES	MODERATE AP(POSSIBLE BIRDS)-MPS-19 TRACK
45	5/12	1103	1214		X	32	NO	6	YES	MPS-19 MYLAR BALLOON TRACKING
46	5/12	≈1300	≈1330		X	33	NO	NO	YES	MPS-19 SIG. GEN. CALIBRATION

APPENDIX A-3

SUMMARY OF PRELIMINARY ANGEL TRACKING TESTS AT NAFEC, OCTOBER 1971

Background

Task II of the APL contract with the Federal Aviation Agency is "Angel Clutter Reduction Techniques." The objective of this effort is to evaluate the effects of angel clutter on ASR radars and to determine cost-effective means of reducing these effects. Angel echoes can be caused by meteorological inhomogeneities, birds, or even insects. Previous experiments have indicated that the majority of angel echoes are due to birds, and the purpose of this field operation was to measure the detailed characteristics of bird angels during the fall bird migration at the FAA's NAFEC facility near Atlantic City, New Jersey. Although wideband video recorder tapes of ASR video had been made previously during the April 1971 migrations, this field operation was the first to record tracking radar data as well as ASR data. Continuous track data is required to fully assess the detailed differences between the radar target characteristics of bird angels and aircraft, and to develop appropriate methods of differentiating between them with the ASR.

Instrumentation

Figure A-3 indicates the equipment used during these tests.

A wideband video recorder (RAVIR Mod 2A) was installed in the NAFEC test facility to simultaneously record MTI and normal ASR video and triggers. A tripod-mounted Polaroid camera was also employed to record single and multiple-scan PPI video presentations. Two portable equipment modules were parked nearby: a 150 KW prime power generator and the Tracking Radar Module. This module consists of an S-Band (AN/MPS-19) tracking radar, a TV system, a Sanborn strip chart recorder to record AGC data, and a SONY PV 120V video tape recorder, which was used to record track radar video and voice annotations of the

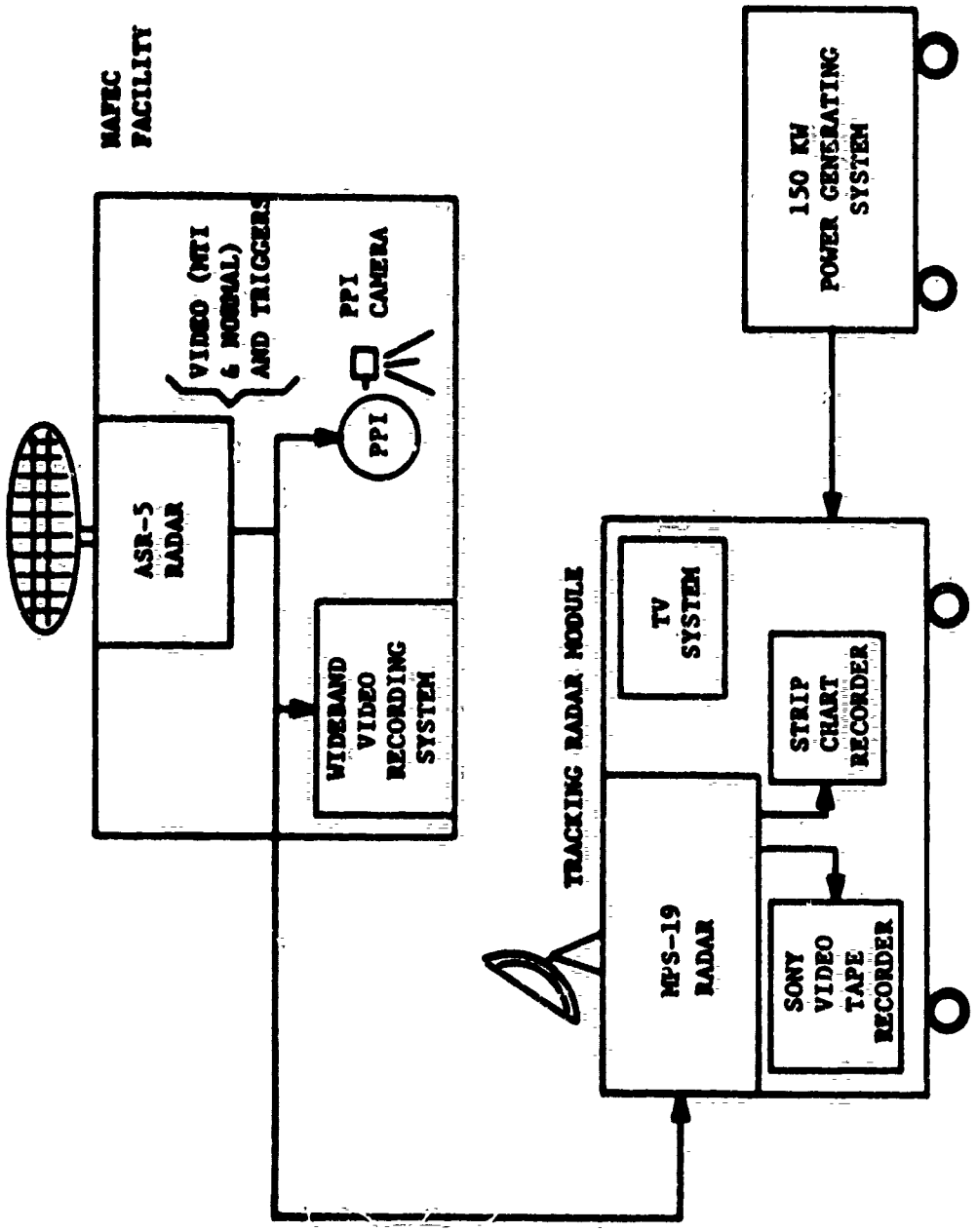

FIGURE A-3 INSTRUMENTATION FOR NAFEC TESTS

type of target and its identifying characteristics and positional data (range, bearing, and elevation as a function of time). The track radar transmitter was synchronized with the ASR transmit pulse to reduce mutual interference.

The S-band tracking radar had been received on loan only three weeks earlier from the Air Force. This precluded the intended full refurbishment of the radar prior to the date of the bird migrations; however, it was decided to conduct the operation at this time rather than to postpone all operations until the spring migrations. The radar on the whole performed well during the test period (due to a strong effort by the test crew) and was adequate for gathering the desired data.

Chronology

The Track Radar Module and Prime Power Generating Module arrived at NAFEC late in the evening of 26 October and the Track Radar Module was in operation the following day. The wideband video recording system was mated to the ASR-5 to record both normal and MTI video simultaneously. Little or no migratory bird activity was observed on the evening of 26 October, primarily due to very poor weather conditions (fog). A combination of fog and night precluded use of the TV system to gather visual data on bird tracks throughout most of the operation.

Early in the evening of 28 October, fog moving in from the south precipitated very heavy bird activity. Bad weather normally precludes migratory activity and local reports had indicated considerable numbers of birds in the area (primarily at the Brigantine Wildlife Refuge) waiting for clearing conditions. The fog on the evening of 28 October was generally low-lying and the moon could be clearly seen above it, indicating acceptable migratory weather. Bird angel activity began shortly after dark and by 1930 EST had reached heavy intensities

A series of five 15-minute wideband video recordings of ASR video were made between the hours of 1541 and 2017 (Table A-6). Almost thirty Polaroid photos were taken between 1607 and 2150 hours (Table A-7); Figures A-4 and A-5 show representative single and multiple-scan PPI presentations for MTI video with and without STC. It is clear from these photographs that neither MTI nor STC is a complete solution to the angel problem during periods of heavy bird activity.

The Tracking Radar Module PPI display presented a similar picture. Aircraft and apparent bird angels were tracked to obtain motional characteristics and recordings of radar video and AGC voltage. Figure A-6 shows three representative AGC recordings and the A-scope video corresponding to each.

Since all required data were recorded on the evening of 28 October, the Tracking Radar Module, generator van, and wideband video recording equipment were returned to APL on 29 October.

Discussion of Preliminary Results

It was possible to make several statements based upon the data gathered during this operation:

(1) AGC recordings of tracking radar video permitted a clear distinction between the angel and aircraft tracks. (Aircraft were identified by their much higher velocity.) This difference is clearly visible from Figures A-6(A) and A-6(B). It should be noted, however, that the AGC output is smoothed data and such distinctions may not be apparent in the short period of time during which the ASR scans past the target.

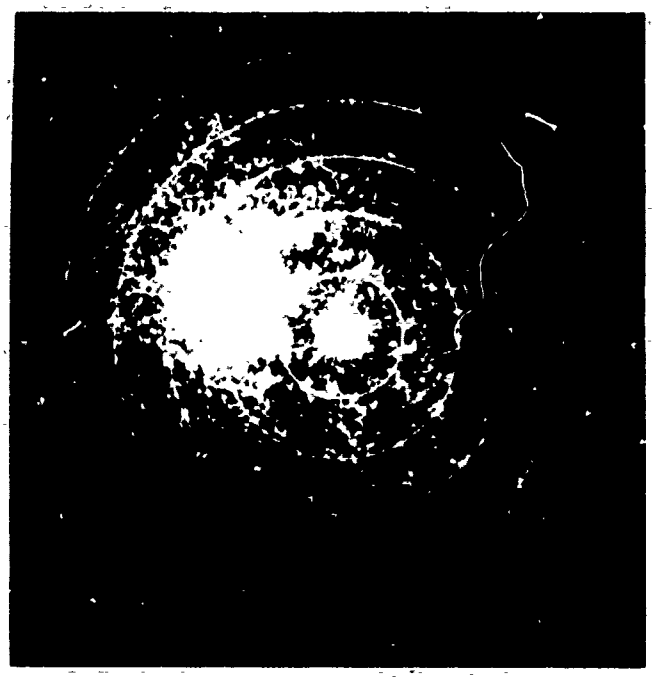

MTI VIDEO, NO STC, SINGLE SCAN

MTI VIDEO, STC, SINGLE SCAN

FIGURE A–4

SINGLE SCAN ASR PPI PRESENTATION
DURING HEAVY BIRD ACTIVITY

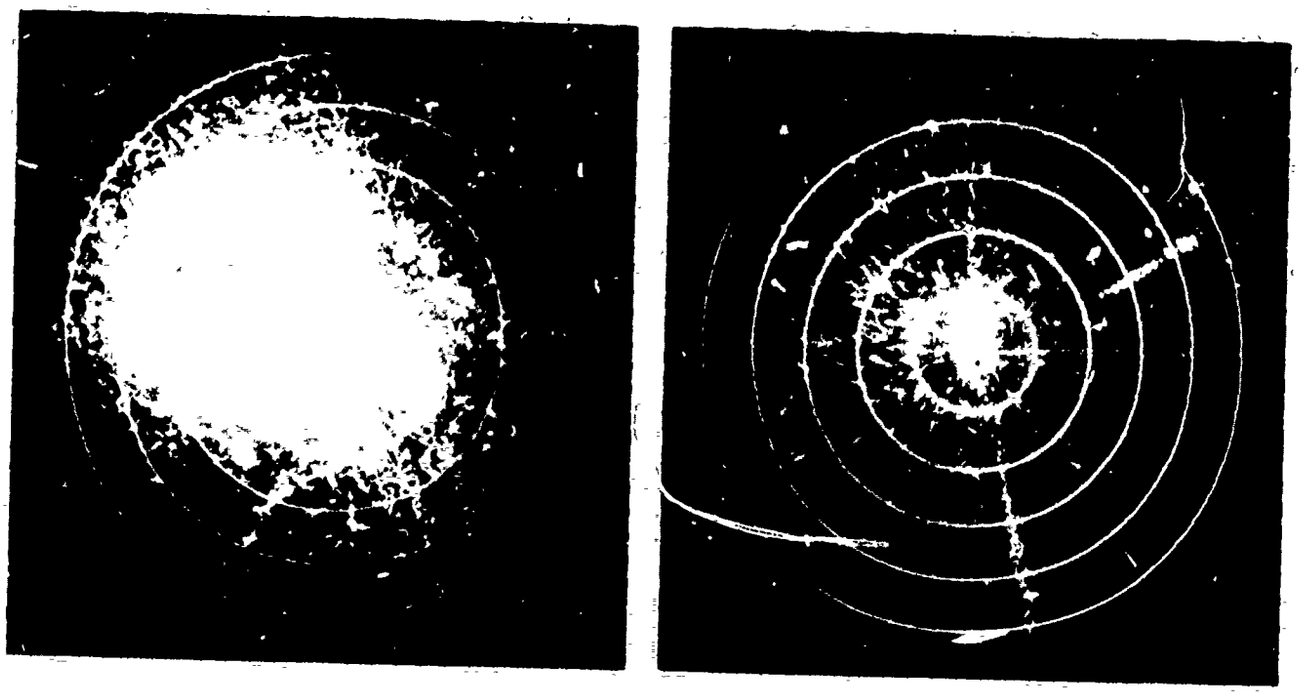

MTI VIDEO, NO STC, 10 SCANS

MTI VIDEO, STC, 15 SCANS

FIGURE A-5_MULTIPLE SCAN ASR
PPI PRESENTATION
DURING HEAVY BIRD ACTIVITY

TABLE A-6

WIDEBAND VIDEO RECORDINGS TAKEN AT NAFEC

28 OCTOBER 1971

Recorder: RAVIR Mod 2A

Channel 1	Normal Video	Track 2
Channel 2	MTI Video	Track 4
Channel 3	MPS-19 Triggers	Track 5
Timing	t_m delayed (-94 μsec)	Track 3

Tape Log

Number	Start	Stop
28-1541	1541 hrs.	1601 hrs.
28-1649	1649	1710
28-1836	1836	1857
28-1917*	1917	--
28-2000*	2000	2017

*Broken tapes. #28-1917 not rewound.

TABLE A-7

ASR-5 VIDEO PHOTOGRAPH LOG

28 OCTOBER 1971

PHOTO NUMBER	APPROX. TIME	RADAR VIDEO NORM	MTI	STC	DURATION	REMARKS
1	1607 hrs.		X		1 scan	Camera Test
2	1608		X		1 scan	Camera Test
3	1609		X		1 scan	
4		X			1 scan	
5			X		60 sec	
6			X		120 sec	
7	1634		X		300 sec	
8	1810		X		1 scan	
9	1818		X		240 sec	
10	1821		X		90 sec	
11	1830		X	X	1 scan	
12	1831		X	X	90 sec	
13	1834		X		1 scan	In Sequence
14	1837		X		90 sec	
15	1839		X		1 scan	
16	1845		X		1 scan	
17	1923		X		1 scan	In Sequence
18	1925		X		90 sec	
19	1926		X		1 scan	
20	1927		X		10 scans	
21	1930		X		1 scan	
22	1931		X	X	1 scan	
23			X	X	1 scan	
24			X	X	15 scans	
25			X		1 scan	In Sequence
26	2140		X		60 sec	
27*	2150	X			1 scan	(20 Mile Range)

*20 mile radius; remainder 10-mile radius with 2 mile range rings. One scan = 4 seconds

AGC RECORD

A SCOPE

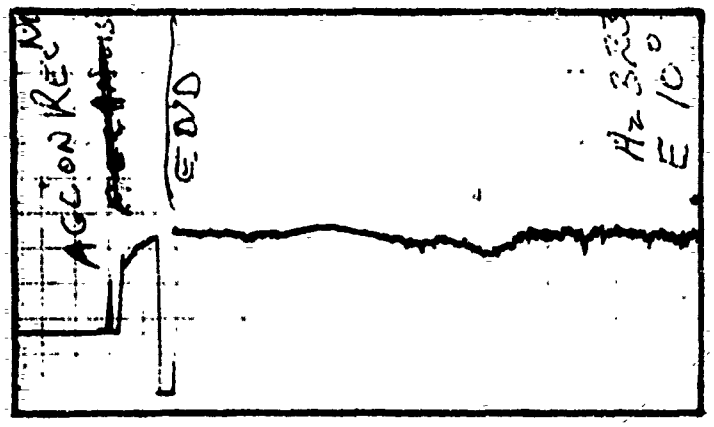

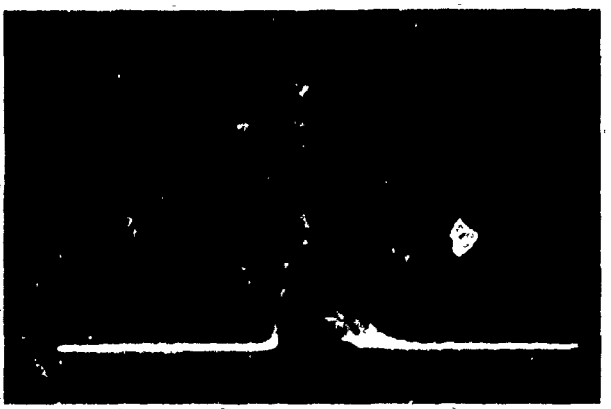

4A ___ MOST COMMON
BIRD ANGEL TARGET

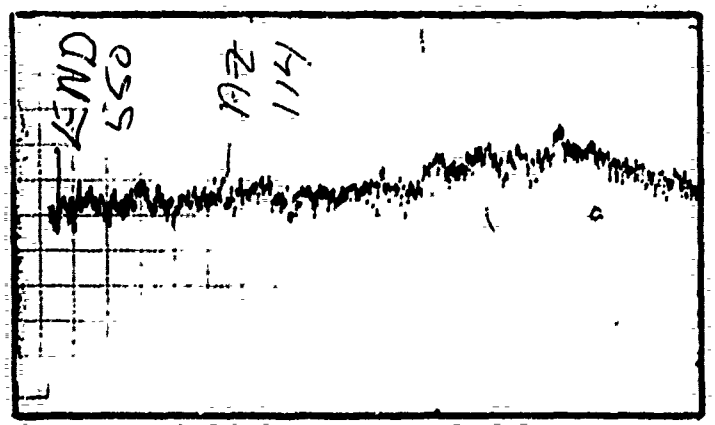

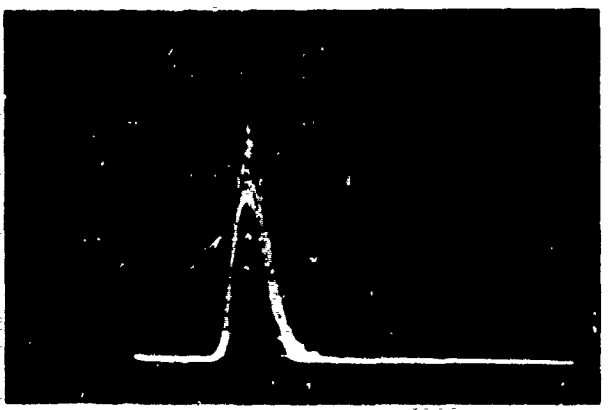

4B ___ LARGE COMMERCIAL
AIRCRAFT

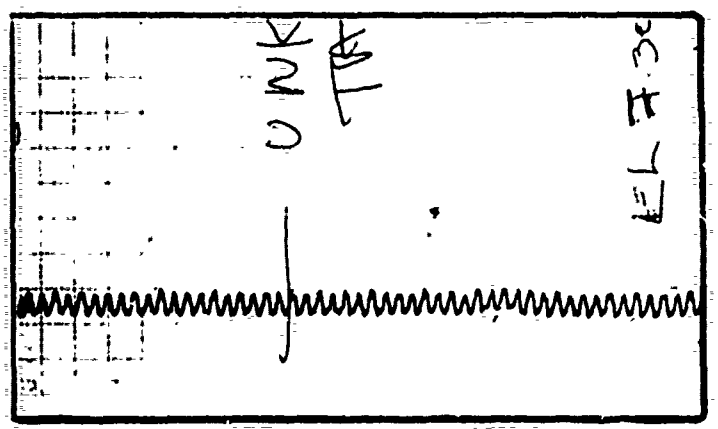

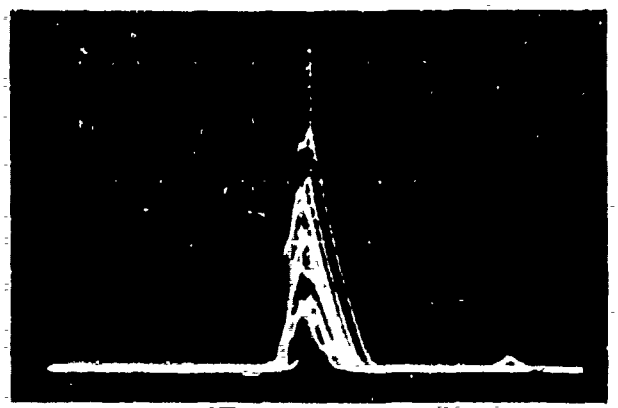

4C ___ HIGH ALTITUDE ANGEL
(6600 FT)

FIGURE A-6 ___ TRACKING RADAR
AGC RECORDINGS & A-SCOPE VIDEO

(2) Visual observation of the A-scope* video (which contains the high frequency amplitude fluctuation components not visible on the AGC recordings) also indicated different fluctuation characteristics for angel and aircraft targets. The observers were able in a number of cases to recognize aircraft and bird angels from the A-scope video, although the AGC recordings appeared to be a more reliable indicator. There was a general feeling that the bird fluctuations could be associated with wing beats, although analysis of the video tape recordings are required to determine if these fluctuations corresponded to wing beats or the fluctuations associated with many birds in the same radar resolution cell.

(3) Two distinct types of angel returns were identified. The majority were of the type shown in the AGC recording of Figure A-6(A). The type shown in Figure A-6(C) were encountered during attempts to determine the maximum altitude of the angel activity. These angels were isolated echoes with 0.5 Hz AGC fluctuations and were encountered at altitudes as high as 6600 feet.

(4) While MTI provided much improvement over normal video, and MTI with STC was even better, a large number of angel echoes remained. It is estimated that there are about 250 angel targets on the MTI-STC single scan photograph in Figure A-4 (excluding the automobile traffic visible on a nearby road).

* A tracking radar A-scope displays signal amplitude (received video) vertically and range (time) horizontally; the horizontal sweep moves to the right with increasing range.

(5) It was possible to distinguish some aircraft returns from angel echoes on the 10-mile PPI display on the basis of angular width (run length), particularly on the MTI-STC display where angel clutter was somewhat reduced. This can be seen at 63° in Figure A-5 (#24). This large aircraft produced a 4° bearing width, indicating detections in the major sidelobes of the ASR radar (1.5° beamwidth). This would not be the case for smaller aircraft.

(6) Preliminary data analysis indicated that the aircraft targets encountered had radar cross-sections of from 25 to 1000 square meters, while the angel returns were in the range 0.0001 to 0.01 square meters. With somewhat limited data reduction, it was not possible to determine the proportions of the angel echoes due to single birds and groups of birds.

APPENDIX A-4

ANGEL CLUTTER TEST SITE SELECTION

Following the initial angel clutter tests at NAFEC and the refurbishment and optimization of field test instrumentation, it was necessary to select a test site for angel clutter data collection during the spring bird migrations. Criteria for this selection were:

(a) A history of migratory or local bird activity in the area,

(b) a history of angel clutter activity with some level of impact on Air Traffic Control functions and coincident with bird activity in the area, and,

(c) a physical situation at the radar site which was appropriate to the location and installation of the necessary instrumentation.

Subsequent to a review of FAA angel clutter field reports, bird migration and weather forecasts, and considering the test period available, four candidate sites were selected. These were Little Rock, Arkansas; Memphis, Tennessee; Minneapolis, Minnesota and Milwaukee, Wisconsin. Following visits to each of the airport FAA facilities by APL personnel, General Mitchell Field, Milwaukee was selected.

Details of the discussions and observations at the four locations are provided in the two APL trip reports included in this Appendix.

I. REPORT ON VISITS TO LITTLE ROCK AND MEMPHIS

March 1972

1. Introduction

APL personnel visited Little Rock Municipal Airport (Adams Field), Little Rock, Arkansas, on March 8-9 and Memphis International Airport, Memphis, Tennessee, on March 10. The purposes of the visits were to observe and discuss local angel clutter problems and to evaluate the potential of the two locations for Task II data collection. Little Rock was considered a likely site for the planned field measurement program; therefore, essential preliminary coordination and planning was carried out with FAA personnel there. Robert Stutzman, SW-432, Task II Coordinator for the Southwest Region, took part in discussions of Little Rock on March 9. This report summarizes the observations and activities of the trip and presents recommendations on Little Rock as a data collection site. Key contacts in Little Rock are listed in Enclosure 1. A brief investigation eliminated Memphis as a possible site for Task II measurements (Section 8).

2. Summary

A visit to Little Rock Municipal Airport on March 8-9, 1972 established that air traffic control there is significantly constrained twice daily in October-November and February-March by radar clutter (Figures 1-4)* and that this clutter is caused by birds which roost near the airport. Frequently-observed "clear-air" clutter (Figure 5) was reported to be as serious a problem as the bird clutter. The nature of the local problem, the physical layout, the facilities, the air traffic load, and the local FAA personnel make Little Rock an excellent site for a field measurement program. However, Little Rock bird experts (Enclosure 1) predict that the birds which cause the radar clutter will start leaving that area around March 15 and that no concentrations are likely to remain after April 1.

The probable bird migration schedule together with the unlikelihood of being able to start data collection in Little Rock before the last week of March prompts the following recommendations:

Most desirable - Locate a suitable airport site in the northern Mississippi Valley where birds will be common in April;

* All figures are grouped at the end of the text.

Alternative - Begin data collection in Little Rock as soon as possible, no later than the last week in March. If birds are gone, or when they go, collect data on clear-air clutter and other local angel clutter.

A visit to Memphis International Airport established that terminal air traffic control there is not affected by birds nor, to any significant extent, by any other forms of "anomalous propagation." Therefore, Memphis is considered to have no value as a data collection site for FAA Task II. Memphis birds migrate at the same time as Little Rock birds.

3. Radar

Little Rock ATC has an ASR 4B radar with parametric amplifier and PIN-diode attenuator. The effect of the latter was described as reducing sensitivity to approximately the level obtained without the parametric amplifier. Antenna height was estimated to be 45 feet. Antenna tilt was reported as +2°.

Standard operating procedure is to use MTI video with STC from 0 to 15 miles and NORMAL video from 15 to 40 miles. NORMAL video is useless inside 10 miles due to ground clutter. With MTI, no ground clutter appears. Surface traffic is observed (Figure 4a, 240°, 9 and 14 miles) and recognized by location and speed, and then is ignored without difficulty. Precipitation returns are reduced by use of circular polarization (CP); attenuation is satisfactory in light rain and is useful but inadequate in heavy rain. When AP and bird clutter appear, sensitivity is reduced by means of the PIN diode attenuator, known locally as "the bird switch." Slight clutter reduction occurs; the loss of sensitivity on aircraft is objectionable. FTC, IAGC and CSS (Cross Section Sensitivity, similar to STC) are available but are seldom used on the ground that they offer no significant performance improvement in clutter.

4. Radar Clutter Reports

AP, "anomalous propagation", was found to be loosely used to refer to many observed radar returns not identifiable as aircraft, surface vehicles, weather, or normal ground clutter. It may include returns from birds, insects, atmospheric inhomogeneities, normally-undetected ground features, etc. In information-gathering discussions it proved important to establish a common working definition of the

term and then to distinguish clearly between observations of AP and interpretations. An effort is made to preserve this distinction in the following. For present purposes, birds are considered separately and AP is defined as follows:

> AP: Any observed radar returns which cannot be associated with aircraft, surface vehicles, birds, weather or normally-detected ground clutter.

The following is a distillation of conversations with approximately 15 FAA personnel at Little Rock including controllers, radar technicians, supervisors, and administrators. A high degree of consistency was noted among the reports.

Bird clutter at Little Rock imposes operational limitations on traffic flow. Aircraft not equipped with beacons cannot be tracked through sectors in which bird clutter appears. Beacon-equipped aircraft must be skin-painted to initiate tracking; this is impossible in dense bird clutter. When bird clutter is strong, controllers advise aircraft of the lack of radar coverage in certain areas. A NOTAM is normally not issued.

Bird clutter is observed throughout October, November, February and March. It occurs twice daily, at dawn and at dusk, for a period of 30 to 90 minutes. Radar clutter is correlated in location and time of appearance with dense streams of birds observed visually from the tower.

The appearance of bird clutter on a PPI is shown in Figures 1 through 4. The clutter in these photographs, taken on March 8 and 9, was considered typical by Little Rock personnel. The characteristics of the clutter are discussed in Section 5.

AP which is thought to result from causes other than birds, is usually observed to the northeast and southwest; sometimes, it is seen to approach from the west. It appears on a PPI as a moving swarm of discrete point echoes resembling aircraft returns (Figure 5). The AP occurs frequently; we were assured that, if we stayed for two days, we would definitely see it. It occurs more often at night than during the day. The AP often occurs in a visually clear atmosphere and cannot be associated with any visible clouds or precipitation. MTI is useful in reducing the clutter, but does not eliminate it. A figure-8 distribution, as seen in Figure 5, is typical, although occasionally the clutter appears at all azimuths. CSS (Cross Section Sensitivity) is of some use in attenuating the clutter; it attenuates aircraft returns as well. FTC and IAGC are of no use.

At both Little Rock and Memphis, returns like those just described were frequently attributed to "ducting." Other characteristic effects ascribed to ducting were a reduction in aircraft detection range and an increased intensity and extent of ground clutter return. Information on the actual presence of ducts has not been sufficient to permit a correlation to be established between ducts and radar effects. The extended detection ranges commonly attained with marine radars in ducts were never noticed.

5. Observations

Radar clutter was observed and photographed on a PPI on the evening of March 8 and the morning of March 9. Table 1 is a log of all photographs taken. Figures 1 through 4 are photographs selected to show the major features of observed clutter.

Ground clutter (Figure 1a) extends in range to between 7 and 15 miles in different sectors. It renders NORMAL video useless inside 10 miles. Usually, MTI video with STC is used inside 15 miles and NORMAL is used between 15 and 40 miles, the customary maximum surveillance range. No residual ground clutter was evident with MTI.

In the evening, March 8, clutter was observed to appear rather abruptly, within several minutes, on a scope which had previously shown a practically black background. It lasted without major variation from 15 minutes before sunset until about 45 minutes after sunset, 1800 to 1900 CST. The occurrence of the evening air traffic peak in this interval increases the impact of the clutter on controllers. The clutter was most dense to the north, northeast and east, where bird roosts are known. This specific geographic relation of airport and roosts aggravates the problem. Because the two principal runways run north-south and northeast-southwest, either departure or approach paths pass directly through the bird clutter region on controllers' PPI's.

Morning clutter began in the east about 40 minutes before sunrise, 0628 CST. It faded almost to the point of disappearance after about 30 minutes. Clutter then reappeared, most strongly in the north and south quadrants, and remained for over an hour. It persisted on into the beginning of the morning air traffic peak. At times the clutter extends to ranges of approximately 12 miles (Figure 4).

Although the gross clutter patterns differed somewhat between evening and morning (Figures 2 and 3), the fine detail visible on the PPI looked identical on both occasions. The video consisted of clouds of discrete, sharply-defined returns. The PPI blips appeared to be equal to or smaller in size than those from a small aircraft. No diffuse or extended returns were noted. (The evident merging of returns in the photographs is a photographic effect.) Some blips could be singled out and could apparently be tracked by eye for several scans. The echoes to the south in Figure 4b were tracked in this way for more than a minute; each appeared to maintain an identity and a fairly steady southerly course for that long. Eventually, the echoes faded. Other echoes, strong and clear on one scan, would fail to reappear in the same neighborhood during the next three or four scans.

Visual observations were made at about the time Figure 4a was taken. A serpentine stream of blackbirds was seen flying south past the airport from the vicinity of a large roost known to lie several miles to the north. The stream was estimated as about 100 - 300 feet wide and the same in thickness. It extended to the limits of visibility to the north and to the south at an estimated altitude of 500 - 1000 ft. Similar large concentrations could be detected at greater ranges. A few flocks of 20 - 50 birds were visible, also heading southward. The locations and extent of the bird concentrations correlated plausibly with observed PPI clutter when the effect of MTI was included. As figures show, MTI cancellation was more effective toward the west, where the birds' southerly track was roughly tangential, than to the north and south, where the motion of the birds was approximately radial with respect to the radar.

6. Bird Information

Mr. and Mrs. Henry Halberg, Thurman Booth and Robert Pierce, experienced Little Rock bird observers, provided much useful consistent information, pertinent parts of which are summarized below.

Several million blackbirds, grackles and starlings roost (sleep) in railroad yards several miles north of the airport, and about one million roost near the river to the east of the airport, locations corresponding to the regions of dense clutter shown in Figures 2-4. The birds disperse to feed after first light and then return to the roost in a more concentrated, briefer flow at sunset, as observed on radar. In previous years bird populations have been as much as ten times greater. The birds roost around Little Rock in large quantities (2 - 50 million) from about October through March. Usually, Little Rock roosts begin to break up in mid-March and the large concentrations have disappeared by about April 1. It was reported as very probable that those birds causing the ASR clutter

would be gone before April 1. This year, migration may be occurring about a week earlier than usual. Resident birds, in the area throughout the summer, appear in small numbers and small concentrations.

After blackbirds begin migrating, temporary roosts form to the north, lasting from several days to several weeks. Day-to-day bird motion is strongly affected by local weather; on a weekly time scale, the long-term weather, e.g., "a warm winter," is the major influence on when bird migrate.

7. Little Rock Facilities

The ASR is sited on airport property in an FAA-controlled, fenced compound of adequate size to contain three vans within approximately 100' of each other and within 100' of the ASR building. The ASR site is within a mile of the Tower/IFR room. Clear radar surveillance is possible on all azimuths except through the tower. Surrounding terrain is very flat with the exception of low hills about 10 miles to the south. The ASR site is accessible from public roads.

Adequate prime power (30 KVA plus) is available from main feed lines at the ASR site. Local loads are automatically switched to a generator if the normal supply fails. In the event of a power failure when APL test equipment was on line, the APL load would not be switched to the FAA generator but would be dropped.

We indicated our intention to provide the following protection at interfaces with the local system:

a) Fused prime power lines to APL equipment
b) Master cutoff switch(es) in APL prime power lines
c) Isolation amplifiers in signal lines (as at Friendship)

An intercom on the ASR tower can be relocated to provide communication between the APL van and the controller/technician location in the tower building.

8. Memphis Angel Clutter Situation

For the last three years Memphis International Airport has had no operational interference from birds. Other "anomalous propagation" returns cause no significant problems in air traffic control. Informal discussions on March 10 with Memphis Tower Chief James Arthur, Deputy Tower Chief Parsons and three watch-standing traffic control supervisors are summarized as follows.

Until three years ago Memphis ATC observed on radar heavy concentrations of birds during fall, winter and spring. Returns occasionally extended as far as 40 miles. Traffic control was affected because primary radar coverage was impossible in some approach and departure sectors. Three years ago the city dump in which the birds roosted, located near the edge of the airport, was eliminated and the bird problem disappeared. No modifications to the radar were made at or around this time. Since then birds have been no problem. Occasional groups of migrating birds are observed in transit through the area; these have no effect on operations. Occasional AP in the form of moving clouds of discrete echoes is observed, but it is not considered an operationally significant problem.

The Memphis TRACON, located in the tower, uses an ASR-5 sited on the opposite side of the airport. Memphis ARTCC is located near the ASR; an ARSR radar is about 15 miles away. The Memphis TRACON handles about 800 to 1000 operations on an average day. As a rough indication of radar operation, radar handoffs between terminal and enroute facilities were claimed to be normally accomplished without difficulty in the range interval 30 to 40 miles from the ASR, for small aircraft as well as for large.

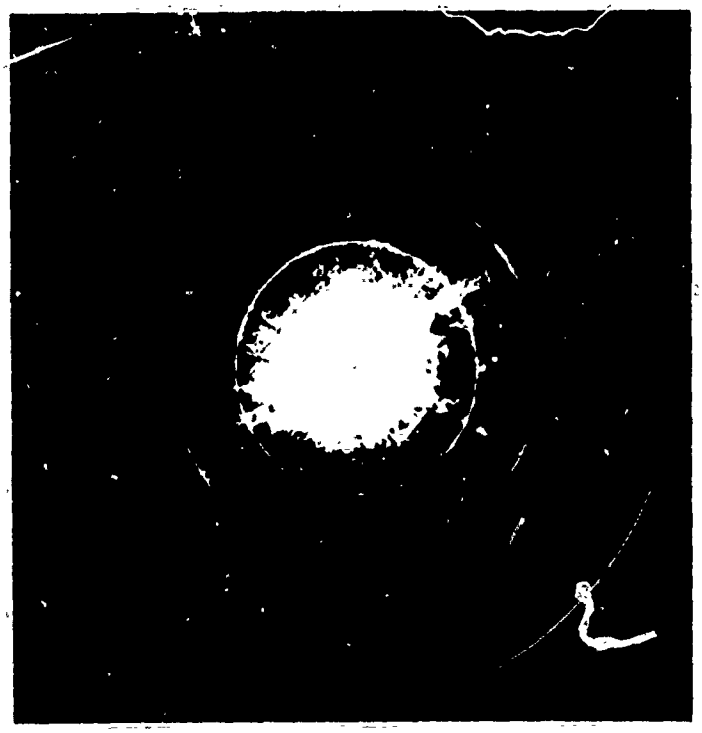

A. 0540CST
MTI AND STC WITH NORMAL BACKGROUND. TWO SCANS, 10 MILE SCALE, 2 MILE RANGE RINGS. MARCH 9. BIRD CLUTTER STARTING TO GROW AT 085°, 4.5 MI.

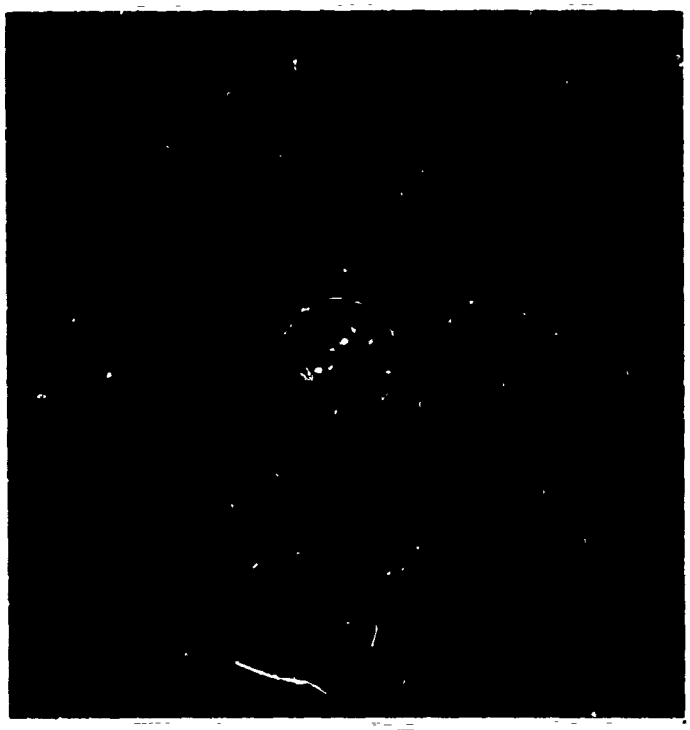

B. 0604CST
MTI AND STC. ONE SCAN, 2 MILE RANGE RINGS. MARCH 9. NO AIRCRAFT KNOWN TO BE IN AREA.

FIGURE 1

A. 1810—SCALE 10 MILES,
2 MILE RANGE RINGS

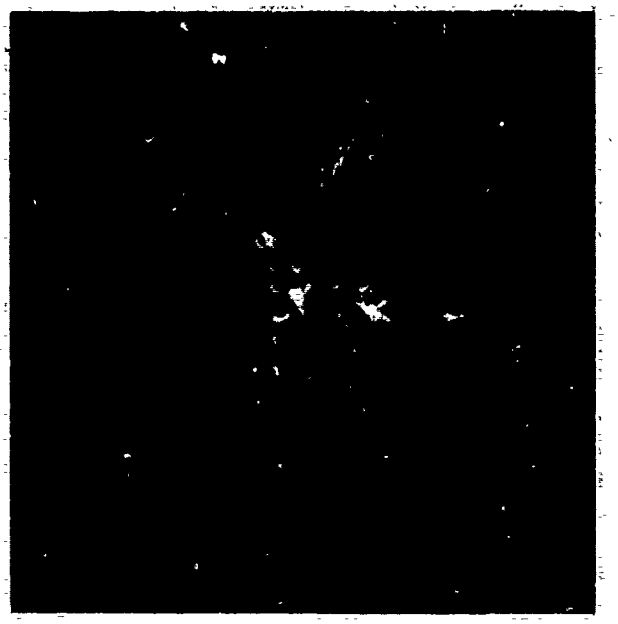

B. 1815—SCALE 10 MILES,
2 MILE RANGE RINGS

C. 1820—SCALE 6 MILES,
2 MILE RANGE RINGS

D. 1825—SCALE 20 MILES,
5 MILE RANGE RINGS

FIGURE 2

DUSK CLUTTER, MARCH 8. MTI & STC. TWO SCANS

A. 0600

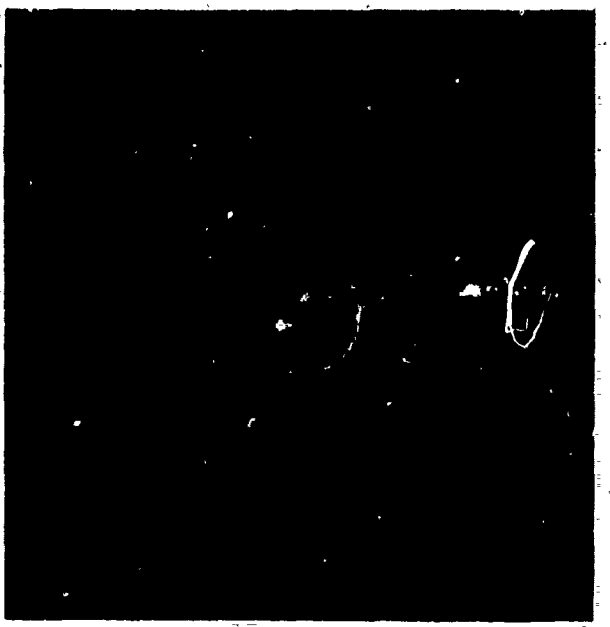

B. 0603

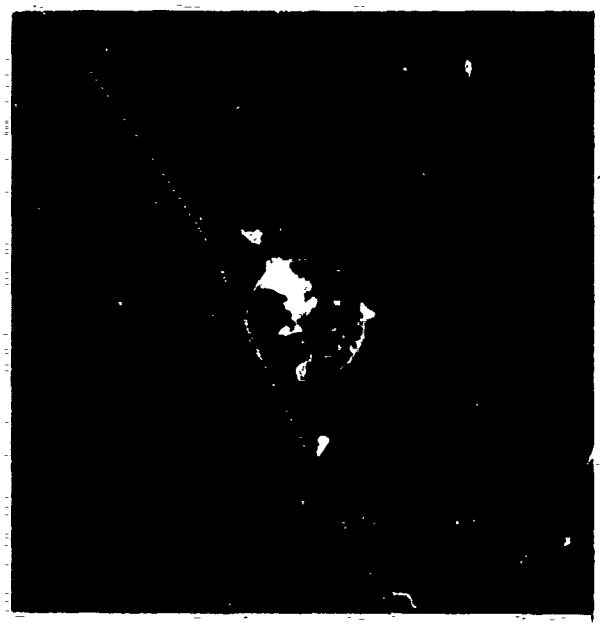

C. 0609

D. 0613

FIGURE 3

DAWN CLUTTER, MARCH 9, MTI & STC
TWO SCANS, 10 MILE SCALE
2 MILE RANGE RINGS

MAGNETIC NORTH TOWARD TOP OF PAGE

TIMES___CST

A. 0635__MTI & STC. TWO SCANS, 20 MILE SCALE, 5 MILE RANGE RINGS. MAR 9

B. 0702__MTI & STC. TWO SCANS, 6 MILE SCALE, 2 MILE RANGE RINGS. MAR 9

FIGURE 4

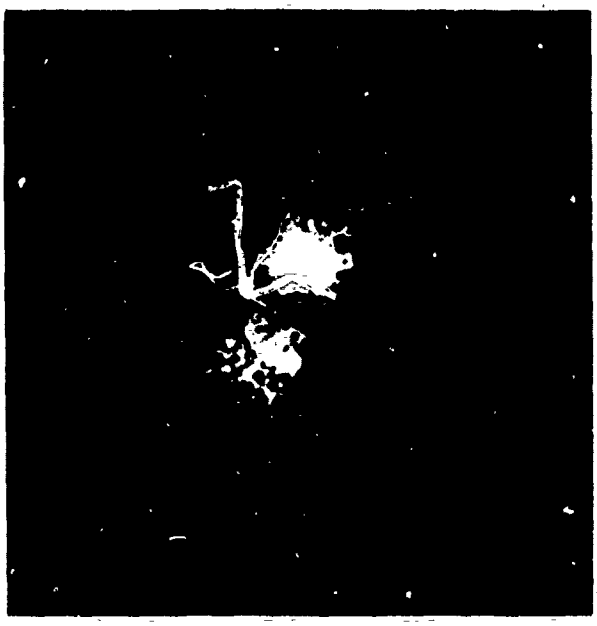

A—2300 CST

B—2320 CST

FIGURE 5
ANGEL CLUTTER ON LITTLE ROCK ASR

(30 MILE RANGE, COURTESY OF
E. GRAHAM, FAA, LITTLE ROCK)

TABLE 1

Little Rock ASR 4B PPI Photographs

March 8-9, 1972

Unless otherwise indicated, photos show MTI video, STC on, parametric amplifier on, 10 mile scale, 2 mile range rings (RR), two sweeps/photo.

Polaroid camera with portrait lens, f/5.6, exposure 8 seconds (2 sweeps) unless otherwise indicated, ASA 3000 film, 21.5" from portrait lens to PPI plastic overlay (approx. 22.5" to CRT face).

No.	Time (CST)	Remarks
2	1805	
3	10	
-	11	Sunset
4	12	
5	15	Parametric amplifier off
6	15+	
11	20	6 mi scale, 2 mi RR
12	22	6 mi scale, 2 mi RR, 1 sweep
13	25	20 mi scale, 5 mi RR
21	0540	MTI with NORMAL background (low NORMAL video gain)
22	48	MTI with NORMAL background, aircraft, birds 090/10
23	50	
24	52	(wind reported 250/4 KTS)
25	53	
26	56	Some birds beginning to appear at ∿ 010
27	0600	
28	03	Birds to east fading
29	04	1 sweep
30	08	Birds appearing to north
31	08+	20 mi scale, 5 mi RR
32	09	
33	13	

Table 1 Continued

No.	Time (CST)	Remarks
34	15	40 mi scale, 10 mi RR, 4 sweeps, surface vehicles 240, 9 mi, aircraft NE 35 mi
35	22	MTI and NORMAL
36	23	MTI and NORMAL
37	0624	6 mi scale, 2 mi RR, MTI and NORMAL
38	26	6 mi scale, 2 mi RR,
-	28	Sunrise
39	32	20 mi scale, 5 mi RR
40	35	20 mi scale, 5 mi RR; 200-600 discrete blips to north
-	37-45	Visual observations of bird streams (see text)
41	48	20 mi scale, 5 mi RR, 5 sweeps
42	0702	6 mi scale, 2 mi RR; clumps to south are moving south; runway MTI beacons NE and SW approx. 1 mi

Enclosure (1)

Principal Contacts in Little Rock

FAA, Little Rock

FAA Sector Chief Noteboom
Asst. Sector Chief Daniel Gardner
Radar Unit Chief Everett Graham
Tower Chief Hunsekker

Airway Facilities Sector
Building C-8, Adams Field
Little Rock, Arkansas 72202
Telephone No. 501-374-9038

Little Rock Avifuana Contacts

Thurman Booth
Federal Blackbird Control Officer
U.S. Fish and Wildlife Service
Room 315, Post Office Building
Little Rock, Ark.
Telephone No. 501-378-5382

Robert Pierce
Cooperative Extension Service
Univ. of Arkansas Graduate Institute of Technology
MacArthur Park, Little Rock, Ark.
Telephone No. 501-376-6301

II. REPORT OF TRIP TO MINNEAPOLIS/MILWAUKEE AIRPORTS

March 1972

The airports and FAA facilities at Minneapolis, Minnesota and Milwaukee, Wisconsin, were visited during the period 15 - 17 March 1972 by APL personnel. The primary purpose of these visits was to determine the feasibility of conducting FAA Task II test operations at either of these locations.

Upon arrival at Minneapolis a tour of the Tower, IFR room and maintenance areas was provided by the Assistant Radar Chief. Discussions with personnel in these areas revealed a history of undefined angel clutter, primarily in the spring and fall. It was expected that the spring clutter problems would begin about 1 April and continue for approximately two months. Controllers interviewed could not recall any occasions when clutter had become an operational problem, although it was an annoyance. Maintenance personnel were cordial and receptive to the possibility of locating Task II equipment at Minneapolis.

Conversations with several local "bird watchers" were consistent, with the arrival of waterfowl anticipated about 1 April followed closely by other types, with peak activity in mid to late April.

Upon arrival at Milwaukee, the Task II requirements were discussed with the Assistant Sector Chief and a tour of the Tower and IFR room was made in company with the evening maintenance technician. All personnel contacted agreed that heavy angel clutter could be anticipated during the spring and fall of each year with the spring clutter historically beginning about 1 April. In contrast with Minneapolis, however, the Milwaukee air controllers interviewed stated that clutter has been an operational problem. The source of the heavy clutter at Milwaukee is undefined after several attempts to correlate with atmospheric conditions. Photographs of previous clutter observations disclosed figure eight patterns centered on the radar and extending, in some cases, to twenty miles. The one point of correlation noted was the tendency of the clutter pattern to align with the wind. Peak clutter periods tend to occur around sunrise and sunset, however, clutter has been observed at all hours.

All facilities at Milwaukee are centrally located providing easy access to the ASR (located on the field in front of the control tower), the tower cab, IFR room, FAA offices, Weather Bureau and Flight Service Station. The Tower Chief and Sector Chief each expressed high interest in the project and their willingness to assist.

The Milwaukee "bird watchers" contacted reported some migratory waterfowl activity beginning now, with overall bird activity expected to reach a peak in April.

In view of the apparently heavier clutter conditions and resultant operational problems, anticipated bird activity and reduced travel distance, it is recommended that Milwaukee Airport be selected as the FAA Task II test site with an equipment arrival date planned for 29 March 1972.

APPENDIX B

SUPPORTING DATA

APPENDIX B-1

STATISTICAL DATA FOR BIRDS AND AIRCRAFT

Spatial Autocorrelation Functions for ASR Video Matrix

The characteristic distributions in azimuth and range of ASR video returns are of importance for the optimization of a video processing scheme. They determine, respectively, the azimuthal extent over which pulse-to-pulse correlation is profitable and the sampling interval in range needed to yield independent video samples. A measure of these characteristics is the one-dimensional autocorrelation function presented below. Initial results include range and azimuth functions for a known, controlled Cessna 172 aircraft and for an angel clutter target. (Figure B-1)

The plotted functions are autocorrelation functions as defined by Bendat and Piersol (Reference *), normalized by the value of the function at zero lag. The input data from each of several scans consisted of a string of ASR amplitude values (37 in azimuth or 40 in range) from a selected row or column in the Data Collect Matrix. The autocorrelation function of each string was found and normalized. Then the average autocorrelation function over the several scans was obtained. Figure B-2 shows range autocorrelation functions for a Cessna 172 aircraft and for an angel track (MKE 16-1, Track 1). Figure B-3 shows azimuth autocorrelation functions for the same two targets.

The range autocorrelation results show that both the aircraft and angel returns usually fall into a single range cell but occasionally appear in two range cells, as is expected from straddling of two range cells. The azimuthal autocorrelation functions show a slight difference for the aircraft and the angel, with the angel track having slightly higher autocorrelation for lags less than 0.45° and slightly lower thereafter. Both targets

---

* Bendat, J. S. and A. G. Piersol, Random Data: Analysis and Measurement Procedures, Wiley-Interscience, New York, 1971

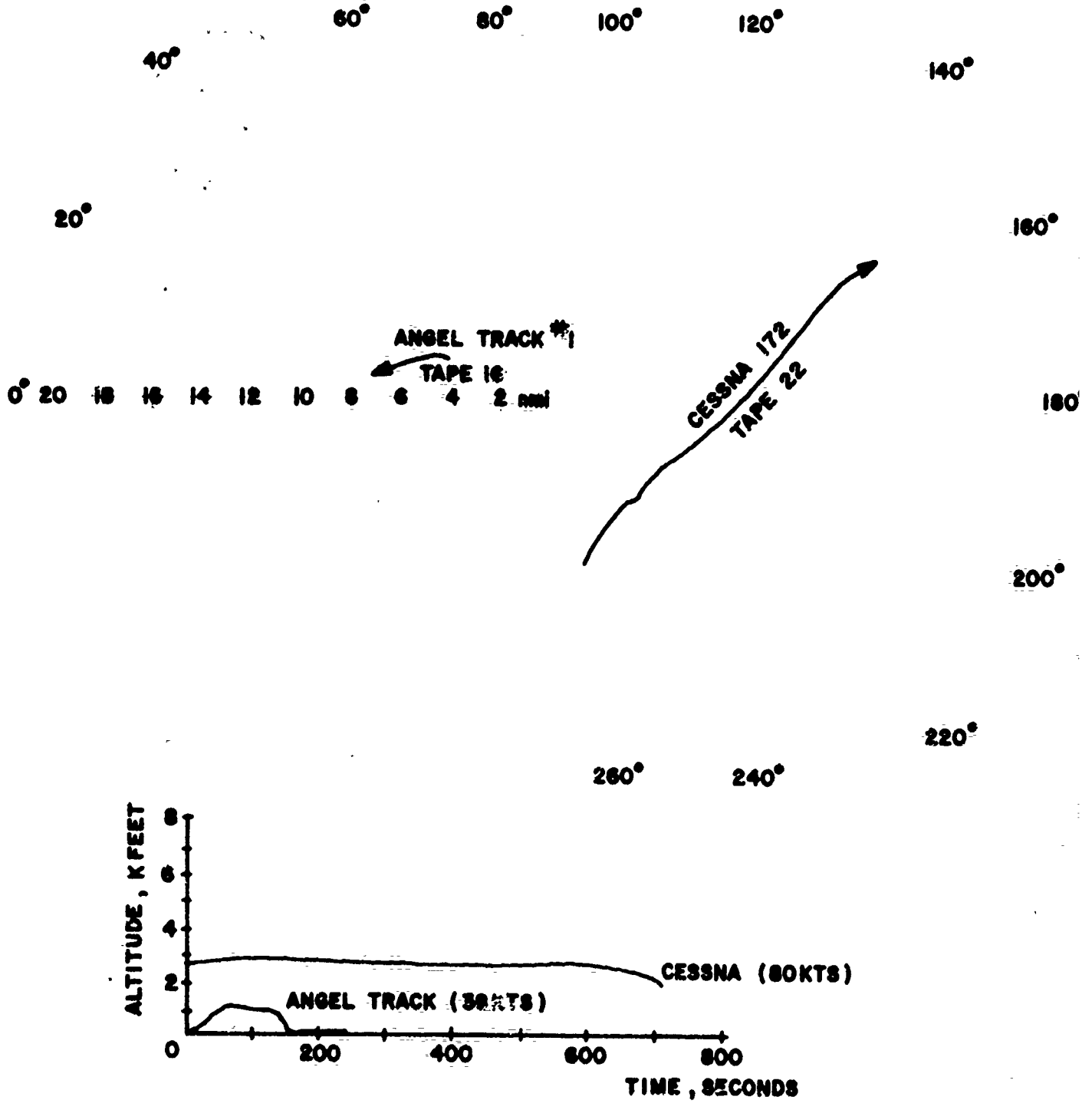

Figure B-1 Tracks Used For Statistical Analysis

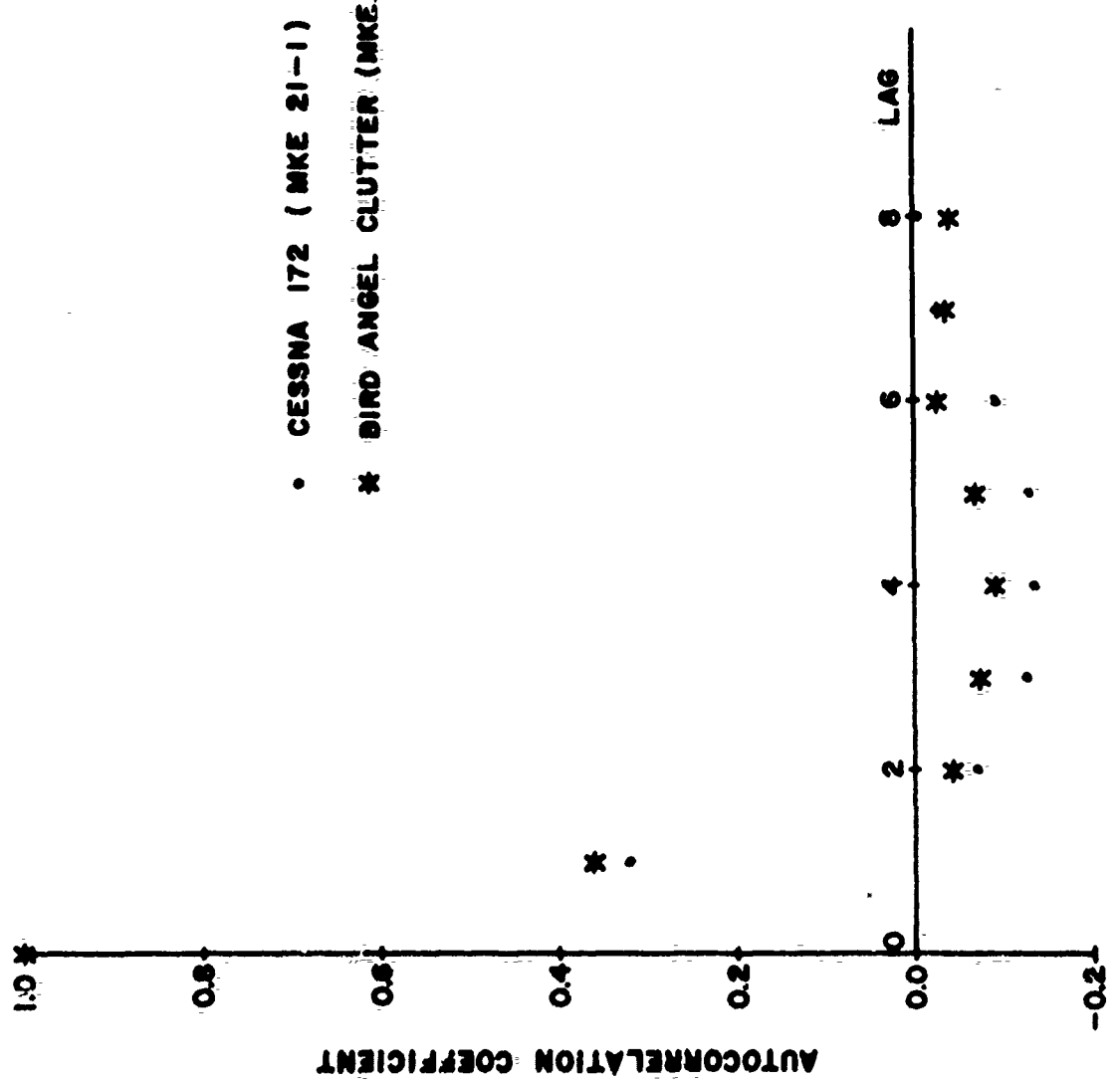

Figure B-2 ASR Mean Range Autocorrelation Coefficient For A Lag Interval Of One Pulsewidth

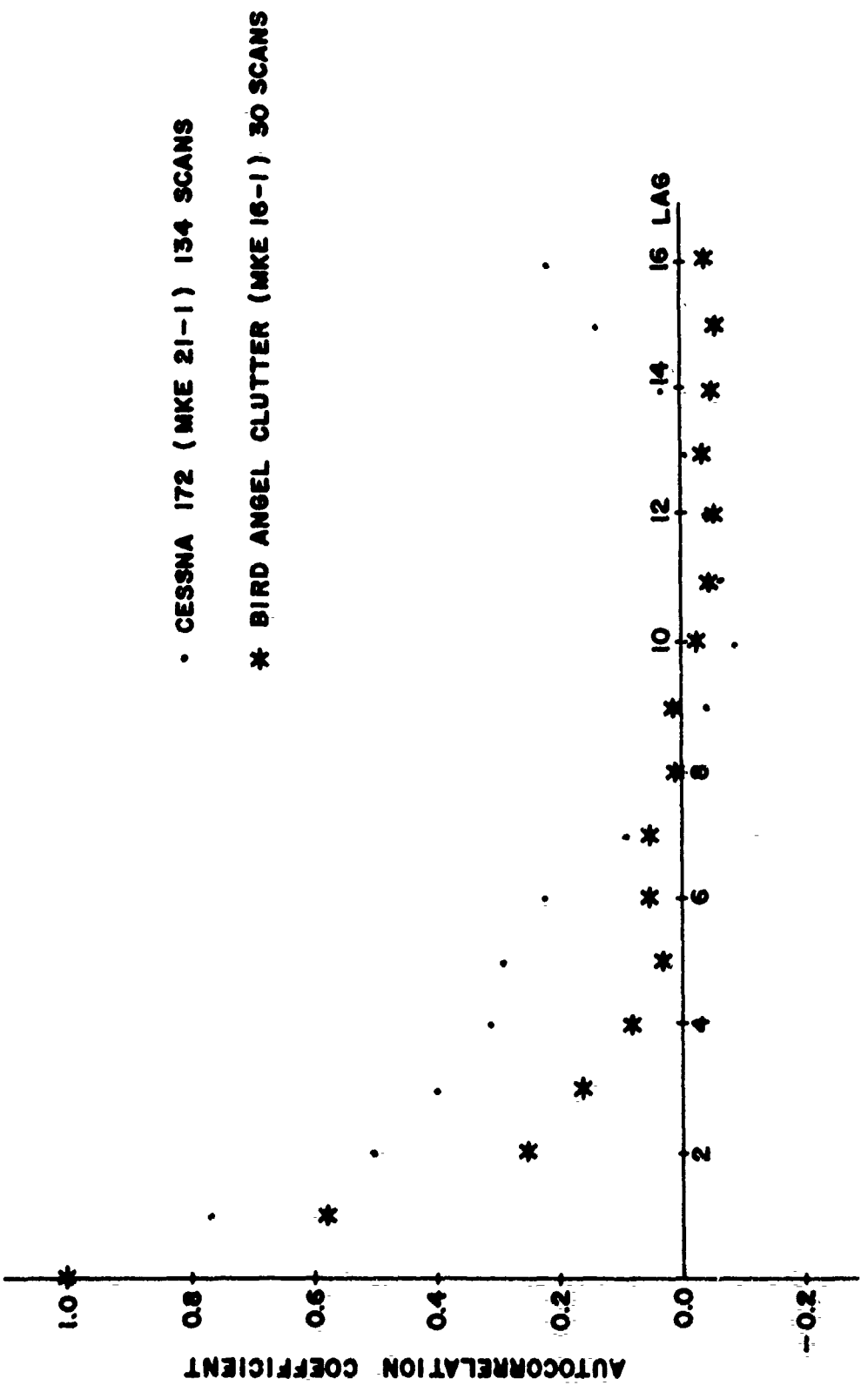

Figure B-3 ASR Mean Azimuth Autocorrelation Coefficient for a Lag Interval of 0.15°

reach a value of 0.5 at 2 lags (0.3°), which is close to the value of 2-3 lags expected due to the antenna pattern itself on a point target. These results confirm single-scan observations, i.e., if targets are smaller than the radar resolution cell (one pulsewidth by one beamwidth) then the run-length similarity for the Cessna and the angel track persists over many scans.

The results are similar for both the aircraft and the angel. From this, one may conclude that angel clutter (presumably birds) resembles general aviation aircraft in their mean spatial distribution. Analysis of additional aircraft and angel data is required to determine whether the angel-aircraft differences in Figures B-2 and B-3 are significant.

Amplitude Distributions for ASR Video Matrix

When the MPS-19 radar tracked an aircraft or angel, the ASR Data Collect Matrix was automatically positioned in the area containing the tracked target. ASR video amplitude in each of the 40 x 37 matrix cells was sampled each scan, while both radars observed the same target and its surroundings. Approximate probability densities in the form of relative amplitude frequency-of-occurrence historgrams and the corresponding cumulative distributions have been plotted.

Frequency-of-occurrence as a function of relative ASR video amplitude is shown in Figure B-4 for a Cessna 172 and in Figure B-5 for two angel tracks. Abscissas in the plots are the logarithm of the range-normalized video amplitude, discussed below; ordinates are the number of occurrences in a target track.

The amplitude distributions were obtained by assuming that the distribution type did not change with target range. Then, the decrease in amplitude with increasing range, e.g. as R^{-2} for a point target, was compensated for by multiplying target amplitudes in the matrix from each scan by the square of the range measured at the time the matrix data were collected. Accurate range was obtained from the continuous target track maintained by the MPS-19.

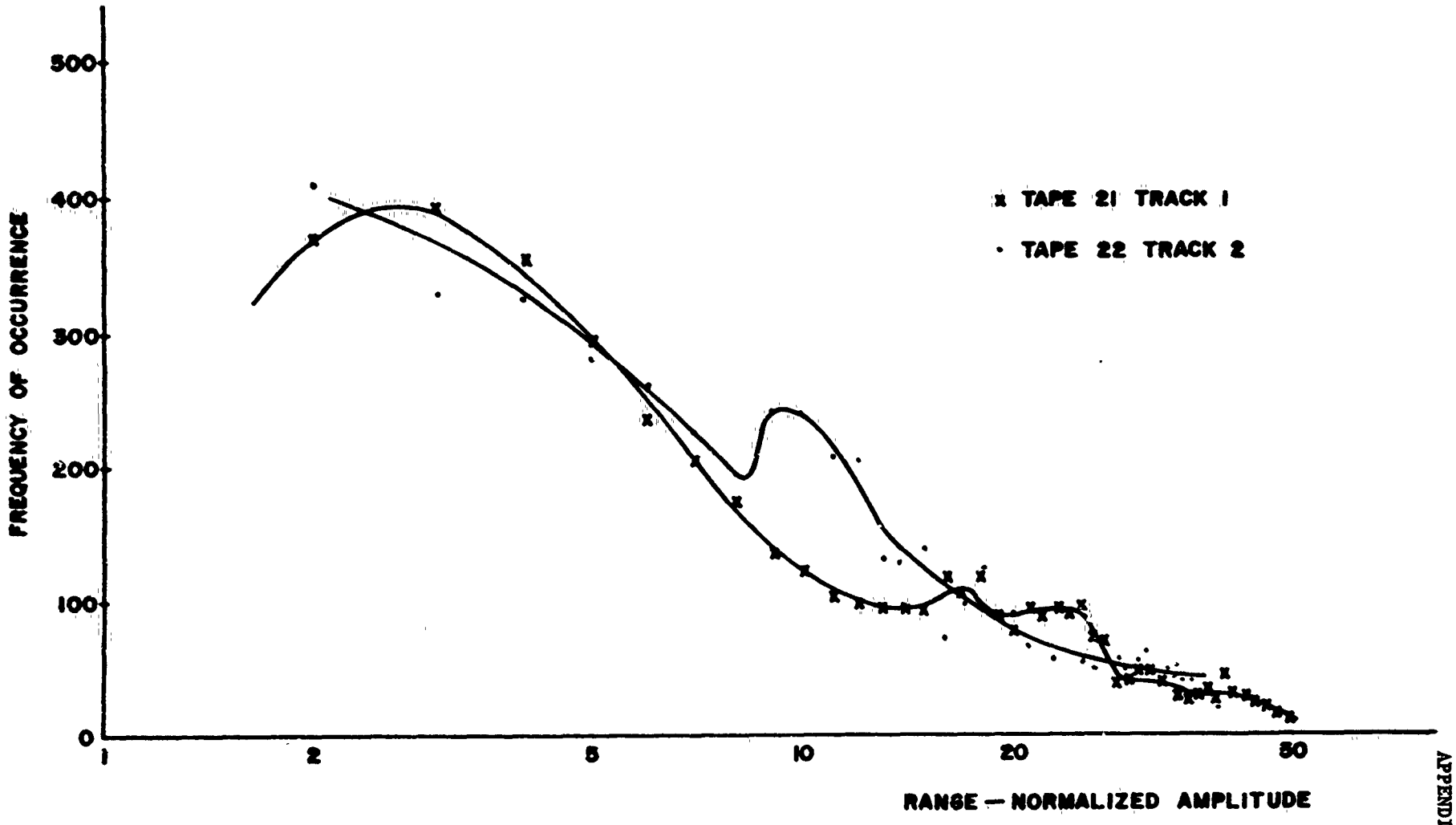

Figure B-4 ASR Amplitude Frequency-Of-Occurrence for Cessna 172

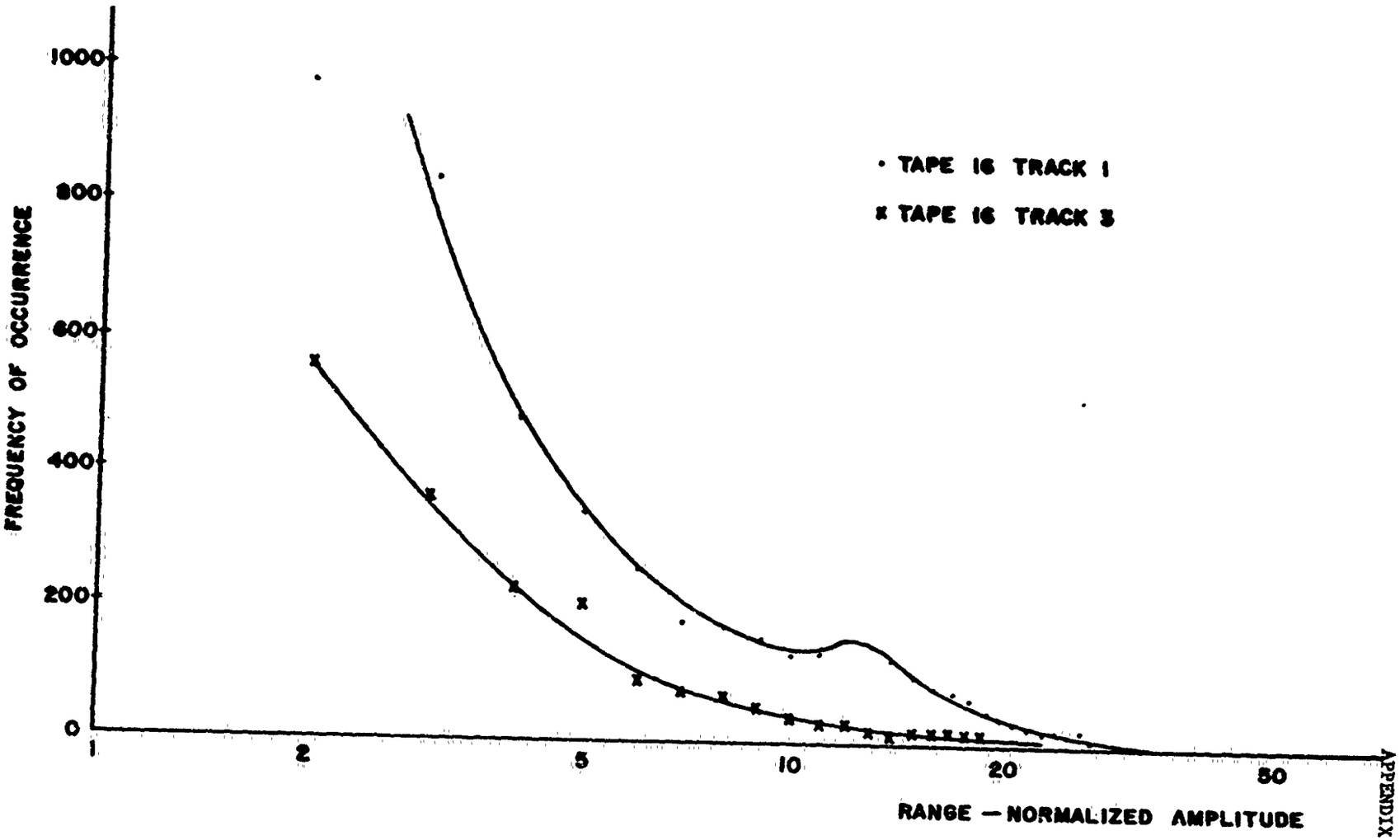

Figure B-5 ASR Amplitude Frequency-Of-Occurrence for Two Angel Targets

In initial data analysis, range factors of R^{-1}, R^{-2}, and R^{-3} were used, and in all cases, the density obtained with the R^{-2} factor had the smallest half-width. This was interpreted as an indication that, among the three range dependences tried, R^{-2} most closely described the target amplitude variation, since compensation with an inapplicable range factor broadens the density. The R^{-2} amplitude dependence (which corresponds to an R^{-4} dependence of signal power) implies that the angel targets behaved approximately as point targets, like aircraft, which is in agreement with the conclusion from single scan analysis above, that the angels were not comparable to or larger in size than an ASR resolution cell.

In addition to amplitude variations caused by target cross-section fluctuation and by target range change, the video amplitude varies due to the gain change in the direction of the target as the antenna rotates. The result is a smearing of the target amplitude density toward lower amplitudes. To deduce target characteristics from the observed distribution, the known antenna contribution must be removed. In the present problem, it is the ASR video characteristics, including the antenna effect, which are of interest. These are shown in the figures.

At low amplitudes (0, 1, 2, 3, on a 0-31 scale), the distributions of target amplitude and of Data Collect Matrix background, which consists of receiver noise and MTI residue, overlap and initially cannot be separated. Therefore, the histograms shown were formed from all 740 independent samples in a matrix. In these histograms, over 90% of the total number of samples lie in the first two intervals. These are predominantly matrix background amplitudes; the typical mean value of background was between 0.7 and 1.0. Occasional returns from targets other than the one being tracked may be received; these targets pass

through the Data Collect Matrix within a few scans and their contributions to the resulting histograms, which are accumulated over many scans, are negligible. Amplitudes greater than approximately three are therefore assumed to be due solely to the tracked target, with high probability.

From the amplitude frequency-of-occurrence data, cumulative probability distributions were formed for the Cessna 172 aircraft and for angels. To reduce the strong effect of background, the densities above were truncated or, equivalently, an amplitude threshold was established. Thresholds of 0, 1, 2, 3 and 4 on a scale of 0-31 were used. The resulting distributions are shown on Weibull distribution plots in Figures B-6 through B-8 for angel targets and Figures B-9 and B-10 for the Cessna. Similar normal probability plots are shown in Figures B-11 for the Cessna and Figure B-12 for an angel target.

The Weibull distribution is a two-parameter distribution with density given by

$$p(x) = \left(\frac{x}{\gamma}\right)^{\beta-1} e^{-\left(\frac{x}{\gamma}\right)}$$

and cumulative distribution

$$P(x) = 1 - e^{-\left(\frac{x}{\gamma}\right)^{\beta}}$$

The Weibull family includes the exponential ($\beta = 1$) and the Rayleigh distribution ($\beta = 2$). The distribution is useful in searching for an analytical description of a measured distribution or in comparing measured to theoretical distributions. A straight line on the Weibull plot indicates exact agreement with the Weibull distribution; the slope of the line can be used to determine the value of the Weibull parameter, β.

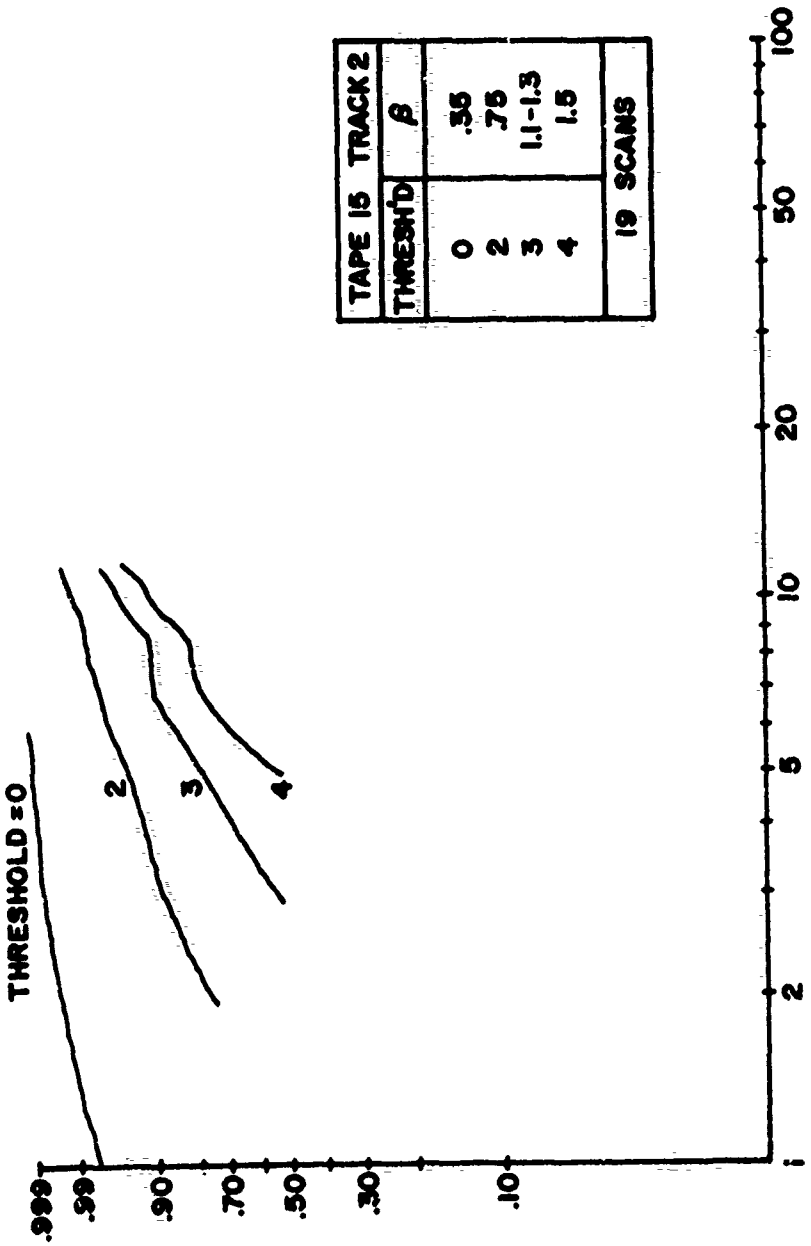

Figure B-6 WEIBULL PLOT OF MATRIX AMPLITUDES - ANGEL TRACK 15-2

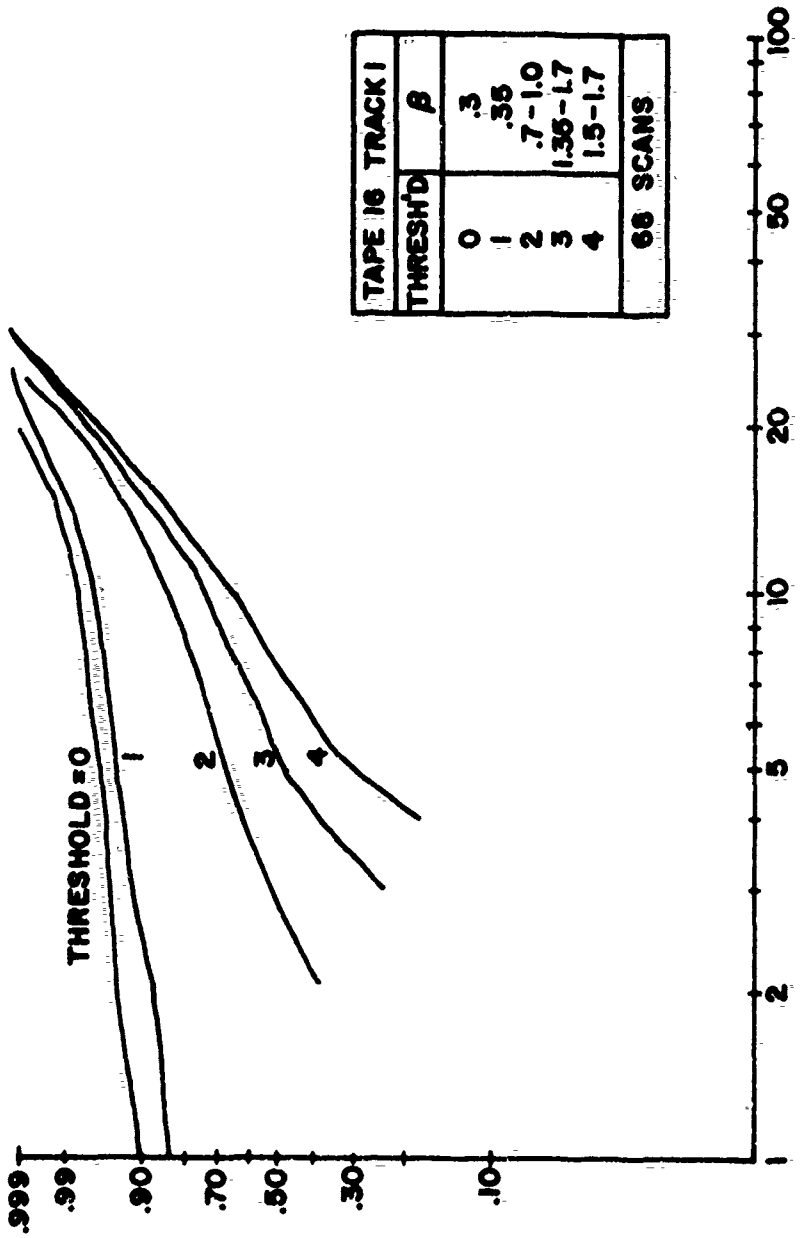

Figure B-7 WEIBULL PLOT OF MATRIX AMPLITUDES FOR ANGEL TRACK 16-1

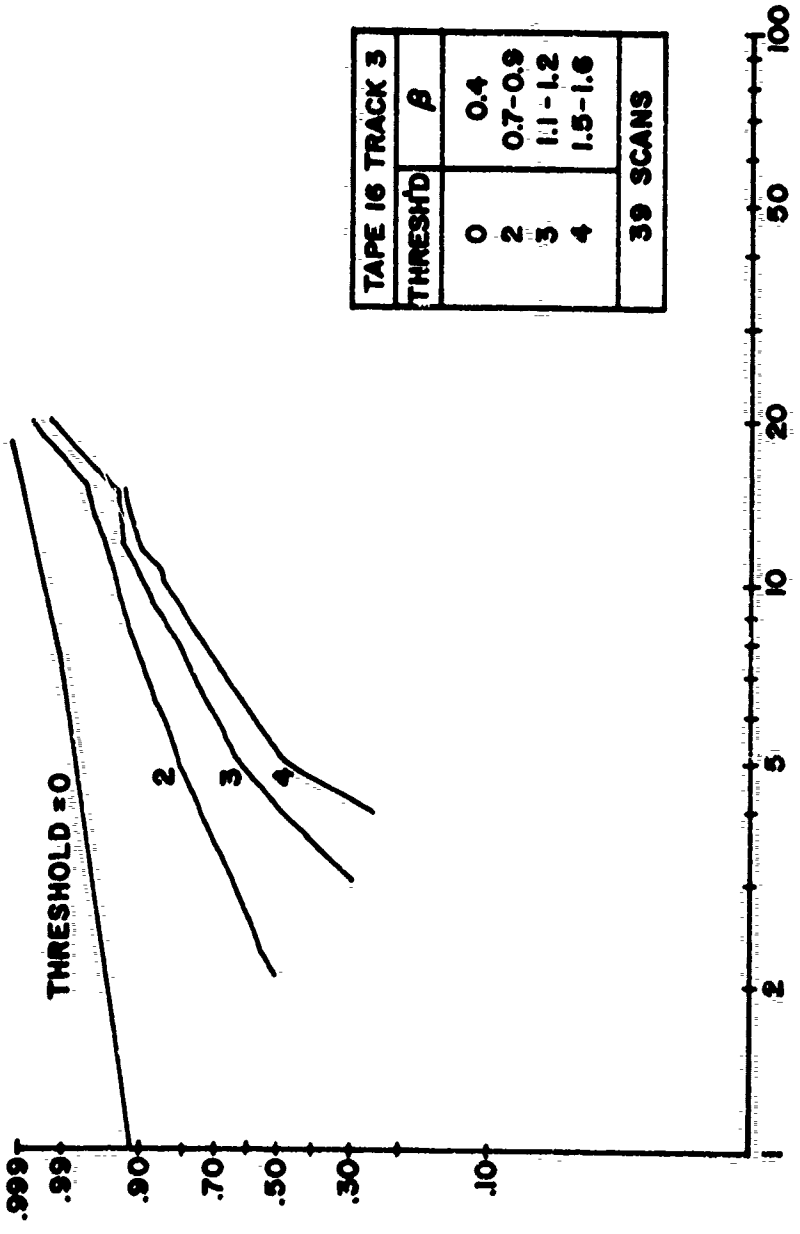

TAPE 16 TRACK 3	
THRESHOLD	β
0	0.4
2	0.7-0.9
3	1.1-1.2
4	1.5-1.6
39 SCANS	

Figure B-8 WEIBULL PLOT OF MATRIX AMPLITUDES - ANGEL TRACK 16-3

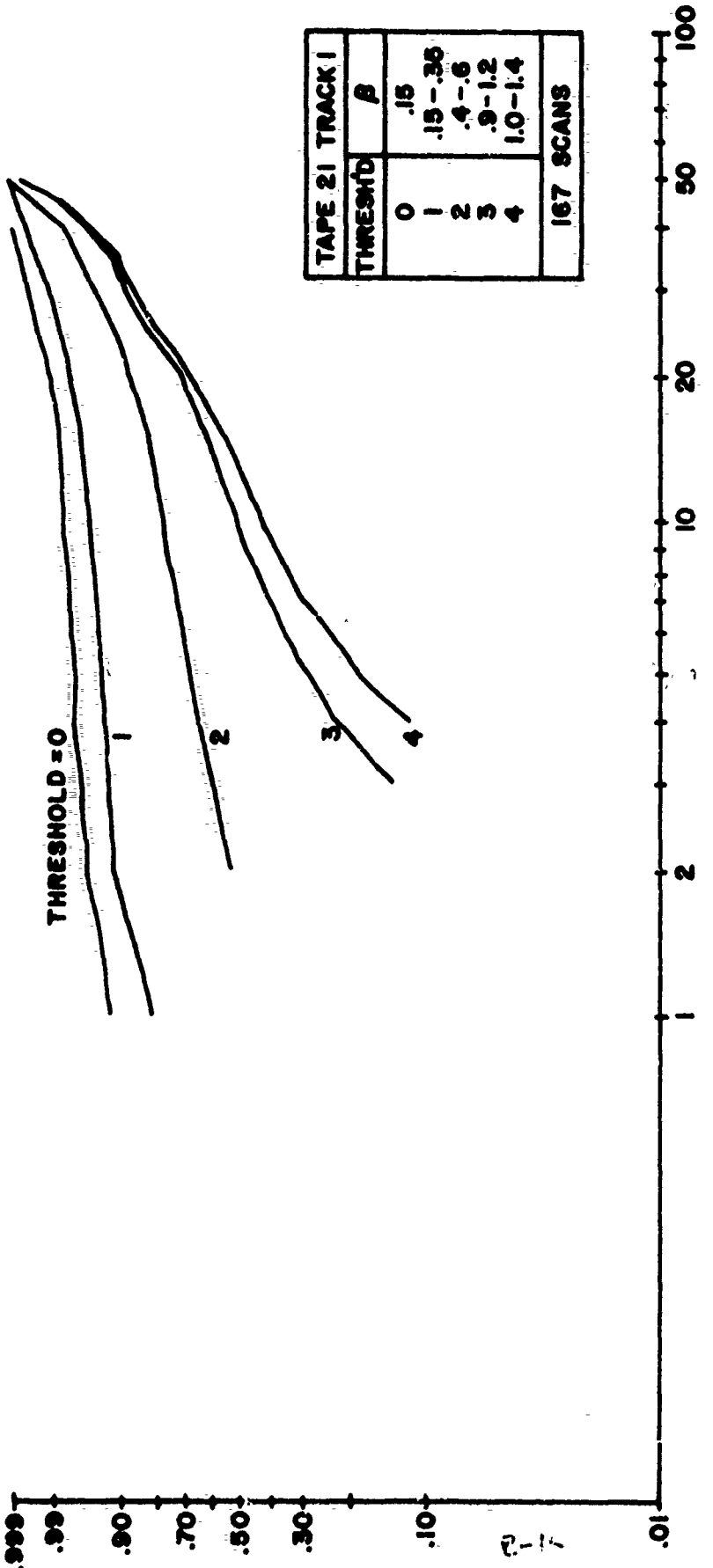

Figure B-9 Weibull Plot of Matrix Amplitudes - Cessna Track 21-1

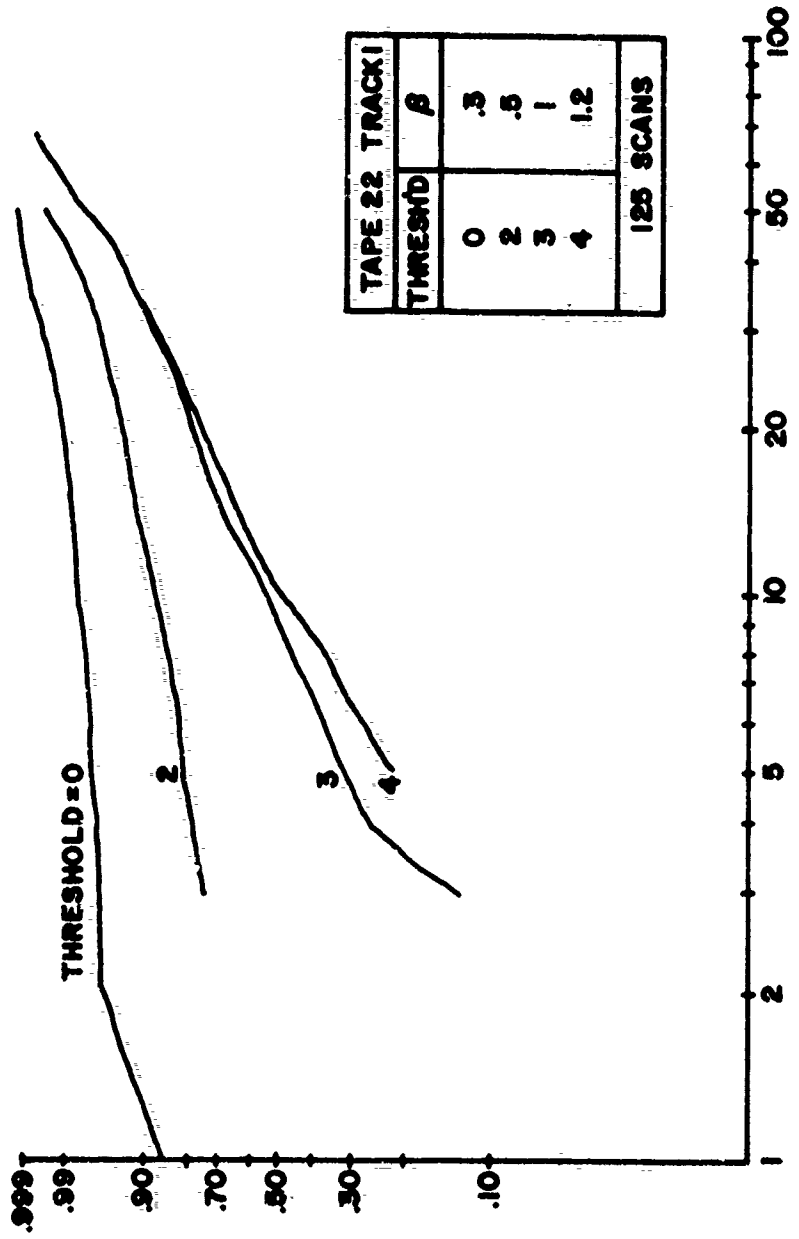

Figure B-10 WEIBULL PLOT OF MATRIX AMPLITUDES FOR CESSNA TRACK 22-1

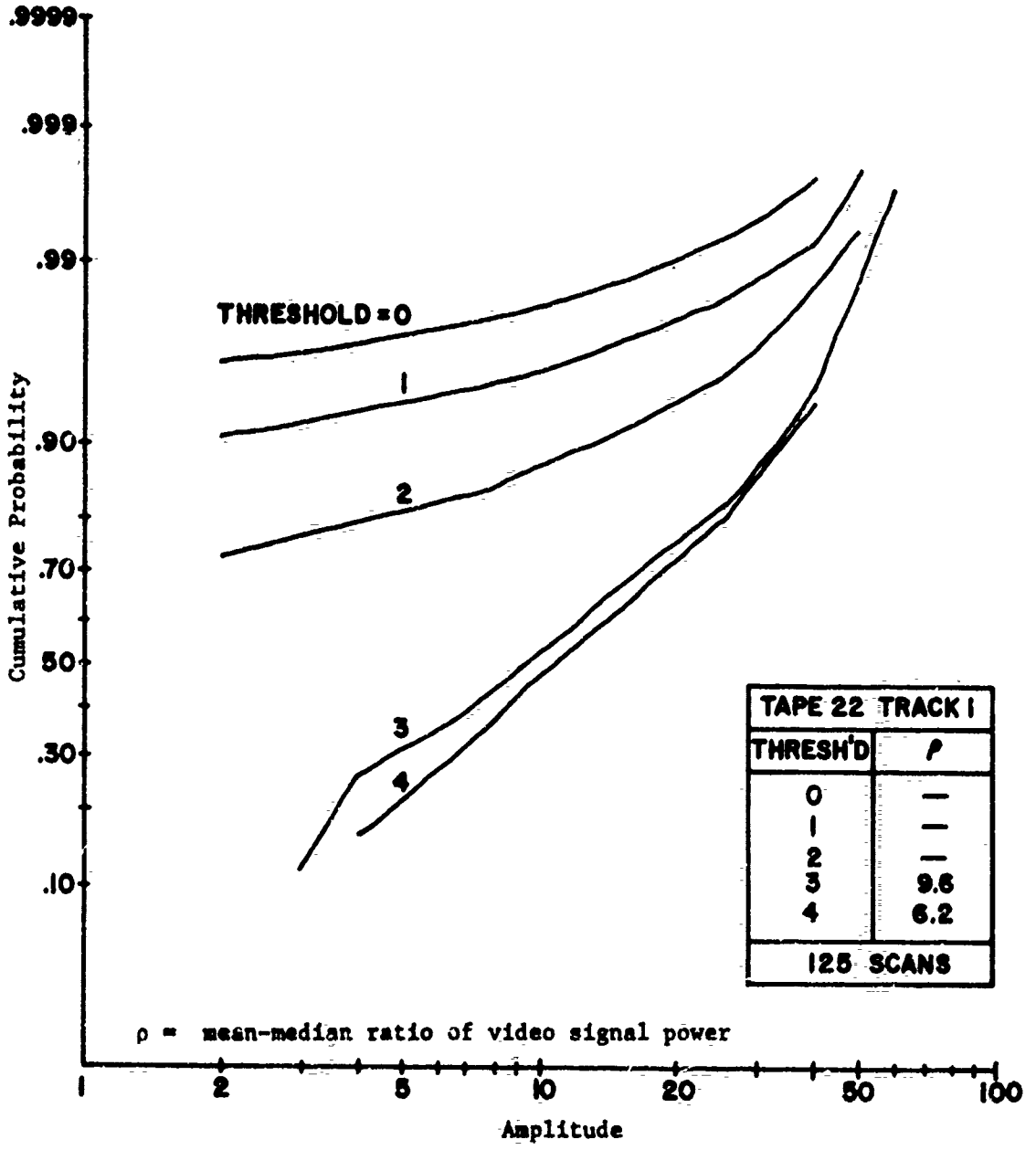

Figure B-11 LOG NORMAL PLOT OF MATRIX AMPLITUDES - CESSNA TRACK 22-1

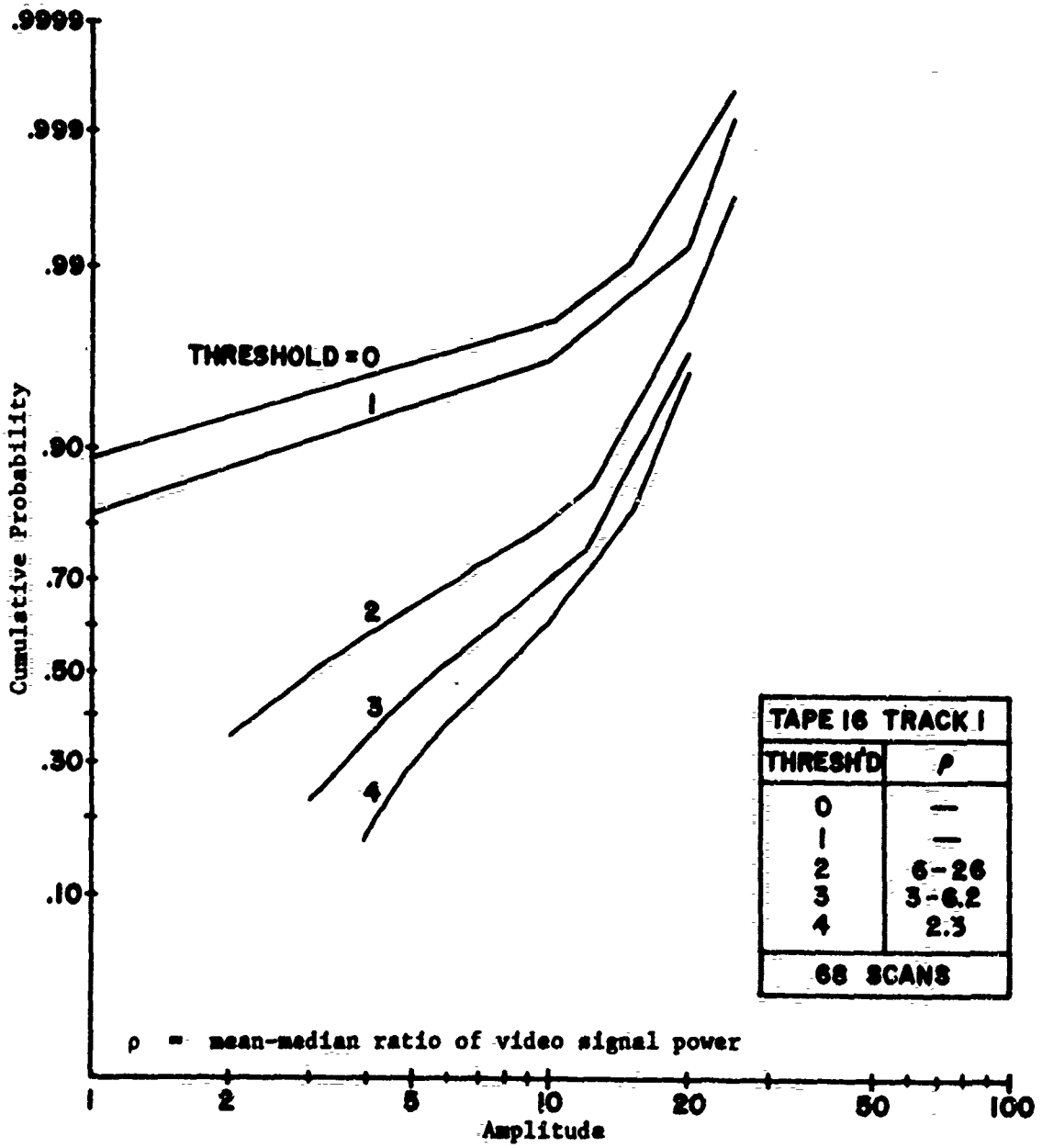

Figure B-12 LOG NORMAL PLOT OF MATRIX AMPLITUDES - ANGEL TRACK 16-1

The Weibull plots of aircraft and angel distributions (Figures B-6 through B-10) show similar features. With threshold values of 0 and 1, the compound nature of the distribution is evident. Background is included and dominates the distribution. When the threshold is raised to three or four, on the other hand, several differences appear. For a given target, the slopes of the curves are quite similar for threshold amplitude $a_T = 3$ and $a_T = 4$. Furthermore, the values of the slopes, giving the parameter β in the Weibull distribution, lie between 0.9 and 1.4 for the aircraft and between 1.1 and 1.7 for the angels; actual values are given in the figures. These results indicate that the observed distributions lie between the exponential and the Rayleigh distributions in type. Small amplitudes are probable but smallest amplitudes (0, 1, and 2) less likely, as shown by the small change when the threshold is raised from 3 to 4. (For the exponential distribution, smallest amplitudes are most probable; for the Rayleigh type, smallest amplitudes are least probable of all amplitudes below the mean).

The plots of cumulative distribution on Log Normal probability paper, Figures B-11 and B-12, are similar to the above in variation as a function of threshold. Again, curves for $a_T = 3$ and 4 lie close with similar slopes. The estimated goodness-of-fit to a straight line is not markedly better for either Weibull or normal plots. For a threshold of 3, the Log Normal parameter ρ (mean-to-median ratio) was about 10 for the aircraft and 3 to 6.2 for the angel track; for a threshold of 4, the values were 6.2 and 2.3 respectively.

Figures B-13 and B-14 show a typical set of angel track video amplitudes recorded by the Track Radar Module. Each track radar pulse is converted to digital format and transmitted to the Data Acquisition Module, where it is written on digital magnetic tape along with range, bearing, and elevation measurements. The ordinate in the figures is the A/D converter level recorded for each pulse. The sample rate was the track radar PRF of half

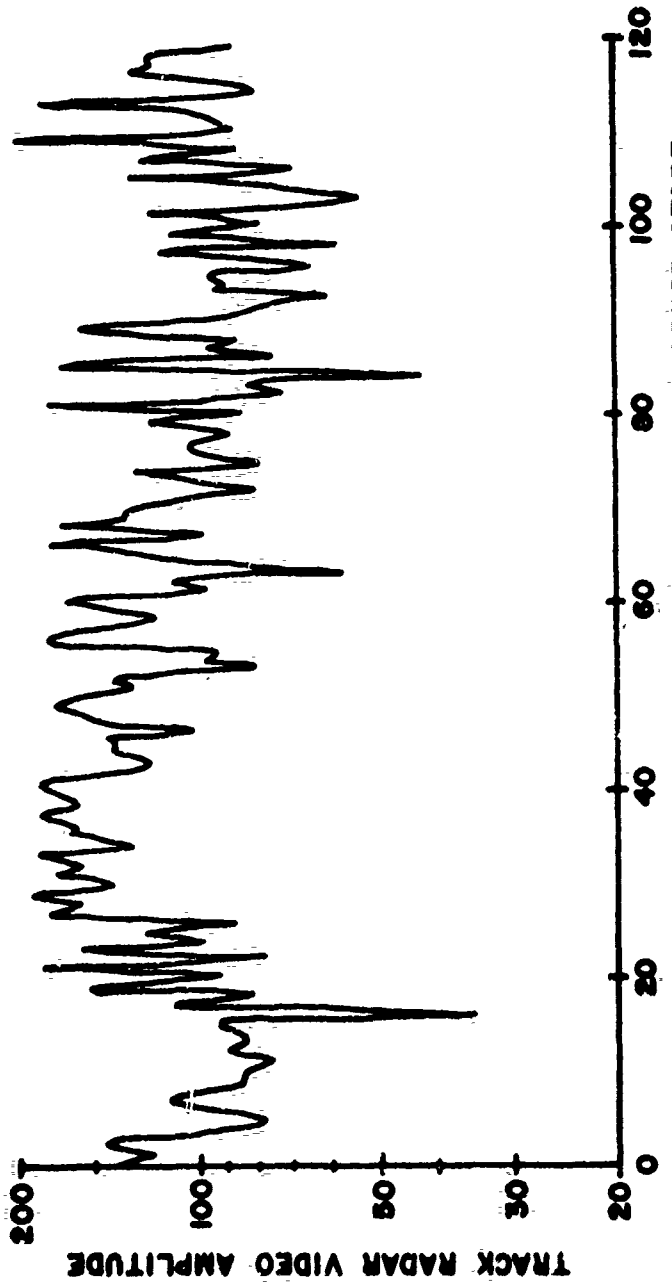

Figure B-13 Angel Track Amplitude Fluctuations Observed With Track Radar

Track
Radar
Video
Amplitude

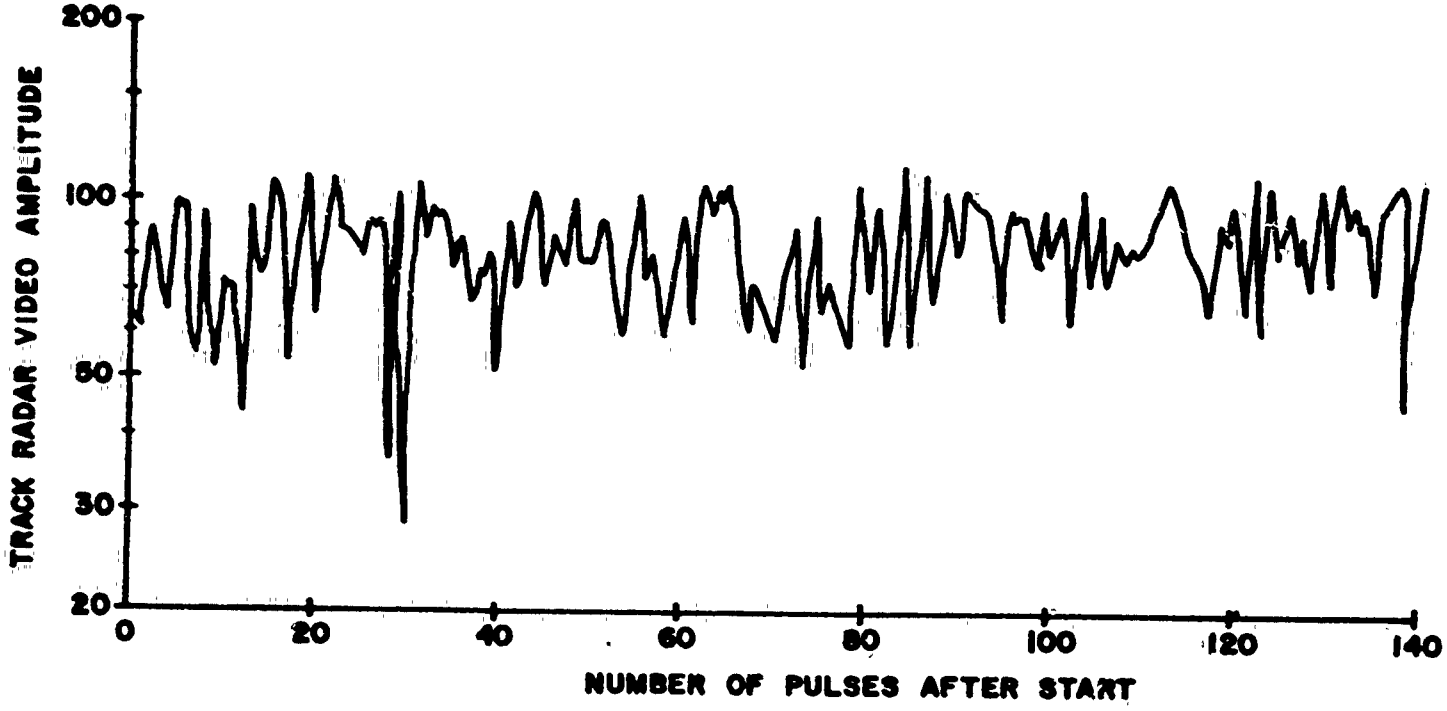

Track #4, Tape 31
Scan #3
PRF = 625 Hz
Auto Range, Manual Amg;e Track

Figure B-14 Angel Track Amplitude Fluctuations Observed With Track Radar

the ASR PRF. Figures B-13 and B-14 thus cover 0.243 and 0.208 seconds, respectively. Both figures were made of the same angel track and were separated in time by four ASR scans or 16 seconds. The track radar was in the automatic range track mode but manual angle track was used to avoid the 30 Hz conical-scan modulations of the MPS-19 angle tracking function. Automatic Gain Control (AGC) was used, maintaining the signal level approximately constant.

Fourier Analysis of MPS-19 Video Fluctuations

To observe the frequency spectra of the target fluctuations, the video from the MPS-19 tracking radar, which was used to place a video gate in the ASR video during the generation of Data Collect Matrices, was simultaneously sampled and recorded for several angel and aircraft targets. These samples, collected every radar pulse while the radar was locked on the target, were used to generate Fourier Spectra of the target fluctuations as seen by the MPS-19. Since the characteristics of the MPS-19 are almost identical to those of the ASR, and as the two radars were colocated in Milwaukee, the results should be representative of the ASR video for the targets. For each spectra, 2^{10} samples were used giving a resolution of approximately 0.6 Hertz for a 600 Hertz sampling rate. The frequency distributions were averaged for 20 consecutive sets of data on each target, representing approximately 34 seconds of video (or ≈ 20,000 samples). Figure B-15 shows two sample frequency distributions for a bird angel and the Cessna 172 which result from this procedure. Note that the ordinate for the aircraft plot covers approximately twice the range of the ordinate for the angel plot. In both plots the conical scan frequency (30.5 Hertz) of the tracking radar is clearly visible.

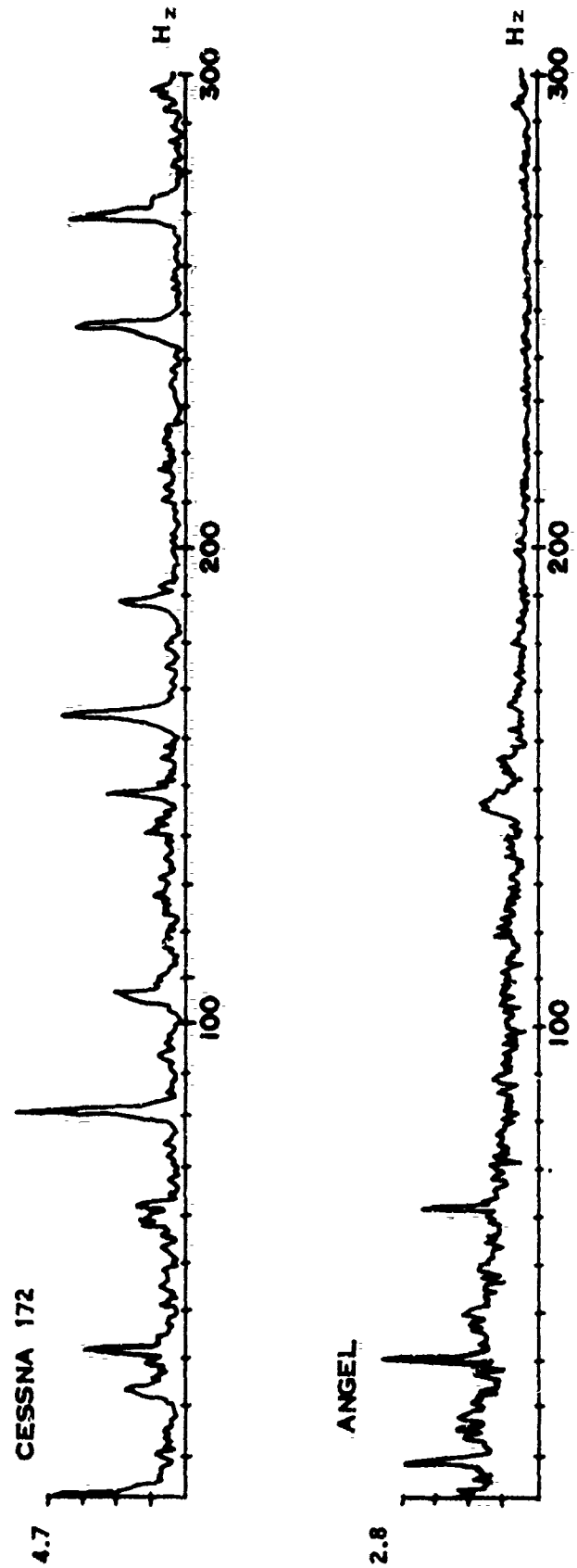

FIGURE B-15 FREQUENCY SPECTRUM OF MPS-19 VIDEO AMPLITUDES

The general characteristics of the plots indicate the angels appear to be represented by low frequency fluctuations, with a prominent peak about 10 Hertz corresponding to the "wing beat" frequencies found by other investigators. The aircraft, on the other hand, had higher frequency modulations, generally characterized by multiple frequency series similar to those found in the normal Fourier decomposition of periodic nonsinusoidal functions. For example, there are peaks at 82 Hertz, 164 Hertz, 248 Hertz. Eighty-two Hertz appears to be the fundamental frequency of this series, with 164, 248, etc., being the first, the second, etc. overtones normally found in the Fourier decomposition. Frequency multiples above the Nyquist frequency, in this case 300 Hertz, are found to be "folded over" and observed at lower frequencies. For example, the series with a fundamental frequency of 80 Hertz has a multiple equal to 320 Hertz which is higher than Nyquist frequency. As a result, this multiple is folded over and observed at 280 Hertz. Similar effects occur for higher multiples. Table I lists the observed and folded frequencies. It is interesting that the aircraft engine used for this run nominally operated at 2400 rpm, which with the two-bladed propeller corresponds to 4800 Hertz per minute, or 80 Hertz per second, the observed fundamental frequency.

The apparent dependence of the major structure of the video frequency spectrum on the Cessna propeller rate points out the fact that great care must be used in developing angel/aircraft discrimination techniques, in order to avoid developing discriminators which operate on characteristics peculiar to certain targets. The most practical way of avoiding this is to collect a large data base of different types of aircraft and angels. While the 80 Hertz lines seen in the track radar video spectrum are not necessarily so prominent in the ASR MTI video, they should be closely investigated in future data collection efforts.

TABLE I

OBSERVED FREQUENCIES AND CORRESPONDING NYQUIST FOLDED FREQUENCIES

Harmonic	Observed Frequency	Folded Frequency	Corresponding Fundamental
1	83.2	83.2	83.2
2	164.6	164.6	82.3
3	248.4	248.4	82.8
4	271.3	328.7	82.2
5	189.3	410.7	82.1
6	107.2	492.8	82.1
7	24.0	576.0	82.3
8	59.8	659.8	82.5

APPENDIX B-2

PROCESSOR SIMULATION RESULTS

Detailed results of each Azimuth Pattern Processor are listed in Tables I - X. The performance curves in the test were derived from the scan-weighted averages of aircraft and angel detection percentages.

The track numbers of each angel and aircraft do not explicitly appear in the tables. However, they can be inferred from the number of scans of data for each track; this number is listed in the left-most column, separated by a vertical line, in each table The correlation between track numbers and number of scans is as follows for the Milwaukee data:

Aircraft Track	Number of Scans
6-1	58-59
6-2	97
3-2	73
3-3	82
21-1	256
22-1	160

Angel Track	Number of Scans
10-1	24
10-6	69-70
11-3	19
11-4	5
11-5	20
11-6	35
11-7	7
16-1	62
16-3	30

For the Baltimore data, the correlation is

Aircraft Track	Number of Scans
2F	120
3-BC	34-35
A/C	308
4C	129-132
4D	163-164
2A	155-180
2B	211-218

A short description of each processor simulation is given below for each table.

1. Simple Amplitude Detector (Milwaukee data)

Table I lists the results of processing the Milwaukee data with a fixed threshold; an aircraft is declared present if at least one amplitude exceeded the threshold. The value of each threshold tested is listed after "THR." in the top line of the table. The maximum video amplitude was 31, corresponding to 5-bit quantization.

All of the Milwaukee data consisted of 37 amplitude samples taken on every other radar sweep (pulse period). The range cell processed was chosen by summing all amplitudes in each range cell for all 37 azimuth samples and choosing the range cell with the largest amplitude sum.

THR.	8	9	10	11	12	13	14	15	16	17	18	19	20	21	22	23	24	25
ANGEL DETECTION PERCENTAGE																		
24	100	100	100	100	100	95	95	70	62	37	12	0	0	0	0	0	0	0
70	100	100	100	100	100	100	100	98	98	94	72	37	20	15	10	8	8	8
19	100	100	94	94	89	84	73	26	26	15	0	0	0	0	0	0	0	0
5	100	100	100	80	80	60	60	20	20	20	20	0	0	0	0	0	0	0
20	100	100	95	95	90	90	90	55	55	40	30	10	10	5	5	5	5	5
35	100	97	97	91	88	88	80	45	42	25	8	0	0	0	0	0	0	0
7	100	100	100	100	100	100	100	28	28	0	0	0	0	0	0	0	0	0
62	100	100	100	100	100	100	100	98	98	96	96	91	90	74	62	45	32	24
30	100	93	90	86	83	83	76	70	66	66	63	43	36	16	6	0	0	0
SCAN WEIGHTED AVERAGES:																		
272	100	99	98	96	95	94	91	74	73	64	52	36	30	23	18	13	10	8
AIRCRAFT DETECTION PERCENTAGES																		
59	94	94	94	94	94	94	94	93	93	93	91	86	84	84	81	67	58	48
97	87	82	73	62	56	52	46	31	31	29	25	21	17	15	10	5	5	5
73	100	100	100	100	100	98	97	94	94	94	93	91	90	83	73	68	61	57
82	100	100	100	100	100	100	100	100	100	100	100	92	79	81	64	32	29	29
256	100	100	100	100	100	99	98	96	96	96	95	93	93	84	67	44	37	25
160	99	98	98	96	96	96	96	94	94	94	94	93	91	85	77	63	55	44
SCAN WEIGHTED AVERAGES																		
727	97	96	95	93	92	90	89	85	85	85	84	81	78	71	61	46	40	33

TABLE I AMPLITUDE DETECTOR RESULTS

2. M/M Azimuth Correlator (Milwaukee data)

Tables II and III list the results of subjecting the data to a fixed threshold and requiring that M consecutive samples exceed the threshold for aircraft detection. Table II applies for M/M = 2/2 and Table III applies for M/M = 3/3 as the thresholds were varied from 4 to 21 out of the 31 possible levels.

M/N DETECTOR FOR N= 2

THR.	4	5	6	7	8	9	10	11	12	13	14	15	16	17	18	19	20	21
ANGEL DETECTION PERCENTAGE																		
24	100	100	100	100	100	100	95	91	87	79	79	37	33	20	9	0	0	0
70	100	100	100	100	100	100	100	100	98	94	92	84	84	72	45	15	2	1
19	100	100	100	89	89	89	78	73	63	63	42	5	5	0	0	0	0	0
5	100	100	100	100	100	100	100	60	60	20	20	0	0	0	0	0	0	0
20	100	100	100	100	100	95	95	80	75	75	55	40	40	25	20	5	0	0
35	100	97	91	91	85	85	80	62	57	54	40	17	17	8	0	0	0	0
7	100	100	100	100	100	100	85	71	57	57	57	0	0	0	0	0	0	0
62	100	100	100	100	100	100	100	100	98	96	93	91	91	90	90	83	82	61
30	100	96	93	86	73	70	66	66	63	60	56	43	43	36	20	16	13	3
SCAN WEIGHTED AVERAGES:																		
272	100	99	98	96	94	93	90	85	82	78	71	55	55	47	35	24	20	14
AIRCRAFT DETECTION PERCENTAGES																		
59	96	96	94	94	94	94	94	94	94	93	93	91	91	89	83	83	83	79
97	95	91	87	79	72	64	58	46	42	41	36	25	25	23	21	15	14	12
73	100	100	100	100	100	100	100	100	100	97	95	93	93	93	91	87	82	76
82	100	98	98	98	97	97	97	95	95	93	93	92	92	92	86	76	64	40
256	100	99	98	98	97	96	95	94	94	94	92	90	90	90	89	85	82	64
160	100	98	96	96	96	96	95	94	94	92	91	91	91	90	90	87	86	79
SCAN WEIGHTED AVERAGES:																		
727	99	97	95	94	93	92	90	88	87	86	85	82	82	81	79	75	71	60

TABLE II 2/2 AZIMUTH CORRELATOR RESULTS

N/N DETECTOR FOR N= 3

THR.	4	5	6	7	8	9	10	11	12	13	14	15	16	17	18	19	20	21
ANGEL DETECTION PERCENTAGE																		
24	100	95	95	95	95	87	87	62	58	54	50	16	16	8	0	0	0	0
70	100	100	100	100	98	98	95	92	90	88	84	70	67	47	25	2	1	0
19	100	78	78	78	73	73	63	52	47	36	26	0	0	0	0	0	0	0
5	100	100	100	80	40	40	0	0	0	0	0	0	0	0	0	0	0	0
20	100	100	100	85	75	70	65	55	40	35	30	15	15	10	0	0	0	0
35	94	88	82	80	68	60	46	40	37	25	17	2	2	0	0	0	0	0
7	100	71	71	71	71	71	71	28	14	14	0	0	0	0	0	0	0	0
62	100	100	98	96	96	96	95	91	90	90	87	83	83	83	75	69	67	45
30	96	86	70	66	60	56	53	43	43	33	30	20	16	16	10	10	6	3
SCAN WEIGHTED AVERAGES:																		
272	98	94	91	88	84	81	76	68	64	60	55	41	40	34	24	17	16	10
AIRCRAFT DETECTION PERCENTAGES																		
256	96	95	94	93	91	91	89	88	87	87	86	81	81	80	76	73	70	52
160	96	95	94	92	92	91	90	90	89	88	88	86	86	85	85	83	82	72
59	94	94	94	94	94	94	94	94	93	93	91	86	86	86	83	81	79	77
97	88	78	74	65	62	55	49	40	38	36	31	19	19	19	19	15	12	11
73	100	100	100	100	100	100	100	98	97	95	94	93	93	90	86	80	78	72
82	100	98	96	96	95	93	92	90	89	86	86	85	85	84	80	54	40	28
SCAN WEIGHTED AVERAGES:																		
727	95	93	92	90	88	87	85	83	82	81	80	75	75	75	73	66	63	52

TABLE III 3/3 AZIMUTH CORRELATOR RESULTS

3. Dual Threshold Processor (Milwaukee data)

This processor uses two thresholds, one low (given by "THR." in the tables) and one high (set "MR." levels above the first). The number of ACI (Azimuth Correlation Intervals) is counted at each threshold. A third threshold is set on the ACI difference. An aircraft is declared if the ACI difference is less than this third value, given by "MN." in the tables.

Table IV lists the results for combinations of the three threshold values when all 37 azimuth samples were processed. Table V applies when only 10 of the 37 samples are processed at any one time; at least one aircraft detection was required as the 10-sample window was swept across the full 37-sample azimuth coverage.

DUAL THRESHOLD

THR.	0	0	2	2	2	2	4	4	4	4	4	4	6	6	6	6	6	6
MR..	2	2	2	6	6	6	2	2	2	6	6	6	2	2	2	6	6	6
MN..	2	3	4	2	3	4	2	3	4	2	3	4	2	3	4	2	3	4

ANGEL DETECTION PERCENTAGE

24	91	95	100	29	62	70	62	91	100	54	62	79	79	91	95	58	79	91
69	97	100	100	65	85	97	78	91	98	63	78	91	84	97	98	69	86	97
19	89	100	100	15	36	63	63	89	94	36	52	68	68	89	100	47	68	73
5	80	100	80	20	40	60	80	100	100	80	80	80	80	100	100	80	80	80
20	90	90	80	45	60	75	90	100	100	60	85	95	100	100	100	45	65	100
35	80	100	97	51	62	85	62	91	100	31	62	82	85	100	100	54	74	91
7	71	71	100	0	0	42	71	100	100	42	71	100	100	100	100	57	71	100
62	75	83	98	88	96	100	95	100	100	90	98	100	98	100	100	91	96	100
30	73	80	100	53	63	83	80	100	100	66	80	96	90	93	100	73	90	96

SCAN WEIGHTED AVERAGES:

271	84	91	97	56	71	86	78	94	99	62	77	90	87	96	99	68	83	94

AIRCRAFT DETECTION PERCENTAGES

58	68	81	77	48	63	77	89	98	98	87	94	98	98	100	100	96	100	100
97	56	69	77	31	52	69	85	94	98	67	81	89	88	97	98	64	87	97
73	42	60	100	98	98	100	100	100	100	98	100	100	100	100	100	95	98	100
82	70	78	100	95	98	100	97	100	100	93	97	100	100	100	100	93	98	100
256	89	91	99	91	98	98	96	98	100	93	96	98	98	100	100	94	98	99
160	99	100	100	93	98	98	96	99	100	90	96	98	98	100	100	92	98	99

SCAN WEIGHTED AVERAGES:

726	78	84	94	81	89	92	94	98	99	88	94	97	97	99	99	89	96	99

TABLE IV 37 SAMPLE DUAL THRESHOLD RESULTS

DUAL THRESHOLD

THR.	0	0	4	4	4	4	6	6	6	6	6	6	8	8	8	8	8	8
MR..	14	14	14	18	18	18	14	14	14	18	18	18	14	14	14	18	18	18
MN..	1	2	3	1	2	3	1	2	3	1	2	3	1	2	3	1	2	3
ANGEL DETECTION PERCENTAGE																		
24	12	29	8	0	0	0	0	0	25	0	0	25	0	8	29	0	8	29
69	52	65	28	0	0	2	0	2	4	0	1	2	0	1	2	0	1	2
19	0	10	10	0	0	10	0	0	15	0	0	15	0	10	36	0	10	36
5	0	0	20	0	0	20	0	20	40	0	20	40	0	0	60	0	0	60
20	15	15	25	0	5	20	0	5	20	0	5	20	0	0	35	0	0	35
35	11	17	8	0	2	11	0	8	28	0	8	28	0	14	40	0	14	40
7	0	0	14	0	0	28	0	28	57	0	28	57	0	42	57	0	42	57
62	56	70	91	35	62	85	56	80	85	19	46	72	33	66	87	4	35	69
30	30	46	60	0	20	46	16	43	80	0	30	70	0	53	83	0	46	80
SCAN WEIGHTED AVERAGES:																		
271	32	44	39	8	17	29	14	26	39	4	16	35	7	25	45	0	17	40
AIRCRAFT DETECTION PERCENTAGES																		
58	12	32	87	60	84	87	74	91	96	53	86	96	79	93	96	43	87	94
97	4	9	52	10	42	74	33	50	82	9	48	82	21	58	90	14	56	90
73	34	41	95	68	86	97	78	91	98	54	82	94	64	87	95	50	80	93
82	60	73	90	23	39	68	47	65	81	7	23	56	19	37	64	3	20	56
256	83	88	84	35	54	70	61	83	92	19	36	62	32	55	74	2	19	50
160	97	100	88	59	71	83	71	85	93	37	58	77	57	71	88	4	31	67
SCAN WEIGHTED AVERAGES:																		
726	62	69	82	40	60	77	58	78	90	26	49	73	41	63	81	12	38	67

TABLE IV 37 SAMPLE DUAL THRESHOLD RESULTS (Cont'd)

DUAL THRESHOLD

THR.	0	0	4	4	4	4	6	6	6	6	6	6	8	8	8	8	8	8
MP..	12	12	12	16	16	16	12	12	12	16	16	16	12	12	12	16	16	16
MN..	1	2	3	1	2	3	1	2	3	1	2	3	1	2	3	1	2	3

ANGEL DETECTION PERCENTAGE

24	16	20	25	0	0	0	0	4	29	0	0	25	0	8	29	0	8	29
69	50	66	40	0	1	4	5	23	30	0	1	2	1	2	5	0	1	2
19	5	5	26	0	0	10	0	0	15	0	0	15	0	10	36	0	10	36
5	0	0	40	0	0	20	0	40	40	0	20	40	0	0	60	0	0	60
20	10	20	30	0	5	20	5	10	20	0	5	20	0	0	35	0	0	35
35	2	11	17	0	2	11	2	8	28	0	8	28	0	14	40	0	14	40
7	0	0	42	0	0	28	0	28	57	0	28	57	0	42	57	0	42	57
62	46	64	91	56	75	88	67	82	93	33	66	83	58	80	88	14	43	75
30	16	40	73	20	26	56	33	60	90	3	33	73	20	66	90	0	46	80

SCAN WEIGHTED AVERAGES:

271	27	40	49	15	20	32	20	34	49	7	21	38	15	30	46	3	19	41

AIRCRAFT DETECTION PERCENTAGES

58	3	20	94	63	84	89	79	94	98	65	94	96	84	94	96	56	89	94
97	1	7	74	15	43	74	25	53	82	14	49	82	23	62	90	16	57	90
73	32	36	100	80	90	98	75	93	98	64	86	97	76	91	95	53	80	93
82	51	68	97	51	69	81	67	87	97	20	40	63	50	65	82	3	20	56
160	92	98	93	71	85	91	73	87	96	58	70	86	73	88	93	36	58	76
256	78	85	94	59	80	89	63	88	96	32	57	74	60	84	96	19	35	62

SCAN WEIGHTED AVERAGES:

726	57	65	92	57	76	87	63	83	94	39	62	80	60	81	92	26	50	73

TABLE IV 37 SAMPLE DUAL THRESHOLD RESULTS (Cont'd)

DUAL THRESHOLD

THR.	0	0	4	4	4	4	6	6	6	6	6	6	8	8	8	8	8	8
MR..	12	12	12	16	16	16	12	12	12	16	16	16	12	12	12	16	16	16
MN..	1	2	3	1	2	3	1	2	3	1	2	3	1	2	3	1	2	3
ANGEL DETECTION PERCENTAGE																		
24	16	29	25	0	0	0	0	4	29	0	0	25	0	8	29	0	8	29
69	57	69	40	0	1	5	5	24	33	0	1	2	1	2	5	0	1	2
19	5	10	21	0	0	10	0	0	15	0	0	15	0	10	36	0	10	36
5	0	0	20	0	0	20	0	40	40	0	20	40	0	0	60	0	0	60
20	10	30	30	0	5	20	5	10	20	0	5	20	0	0	35	0	0	35
35	5	14	14	0	2	11	2	8	28	0	8	28	0	14	40	0	14	40
7	0	0	14	0	0	28	0	28	57	0	28	57	0	42	57	0	42	57
62	58	69	90	56	75	88	67	82	93	33	66	83	56	80	88	16	43	75
30	30	46	60	20	26	56	26	60	90	6	33	73	20	66	90	0	46	80
SCAN WEIGHTED AVERAGES:																		
271	34	45	45	15	20	32	20	35	50	8	21	38	15	30	46	3	19	41
AIRCRAFT DETECTION PERCENTAGES																		
58	13	32	87	63	84	89	79	94	98	65	94	96	84	94	96	56	89	94
97	5	11	53	15	43	74	25	53	82	14	49	82	23	62	90	16	57	90
73	34	41	98	82	91	98	78	93	98	65	87	97	78	93	95	56	82	93
82	60	71	91	51	69	81	67	87	97	20	40	63	50	65	82	3	20	56
256	84	88	86	59	80	89	63	88	96	32	57	74	60	84	96	19	35	62
160	98	100	89	71	85	91	73	87	96	58	70	86	73	88	93	36	58	76
SCAN WEIGHTED AVERAGES:																		
726	63	69	84	57	76	87	63	83	94	39	62	80	60	81	92	27	50	73

TABLE IV 37 SAMPLE DUAL THRESHOLD RESULTS (Cont'd)

DUAL THRESHOLD

THR.	0	0	6	6	6	6	8	8	8	8	8	8	10	10	10	10	10	10
MR..	8	8	8	12	12	12	8	8	8	12	12	12	8	8	8	12	12	12
MN..	2	3	4	2	3	4	2	3	4	2	3	4	2	3	4	2	3	4

ANGEL DETECTION PERCENTAGE

24	37	58	75	12	29	45	29	62	79	12	29	62	8	33	79	12	33	70
69	86	100	84	26	33	47	44	78	88	4	5	23	24	40	63	2	11	28
19	15	42	63	0	15	47	26	47	84	10	36	84	26	78	89	26	78	89
5	20	40	80	40	40	80	20	60	80	0	60	80	20	100	100	20	80	100
20	45	50	85	15	20	50	20	50	75	0	35	45	25	55	80	10	40	65
35	45	65	82	8	28	60	22	54	80	14	40	62	25	68	91	25	62	91
7	14	14	100	28	57	71	42	57	100	42	57	100	42	85	100	42	85	100
62	74	87	95	82	93	98	87	96	100	80	88	100	93	100	100	74	85	91
30	46	63	90	63	90	90	80	96	100	70	90	100	83	100	100	53	93	100

SCAN WEIGHTED AVERAGES:

271	58	73	85	37	50	66	50	74	89	31	46	66	45	69	85	31	55	72

AIRCRAFT DETECTION PERCENTAGES

58	34	55	100	94	98	100	94	100	100	94	96	100	98	100	100	94	100	100
97	17	35	85	53	82	94	69	91	98	62	90	98	80	91	97	76	90	97
73	43	56	100	93	98	98	93	95	98	93	95	98	90	100	100	86	100	100
82	74	80	98	87	97	98	92	97	100	65	82	93	96	98	98	35	69	87
256	88	91	98	88	96	98	93	99	99	84	96	99	93	99	100	57	75	88
160	100	100	98	87	96	98	91	97	99	88	93	99	92	98	100	77	87	98

SCAN WEIGHTED AVERAGES:

726	70	77	96	83	94	97	89	96	98	81	92	98	91	97	99	67	83	93

TABLE IV 37 SAMPLE DUAL THRESHOLD RESULTS (Cont'd)

DUAL THRESHOLD

THR.	0	0	10	10	10	10	12	12	12	12	12	12	14	14	14	14	14	14
MR..	4	4	4	8	8	8	4	4	4	8	8	8	4	4	4	8	8	8
MN..	2	3	4	2	3	4	2	3	4	2	3	4	2	3	4	2	3	4
ANGEL DETECTION PERCENTAGE																		
24	66	87	100	20	33	79	37	70	95	16	41	75	29	58	87	25	54	87
69	95	100	97	30	40	63	62	89	97	8	18	47	34	63	82	10	26	57
19	63	78	100	26	78	89	63	84	94	42	78	94	47	84	100	47	84	100
5	40	80	100	20	100	100	60	100	100	40	100	100	100	100	100	100	100	100
20	55	70	95	30	55	80	55	80	90	15	50	80	45	80	100	25	65	95
35	71	85	100	25	68	91	62	85	97	45	71	91	62	74	88	60	71	85
7	28	42	100	42	85	100	85	100	100	71	100	100	71	100	100	71	100	100
62	72	82	100	93	100	100	95	98	100	85	93	98	95	100	100	72	90	93
30	60	76	100	86	100	100	96	100	100	86	100	100	96	100	100	70	100	100
SCAN WEIGHTED AVERAGES:																		
271	72	84	98	48	69	85	71	89	97	44	63	80	61	80	92	45	67	83
AIRCRAFT DETECTION PERCENTAGES																		
58	43	56	100	98	100	100	96	98	100	93	98	98	100	100	100	96	100	100
97	21	39	95	80	91	97	92	97	98	84	97	98	87	98	100	82	97	100
73	43	57	100	90	100	100	97	100	100	94	100	100	97	98	100	93	97	100
82	70	82	100	96	98	98	97	100	100	70	87	96	97	100	100	36	68	85
256	89	92	100	93	99	100	96	100	100	88	97	99	97	99	100	57	77	92
160	99	100	100	92	98	100	96	98	100	92	97	100	96	100	100	75	92	98
SCAN WEIGHTED AVERAGES:																		
726	71	79	99	91	97	99	95	98	99	87	96	98	95	99	100	68	85	95

TABLE IV 37 SAMPLE DUAL THRESHOLD RESULTS (Cont'd)

DUAL THRESHOLD

THR.	0	0	2	2	2	2	4	4	4	4	4	4	6	6	6	6	6	6
MR..	14	14	14	18	18	18	14	14	14	18	18	18	14	14	14	18	18	18
MN..	2	3	4	2	3	4	2	3	4	2	3	4	2	3	4	2	3	4
ANGEL DETECTION PERCENTAGE																		
24	33	50	29	0	0	8	0	0	33	0	0	20	0	25	41	0	25	41
70	72	82	61	4	8	21	15	32	40	0	2	11	2	5	20	1	4	15
19	10	15	5	0	0	0	0	10	26	0	10	26	0	15	47	0	15	47
5	0	20	20	0	0	20	0	40	80	0	20	80	20	40	80	20	40	80
20	15	35	35	0	5	10	10	20	50	5	20	35	5	20	40	5	20	40
35	17	34	31	0	2	14	2	11	20	2	11	17	8	28	57	8	28	57
7	14	14	14	0	0	0	0	28	57	0	28	57	28	57	71	28	57	71
62	74	83	93	67	88	96	87	91	100	62	85	88	80	85	98	46	72	85
30	46	56	66	36	46	63	36	70	86	26	46	76	43	80	90	30	70	90
SCAN WEIGHTED AVERAGES:																		
272	47	59	54	20	27	37	28	41	56	17	29	42	25	40	57	16	35	53
AIRCRAFT DETECTION PERCENTAGES																		
58	34	56	72	44	62	75	86	93	98	84	87	98	91	96	100	86	96	100
97	9	22	37	11	26	47	45	74	86	42	74	86	50	82	94	48	82	93
73	42	57	100	91	98	100	93	98	100	86	97	100	91	98	98	82	94	98
82	73	81	98	68	81	92	86	96	100	39	68	89	65	81	93	23	56	81
256	89	91	94	80	89	94	83	93	97	54	70	83	83	92	98	36	62	83
160	100	100	93	83	90	95	87	92	95	71	83	93	85	93	96	58	77	91
SCAN WEIGHTED AVERAGES:																		
726	69	76	85	68	78	86	80	91	95	60	77	89	78	90	97	49	73	88

TABLE V 10 SAMPLE DUAL THRESHOLD RESULTS

DUAL THRESHOLD

THR.	0	0	2	2	2	2	4	4	4	4	4	4	6	6	6	6	6	6
MR..	16	16	16	20	20	20	16	16	16	20	20	20	16	16	16	20	20	20
NM..	2	3	4	2	3	4	2	3	4	2	3	4	2	3	4	2	3	4
ANGEL DETECTION PERCENTAGE																		
24	12	16	16	0	0	8	0	0	20	0	0	20	0	25	41	0	25	41
70	60	74	45	0	5	18	1	5	17	0	2	11	1	4	17	1	4	15
19	0	0	0	0	0	0	0	10	26	0	10	26	0	15	47	0	15	47
5	0	20	20	0	0	20	0	20	80	0	20	80	20	40	80	20	40	80
20	10	25	20	0	5	10	5	20	35	5	20	35	5	20	40	5	20	40
35	2	8	11	0	2	14	2	11	17	2	11	17	8	28	57	8	28	57
7	0	0	0	0	0	0	0	28	57	0	28	57	28	57	71	28	57	71
62	74	83	91	54	75	93	74	88	100	43	72	87	66	83	90	43	64	83
30	46	56	63	20	36	60	23	56	80	16	43	73	30	73	90	30	70	90
SCAN WEIGHTED AVERAGES:																		
272	39	48	43	14	22	36	20	32	47	12	26	41	21	38	55	15	33	53
AIRCRAFT DETECTION PERCENTAGES																		
59	33	57	71	42	59	76	81	88	96	76	86	96	93	94	100	79	93	100
97	9	17	36	10	23	47	40	74	86	41	74	85	49	82	94	47	82	93
73	29	56	100	89	97	98	91	98	100	84	95	100	87	97	98	82	93	100
82	73	81	96	43	71	86	69	81	95	29	58	84	40	63	84	23	56	81
256	89	91	92	58	71	84	80	89	96	39	59	78	57	74	87	19	50	78
160	100	100	93	73	83	93	85	91	95	60	76	88	70	86	95	32	68	89
SCAN WEIGHTED AVERAGES:																		
727	69	75	84	55	68	82	75	87	94	50	70	85	62	80	91	37	66	86

TABLE V 10 SAMPLE DUAL THRESHOLD RESULTS (Cont'd)

DUAL THRESHOLD

THR.	0	0	8	8	8	8	10	10	10	10	10	10	12	12	12	12	12	12
MR..	14	14	14	18	18	18	14	14	14	18	18	18	14	14	14	18	18	18
MN..	2	3	4	2	3	4	2	3	4	2	3	4	2	3	4	2	3	4
ANGEL DETECTION PERCENTAGE																		
24	37	50	45	8	29	62	8	33	70	12	33	70	16	41	75	16	41	75
70	72	82	17	1	2	21	2	11	28	1	10	27	2	17	45	1	15	45
19	10	15	57	10	36	84	26	78	89	26	78	89	42	78	94	42	78	94
5	0	20	80	0	60	80	20	80	100	20	80	100	40	100	100	40	100	100
20	15	35	45	0	35	45	10	40	65	10	40	60	15	45	80	15	45	80
35	17	34	54	14	40	62	25	62	91	25	62	91	45	71	91	45	71	91
7	14	14	100	42	57	100	42	85	100	42	85	100	71	100	100	71	100	100
62	72	83	88	37	69	87	45	75	91	35	67	88	33	70	87	27	66	85
30	46	56	90	46	80	100	43	90	100	46	90	100	56	96	100	56	96	100
SCAN WEIGHTED AVERAGES:																		
272	47	59	56	18	40	62	23	52	72	21	50	70	28	56	77	26	55	77
AIRCRAFT DETECTION PERCENTAGES																		
58	34	56	98	87	94	98	86	100	100	77	98	100	82	96	96	77	96	96
97	9	22	91	56	90	98	76	90	97	76	90	97	79	97	98	79	97	98
73	42	57	97	80	93	98	82	98	100	82	95	100	87	97	100	84	95	100
82	73	81	74	20	56	82	20	58	81	20	56	81	21	54	80	19	45	73
256	89	91	76	19	50	78	37	69	82	15	47	76	18	49	78	14	46	78
100	100	100	85	31	67	88	59	76	93	24	65	85	31	86	97	28	69	95
SCAN WEIGHTED AVERAGES:																		
726	69	76	84	38	67	86	53	74	89	37	65	85	41	67	86	36	65	85

TABLE V 10 SAMPLE DUAL THRESHOLD RESULTS (Cont'd)

4. M/M Azimuth Correlator (Baltimore data)

The additional aircraft data gathered at Baltimore's Friendship airport sampled 40 consecutive radar sweeps, rather than 37 alternate sweeps as done at Milwaukee. Results for a 4/4 Azimuth Correlator are given in Table VI; Table VII applies to 5/5.

To evaluate the effects of using only alternate sweeps, the processor was also run for 2/2 on alternate sweeps. Table VIII applies to the even samples and Table IX applies to the odd samples from the Baltimore data.

N/N DETECTOR, N= 4

THR.	4	5	6	7	8	9	10	11	12	13	14	15	16	17	18	19	20	21
AIRCRAFT DETECTION PERCENTAGES																		
120	83	76	75	73	72	68	68	65	62	59	55	50	50	50	49	48	44	35
35	97	97	97	97	97	97	97	97	97	97	97	94	94	91	91	85	77	68
308	94	91	89	89	88	86	85	85	85	84	83	80	80	79	78	75	74	71
132	86	78	75	71	70	68	66	63	62	62	59	53	52	52	50	46	43	33
164	86	84	79	75	75	72	70	65	62	61	60	54	53	53	50	47	44	35
180	78	76	75	75	72	71	68	67	64	64	64	61	60	60	56	43	34	17
218	89	87	85	82	80	78	77	76	75	74	71	60	59	59	56	32	24	8
SCAN WEIGHTED AVERAGES:																		
1157	87	84	81	80	78	76	75	73	71	71	69	63	63	62	60	52	47	37

TABLE VI 4/4 AZIMUTH CORRELATOR

BALTIMORE DATA, EVERY RADAR SWEEP

M/N DETECTOR, N= 5

THR.	4	5	6	7	8	9	10	11	12	13	14	15	16	17	18	19	20	21
AIRCRAFT DETECTION PERCENTAGES																		
120	75	68	64	61	60	58	55	52	50	48	46	38	38	37	36	35	31	25
35	97	94	94	94	88	88	88	85	82	77	77	74	74	74	74	74	68	62
308	91	88	87	86	85	82	82	80	80	78	76	72	72	71	69	67	65	61
132	74	65	61	55	54	53	51	49	49	49	46	44	43	43	41	38	34	25
164	78	75	70	64	62	58	56	51	48	47	43	39	37	37	33	31	29	23
180	74	71	68	67	66	65	64	63	60	60	58	54	53	53	47	36	28	11
218	86	83	82	79	77	75	73	72	72	69	63	51	49	48	39	17	13	2
SCAN WEIGHTED AVERAGES:																		
1157	82	78	75	72	71	69	67	65	64	62	59	53	52	52	48	41	37	28

TABLE VII 5/5 AZIMUTH CORRELATOR

BALTIMORE DATA - EVERY RADAR SWEEP

N/N DETECTOR, N= 2

THR.	4	5	6	7	8	9	10	11	12	13	14	15	16	17	18	19	20	21
ANGEL DETECTION PERCENTAGE																		
	0	0	0	0	0	0	0	0	0	0	0	0	0	0	0	0	0	0
SCAN WEIGHTED AVERAGES:																		
	0	-0	-0	-0	-0	-0	-0	-0	-0	-0	-0	-0	-0	-0	-0	-0	-0	-0
AIRCRAFT DETECTION PERCENTAGES																		
120	85	84	84	84	84	83	83	80	79	78	75	71	71	71	71	70	69	59
34	100	100	100	100	100	100	100	100	100	100	100	97	97	97	97	97	94	82
308	90	90	90	90	89	89	89	89	89	[illegible]	88	87	87	87	86	85	85	84
129	81	79	78	75	75	75	74	74	74	74	72	65	63	63	63	60	59	53
163	84	84	84	83	83	82	80	77	77	77	77	76	76	76	75	73	71	66
155	89	89	88	88	87	87	87	87	85	85	85	83	82	82	80	64	54	29
SCAN WEIGHTED AVERAGES:																		
909	87	86	86	85	85	85	84	83	83	82	81	79	79	79	78	74	71	63

TABLE VIII 2/2 AZIMUTH CORRELATOR

BALTIMORE DATA - ALTERNATE (EVEN) SWEEPS

N/N DETECTOR,N= 2

THR.	4	5	6	7	8	9	10	11	12	13	14	15	16	17	18	19	20	21
MR..	2	2	2	3	3	3	2	2	2	3	3	3	2	2	2	3	3	3
	0	0	0	0	0	0	0	0	0	0	0	0	0	0	0	0	0	0

ANGEL DETECTION PERCENTAGE

0	2	3	4	2	3	4	2	3	4	2	3	4	2	3	4	2	3	4

SCAN WEIGHTED AVERAGES:

0	-0	-0	-0	-0	-0	-0	-0	-0	-0	-0	-0	-0	-0	-0	-0	-0	-0	-0

AIRCRAFT DETECTION PERCENTAGES

120	84	84	84	84	84	82	80	80	80	79	78	76	75	75	73	71	70	60
34	100	100	100	100	100	100	100	100	100	100	100	100	100	100	100	100	100	91
308	90	89	89	89	88	88	88	88	88	87	87	86	86	85	85	84	83	81
129	81	79	79	79	79	79	78	75	75	75	73	69	68	68	67	67	64	52
163	84	84	84	82	82	81	81	79	78	78	77	75	74	74	74	71	69	68
155	89	89	89	88	88	87	87	85	85	84	84	80	80	80	76	65	56	36

SCAN WEIGHTED AVERAGES:

909	87	86	86	85	85	84	84	83	83	82	82	79	79	79	77	74	72	64

TABLE IX 2/2 AZIMUTH CORRELATOR

BALTIMORE DATA - ALTERNATE (ODD) SWEEPS

5. Dual Threshold Processor (Baltimore data)

This processor was identical to that used on the Milwaukee data except that 40 consecutive radar sweeps, as opposed to 37 alternate radar sweeps were processed. Table X lists the results.

DUAL THRESHOLD

THR.	8	8	8	8	8	8	10	10	10	10	10	10	12	12	12	12	12	12
MB..	16	16	16	20	20	20	16	16	16	20	20	20	16	16	16	20	20	20
MM..	2	3	4	2	3	4	2	3	4	2	3	4	2	3	4	2	3	4

AIRCRAFT DETECTION PERCENTAGE

120	32	43	59	5	20	32	13	27	37	5	15	30	5	18	36	4	15	34
34	58	67	79	14	17	29	20	38	61	8	14	29	14	17	32	8	14	32
308	71	81	90	53	64	75	66	75	82	42	53	64	51	62	68	11	28	42
129	21	36	51	10	20	37	17	29	47	5	18	35	11	27	43	5	23	37
163	36	50	64	15	23	39	22	34	47	6	15	30	14	22	39	6	15	33
155	18	36	51	16	35	51	18	34	50	5	22	45	15	32	50	3	18	45
211	6	18	31	5	17	27	6	14	28	3	9	18	6	11	24	3	8	17

SCAN WEIGHTED AVERAGES:

1120	35	48.	61	22	33	47	28	40	52	15	25	39	21	32	45	6	18	34

TABLE X DUAL THRESHOLD RESULTS
BALTIMORE AIRCRAFT DATA

DUAL THRESHOLD

THR.	10	10	10	10	10	10	12	12	12	12	12	12	14	14	14	14	14	14
MR..	4	4	4	8	8	8	4	4	4	8	8	8	4	4	4	8	8	8
MN..	2	3	4	2	3	4	2	3	4	2	3	4	2	3	4	2	3	4

AIRCRAFT DETECTION PERCENTAGE

120	92	97	98	82	90	95	90	98	99	85	93	96	93	96	99	58	75	89
34	100	100	100	94	97	100	94	100	100	85	97	100	97	97	100	73	85	94
308	89	93	93	87	92	93	87	91	92	82	90	92	86	90	91	79	86	89
129	92	99	100	74	89	97	82	95	97	75	89	95	84	95	99	48	71	85
163	92	96	98	81	94	96	87	96	97	80	89	96	92	98	99	64	79	88
155	93	96	96	76	86	93	81	86	92	54	67	78	77	88	92	27	41	61
211	92	95	96	75	87	92	86	91	94	48	62	74	79	89	92	16	26	41

SCAN WEIGHTED AVERAGES:

1120	91	95	96	80	90	94	85	92	94	71	81	88	85	92	94	51	64	75

TABLE X DUAL THRESHOLD RESULTS (Cont'd)

BALTIMORE AIRCRAFT DATA

DUAL THRESHOLD

THR.	2	2	2	2	2	2	4	4	4	4	4	4	6	6	6	6	6	6
MR..	2	2	2	6	6	6	2	2	2	6	6	6	2	2	2	6	6	6
MN..	2	3	4	2	3	4	2	3	4	2	3	4	2	3	4	2	3	4

AIRCRAFT DETECTION PERCENTAGE

120	88	97	100	75	90	95	92	100	100	81	95	100	96	100	100	86	98	99
34	94	100	100	94	100	100	100	100	100	94	100	100	94	100	100	94	97	100
308	95	99	100	86	92	96	85	92	97	77	86	91	86	92	94	77	88	93
129	86	96	98	84	89	93	89	95	99	80	88	95	96	99	100	79	93	98
163	93	98	100	84	92	96	94	98	99	82	91	95	93	99	100	82	95	98
155	86	92	98	83	89	94	94	99	99	85	95	98	97	98	98	91	96	97
211	87	94	98	85	89	93	93	97	99	88	94	98	96	97	98	89	95	97

SCAN WEIGHTED AVERAGES:

1120	90	96	99	83	90	94	90	96	98	82	91	95	92	96	97	83	93	96

TABLE X DUAL THRESHOLD RESULTS (Cont'd)

BALTIMORE AIRCRAFT DATA

DUAL THRESHOLD

THR.	6	6	6	6	6	6	8	8	8	8	8	8	10	10	10	10	10	10
MR..	8	8	8	12	12	12	8	8	8	12	12	12	8	8	8	12	12	12
MN..	2	3	4	2	3	4	2	3	4	2	3	4	2	3	4	2	3	4

AIRCRAFT DETECTION PERCENTAGE

120	85	94	98	75	88	94	73	92	96	58	88	93	82	90	95	51	70	82
34	91	97	100	85	97	100	91	97	100	85	94	97	94	97	100	76	79	94
308	79	88	91	75	85	91	84	91	95	82	89	94	87	92	93	80	88	92
129	75	92	97	66	79	89	72	84	93	66	81	90	74	89	97	45	65	79
163	82	92	96	77	86	92	80	92	96	73	82	95	81	94	96	63	72	82
155	90	96	97	76	85	92	78	88	91	57	70	78	76	86	93	29	47	61
211	89	92	96	75	88	92	82	92	96	53	64	72	75	87	92	19	30	45

SCAN WEIGHTED AVERAGES:

1120	83	91	95	75	85	91	80	90	94	68	79	87	80	90	94	51	64	74

TABLE X DUAL THRESHOLD RESULTS (Cont'd)

BALTIMORE AIRCRAFT DATA

DUAL THRESHOLD

THR.	4	4	4	4	4	4	6	6	6	6	6	6	8	8	8	8	8	8
MR..	12	12	12	16	16	16	12	12	12	16	16	16	12	12	12	16	16	16
MN..	1	2	3	1	2	3	1	2	3	1	2	3	1	2	3	1	2	3
AIRCRAFT DETECTION PERCENTAGE																		
120	50	70	84	47	66	80	50	75	88	35	50	65	56	68	88	15	32	43
34	64	91	97	67	79	94	67	85	97	67	76	82	73	85	94	41	58	67
308	63	76	83	62	75	83	64	78	85	60	75	83	65	82	89	53	71	81
129	51	67	78	49	64	75	46	66	79	30	42	58	41	66	81	17	21	36
163	56	76	83	53	71	80	54	77	86	43	59	68	51	73	82	24	36	50
155	61	77	87	47	61	73	60	76	85	18	32	49	40	57	70	9	18	36
211	67	80	91	55	54	70	62	75	88	9	22	38	36	53	64	0	6	18
SCAN WEIGHTED AVERAGES:																		
1120	59	75	85	52	66	77	58	75	85	36	50	62	50	68	79	24	35	48

TABLE X DUAL THRESHOLD RESULTS (Cont'd)
BALTIMORE AIRCRAFT DATA

APPENDIX B-3

AZIMUTH PATTERN VIDEO AMPLITUDE DATA

Azimuth Pattern Analysis

To help visualize the type of returns used in the calculations, a computer was programmed to plot data. The amplitudes for the video (in the row with the maximum sum of amplitudes) from the Data Collect Matrix for each scan were used. The enclosed figures illustrate three examples of two scans for each of these plots. Each plot has target amplitude plotted on the ordinate and target azimuth on the abscissa. The amplitude is scaled 0 to 31 and the azimuth integers correspond to alternate scans. (The plus signs along the edges represent 5 amplitude divisions). Figures B-16 and B-17 are angel returns illustrating the large variety of returns found for angels. These examples are typical of the plots obtained for angel tracks. The most striking characteristic of these plots is their width. Whereas the aircraft plots, of which Figure B-18 is typical, appear to be generally confined to about 40 dwells in azimuth. The angels appear to fill the full 74 (twice 37) dwells observed, indicating that perhaps an extended bird flock was tracked, or perhaps several flocks. In addition, scan-to-scan, the angel plots do not vary in a consistent manner, while the aircraft track almost always consists of one principle peak with few, if any, side peaks. This peak appears to be one of the principle reasons for the success of the 5/5 detector. The width difference also explains the reason for degradation in the discrimination capabilities of other detectors employed, as the width of the sampled region was decreased. Another general characteristic was, that except for small fluctuations, the larger fluctuations for aircraft almost always vary from zero to a maximum or vice versa. Angels, on the other hand, appear to have more intermediate types of fluctuation, which accounts for the capabilities of the dual threshold detector.

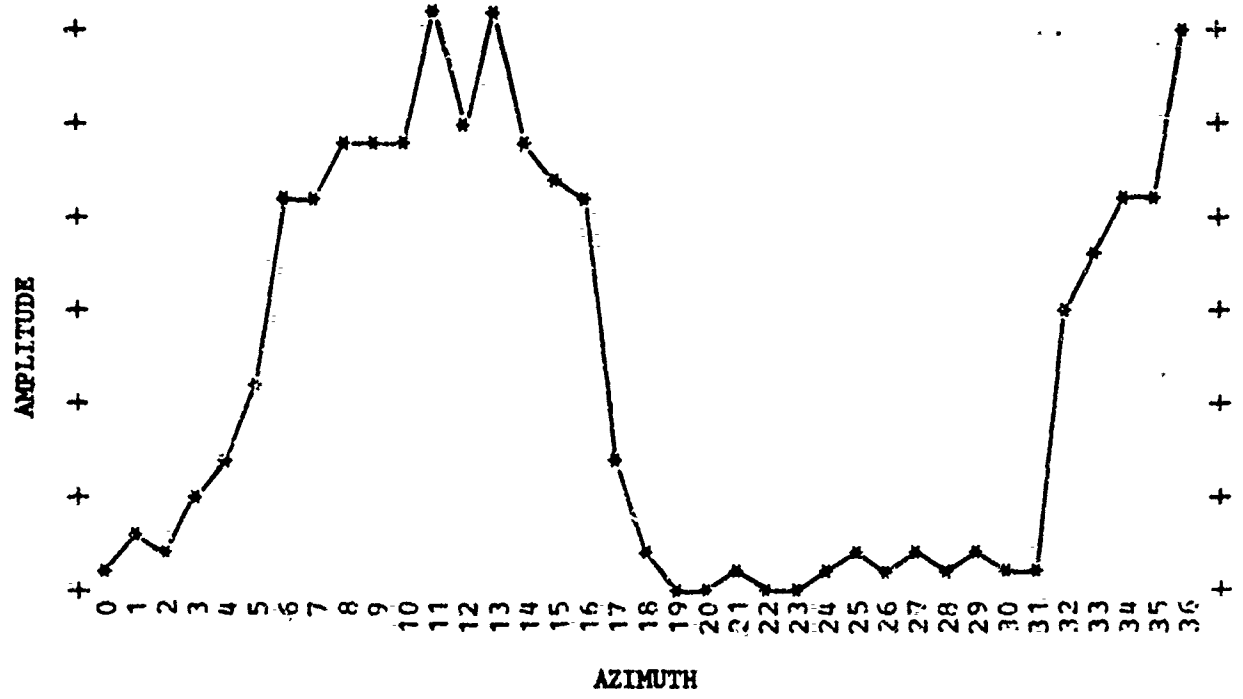

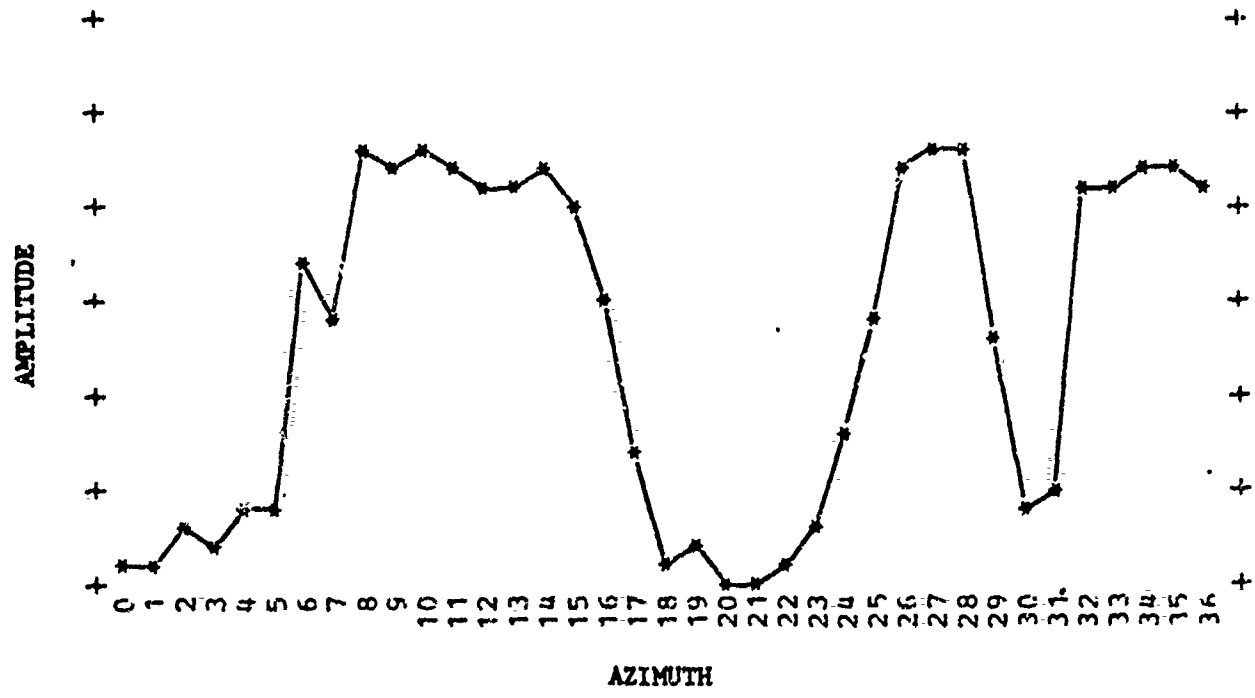

Figure B-16 Angel Azimuth Patterns

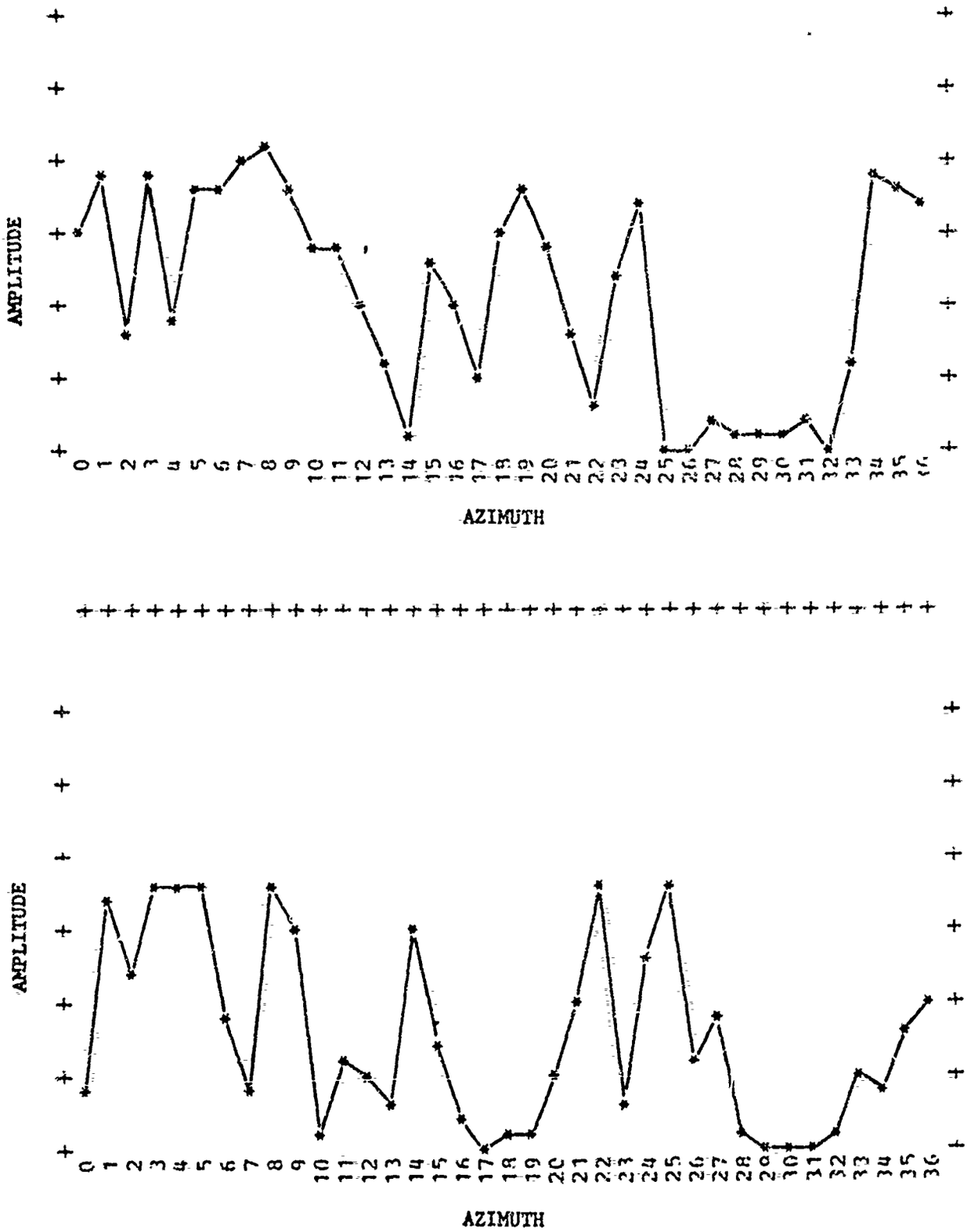

Figure B-17 Angel Azimuth Patterns

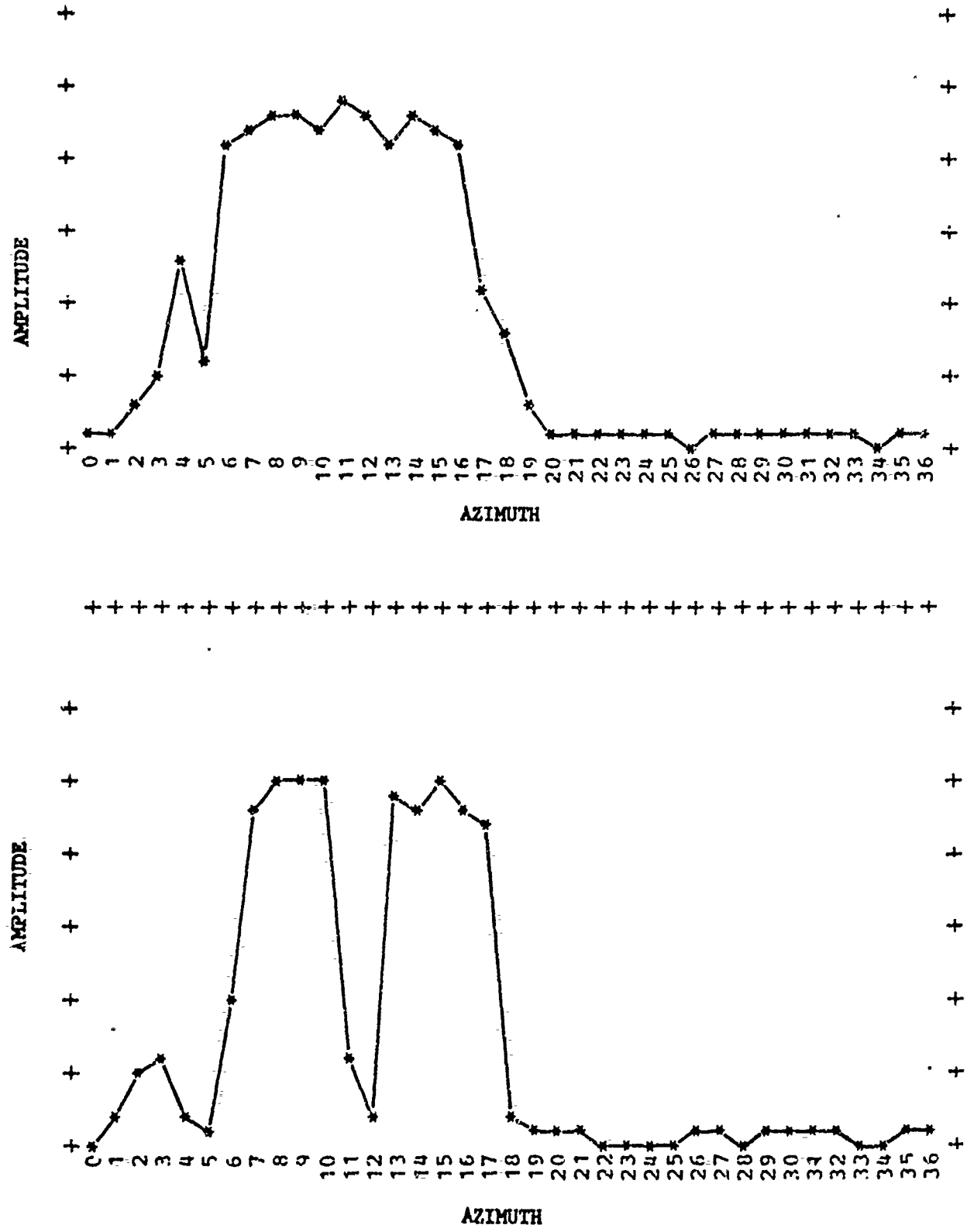

Figure B-18 Aircraft Azimuth Patterns

APPENDIX B-4

ASR ANGEL CLUTTER DENSITY OBSERVATIONS

Introduction

Total numbers and densities of angels as observed, for example, on a PPI are of interest because they are numerical measures of what is meant by "an angel clutter problem" in the present air traffic control system. Furthermore, they are indicative of the angel clutter which must be handled in some way by the developing automated traffic control systems. This Appendix presents some quantitative results on observed numbers and densities of angels based on data collected for FAA Task II. Observed densities depend strongly on signal processing and antenna tilt as well as on angel cross sections and spatial distributions. The results presented below are from ASR's which were set up primarily for a satisfactory tradeoff between aircraft and ground clutter detections. The data represent typical conditions of moderate-to-heavy angel clutter in Milwaukee, Little Rock and Atlantic City (NAFEC).

Observed Angel Numbers and Densities

Several PPI photographs of ASR MTI video were examined; the photographs, obtained in preparation for and during FAA Task II, are identified in Table 1. The number of angels detectable by eye were counted in two-mile range intervals. The results are shown in Figure B-19. In areas of densest clutter, clustered angels could not be accurately counted by eye. In these areas, the count given is an underestimate. The actual number of detectable targets in these range intervals could be as much as fifty per cent higher than the number given. The total counts of detectable angels are listed in Table 1. The identity of the source of these angels is of some interest in the search for angel clutter reduction techniques; it is considered later.

TABLE 1

Angels in ASR MTI Video

PPI Photograph Date	Time	CSS/STC	Total Angels Counted	Reference
Milwaukee (1972)				
April 15	2122 CST	CSS-2	225	a.
April 17	0620	CSS-2	310	a.
April 18	0602	None	284	b.
Little Rock (1972)				
March 8	1805 CST	STC	230	c.
March 9	0553	STC	167	c.
NAFEC (1971)				
October 28	1931 EDT	STC	225	d.

References:

a. Figure 5.2.1-1, MSO-F-133, Task II Interim Report, 22 May 1972
b. Figure 5.2.1-3, MSO-F-133, Task II Interim Report, 22 May 1972
c. On file; similar to Figures 2 and 3, MFS-0-197, 23 March 1972
d. Figure 2, MRD-3-394, 10 November 1971

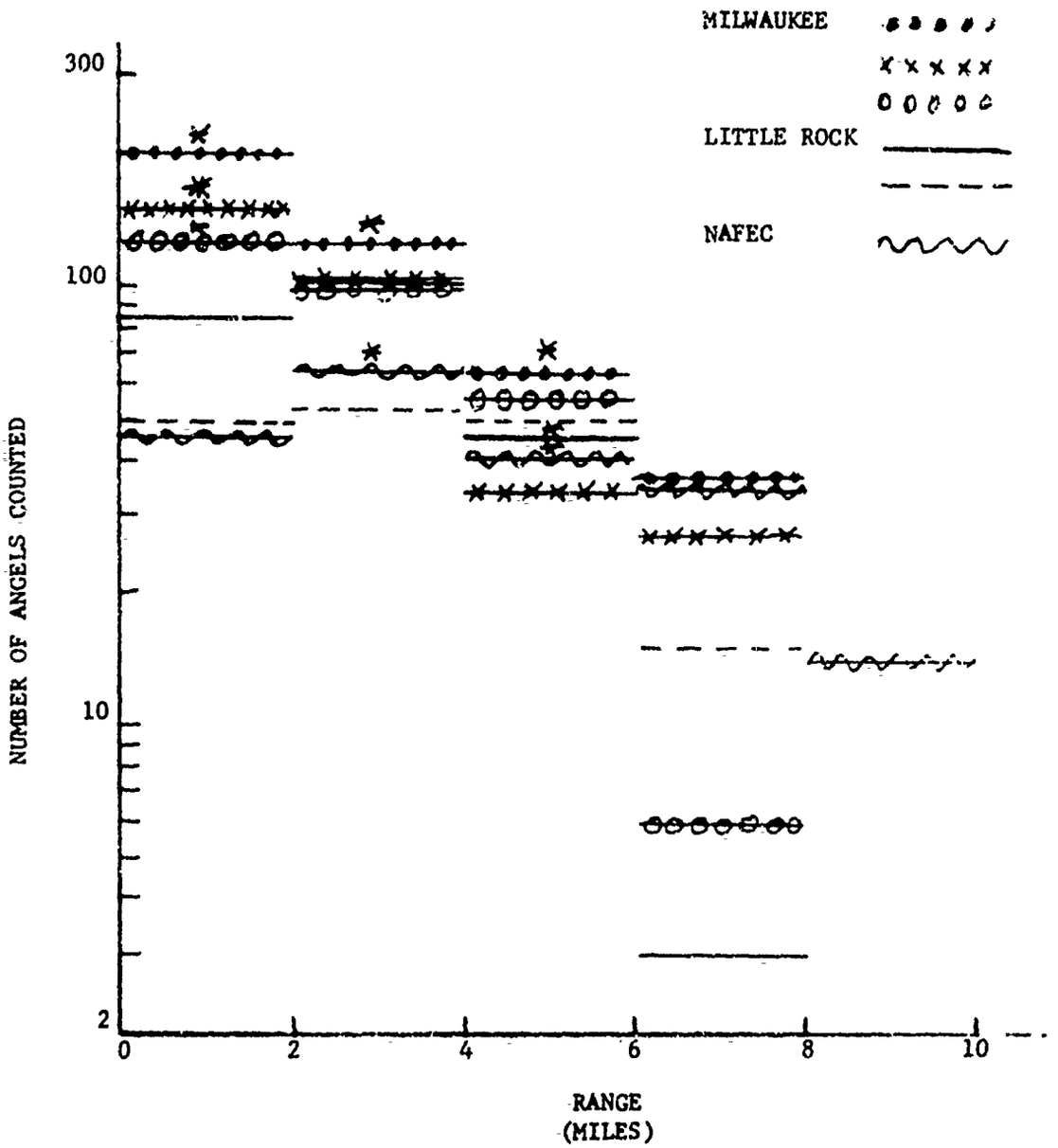

Figure B-19 Number of angels counted per range interval in PPI photographs of ASR MTI video. Probable underestimates shown by * (see text).

Mean angel densities were determined from the data of Figure B-19 by dividing the number of angels counted in a range interval by the area of the interval. Table 2 gives the results. Included in the Table are results, obtained in the same way, for several additional photographs of Little Rock video. These photographs were taken within minutes of ones listed in Table 1.

Mean densities in Table 2 are, for the most part, on the order of 1 per square mile with a range of about two orders of magnitude. The minimum densities shown represent a few angels in 88 square miles. Inside six miles, these densities must be considered underestimates for two reasons. First, as indicated above, where density is high, some echoes appear to be merged. An effective automatic detection system or an optimized combination of PPI and camera would probably often show two distinct angels where the visual counting yielded one. Second, angels are usually not distributed uniformly in azimuth. Large sectors of a particular range interval may contain few or no angels while, in other sectors, the mean density is several times the tabulated value.

To obtain more detailed information on angel densities, two photographs of Little Rock MTI video were further analyzed. A square grid was superimposed on each photograph and the number of angels detectable in each cell was counted. The grid and results are shown in Figure 20. (Note that cell size in miles differs in the two cases.) The azimuthal nonuniformity which was mentioned above is evident. Although detection density generally decreases with range, the variation is not smooth. In Figure 20a, the distribution appears to peak about four to six miles from the radar. These distributions are fully consistent with the known, customary paths of the birds believed to be the source of these angels.

TABLE 2

Observed Mean Angel Densities ($mile^{-2}$)
in Range Intervals

		Range Interval (miles)			
		0-2	2-4	4-6	6-8
Milwaukee					
April 15		>16	3.3	1.0	0.4
17		11.7	2.7	0.5	0.3
18		9.9	2.6	0.9	0.07
Little Rock					
March 8	1805	6.8	2.7	0.7	0.03
	1812	8.3	2.4	0.5	0.03
March 9	0552	3.1	1.5	0.7	0.1
	0553	3.9	1.4	0.8	0.2
	0556	3.3	2.4	0.6	0.4
	0648	5.0	1.8	0.7	0.1
NAFEC					
October 28		3.6	1.7	0.7	0.4

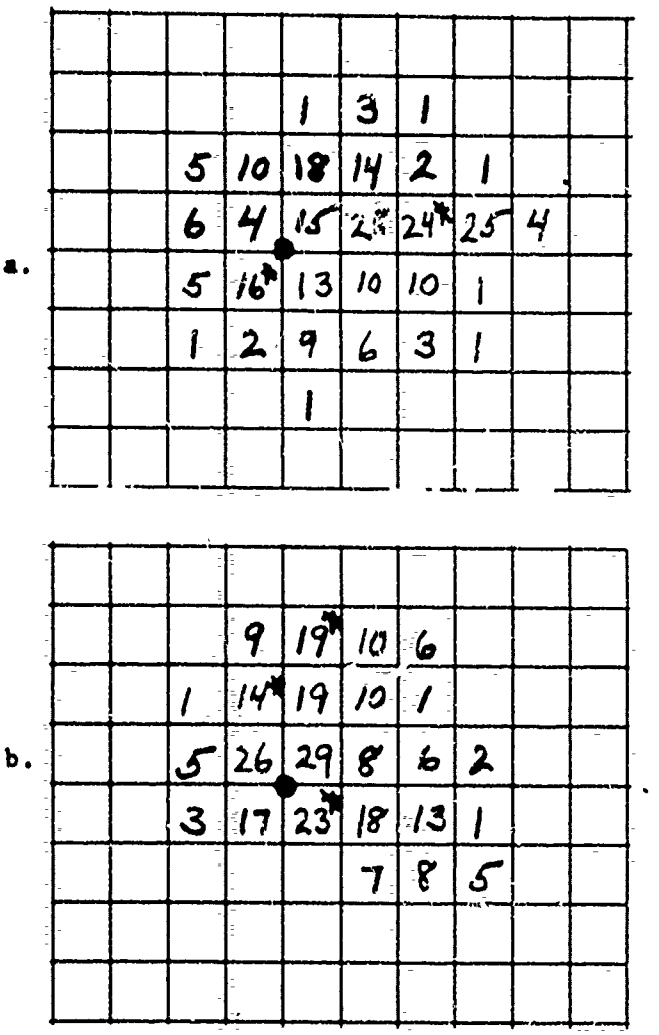

Figure B-20 Angels counted in PPI photographs of Little Rock ASR MTI video. Underestimates are shown by *.

a. Cell size 1.9 x 1.9 miles. 0556CST, 9 March 1972

b. Cell size 1.56 x 1.56 miles. 1805CST, 8 March 1972

Cumulative distributions of the mean densities calculated from the data of Figure 20 are given in Figure 21. Maximum angel densities observed were near 10 mi^{-2}. Note that this value depends on the cell size chosen. If smaller cells had been used, higher maximum densities would probably have been found. Mean densities taken over all non-empty cells were 2.4 mi^{-2} over 105 square miles and 4.4 mi^{-2} over 58 square miles.

Angel Identification

For the data given, a strong circumstantial argument can be made that the angels were due to birds. At Little Rock, the appearance, disappearance and approximate spatial distribution of angels was very closely correlated with easily-observed mass movements of blackbirds near the airport. Local air controllers confirmed that this correlation was normal. At Milwaukee, migratory activity in the area was common and widespread during the times of observation. At NAFEC, the area of angel activity was a bird sanctuary known to be active, and early-evening bird activity was a regular occurrance. In all cases, angels which could be followed on the PPI behaved like birds and not like ground clutter, air or ground vehicles, or recognizable atmospheric phenomena. Weather was clear and stable enough in each case to be eliminated as a plausible clutter source. Satisfactory MTI cancellation of stationary targets and ground clutter was verified before and after angels became numerous and was verified in clear sectors and at longer ranges while angels were present. These latter observations also confirmed that equipment noise was not a factor. The conclusion drawn on the identity of the observed angels is that, with high probability, almost all were due to birds. Although some may have been due to individual birds, the characteristics of typical bird activity at each site during the period when observations were made suggests that most angels were probably due to groups of several birds or more.

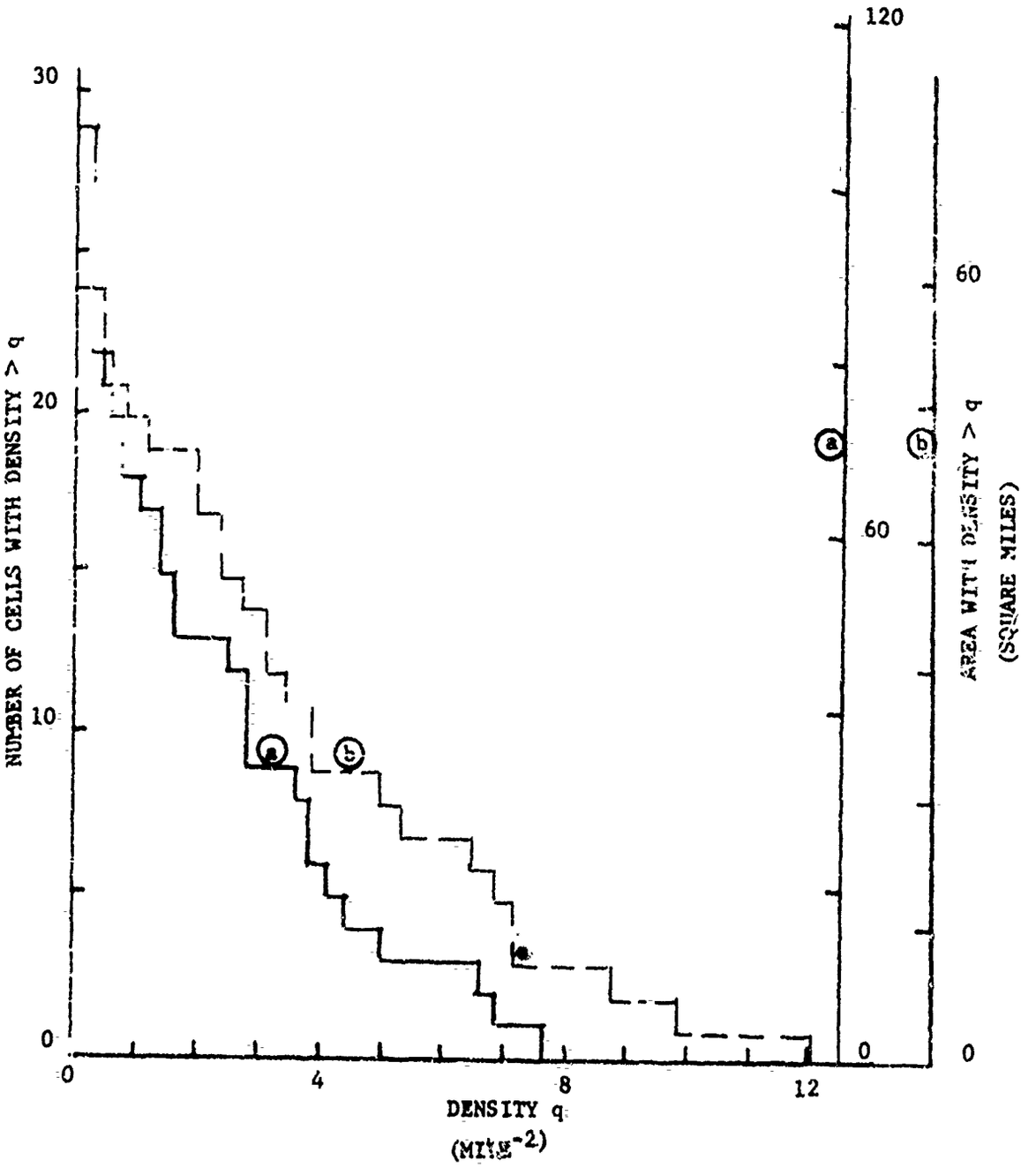

Figure B-21 Cumulative distribution of mean angel densities in Little Rock ASR MTI video. (a) and (b) refer to Figure B-20.

APPENDIX B-4

Summary

In PPI photographs of MTI video at three ASR sites, typical angel densities on the order of 1 mi^{-2} were found in moderate-to-heavy clutter. Maximum mean densities of approximately 10 mi^{-2} were observed in averages over areas of six to eight square miles. The total number of detectable angels ranged between approximately 150 and 300. With high probability, the angels were due to birds in groups.

APPENDIX C

SUPPORTING ANALYSES

APPENDIX C-1

ANALYTIC MODEL OF PPI-OBSERVER INTERACTION

Abstract

An analytic model of PPI-observer interaction is investigated with a view toward evaluating the impact of Clutter Reducing Devices (CRD) on the detectability of selected target types. Optimum conditions are found within this model for the reduction of clutter masking effects and several properties of this system are illustrated using particular examples of the model.

The results indicate that as the clutter component increases the strength of the clutter reducing device, as measured by the percentage of valid targets rejected, must be increased to produce an increase in target detectability: i.e., although a greater percentage of valid targets are rejected by the CRD, more targets become detectable due to a reduction in clutter masking effects. Also, as the clutter increases, the gain in target detectability for this optimum CRD increases. This result can be misleading, however, as an improvement of from one to ten targets detectable out of a thousand possible targets amounts to a ten to one increase in detectability but is not sufficient improvement for the conditions. Thus, eventually this "real life" device also "saturates" as far as usefulness is concerned. Finally, the receiver will be shown, in the models considered, to actually increase target detectability slightly.

Introduction: Clutter Elimination and Target Detectability

In designing a radar system, the objective is always to obtain the maximum detectability of some given target type. Increasing detectability, however, implies increasing the sensitivity of the radar, increasing clutter which can reduce detectability by obscuring or masking valid targets. Thus, tradeoffs must be made between the cost of not detecting a target and the amount of clutter

masking that can be tolerated in order to maximize the probability of detecting a target. It is, however, possible to use the characteristics of the expected targets and clutter to build devices which will selectively reject clutter while retaining valid targets, increasing detection probability. Ideally such a device would reject only clutter and pass only targets, so that the sensitivity of the radar could be made as high as desired and target detectability could be chosen at will. Unfortunately, real life devices will always pass some clutter and reject some targets so that some reduction in actual number of targets on the PPI occurs, and some targets are still masked by clutter when the device is incorporated into the system. If this Clutter Reducing Device (CRD) is designed properly, however, large numbers of targets previously obscured by clutter will now be easily detected so that an overall increase in detectable targets occurs. In addition, as a large amount of clutter has been eliminated, the sensitivity of the system can be increased until the clutter passed by the CRD reaches maximum tolerable levels. With proper design this can compensate for some of the targets rejected by the CRDs (perhaps even increase the efficiency of the CRD) and contribute to the overall increase in detectability of the desired targets. The problem comes in finding the parameters for the CRD which will maximize this detectability, particularly in view of the probability of rejecting a valid target during the processing. If one is too worried by the possibility of the CRD rejecting a valid target, the parameters may be chosen to minimize target rejections so all targets appear on the PPI. Unfortunately, this situation also implies that a large amount of clutter will be passed by the CRD and obscure many of the targets on the PPI, producing the same effect as a rejection. Thus, little or no improvement is obtained. The opposite extreme also yields no improvement. However, if the designer is willing to experience the loss of a few targets due to CRD rejection, many other targets may become detectable yielding a net increase of targets detected. The choice of parameters determines which case occurs and, by a proper choice of the operating parameters, the maximum improvement for a given device can be obtained. (Figure 1 shows how a CRD might be incorporated into a radar system).

The purpose of this memo is to provide an analytic approach for optimizing the parameters of a CRD in the above situation and to illustrate the results for a particular model of aircraft detectability

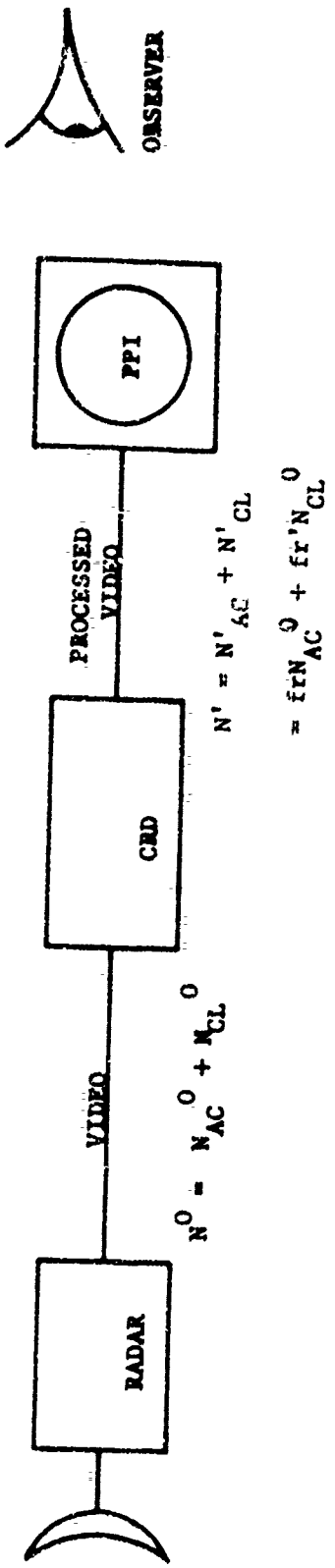
OBSERVER
PPI
PROCESSED VIDEO
CRD
VIDEO
RADAR
$N' = N'_{AC} + N'_{CL}$
$= \epsilon r N^0_{AC} + \epsilon r' N^0_{CL}$
$N^0 = N^0_{AC} + N^0_{CL}$

FIGURE 1

for a man-radar system. In particular, the characteristics of a device designed to detect aircraft amidst angel returns will be used to characterize the decision making scheme. The concept of this device was derived from the results of angel clutter study conducted for the FAA and so represents a possible system.

General Considerations

Basically the problem is formulated as follows. At any given time there is generally some finite number of aircraft targets (N_{AC}^{o})on a PPI display. Due to the interaction of clutter with these targets and to basic limitations in the skill of the operator observing the PPI, some targets go undetected by this observer. In principle, however, all targets could be found given sufficient time and information. The actual number of targets detected (N_{AC}) is, therefore, some fraction of the actual number of targets and can be related to this actual number by

$$N_{AC} = N_{AC}^{o} \; F(N_{CL}), \qquad 0 \leq F \leq 1 \tag{1}$$

where F(x) represents the observer's skill in detecting targets as a function of a clutter parameter (N_{CL}). Here F(x) is a function with range $[0, 1]$, and N_{CL} is a measure of the clutter density appearing on the PPI prior to application of the CRD. The nature of F(x) depends on the capabilities of the PPI observer but can be generally expected to be a monotonically decreasing function of x. This follows from the assumption that an increase in the clutter will lead to a reduction in the number of targets detected by the observer. Thus in general, for

$$X < Y \tag{2a}$$

$$F(x) \geq F(y) \tag{2b}$$

with $$0 \leq F(x) \leq F(y) \leq 1 \tag{2c}$$

If now a CRD is incorporated into the system, the number of targets actually on the PPI is reduced to

$$(N_{AC}{}^{o})' = N_{AC}{}^{o} \; fr \tag{3}$$

while, at the same time, the clutter has been reduced to

$$(N_{CL})' = N_{CL} \; fr' \tag{4}$$

Here 1 -fr and 1 -fr' are the fraction of targets and clutter, respectively, removed by the CRD. Both of these fractions are a function of the design parameters at the CRD and may vary between 0 and 1 as determined by the operating characteristics of the device.

Presumably the detecting capabilities of the PPI observer are unchanged by the CRD, so the number of targets actually detected by the observer should be related to the targets actually displayed in the same manner as prior to installation of the device, i.e.,

$$(N_{AC})' = (N_{AC}{}^{o})' \; F((N_{CL})') = fr \; N_{AC}{}^{o} \; F(fr' \; N_{CL}) \tag{5}$$

The object of building such a device is that

$$(N_{AC})' > N_{AC} \tag{6}$$

i.e., more targets are detected with the device than without it. In other words,

$$\text{Improvement factor} = \frac{(N_{AC})'}{N_{AC}} > 1 \tag{7}$$

which in terms of characteristics of the observer and a CRD, becomes,

$$\frac{fr \; F(fr' \; N_{CL})}{F \; (N_{CL})} > 1 \tag{8}$$

If this inequality is not satisfied for a CRD, then it is actually decreasing target detectability and should no longer be considered.

Note that the dependence on the desired target numbers has cancelled out, so that only the operating characteristics of the CRD and the observer as functions of the initial clutter density remain. The optimization occurs by choosing the values of fr and fr' which maximize this ratio. As fr and fr', which describe the operating point of the CRD, are dependent parameters, differentiation with respect to one of these parameters will lead to a maximizing condition, i.e.,

$$\frac{d}{d\ fr}\left[fr\ \frac{F\left[fr'\ N_{CL}\right]}{F\left[N_{CL}\right]} \right] = 0 \qquad (9)$$

This leads simply to

$$fr\ \chi(fr'\ N_{CL})\ N_{CL}\ \frac{d\ fr'}{d\ fr} = 1 \qquad (10)$$

where

$$\chi(x) = \frac{-1}{F(a)} \left[\frac{d}{dx}\ F(x) \right]_{x=a} \qquad (11)$$

As F(x) is monotomic decreasing, $\chi(x)$ is positive, although the exact form depends on the model assumed for the observer. In view of this result, maximization of the detectability requires that the operating parameters of the CRD must <u>not</u> be selected to place the operating point on a portion of the CRD's characteristic operating curve with negative slope for all other terms in equation 10 are positive. The exact point of operation, of course, depends on the exact characteristics of the device used. Once both functions are known, however, the exact optimum operation point can be found.

The second criteria for a maximum, (the third criteria for an operational CRD), namely

$$\frac{d^2}{d\ fr^2}\ fr\ \frac{F\ (fr'\ N_{CL})}{F\ (N_{CL})} < 0 \qquad (12)$$

leads to the expression

$$y\ (fr'\ N_{CL}) < \frac{1}{fr\ (N_{CL}\ g)^2} \left(\frac{2}{fr} + \frac{1}{g}\ \frac{d}{d\ fr}\ g \right) \qquad (13)$$

where

$$y(x) = \frac{1}{F(k)} \quad \frac{d^2}{dx^2} \quad F(x)$$

$$g = \frac{d}{d\ fr} \quad fr'$$

If this condition is not satisfied no real optimum operating point exists for the clutter conditions and the device provides no benefit to the observer. In this case, the optimum possible situation is to switch the device from the circuit, and allow the observer to select targets on his own.

Exponential Observer

To illustrate the technique just described, it will be useful to assume an exponential model for the operating characteristics of the observer. The exact relation assumed is

$$F\ (N_{CL}) = e^{-N_{CL}/\tau} \tag{14}$$

where τ is a parameter describing the operator's clutter handling capability. As one operator's "heavy clutter" is another operator's "light clutter", only the ratio N_{CL}/τ allows some measure of the "clutter situation" for each observer. Thus, when this ratio is large, the clutter level is sufficient to cause the operator to lose many targets, although another operator, viewing with the same clutter level, may have enough experience to result in a smaller ratio of N_{CL}/τ and therefore, a smaller fraction of lost aircraft. This ratio then determines which is heavy, and which is light clutter for each observer and is the characteristic parameter describing the man-clutter situation. The lower curve in Figure 2 illustrates this exponential function where regions of light, moderate, and heavy clutter have been more or less arbitrarily assigned.

In principle a CRD can be constructed to separate any two (or more) target types. By way of example, however, it will be

FIGURE 2

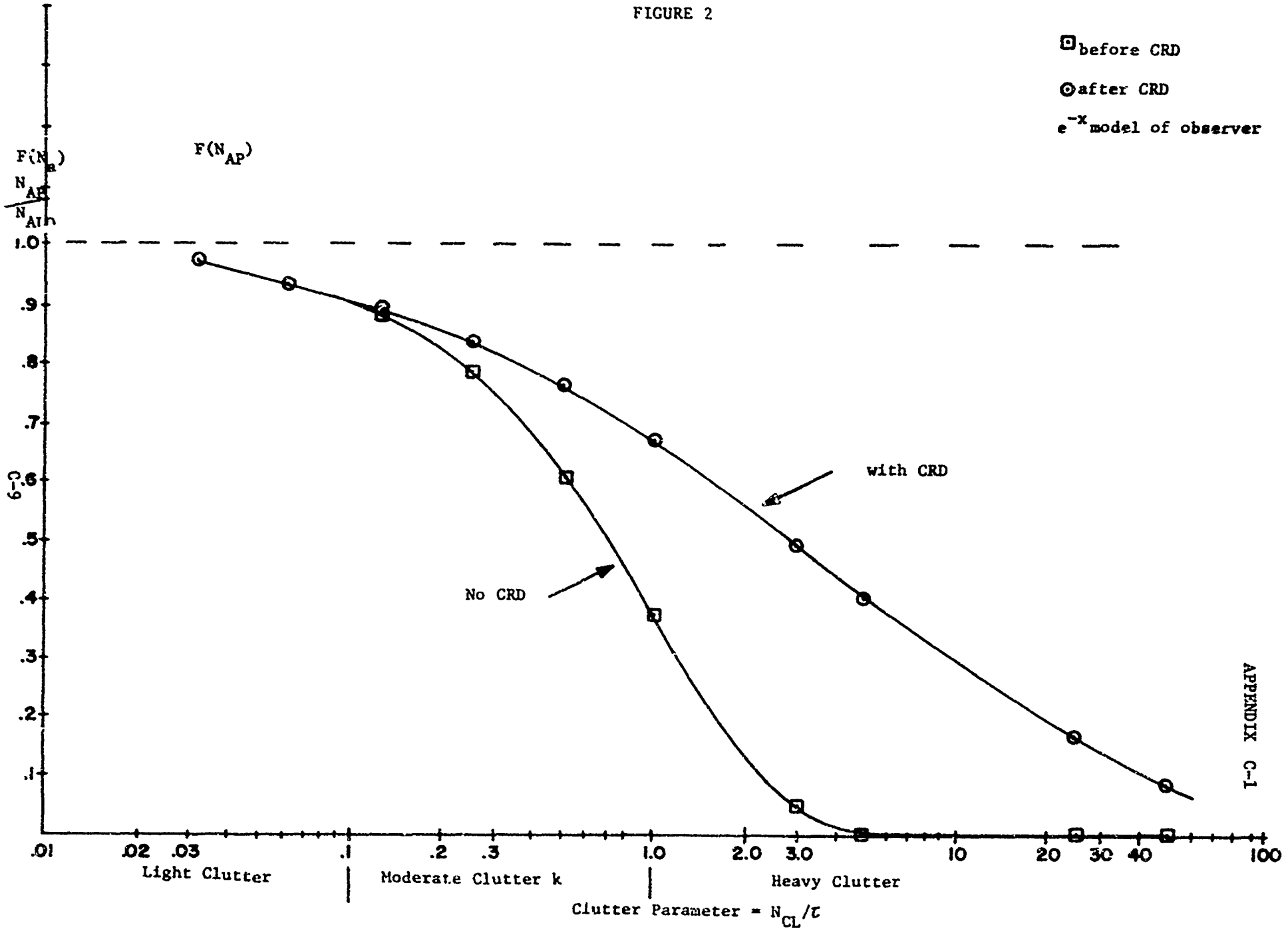

APPENDIX C-1

assumed that the desired targets are aircraft, and the clutter is produced by angel returns generally from birds and anomonalous propagation effects. A device capable of discriminating between these two types of returns based on the azimuth run-length characteristics of the video has been devised in response to a study program conducted by APL for the FAA. Figure 3 is a plot of the operating curve for this device as derived from actual data collected from angel and aircraft video returns. Also plotted is a hyperpolic fit to this data given by

$$fr' = \frac{.0636}{1.06-fr} - 0.6 \qquad (15)$$

which is the desired relationship between fr and fr' for this device.

Using these relationships, the improvement in target detections can be calculated. Figures 4 and 5 show improvement curves for both moderate and heavy clutter situations with this approximation of the CRD operating curve. The improvement factor, (N_{AC}'/N_{AC}) can be seen to decrease below one for some values of fr indicating that this region of operation is to be avoided as more aircraft are lost by the device than are gained by the reduced clutter level. The optimum operating point is that which maximizes the improvement factor, and is indicated on each plot. Both plots also indicate that both the maximum improvement factor and the optimum operating point change with changing clutter conditions. Figure 6 shows a plot of the maximum improvement factor as a function of the clutter parameter N_{AP}/τ. Interestingly this device yields little improvement in light or moderate clutter but results in considerable improvement in severe or heavy clutter, although this is model dependent. Figure 7 shows how the optimum operating point for this CRD varies with clutter conditions. To implement this device, some means of adjusting the operating point must be incorporated so as to allow adjustment to the optimum parameters for the clutter situation as required by this curve.

FIGURE 3

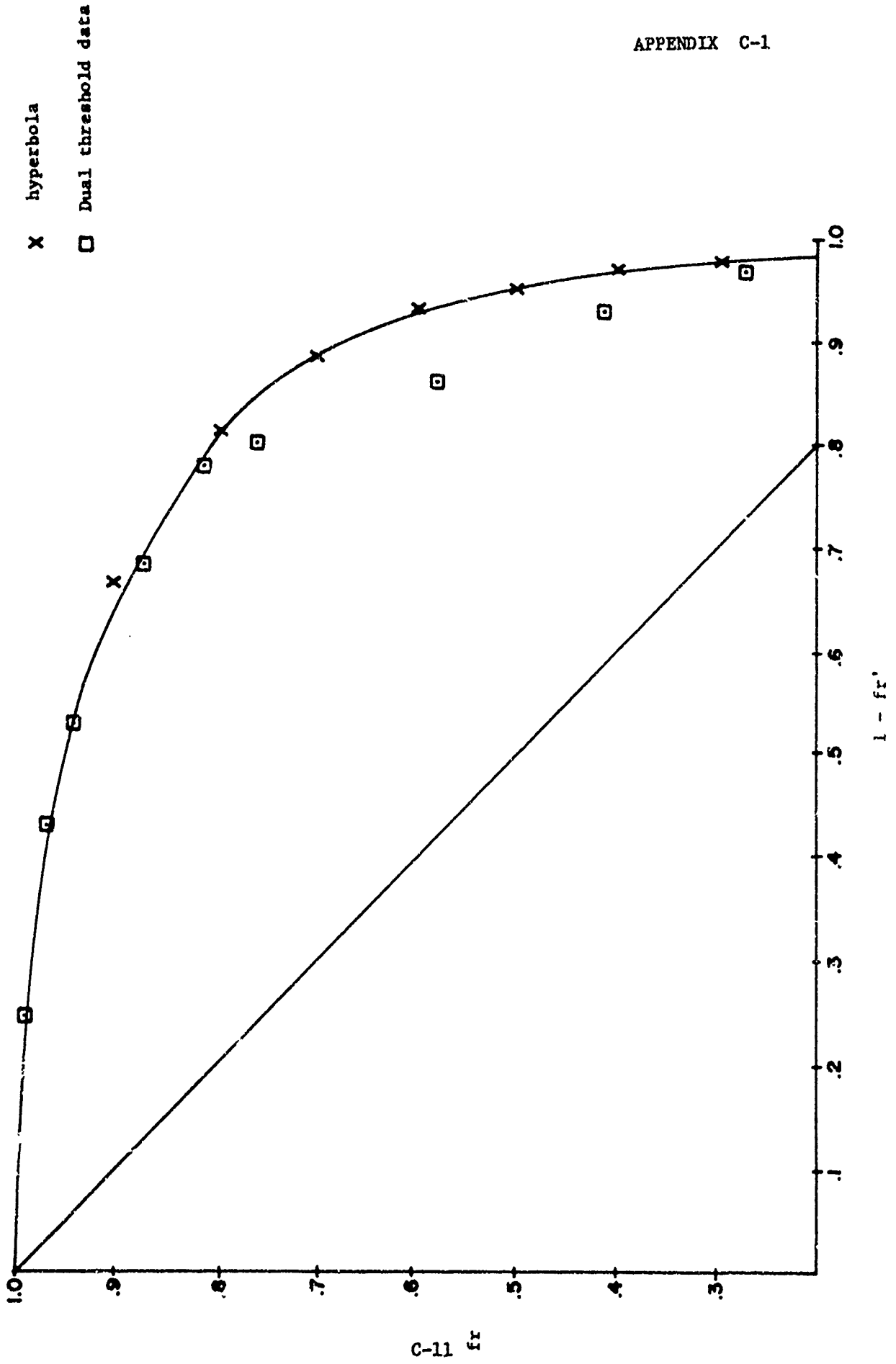

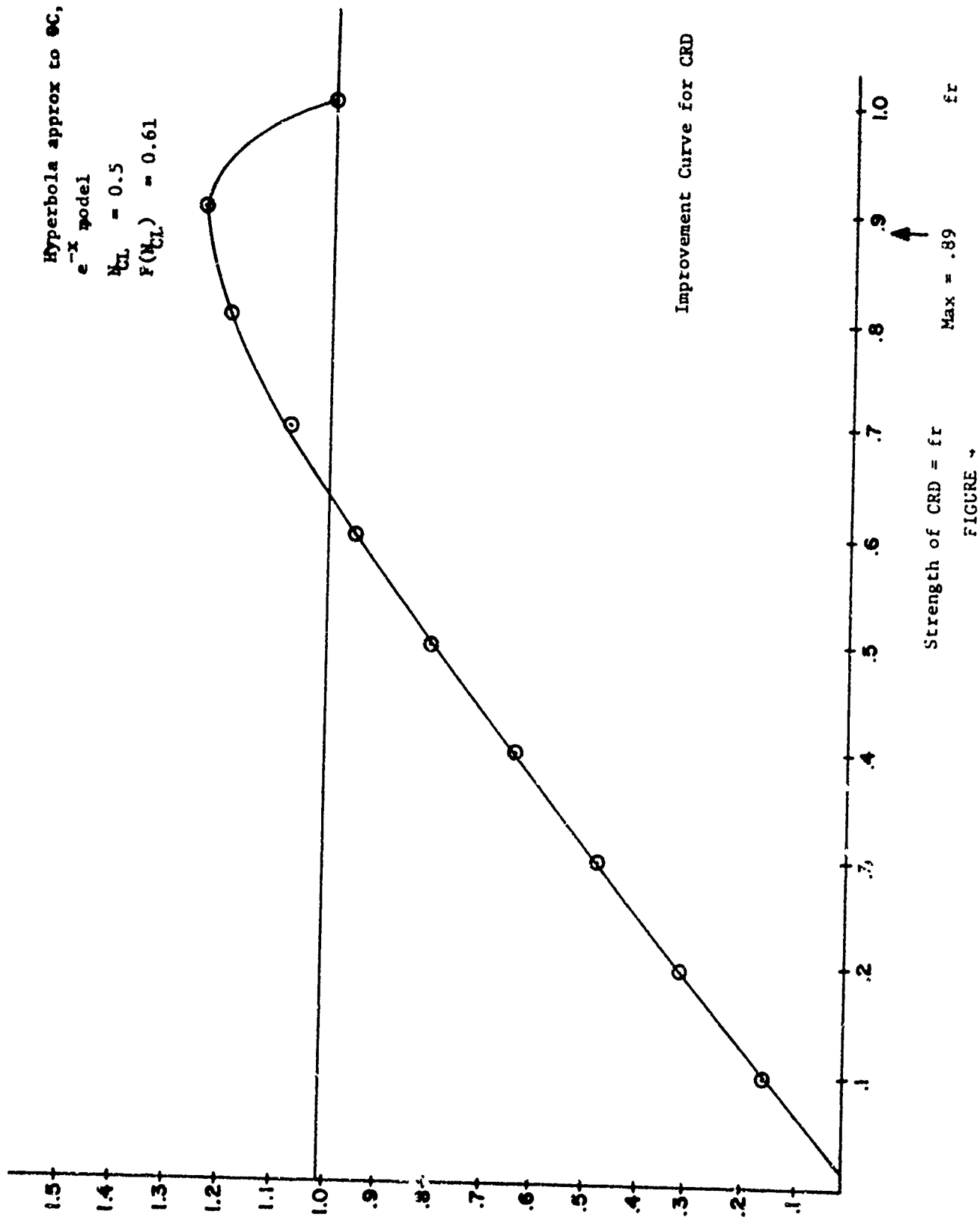
Hyperbola approx to e^{-x} model
N_{CL} = 0.5
$F(N_{CL})$ = 0.61
Improvement Curve for CRD
Strength of CRD = fr
Max = .89
fr
Improvement of Aircraft Observability = N_{AC}'/N_{AC}

FIGURE

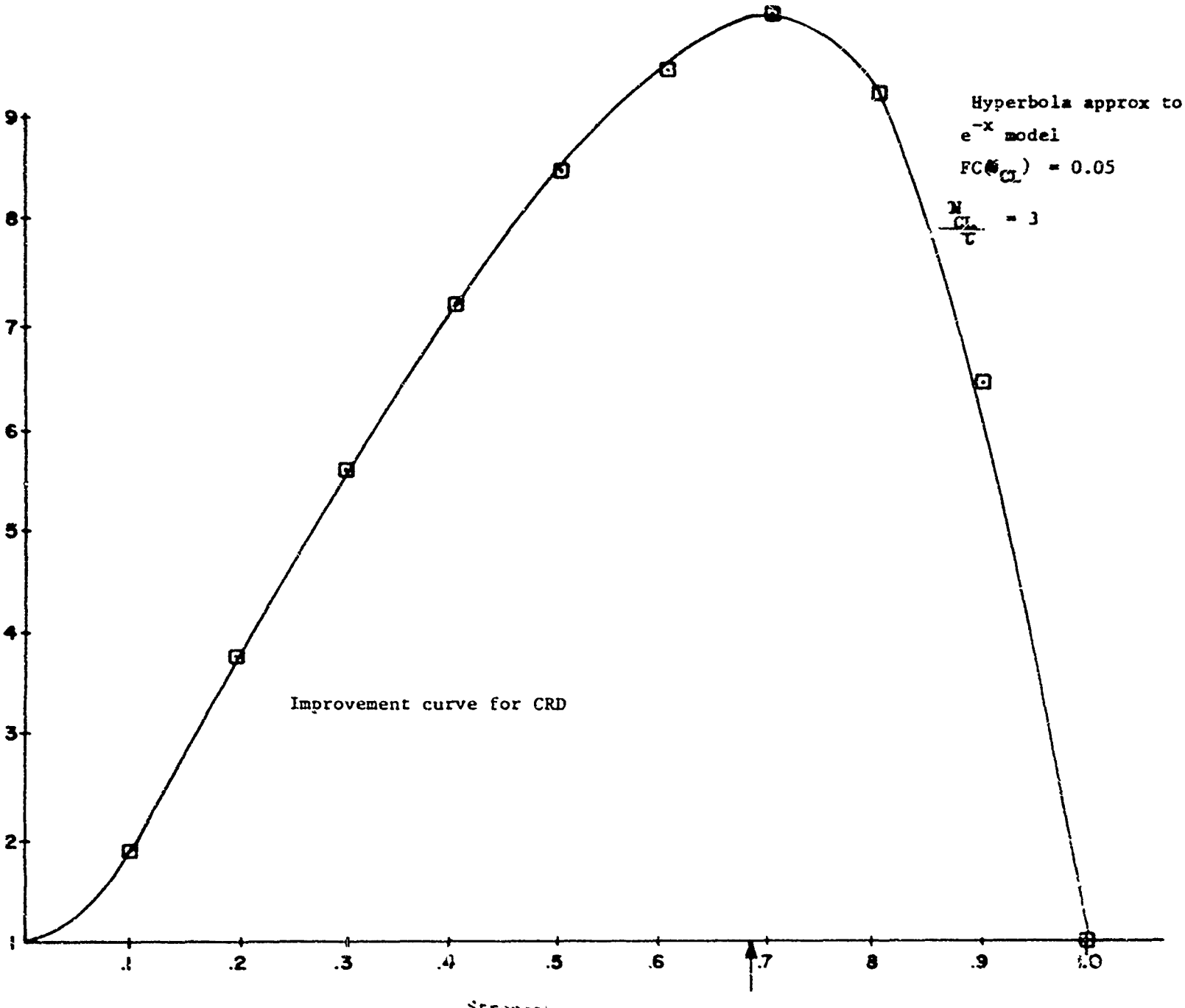

APPENDIX C-1

Figure 3

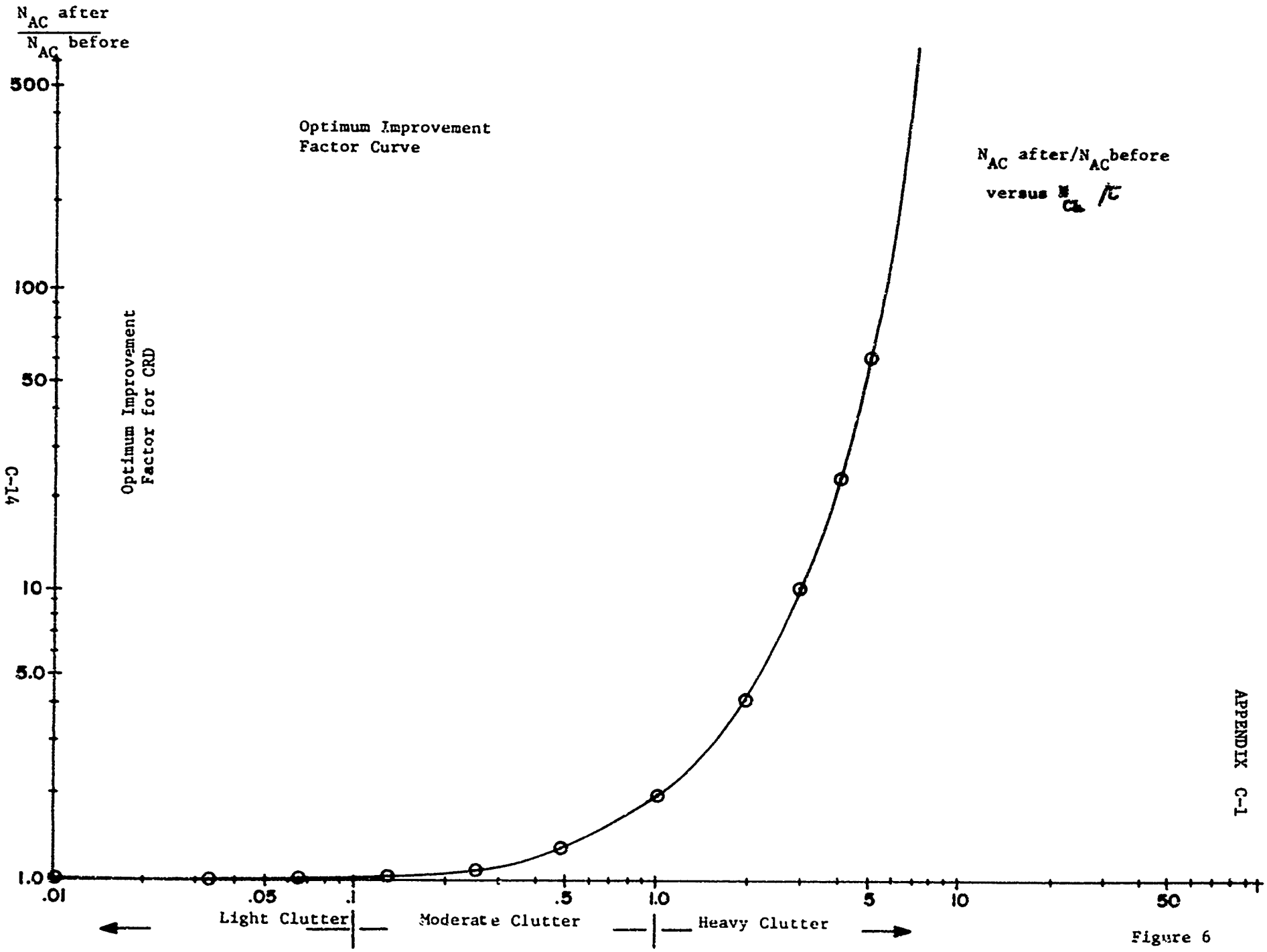
N_{AC} after / N_{AC} before
500
100
50
10
5.0
1.0
Optimum Improvement Factor Curve
N_{AC} after/N_{AC} before versus N_{CL}/C
Optimum Improvement Factor for CRD
C-14
.01
.05
.1
.5
1.0
5
10
50
Light Clutter
Moderate Clutter
Heavy Clutter
APPENDIX C-1

Figure 6

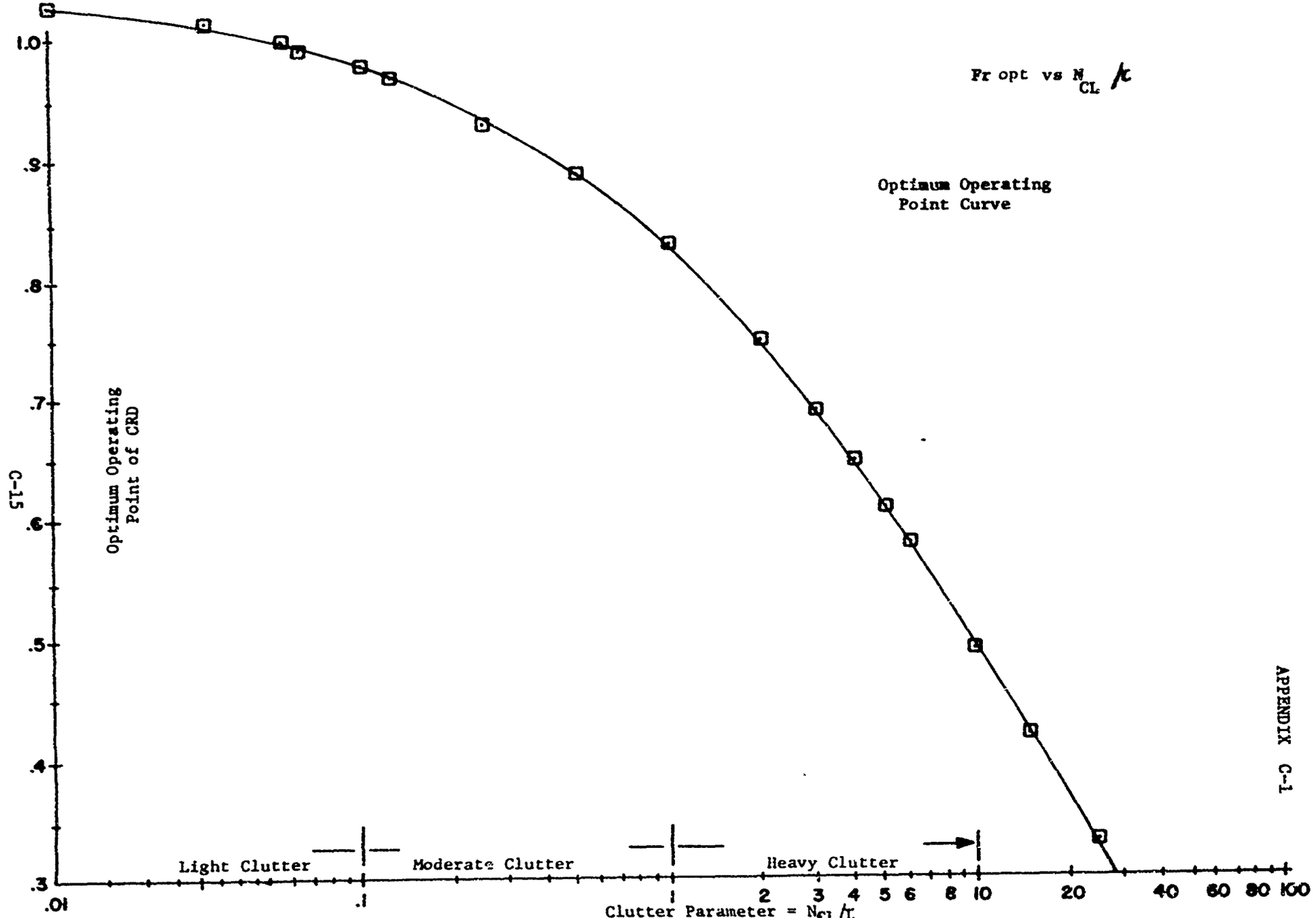
Fr opt vs N_{CL}/τ
Optimum Operating Point Curve
Optimum Operating Point of CRD
C-15
1.0
.9
.8
.7
.6
.5
.4
.3
.01
.1
Light Clutter
Moderate Clutter
Heavy Clutter
2
3
4
5
6
8
10
20
40
60
80
100
Clutter Parameter = N_{CL}/τ
APPENDIX C-1

Figure 7

Finally returning to Figure 2, the upper curve represents the new operating curve for the radar-CRD-man system and indicates the maximum improvement which can be achieved within this model for this device. This improved curve is very much model dependent as Figure 8 illustrates. Here the same calculations have been performed with an e^{-x^2} model. In both cases, the horizontal dashed line represents the ideal case of no target losses regardless of clutter conditions and the closer the final curve approaches this line, the more effective is the CRD.

It is perhaps of interest to consider these two sets of curves in more detail in order to gain some appreciation of the effect of this process. Table 1 illustrates the pertinent points. For the e^{-x^2} model in moderate clutter and before application of the CRD, the radar-man system is finding 78% of targets actually there Afterwards, the radar-CRD-man system finds 92% of the original number of targets. As the clutter level increases, the improvement also increases, although as can be seen for the simple exponential model, an improvement of a factor of 10 to 1 is not enough as only about 51% of the targets are detected after application of the CRD.

There exists an intriguing special case of a CRD for which $f_r = f_r'$ describes the operating curve. This device is utilized almost daily in every radar system in existence. It is the familar gain control Interestingly, if the gain is reduced, both targets and clutter are reduced equally, however, with either of these models, due to the non-linear characteristics of observer, there is an actual increase in the detection capabilities of the system. (This of course assumes no difference in the amplitudes found for the clutter and the targets.) Figures 9 and 10 are the corresponding curves for the two models considered with the gain control used as a CRD. It is clear that some improvement can be achieved by decreasing the gain but only in very heavy clutter situations and even then the fraction of targets detected is still miniscule. Although if it is absolutely necessary to operate with such high clutter densities, then by all means turn the gain down, as the improvement is significant.

If, in fact, amplitude is a useful discriminate between clutter and valid targets, the gain control will act as a CRD and even greater improvement factors can be achieved for such targets.

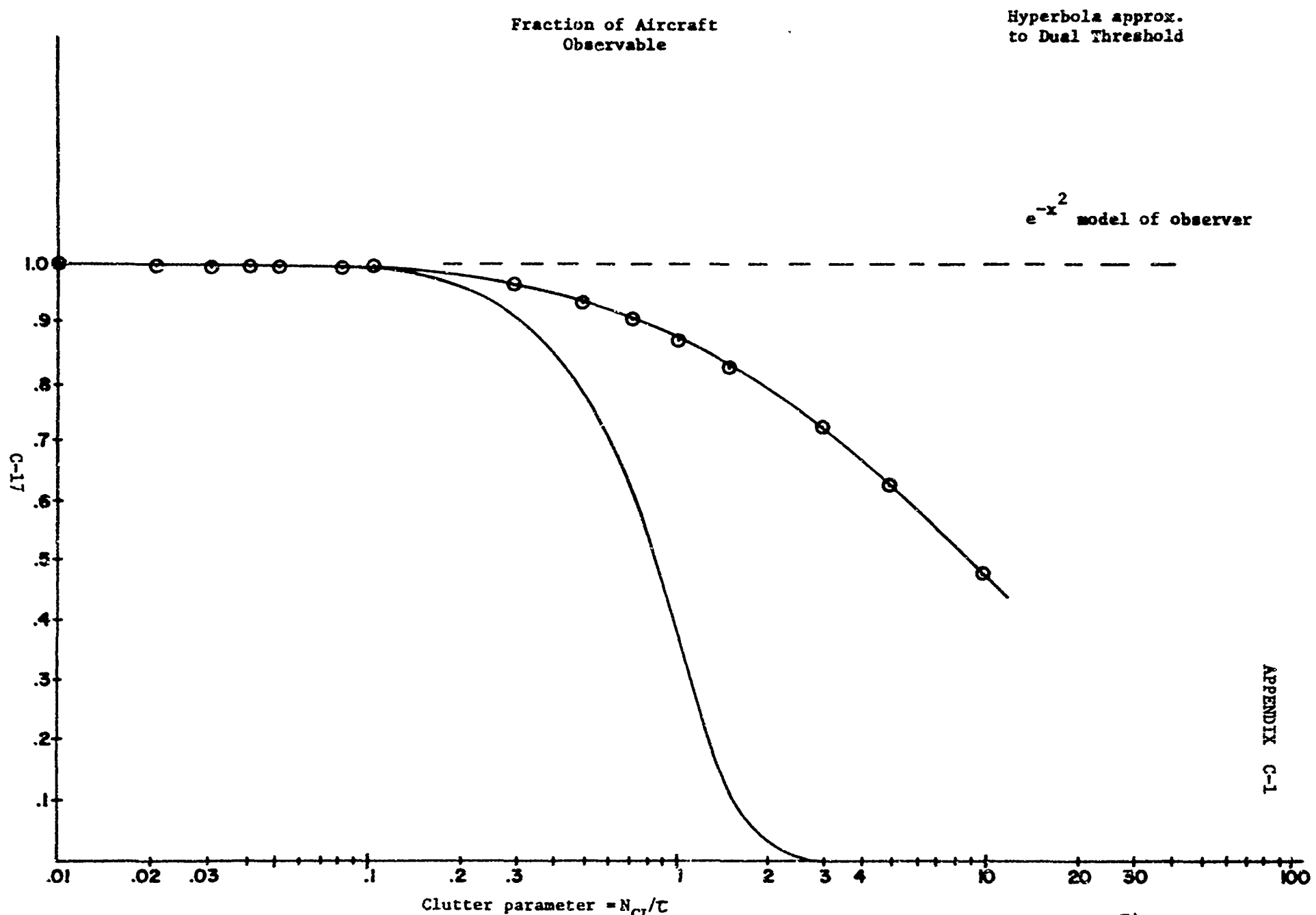

APPENDIX C-1

Figure 8

APPENDIX C-1

TABLE 1

FRACTION OF OBSERVABLE AIRCRAFT

Model Clutter Condition $= N_{CL}/$	e^{-x}		e^{-x^2}	
	Before CRD	After CRD	Before CRD	After CRD
Moderate Clutter .5	.61	.78	.78	.92
Heavy Clutter 3	.05	.51	1.2×10^{-4}	.71

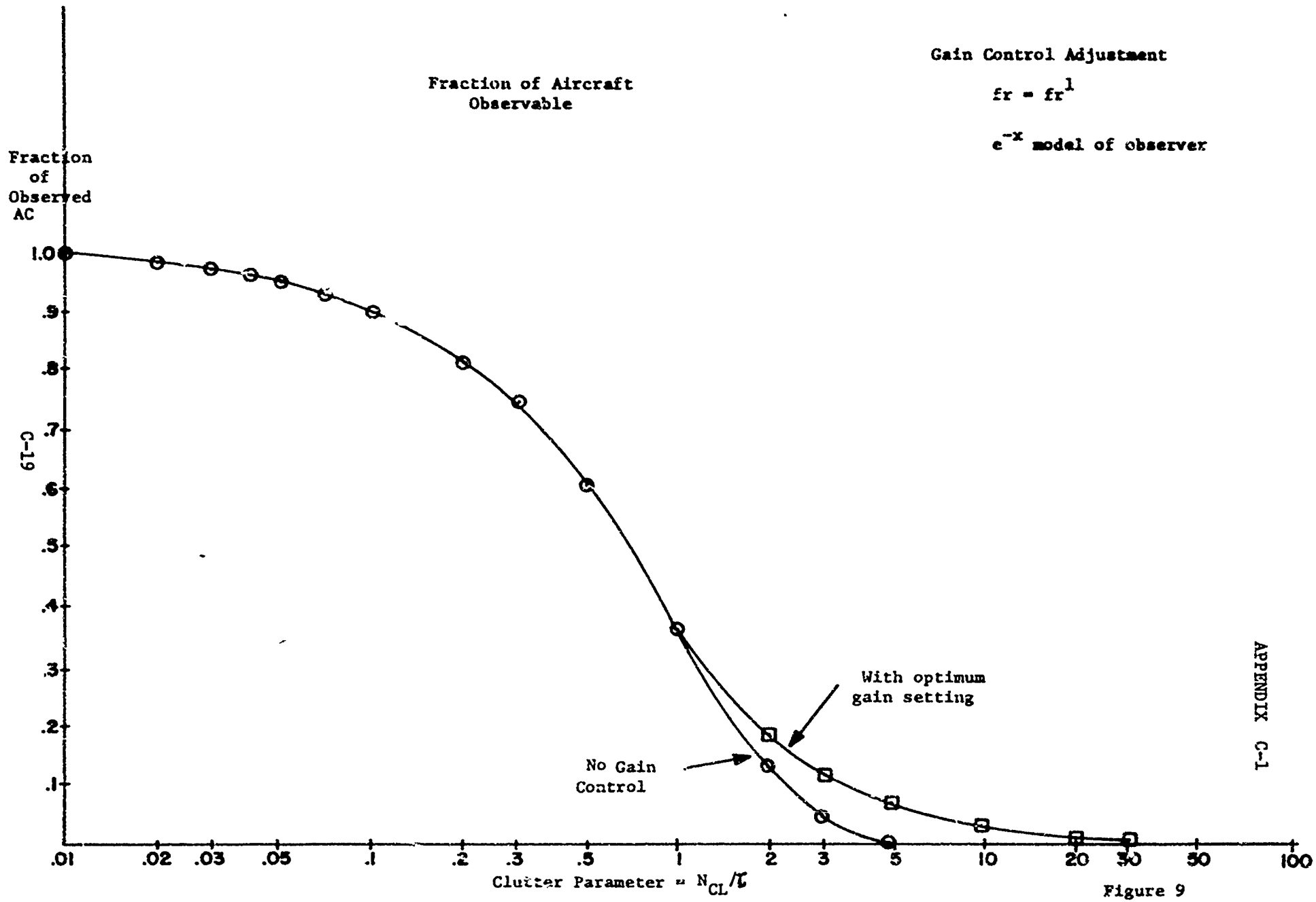
Fraction of Aircraft Observable
Gain Control Adjustment
$fr = fr^1$
e^{-x} model of observer
Fraction of Observed AC
1.0
.9
.8
.7
.6
.5
.4
.3
.2
.1
With optimum gain setting
No Gain Control
.01
.02
.03
.05
.1
.2
.3
.5
1
2
3
5
10
20
30
50
100
Clutter Parameter = N_{CL}/τ

Figure 9

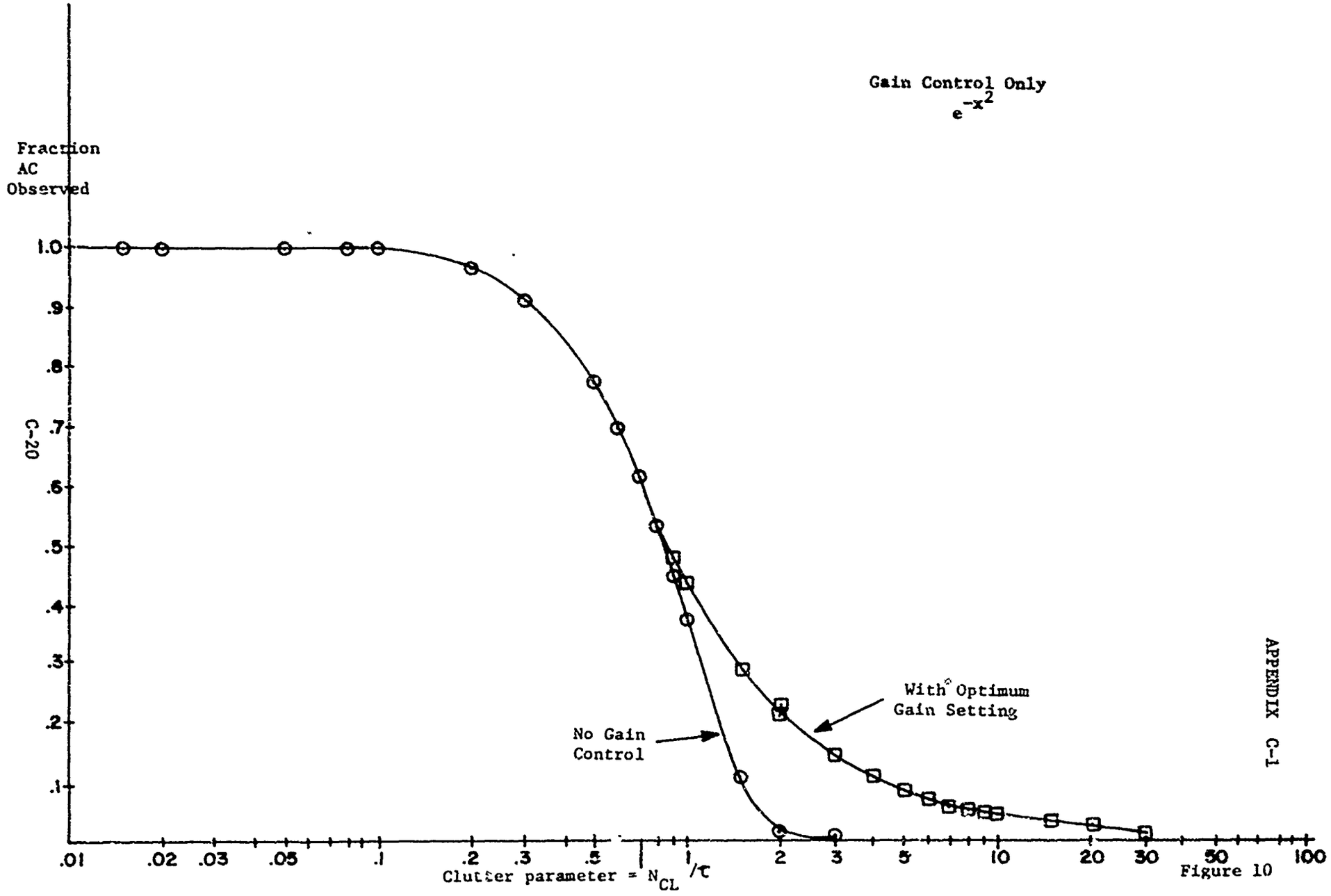

APPENDIX C-1

Figure 10

As it turns out, this is indeed the case for angels and aircraft, as the great preponderance of angels are very weak targets. Thus, reducing the gain can selectively reduce clutter returns, increasing the detectability of aircraft as described above. Figures 9 and 10 therefore, represent the minimum possible improvements within these models for the gain control CRD, with more improvement possible if clutter and targets can be reasonably separated by amplitude.

Other models of the operator-receiver system and other CRD's will yield similar conclusions and although specific results will be model dependent, it is clear that with a monotonic decreasing non-linear operator detection curve similar maximization effects can be found for realistic CRD's. Such devices will, in fact, increase the number of targets which can be detected. The price is the loss of a few targets rejected by the device, but this loss can be made smaller than the increase in targets newly detectable, resulting in a net increase in detectable targets.

Adaptive Systems

The concern so far has been with the effect of clutter masking as viewed over the whole PPI. Normally occurring clutter, appears only in subregions of the PPI, with other subregions remaining relatively clear. This means that subregions of the PPI display should be individually processed by a CRD operation with the optimum parameters for that subregion. This effect can be achieved by use of various adaptive feedback systems. What is needed is some measure of the clutter intensity as indicated by the ratio N_{CL}/τ.

It is possible, by monitoring both the input and output signals of the CRD to calculate the clutter parameter N_{CL}. Figure A below illustrates the operation of the CRD in terms of number of input hits (N^o) and number of output hits (N')

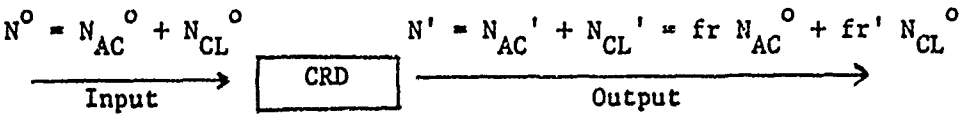

FIGURE A

By observing both these numbers, and from a knowledge of the operating point of the CRD, one finds,

$$N_{CL}^{o} = \frac{(N' - fr\ N^{o})}{fr' - fr} \tag{16}$$

where fr' is given by equation 13. The operator then can dial in a value of r, indicating his particular capabilities with handling clutter. The value of N_{CL}/τ would thus be available for feeding back into the CRD to adjust for the optimum operating point for the clutter conditions. For example, in the linear exponential model, the optimum operating point is characterized by,

$$fr^{optimum} = 1.06\left(1 + .03\,\frac{N_{CL}}{\tau}\right)\left(1 - \left(1 - \frac{1}{(1 + .03\,\frac{N_{CL}}{\tau})^{2}}\right)^{\frac{1}{2}}\right) \tag{17}$$

while for the squared exponential

$$fr^{optimum} = X - P/3 \tag{18}$$

where

$$X = A^{+} + A^{-}$$

$$A^{\pm} = -\frac{b}{2} \pm \left(\frac{b^2}{4} + \frac{a^3}{27}\right)3$$

$$a = 1/3\ (3q - p^2)$$

$$b = 1/27\ (2p^3 - 9pq + 27\ R)$$

and

$$p = .0076\ \left(\frac{N_{CL}}{\tau}\right)^{2} - 3.18$$

$$q = 3.371$$

$$R = -1.191$$

These exact relationships are undoubtedly too complicated for quick evaluation, thus some approximation will most likely be made in practice. In principle, however, the feedback can be accomplished

exactly within these models using this procedure. The feedback delay between the actual calculation of N^o and N' and the actual modification of the operating parameters of the CRD will depend on the type of clutter considered, although a delay of one or two sweeps would appear to be appropriate.

Target Identification

For many purposes it is not desirable to merely eliminate clutter from the PPI-observer system. The elimination of the clutter from the system, as shown, can improve target detectability, but can then result in the observer vectoring aircraft into the clutter regions on the PPI which have been cleared by the CRD. If the clutter consists of birds as in the example considered, the results can be particularly disastrous. Thus it is particularly desirable to display the clutter on the PPI. This, in turn, would reduce target detectability, at least with present display systems.

The obvious conclusion is to have some unique method of identifying targets and clutter on the PPI display (such as color, or symbology). Target detectability is, after all, really "target identification". The analysis so far has considered either the presence or absence of clutter and targets and their interaction as the primary effect. Actually, the same effects and conclusions can be drawn if the problem is viewed as a target identification problem, with all returns continuously on display, but separated now by various display techniques into target types. Now the display of the clutter targets can prevent the vectoring of aircraft into clutter targets, measurably improving system performance and safety.

Generalization

Although the presentation has been covered in terms of the interactions between a radar system and its ovserver, the conclusions actually are more general, applying to any information handling system where some desired information must be sorted from undesired clutter information. In general, this unwanted clutter information will mask the actual information, reducing information transmittal rate of the system and increase the need for redundancy to assure the completeness of information actually transferred. Thus, this more general system may be described by a monotonically decreasing function describing the fraction of the original information received from the

system by the observer in the presence of clutter. This function will satisfy a relation equivalent to equation 1 where the symbols now represent information content instead of target counts. As a result, the derivations of the previous sections can be developed for this system and similar conclusions will be found.

For example, if there exists some sort of clutter reducing device, which of course will also eliminate some of the desired information, and if it is possible to satisfy equation 8 with this device, then the information transmitted can be increased by reducing the effects of clutter masking. This indicates how the generalization to arbitrary systems can be developed, although the existence of the device with the required parameters is not always assured.

APPENDIX C-2

ANALYSES OF AREA MTI PERFORMANCE FOR ANGEL CLUTTER REDUCTION

1. Summary

An analytical model of an Area MTI is derived. The model reflects the interactions of random bird velocity, single-scan thresholding, different area MTI designs, dense angel clutter effects, and operator masking effects. A practical baseline design is evaluated with the model, resulting in the conclusion that the Area MTI improves on single scan processing only if 1) angel densities are light, and 2) aircraft detection by an operator would be severely masked by angel clutter breakthrough.

2. Introduction

Scan-to-scan or Area MTI is a technique which discriminates against slow moving and stationary targets by means of the change in their position from scan-to-scan. The measured position of all declared targets for one scan is stored in a digital memory. On the next scan, the measured positions of new targets are compared with the stored position; if there are any scan-to-scan correlations, corresponding to low velocities, the new data is not displayed. For the ASR scan rate, a 60 knot target moves 410 feet (one pulsewidth) from scan to scan.

While Doppler or pulse-to-pulse MTI discriminates only on the basis of radial velocity (range rate), Area MTI discrimination involves total velocity in any direction. Since bird velocities are, on the whole, significantly smaller than aircraft velocities, Area MTI seems to be of potential value in reducing angel clutter. Area MTI can be interfaced with single-scan processing (such as 5/5 correlation) and an operator as shown in Figure 1.

There are two main types of Area MTI, with several variations on each type: Sector Map and Target Store.

The Sector Map Area MTI divides the surveillance area into a grid on non-overlapping sectors; each range-bearing sector (or cell) is

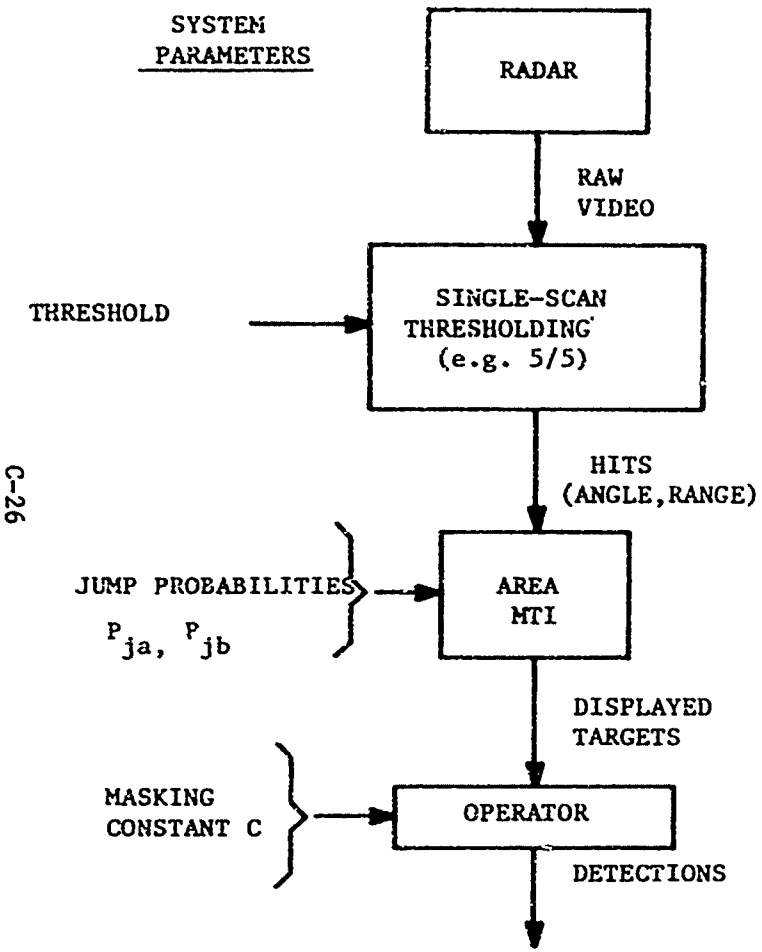

OUTPUT PARAMETERS	MODEL EQUATIONS
P_a, P_b	$P_b = P_a^4$
	$(P_{dis})_a = (p_a(1-p_a) + p_a^2 P_{ja}) e^{-\rho A p_b}$
$(P_{dis})_a$, $(P_{dis})_b$	$(P_{dis})_b = (p_b(1-p_b) + p_n^2 P_{jb}) e^{-\rho A p_b}$
Pd	$Pd = (P_{dis})_a e^{-\rho AC} (P_{dis})_b$

FIGURE 1. AREA MTI INTERFACES

represented by one bit in a sector map. If a target is detected in a certain sector, the storage bit for that sector is set to 1; otherwise, the bit is reset to 0. When the data for the new scan comes in, the cell is displayed only if the old scan-new scan bit pattern is 0, 1.

The sector map can be implemented fairly easily. If cell quantization of 1/16 nmi by 0.75° is used in a map out to 15 nmi, then digital storage of 115,200 bits is required. In addition, fairly simple logic can be constructed to report the presence of a hit within a cell.

The Target Store Area MTI stores the range and bearing of the centroid of each target detected during a scan. When a target is detected on the new scan, data from the old scan are searched to find a target within a range-bearing correlation window corresponding to low velocity. If a correlating target is found, the new target is not displayed.

The Target Store Area MTI is most easily implemented with a small digital computer; the target store, search, and correlation operations make hardware designs fairly complicated. To avoid a delay of the displayed data relative to radar input, two target stores are required: Input (to store new targets as they come in) and Process (to search for correlating targets). If 500 targets are to be processed, about 2K to 4K of sixteen-bit memory is required.

In the following sections, simple analytical models will be derived and used to determine the performance of the Area MTI under various conditions. In Section 3, the basic mechanism for bird-aircraft discrimination is explained and a first-cut design at an Area MTI is suggested Details of this design are attended to in Section 4, 5, and 6. The model is extended in Section 7 to describe the interaction effects of multiple angels in a dense clutter environment. In Section 8, the effect of operator interaction is examined.

3. Display Probability

The performance of any Area MTI in angel clutter can be modeled very simply by two numbers. One represents the probability that an aircraft leaves the correlation bin it was in during the last

scan; the other is the probability an angel leaves the bin. The bin corresponds to a sector cell in the Sector Map Area MTI or to the correlation window in the Target Store Area MTI. An ideal Area MTI would be configured so that all aircraft move so fast that they always leave their original bins, while birds never leave their original bins. Denoting the aircraft and bird "jump" probabilities by P_{ja} and P_{jb} respectively, the ideal Area MTI has $P_{ja} = 1$, $P_{jb} = 0$. A practical design objective might be $P_{ja} = .9$, $P_{jb} = .2$; 90% of the aircraft and 20% of the birds, on the average, leave the bins from scan to scan.

The probability that a bird or angel target is displayed can be found easily by enumerating the two ways display can come about. First, if a given target is detected by the radar on the present scan but not on the previous scan, the Area MTI detects no correlation and thus displays the target (It is assumed here that there is no interaction from other targets; angel densities are frequently low enough so that this assumption is approximately valid The more general case is treated in Section 7.) The other way a target can be displayed is if it is detected on both scans and also jumps out of its correlation bin between the scans. If aircraft and bird detection probabilities are denoted by p_a and p_b and detection is assumed independent from scan-to-scan, then the aircraft and bird display probabilities, $(P_{dis})_a$ and $(P_{dis})_b$ respectively, can be found:

$$(P_{dis})_a = p_a (1 - p_a) + p_a^2 P_{ja} \quad (1)$$

$$(P_{dis})_b = P_b (1 - P_b) + P_b^2 P_{jb} \quad (2)$$

Figure 2 shows how the display probability depends on detection and jump probabilities, which are a function of bin size relative to angel and aircraft motion between scans and the target position within the initial bin. For a properly selected bin size, aircraft would tend to fall on one of the curves with high P_j (0.8 to 1.0); birds on a curve with low P_j (0.0 to 0.2). It is interesting to note that an Area MTI which is effective against birds ($P_j = 0.0$) discriminates better with a P_b of 1.0 than with a P_b of 0.5. This corresponds to the fact that stationary targets are displayed only when a miss-hit pattern occurs; this pattern is most likely at $P_b = 0.5$.

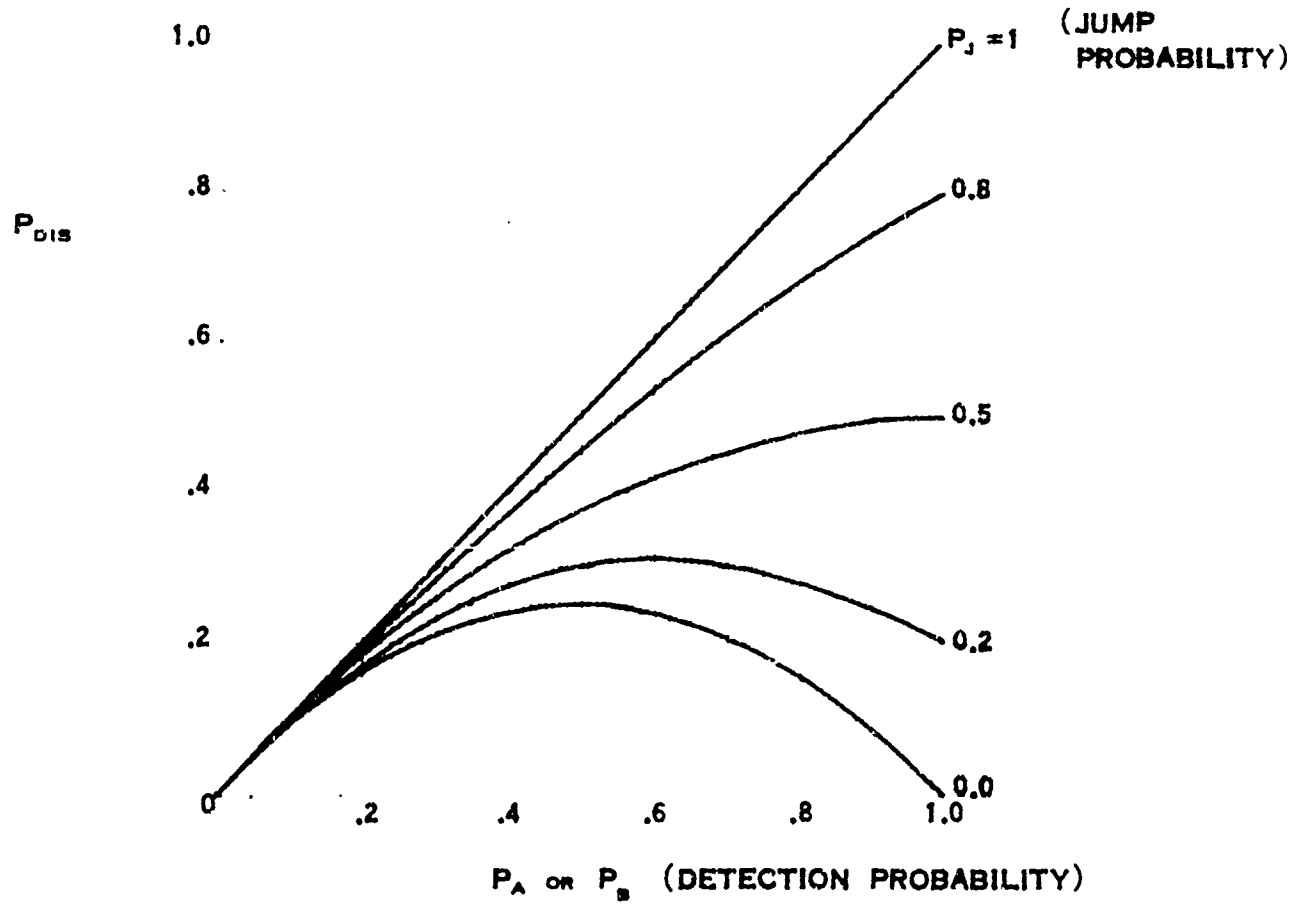

FIGURE 2 DISPLAY PROBABILITY FOR AREA MTI

Figure 3 illustrates the effect of an Area MTI on aircraft and bird display probabilities. Both curves show display probability with Area MTI versus display probability without Area MTI. Note that in all cases, the Area MTI reduces display probability (all points are below the 45° line). The significant point about Figure 3 is that birds with a high display probability before Area MTI turn out with much lower display probability after Area MTI; for example, 80% display probability is reduced to 29% by Area MTI. This means that birds which single-scan processing fails to remove are removed by Area MTI. When single-scan processing is effective, i.e , P_b = .2 or less, Area MTI does little to reduce this probability further. Thus, Area MTI might be viewed as insurance on single scan processing which becomes effective precisely when the latter fails.

The single-scan detection probabilities, p_a and p_b are related to each other by means of the single-scan thresholding technique used prior to the Area MTI. Desirable single-scan processing techniques maximize p_a while minimizing p_b. Figure 2.5-6 of Reference 2 in effect shows p_a versus $1 - p_b$ for three detectors: an amplitude-only threshold, a maximum run-length detector, and an M/N detector. The values of p_a and p_b are average values for the bird and aircraft tracks analyzed. To illustrate the relationship between single-scan processing effectiveness and Area MTI effectiveness, we will consider $p_a = (p_b)^{\frac{1}{4}}$ as a reasonable approximation to the measured points of the first of these three curves. This function is shown in Figure 4 as a dashed line. (Actually, what is shown as a dashed line is the display probabilities for an Area MTI which passes all aircraft and birds. From equations (1) and (2), if $P_{ja} = P_{jb} = 1$, then $(P_{dis})_a = p_a$ and $(P_{dis})_b = p_b$. Thus, the meaning of the dashed curve is that with no Area MTI, both display probabilities are low for very effective single-scan processing which detects few birds and few aircraft; as single scan processing is weakened, thus passing more birds and more aircraft on to the Area MTI, the locus of $(P_{dis})_a$ and $(P_{dis})_b$ follows the dashed path.

If an Area MTI is used, $(P_{dis})_a$ and $(P_{dis})_b$ are related to p_a and p_b by equations (1) and (2). If a particular set of Area MTI parameters is chosen, P_{ja} and P_{jb}, the jump probabilities, are fixed so that a particular curve $(P_{dis})_a$ vs $(P_{dis})_b$ is traced out as the

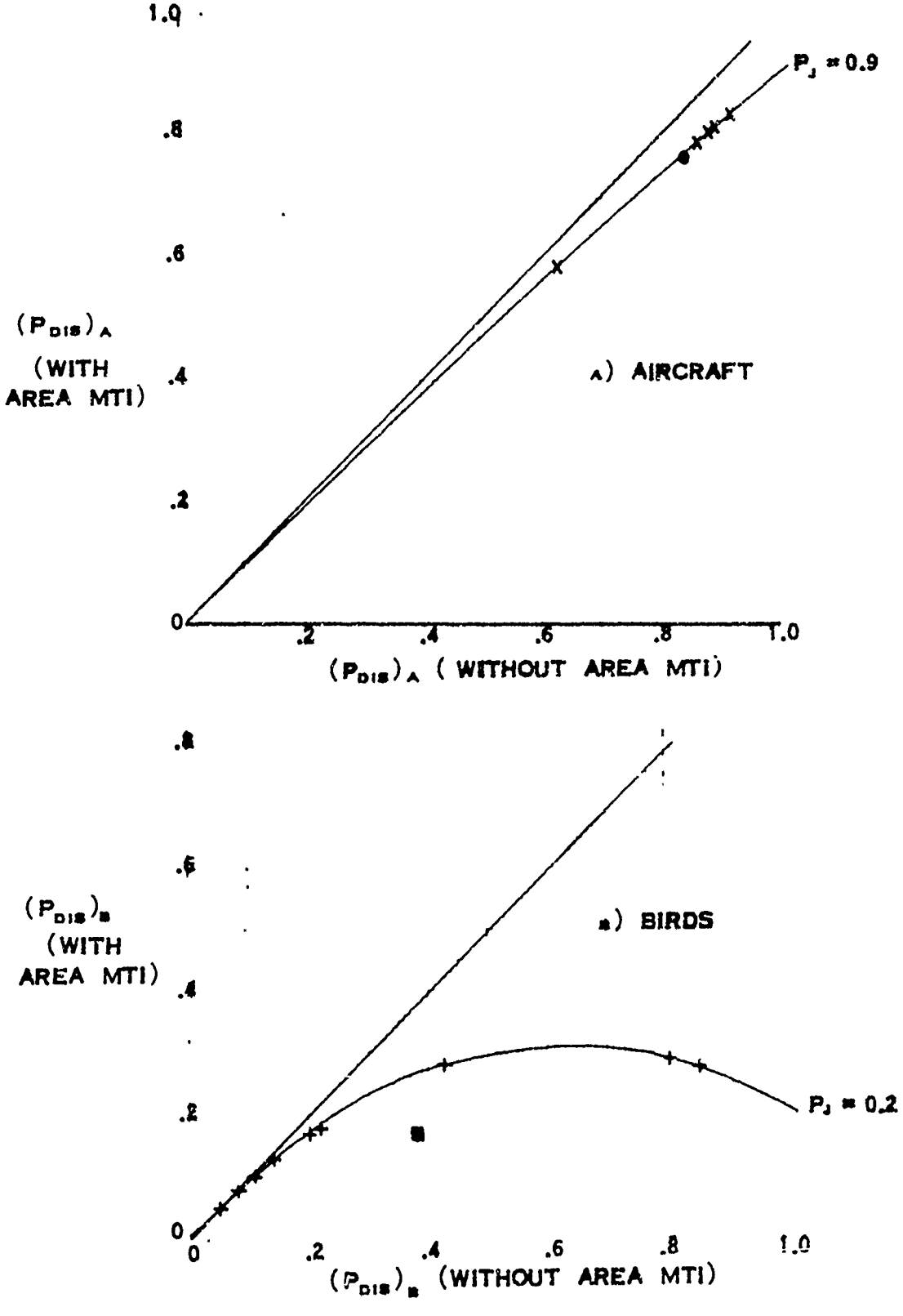

FIGURE 3 EFFECT OF AREA MTI ON AIRCRAFT AND BIRDS

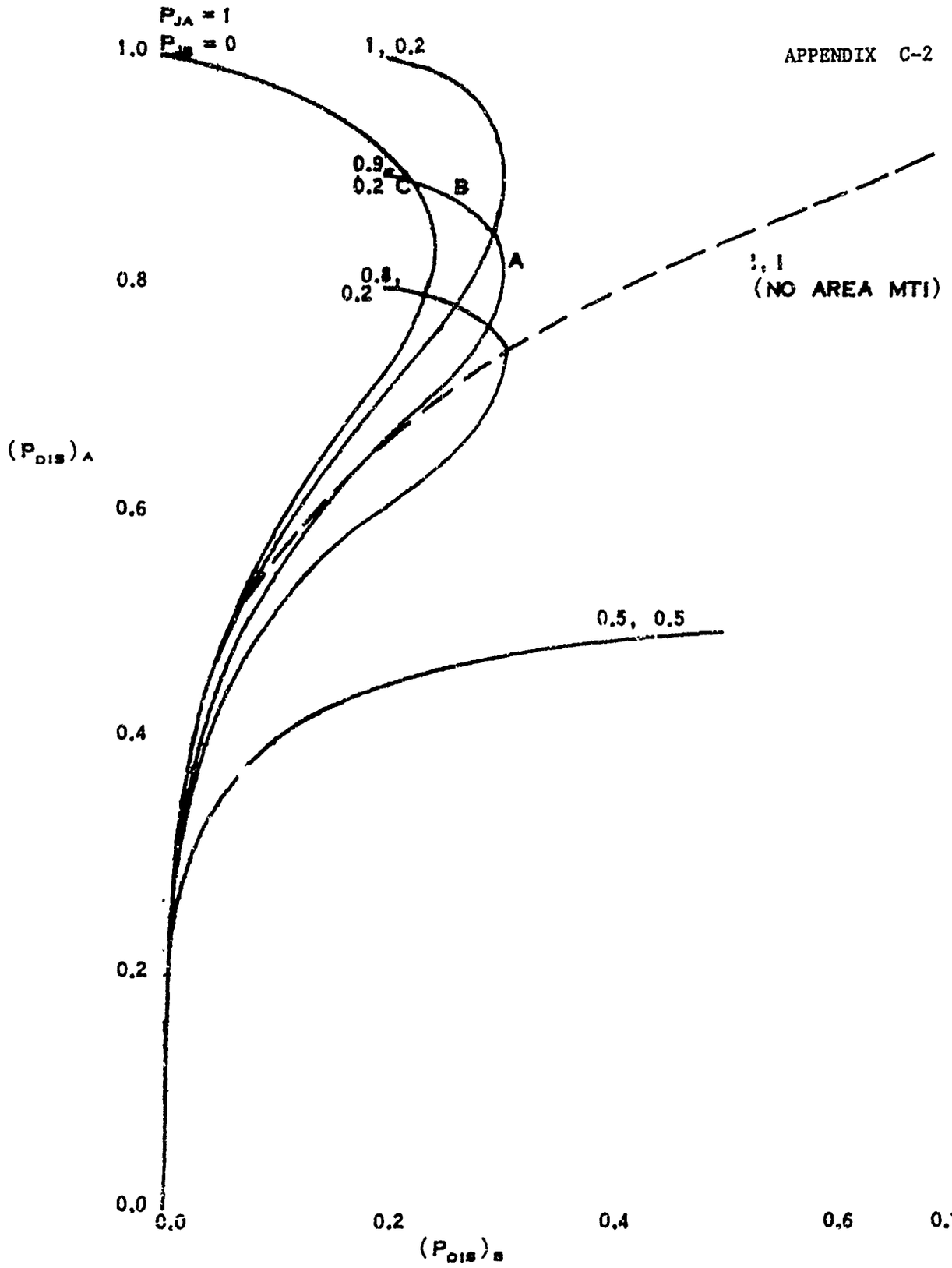

FIGURE 4 AIRCRAFT AND BIRD DISPLAY PROBABILITIES WITH AREA MTI

(PARAMETERS ARE AIRCRAFT AND BIRD JUMP PROBABILITIES P_{JA} AND P_{JB})

first threshold is varied parametrically. Thus, each pair (P_{ja}, P_{jb}) defines a different performance curve which can be used to judge various Area MTI parameters using display probabilities as criteria. Several of these curves are shown in Figure 4.

For example, it can be seen that any Area MTI that treats aircraft and birds equally (i.e., $P_{ja} = P_{jb}$) will actually degrade performance relative to no Area MTI at all. This is proved in Enclosure II. As an example, the case of $P_{ja} = P_{jb} = .5$ is shown. Every point on this curve lies <u>downward</u> and to the <u>right</u> of the dashed curve; in other words, a (.5, .5) Area MTI will decrease the aircraft display probability and increase the angel display probability.

An ideal Area MTI ($P_{ja} = 1$, $P_{jb} = 0$) always does better than no Area MTI at all; its points lie up and to the left of the dashed line.

A practical Area MTI design might achieve $P_{ja} = 0.8$, $P_{jb} = 0.2$. Figure 4 indicates that this Area MTI improves on single scan processing for some values of the single-scan threshold, and does worse for other threshold values. In order for the (.8, .2) curve to lie to the upper left of the dashed line, it turns out that p_b must be larger than 66%. Thus for this Area MTI, single scan processing must pass <u>at least</u> 66% of the bird reports in order to make Area MTI worthwhile.

A more desirable Area MTI would correspond to the (.9, .2) curve in Figure 4. In this case, p_b must exceed 24% in order to improve on single scan processing Points A, B, and C on this curve which correspond respectively to p_b = .5, .75, and 1.0, illustrate that performance is improved as p_b is raised. A reasonable design point might be point B, for which:

$$P_{ja} = .9 \tag{3}$$

$$P_{jb} = .2 \tag{4}$$

$$p_a = .93 \tag{5}$$

$$P_b = .75 \quad (6)$$

$$(P_{dis})_a = .875 \quad (7)$$

$$(P_{dis})_b = .27 \quad (8)$$

4. Area MTI Design

Design parameters such as type of Area MTI (Sector Map or Target Store), correlation box size, and data quantization will now be selected to satisfy equations (3) and (4).

The objective of this design is to pick the smallest possible bin size and largest possible range-angle quantization LSB size satisfying the 20% jump probability for birds. The smaller the bin, the more sensitive the Area MTI will be to slow-moving aircraft. The larger the quantization LSB the fewer bits that will be needed to store Area MTI data.

A reasonable bird model would include random heading of birds, a Rayleigh distribution of air speed, and a ground velocity which is the vector sum of air velocity (i.e., bird velocity with respect to the wind) and wind velocity. It is shown in Enclosure I that this model corresponds to a joint Gaussian velocity vector with a 30 knot standard deviation and a mean velocity in the direction of the wind. Wind speed will be modeled as 0 knots on a quiet day and 30 knots on a windy day.

With a jointly Gaussian velocity vector, it turns out that leaving the bin in the angle direction (probability P_θ) and leaving the bin in the range direction (probability P_R) are independent events, so that the total probability of leaving a bin is:

$$P_{jb} = P_R + P_\theta - P_R P_\theta \quad (9)$$

The Area MTI will be designed so that P_R and P_θ are approximately equal; in order that $P_{jb} = 0.2$, P_R and P_θ must be about 0.1.

5. Range Parameters

The correlation bin is first considered in the range dimension only. Let the bin length be Δ. A stationary bird has no chance of leaving the bin in one scan, while a bird traveling with a radial speed of Δ/T (where T is the scan period, 4 seconds) will always leave the bin in one scan. If the bird is randomly located in the bin, then velocities between 0 and Δ/T result in intermediate jump probabilities, as shown in Figure 5(a). This is the case for a target with deterministic velocity and the Sector Map Area MTI.

If a Target Store Area MTI is used with infinitely fine quantization of the range measurement, the target is certain to leave the bin if its velocity exceeds $\Delta/2T$, since it always starts out exactly in the center of the bin. Any velocity less than $\Delta/2T$ ensures that the target never leaves the bin from scan to scan. These conclusions are reflected in Figure 5(b).

Finally, if quantization q is used with the Target Store Area MTI, the resultant uncertainty in target position spreads out the slope of the curve, resulting in Figure 5(c). This curve can be viewed as intermediate between Figures 5(b) and (a).

If the above jump probabilities are integrated over the Gaussian bird velocity distribution derived above (30 knot standard deviation, 0-30 knot mean) then the average jump probabilities of Figure 6 are obtained. The solid and dashed lines represent the limiting cases of coarse and fine quantization (Figures 5(a) and (b)) respectively. See Enclosure III for the mathematical derivation.

In order to achieve the design goal of $P_R = 0.1$, it is evident from Figure 6 that Δ/T must be at least 120 knots and that some finite quantization (intermediate between the solid and dashed lines) will be acceptable. For example, a range quantization cell of q = 410 ft. with a range bin size of Δ = 1230 ft, gives $P_R = 0.031$ for zero mean wind and $P_R = 0.041$ for 30 knot mean radial wind.

Although these values (q = 410 ft., Δ = 1230 ft.) give conservatively low P_R, they will be chosen for practical reasons. The quantization corresponds to the ASR pulsewidth (1/16 nmi or 0.833 μsec) thus simplifying the radar-Area MTI interface. $\Delta = 3q$ corresponds to a quantized range window of $\pm 2q = \pm 1/8$ nmi, which is also easy to implement. Since $q < \Delta$, the design has taken on the

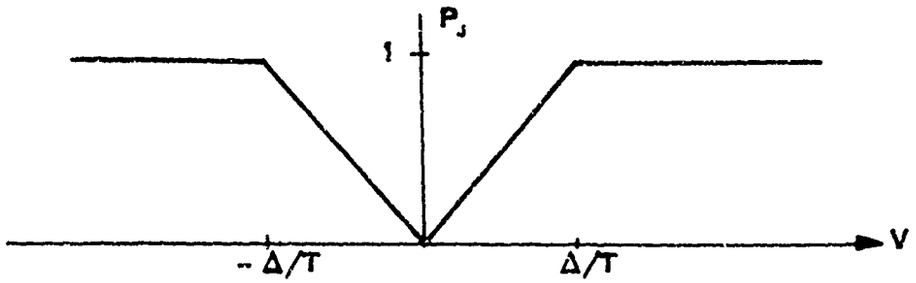

A) SECTOR MAP (QUANTIZATION = BIN SIZE, I.E. $Q = \Delta$)

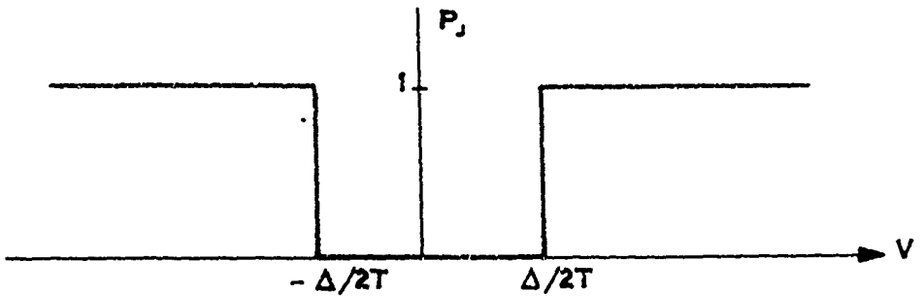

B) TARGET STORE - INFINITE QUANTIZATION ($Q = 0$)

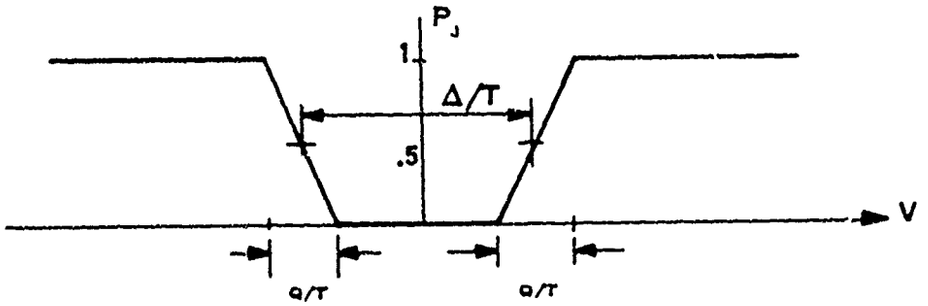

C) TARGET STORE - FINITE QUANTIZATION Q , $Q < \Delta$

FIGURE 5 JUMP PROBABILITY VERSUS VELOCITY

- ONE DIMENSIONAL BIN
- DETERMINISTIC VELOCITY
- RANDOM LOCATION IN QUANTIZATION CELL

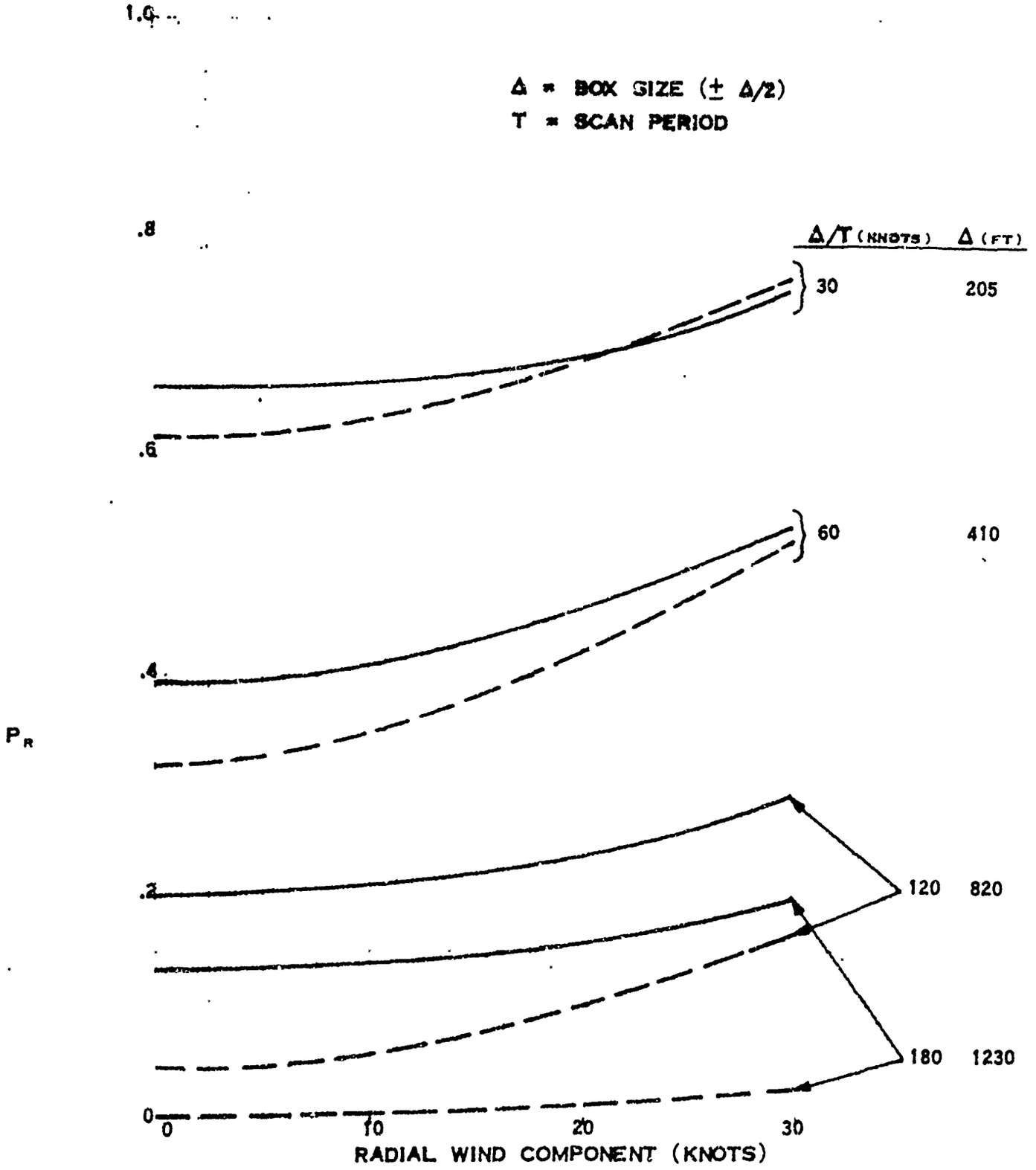

FIGURE 6 PROBABILITY OF TARGET LEAVING BOX IN RANGE

ONE-DIMENSIONAL BOX
RMS BIRD VELOCITY = 30 KNOTS
——— RANDOM LOCATION WITHIN BOX (Q = Δ)
- - - - - BOX EXACTLY CENTERED ON TARGET (Q = 0)

form of the Target Store Area MTI. This is not offered as the only possible design, but rather as a reasonable first-cut design.

With the above design, an aircraft moving in a radial direction must have a ground speed of about 120 knots or more in order to attain a 90% probability of leaving the bin in range and thus escaping cancellation by the Area MTI. This can be seen from Figure 5(c):

$$P_j \quad 0.9 \text{ for } v \quad \Delta/2T + q/2T = 120 \text{ knots}$$

6. Angle Parameters

Selection of quantization and bin size in angle is complicated by the fact that angle measurement errors at each scan effectively contribute to the apparent bird velocity fluctuations. At long range (i.e., approaching 15 miles) these measurement errors dominate the effective velocity standard deviation Thus, the angle parameters must be range dependent to ensure $P_\theta = 0.1$, which is the design goal of Section 4.

An RMS angle measurement error $\sigma_\theta = 0.2^o$ is a reasonable value for the ASR. This results in an effective bird velocity standard deviation in the tangential or angle direction as shown in Figure 7. Also shown is the apparent RMS velocity of an aircraft, for which the only contributing term is the angle measurement error

Since the highest probability of leaving the cell in angle occurs when the wind heading is tangential (i.e., perpendicular to radial) a worst-case 30 knot mean tangential bird velocity is assumed.

The simplest design, for angle parameters considered first, is the Target Store Area MTI with infinitely fine quantization (corresponding to the jump probability of Figure 5(b)). With this design, Δ must be large enough so that $\Delta/2T$ is about 1.28 standard deviations away from the mean velocity of 30 knots, since a Gaussian variable has a 10% chance of being more than 1.28 σ-units larger than its mean. This is illustrated in Figure 8. The lightly shaded area is the probability that birds leave the bin tangentially, P_θ; this must be set to 0.1. Thus given σ_{vb}, the bird velocity standard

FIGURE 7 RMS VELOCITY IN TANGENTIAL DIRECTION

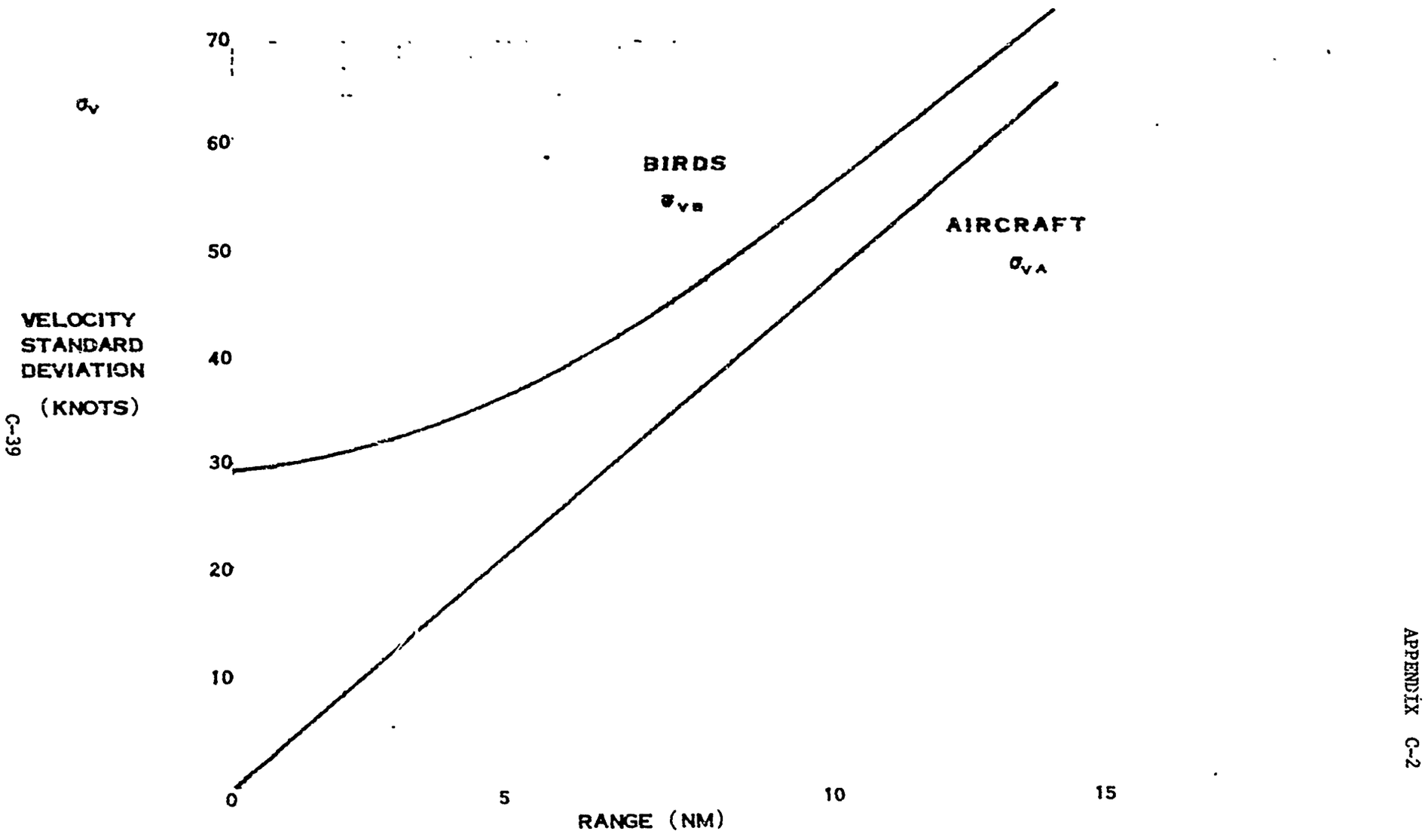

FIGURE 8 BIRD AND AIRCRAFT TANGENTIAL VELOCITY DENSITIES WITH TARGET STORE AREA MTI

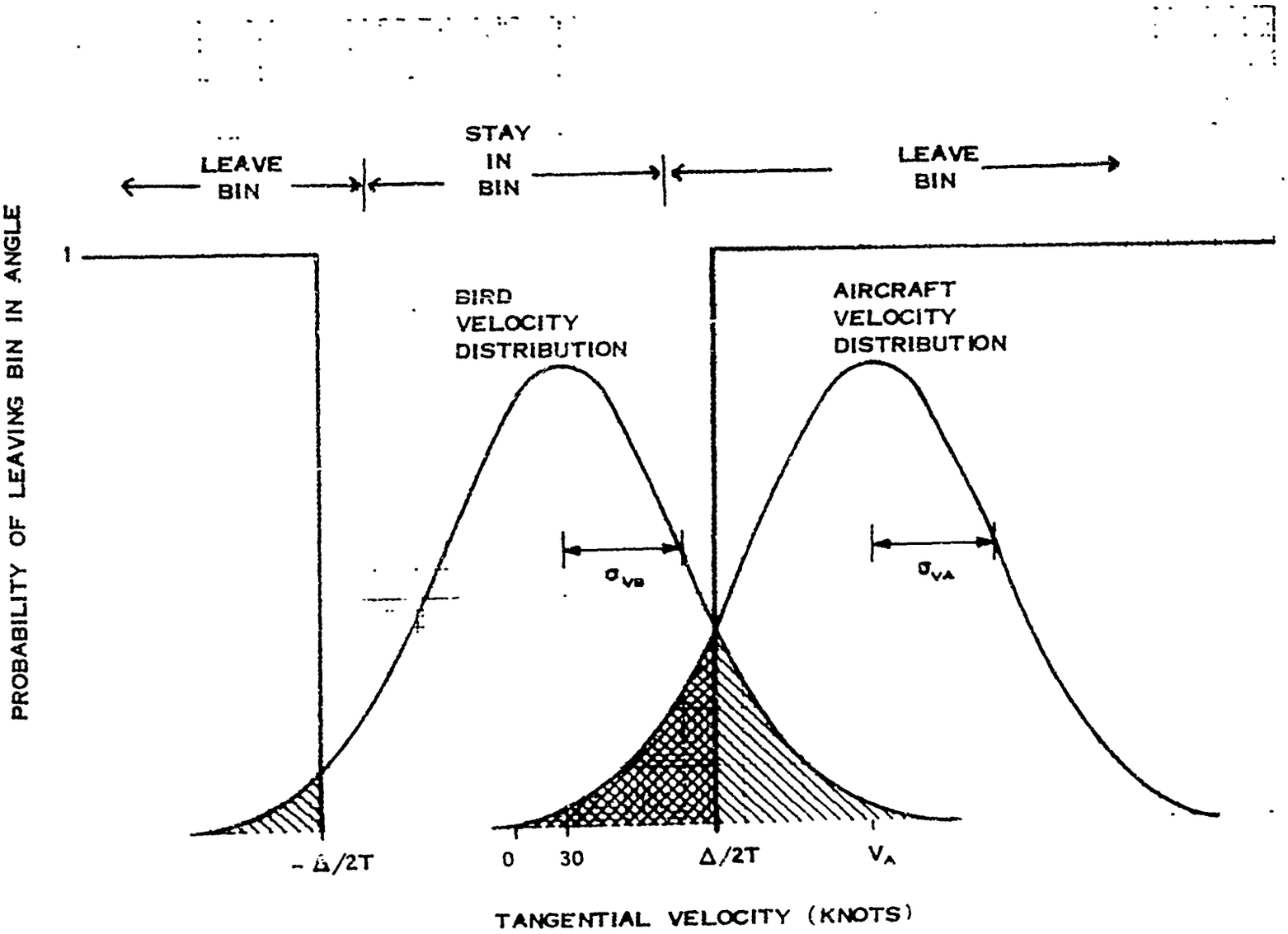

deviation, the bin size must satisfy:

$$\frac{\Delta}{2T} = 30 \text{ knots} + 1.28\ \sigma_{vb} \tag{10}$$

The resulting Δ is given in Figure 9 as a function of range. Δ varies from 0.15 nmi at close range to 0.27 nmi at 15 nmi.

With this bin size Δ, how fast must a tangential aircraft travel in order to achieve a 90% probability of leaving the box? Figure 9 indicates the answer is:

$$V_a = \frac{\Delta}{2T} + 1.28\ \sigma_{va} \tag{11}$$

With these values of V_a and Δ, the dark shaded area of Figure 8 can be held to 10%. The resulting aircraft ground speed is shown in Figure 9; V_a varies between 70 knots at close range and 210 knots at 15 nmi.

Up to this point is has been assumed that infinitely fine quantization has been used. In fact, angle quantization of 11 bits (LSB = 0.175°) turns out to give false alarm and detection performance essentially identical to infinitely fine quantization. Use of 10 bits or less essentially inhibits detection of aircraft moving less than 250 knots between 10 and 15 nmi. Thus 11 bits of angle quantization are necessary.

7. Effects of High Angel Density

Equation (1) and (2) of Section 3 give the conditional display probabilities for aircraft and birds, given that no other birds were detected in the target's new bin on the previous scan. If one or more were detected last scan, display would be inhibited this scan. The unconditional display probabilities are the right hand side of Equations (1) and (2), multiplied by the probability that no birds were detected in the given bin last scan.

It is assumed in this model that birds bunch randomly; i.e., have positions completely independent of each other. If the two

FIGURE 9 REQUIRED BIN SIZE IN ANGLE AND AIRCRAFT VELOCITY TO SATISFY TANGENTIAL DESIGN REQUIREMENTS

(P_θ = .1, P_{JA} = .9)

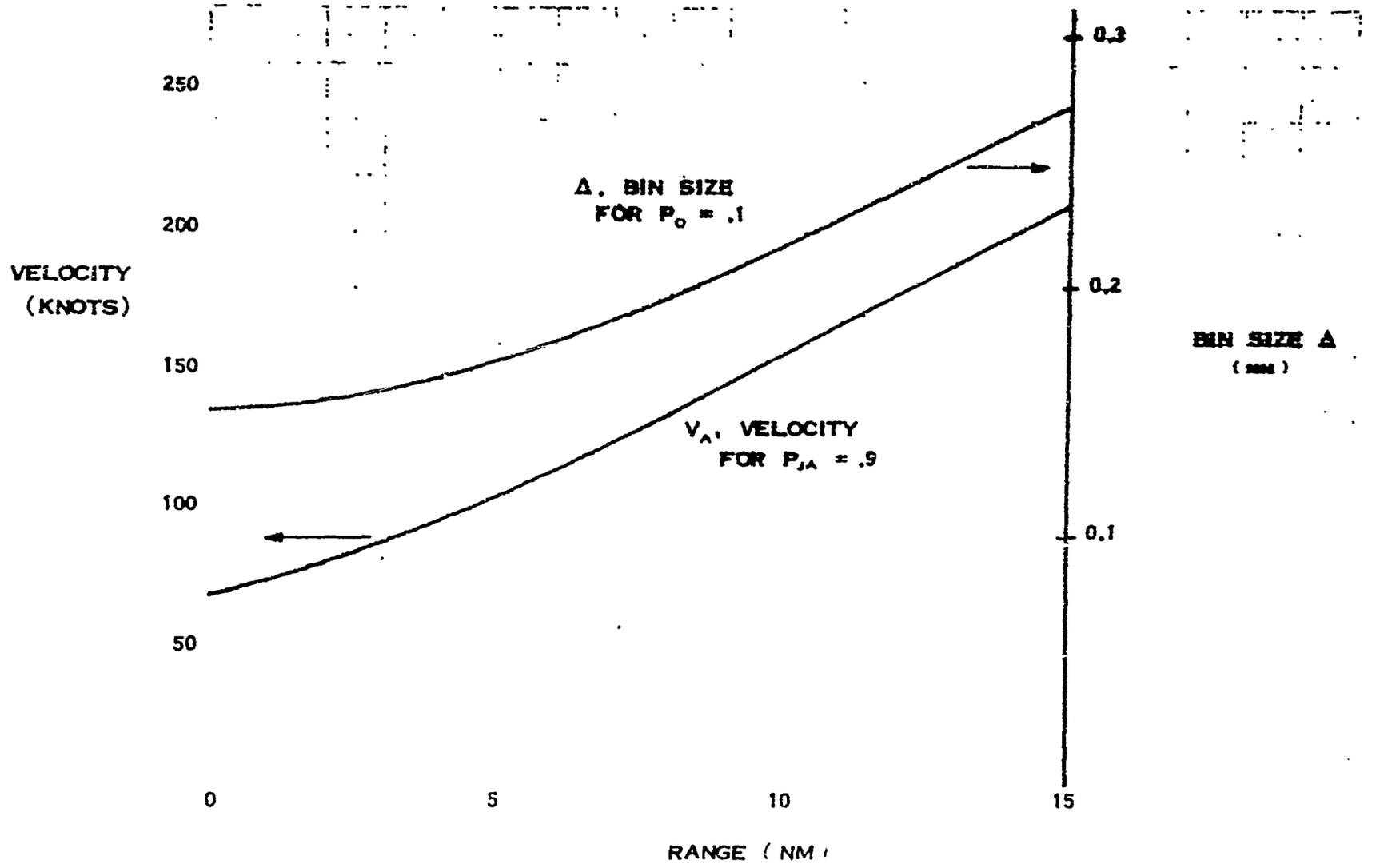

dimensional bird density is ρ birds/nmi^2 before single-scan processing, then it is $\rho\ p_b$ birds/nmi^2 after single scan processing. We can now conceptually divide a bin with area A into N cells, each with area A/N. If N is large, A/N is incrementally small, so that the probability that one or more birds are in a cell is $\rho\ p_b\ A/N$. The probability that there are no birds in a cell is $1 - \rho\ p_b\ A/N$. The probability that there are no birds in a bin (of area A) is just $(1 - \rho\ p_b\ A/N)^N$ which, for infinitely large N, approaches

$$P_r\ [\text{no birds in bin}] = e^{-\rho\ A\ p_b} \tag{12}$$

Combining this with equations (1), (2) we have:

$$(P_{dis})_a = (p_a\ (1 - p_a) + p_a^2\ P_{ja})\ e^{-\rho\ A\ p_b} \tag{13}$$

$$(P_{dis})_b = (p_b\ (1 - p_b) + p_b^2\ P_{jb})\ e^{-\rho\ A\ p_b} \tag{14}$$

Figure 10 shows the effect of varying clutter density (ρ A) on display probabilities. Each of the curves represents the locus of possible pairs of aircraft and bird display probabilities for constant ρ A and varying first threshold (i.e., varying p_a and p_b). Note that for $\rho\ A \geq 0.5$, the Area MTI always does worse than no Area MTI at all (i.e, the solid lines are below the dotted line meaning the Area MTI provides a lower $(P_{dis})_a$ for the same $(P_{dis})_b$ as no Area MTI). For $\rho\ A \leq 0.1$, the Area MTI is useful, but only if no single-scan processing is used (i.e., $p_a = p_b = 1$).

The important conclusions to be drawn from this model are that heavy angel clutter renders the Area MTI useless and that Area MTI helps in light clutter only if no single-scan processing is used.

8. Operator Detection with Area MTI

The Area MTI mathematical model at this point (reflected by equations (13) and (14)) describes the probability that a given bird or a given aircraft will appear on a display fed by information from an Area MTI. Additional bird/aircraft discrimination must be

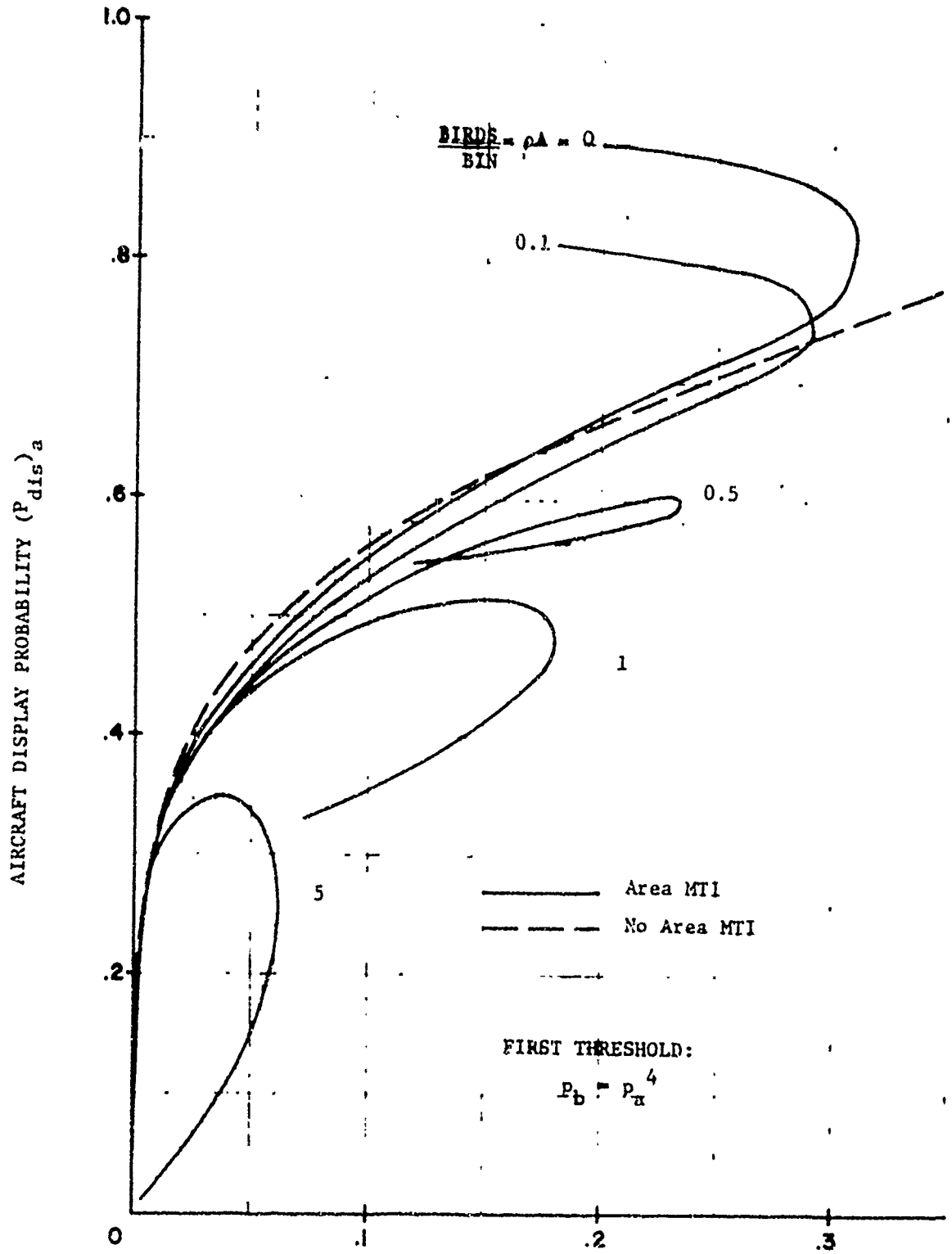

FIGURE 10. AREA MTI IN HEAVY ANGEL CLUTTER, $P_{ja} = 0.9$, $P_{jb} = 0.2$

supplied by an operator. Unfortunately, even if an aircraft is displayed, it may be rejected by the operator as a valid target if it is in a group of false alarms due to birds. This is called masking. At present we have only a rough qualitative concept of the effects of bird masking on operator detection; psychometric experimentation would be needed to quantify these concepts. However, a (somewhat speculative) model is proposed here to indicate the general trend. This model is due to J. Miller (Reference 3).

The basis of the model is a masking function, F(n) having the properties $0 \leq F(n) \leq 1$, $F(0) = 1$, and $F(n) \to 0$ as $n \to \infty$. In the masking model, F(n) is the probability that the operator detects an aircraft, given that the aircraft is displayed. In other words, it is the probability that the aircraft is not masked. Here n is the "effective average number of masking birds". For example, suppose the operator looks over an area A_{op} on the PPI (suppose A_{op} consists of many bins , each bin consisting of area A). The average number of birds in this area is ρA_{op}. The average number which "survive" Area MTI processing is $n = \rho A_{op} (P_{dis})_b$. This is the average number of birds which are effective in masking an aircraft. The unconditional probability that an aircraft is detected by the operator is:

$$Pd = (P_{dis})_a F(n) \tag{15}$$

The function F(n) is unknown, but Reference 3 suggests two possible functions satisfying the requirements: $F(n) = \exp(-C_1 n)$ and $F(n) = \exp(-C_2 n^2)$. We will consider the first of these two.

Thus,

$$Pd = (P_{dis})_a \exp(-C_1 \rho A_{op} (P_{dis})_b)$$

or

$$Pd = (P_{dis})_a \exp(-C \rho A (P_{dis})_b) \tag{16}$$

where $C = C_1 A_{op}/A$ and $(P_{dis})_a$ and $(P_{dis})_b$ are found from equations (13) and (14). Figure 11 shows operator detection probability Pd as a function of single scan aircraft detection probability P_a for varying clutter levels ρA. The masking constant C is 10 in Figure 11.

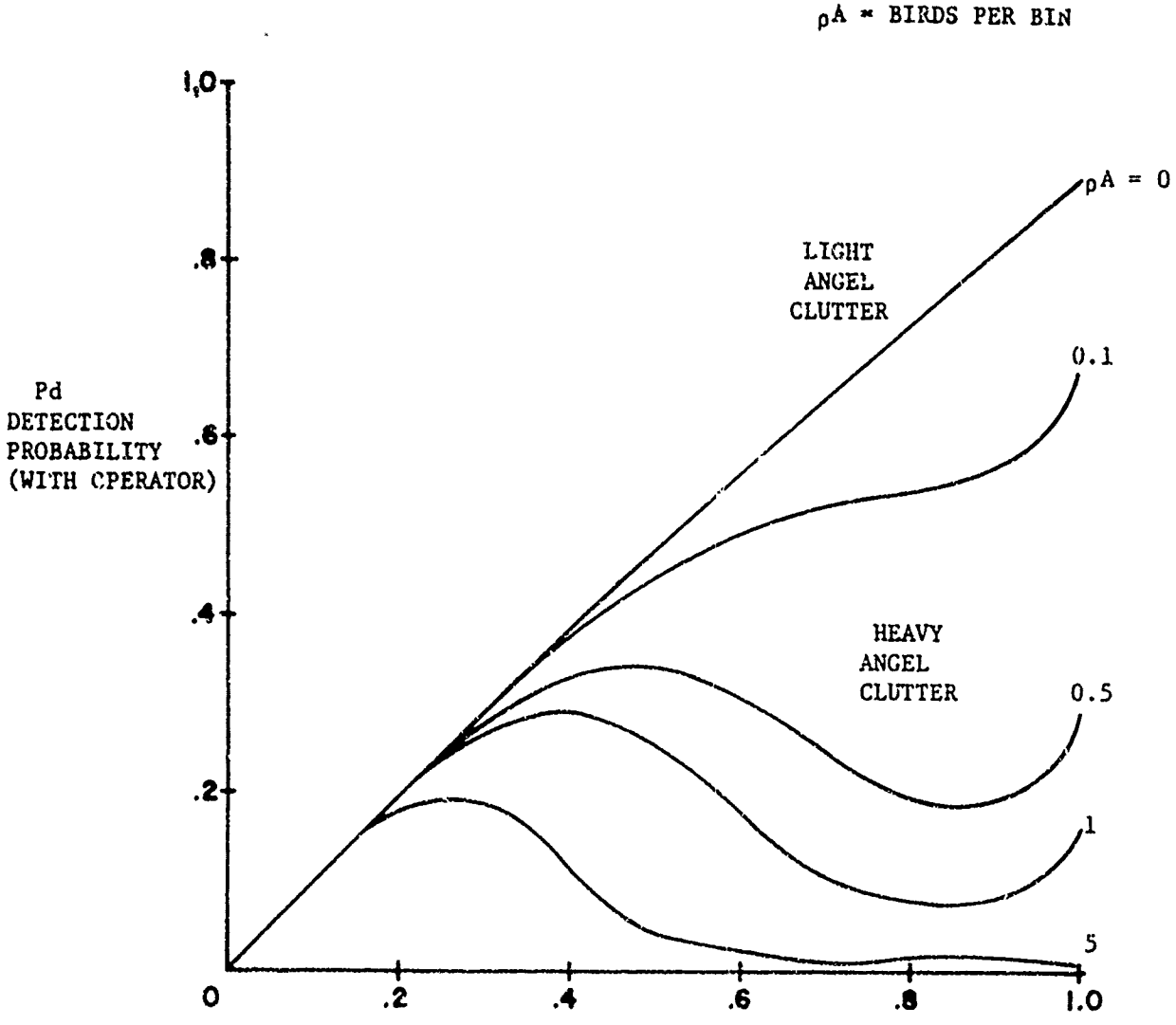

FIGURE 11. OPERATOR DETECTION PERFORMANCE WITH AREA MTI
(MASKING CONSTANT C = 10)

Note that for light angel clutter (i.e., $\rho A \leq 0.1$), optimum Pd occurs for $p_a = 1$, i.e., no single-scan processing. For heavy angel clutter ($\rho A \geq 0.5$), optimum Pd is attained for p_a smaller than unity.

Figure 11 shows the effect of operator masking with Area MTI. Without Area MTI, similar masking would occur, yielding

$$Pd = p_a \exp(-C \rho A p_a^4) \quad (17)$$

Curves similar to Figure 11 were found for the "no Area MTI" case, and the optimum Pd attainable was cross-plotted in Figure 12. Also plotted were optimum Pd with and without Area MTI for light masking, C = 1. As was noted before, the masking constant C is unknown. However, C = 10 seems more reasonable since it implies that with 0.1 birds/bin, the masking function is exp (- (0.1)(10)) = 37%, meaning that an aircraft has a 63% chance of being lost due to operator confusion. If C = 1, than there is a 9% chance of being lost due to operator confusion with 0.1 birds/bin. The former of these two seems more reasonable.

Figure 12 supports the following major conclusion. Area MTI improves slightly on single-scan processing if the angel clutter is light ($\rho A < 0.4$) and if masking of targets due to angel breakthrough is heavy. If masking is light and/or clutter is heavy, Area MTI is of little use.

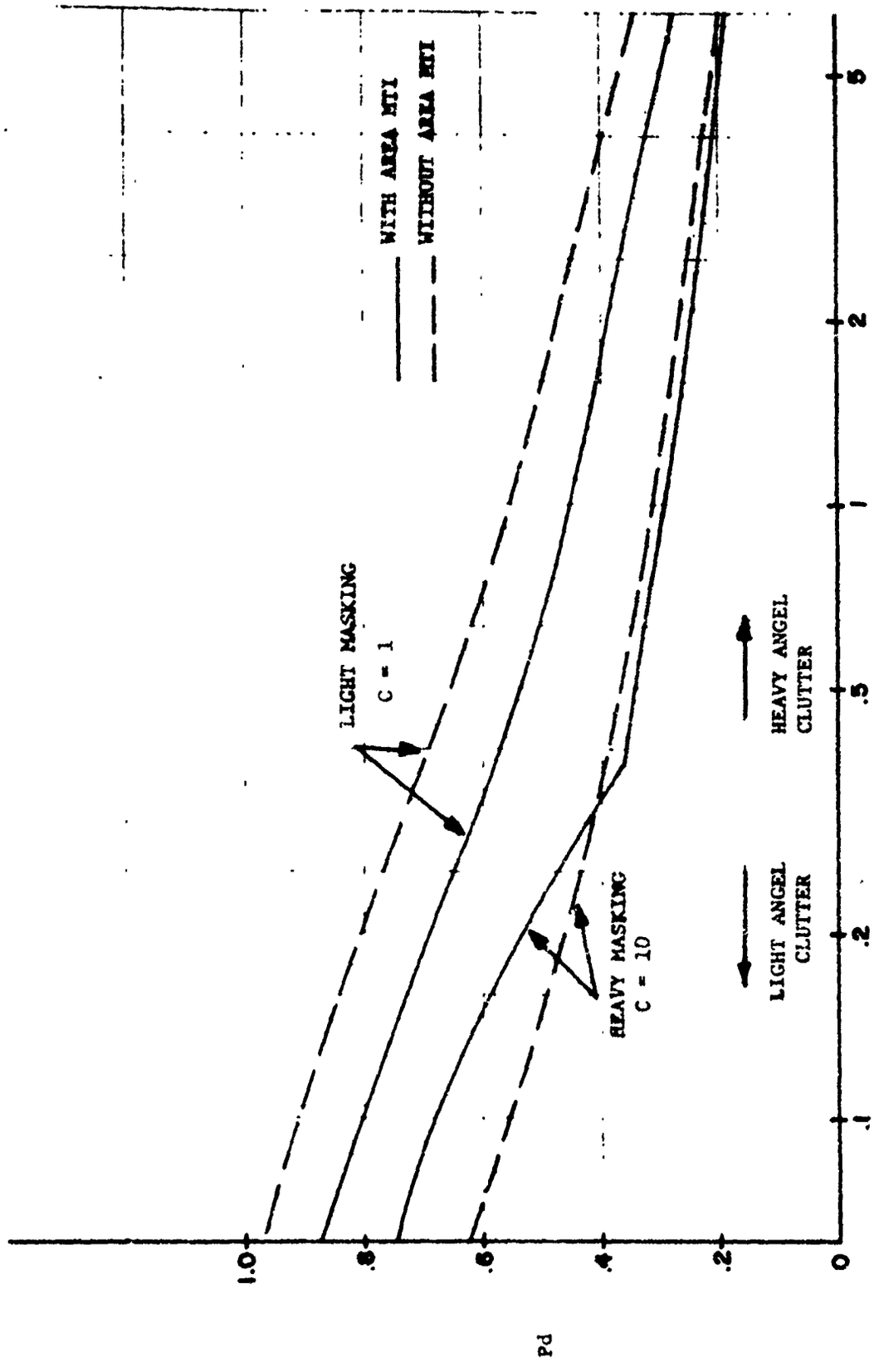

FIGURE 12. OPTIMUM DETECTION PROBABILITY WITH AND WITHOUT AREA MTI

ENCLOSURE A

BIRD MODEL

In Reference 4, an exhaustive survey of existing angel literature formed the basis for a mathematical model of angel returns due to birds. One part of the model was the distribution of angel speed (i.e., magnitude of the velocity vector), which was found to be chi-square with six degrees of freedom in the absence of wind:

$$f(v) = \frac{v^2}{2\,v_o^2}\, e^{-\frac{v}{v_o}}, \quad v_o = 9 \text{ knots} \tag{A1}$$

This distribution does not lend itself to calculation of the distributions of radial and tangential velocity components. However, a slight modification of f(v) to g(v):

$$g(v) = \frac{v}{\sigma^2}\, e^{-\frac{v^2}{2\sigma^2}} \tag{A2}$$

permits one to find the radial and tangential components of angel velocity.

We assume that the angel's heading, ϕ, is a random variable between 0 and 2π (which is reasonable for local, non-migratory flight). Thus, defining α as $\phi-\theta$, where θ is the angel bearing, we see that α too is uniform from 0 to 2π. The radial and tangential components of velocity are then

$$v_r = v \cos \alpha \tag{A3}$$

$$v_t = v \sin \alpha \tag{A4}$$

respectively. Simple transformation of variables shows that v_r and v_t are both Gaussian with zero mean and variance σ^2. In view of the simplicity of this result, the alternate bird speed model (A2) was adopted with σ = 30 knots. This results in an average air speed of

$\bar{v} = \sqrt{\frac{\pi}{2}}\,\sigma$ = 37.6 knots from (A2) which is consistent with observation of angels. (Reference 1 and 2).

The above model describes bird velocities with no wind effects. However, the Gaussian model is excellently suited to include the effect of a mean wind by adding the radial (or tangential) wind component in as a non-zero mean. In addition, these wind effects must be considered in analyzing an Area MTI which would be seriously affected by additional bird velocity. Thus, if the wind direction and magnitude are β and W respectively, then:

$$v_r = v \cos \alpha + W \cos (\beta - \theta) \qquad (A5)$$

$$v_t = v \sin \alpha + W \sin (\beta - \theta) \qquad (A6)$$

i.e., radial and tangential components of the net angel velocity are Gaussian with a mean component in the direction of the wind.

ENCLOSURE B

EFFECT OF AREA MTI WHEN $P_{ja} = P_{jb}$

It is shown here that any aircraft which treats aircraft and birds equally (i.e., $P_{ja} = P_{jb}$) actually degrades performance relative to no Area MTI at all. We first prove the following theorem:

Theorem: Given $h(x)$ and $g(x)$, with $h(x) \leq x$, $g(x) \leq x$, $h(0) = g(0) = 0$, $\ddot{h}(x) \geq 0$ and $\ddot{g}(x) \leq 0$, then $h(g(x)) \leq g(h(x))$.

Proof: Since $h(x)$ is concave upward ($\ddot{h}(x) \geq 0$), we must have

$$h(\lambda x_1 + (1-\lambda) x_2) \leq \lambda h(x_1) + (1-\lambda) h(x_2), \quad 0 \leq \lambda \leq 1 \qquad (B1)$$

In particular let $x_2 = 0$ and define $t = \lambda x_1$, whence:

$$h(t) \leq \frac{t}{x} h(x) \qquad 0 \leq t \leq x \qquad (B2)$$

Similarly. $g(x)$ is concave downward. yielding

$$g(t) \geq \frac{t}{x} g(x) \qquad 0 \leq t \leq x \qquad (B3)$$

Since $g(x) \leq x$, we can substitute $g(x)$ for t in (B2):

$$h(g(x)) \leq g(x) \frac{h(x)}{x} \qquad (B4)$$

Since $h(x) \leq x$, we can substitute $h(x)$ for t in (B3):

$$g(h(x)) \geq h(x) \frac{g(x)}{x} \qquad (B5)$$

From (B4) and (B5) we have

$$h(g(x)) \leq g(h(x)) \qquad (B6)$$

We now let h be the function relating single-scan detection probabilities, $p_b = h(p_a)$. This function is the well-known Receiver Operating Curve (ROC) which satisfies the hypotheses of the theorem for h (Reference 5

We let $g(x) = x - (1-P)\, x^2$, where $P = P_{ja} = P_{jb}$. Clearly, g(x) satisfies the hypotheses of the theorem.

Given any p_a, then we have

$$p_b = h(p_a)$$

$$(P_{dis})_a = g(p_a)$$

$$(P_{dis})_b = g(h(p_a)) \geq h(g(p_a))$$

$$(P_{dis})_b \geq h((P_{dis})_a) \qquad \text{(B7)}$$

for the Area MTI, while with no Area MTI, we have $(P_{dis})_b = p_b = h(p_a)$

$$(P_{dis})_a = p_a$$

$$(P_{dis})_b = h((P_{dis})_a) \qquad \text{(B8)}$$

Thus if $P_{ja} = P_{jb}$ and a certain value of $(P_{dis})_a$ is required, the Area MTI will have a higher $(P_{dis})_b$ than with no Area MTI.

ENCLOSURE C

CALCULATION OF JUMP PROBABILITY

Appendix A describes a model for the distribution of radial bird velocity, resulting in a Gaussian distribution with mean V knots and standard deviation σ knots, where $0 \leq V \leq 30$ and $\sigma = 30$.

The conditional jump probability (given radial velocity) is $P_j(v)$ and is shown in Figure C1 (reproduced from Figure 5(c). Superposed is the radial velocity distribution $f(v)$.

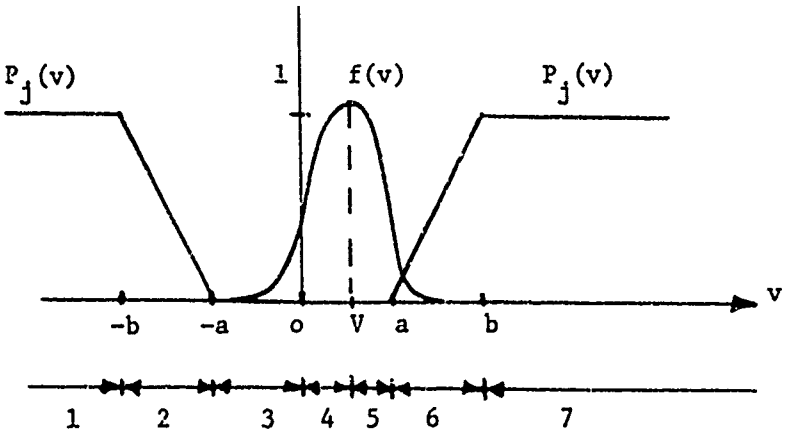

Figure C1

Since the unconditional jump probability is

$$P_j = \int_{-\infty}^{\infty} P_j(v)\, f(v)\, dv \qquad (C1)$$

we have only to integrate over the seven regions indicated in Figure (C1), yielding the general result:

$$P_j = 2\left(\frac{b+V}{b-a}\right)\phi\left(\frac{b+V}{\sigma}\right) - \left(\frac{b-V}{b-a}\right)\phi\left(\frac{b-V}{\sigma}\right) + \left(\frac{a+V}{b-a}\right)\phi\left(\frac{a+V}{\sigma}\right) + \left(\frac{a-V}{b-a}\right)\phi\left(\frac{a-V}{\sigma}\right)$$

$$+ \frac{2\sigma}{\sqrt{2\pi}\,(b-a)}\, e^{-\frac{V^2}{2\sigma^2}} \left[e^{-\frac{a^2}{2\sigma^2}} \cosh\frac{aV}{\sigma^2} - e^{-\frac{b^2}{2\sigma^2}} \cosh\frac{bV}{\sigma^2} \right] \qquad \text{(C2)}$$

where

$$\phi(x) = \int_{-a}^{x} \frac{1}{\sqrt{2\pi}}\, e^{-\frac{t^2}{2}}\, dt$$

Figure 5 can be used to substitute appropriate values of a and b for a particular Area MTI:

(a) Sector Map: $a = 0$, $b = \Delta/T$

(b) Target Store: $a = (\Delta-q)/2T$, $b = (\Delta+q)/2T$

(c) Target Store with infinitely fine quantization: $q = 0$ in (b), so $a = b = \Delta/2T$

For (c) above, P_j reduces to:

$$P_j = 2 - \phi\left(\frac{\Delta/2T + V}{\sigma}\right) - \phi\left(\frac{\Delta/2T - V}{\sigma}\right) \qquad \text{(C3)}$$

Special cases (a) and (c) were used to generate the curves of Figure 6

APPENDIX C-2 REFERENCES:

1. Third Task II Interim Report: Angel Clutter Reduction Program: Detailed Design of Selected ASR Alterations, MSO-F-156, August 1972

2. Second Task II Interim Report: Angel Clutter Reduction Program-Alterations to ASR Radar, MSO-F-148, 15 July 1972

3. J. T. Miller, Analytic Model of PPI Observer Interaction,MRD-2-340, March 20, 1973

4. A Study of Radar Angel Phenomena, G. Heidbreder, et al TSC Report, April 1971

5. Detection, Estimation and Modulation Theory, (Part I), H. L. Van Trees, J. Wiley, 1968

APPENDIX D

PATTERN RECOGNITION TECHNIQUES

APPENDIX D-1

SIMPLIFIED THEORY OF OPERATION FOR PATTERN RECOGNIZER TECHNIQUES

Operation

Basically a pattern recognizer uses measured data to characterize the object which the data represents. Normally, the characterization is accomplished by selecting among several possible alternatives which most closely fit the measured and/or extracted data.

To arrive at this decision, all pattern recogniation devices follow a three step procedure, illustrated in general terms by Figure 1. The sample space is formed from the set of all measurements of a given target which will be used by the recognizer. For this report, all 37 alternate-dwell amplitude samples from the range cell of the data collect matrix containing the target formed the sample space. If these 37 samples are considered as independent, then the resultant sample space is considered to be 37 dimensional with one dimension for each amplitude sample. Each complete measurement will then consist of a full 37 samples which are viewed as producing a 37-component vector* in this space. Each target return produces a vector in this sample space. Presumably, similar targets will produce similar vectors, possibly allowing a partitioning of this space into regions containing only vectors for each type of target

Feature Selection

Generally, either this space is of too high a dimensionality, or a complete separation of target types is not possible with the measurements alone, so that some sort of data reduction is necessary. This reduces the dimensionality and increases the separation of target types, if the appropriate reductions are used. The results of these reductions are called features and form another space, called feature space Now, each reduced result is considered as independent and

*An n-vector is an n-dimensional vector, i.e., has n components.

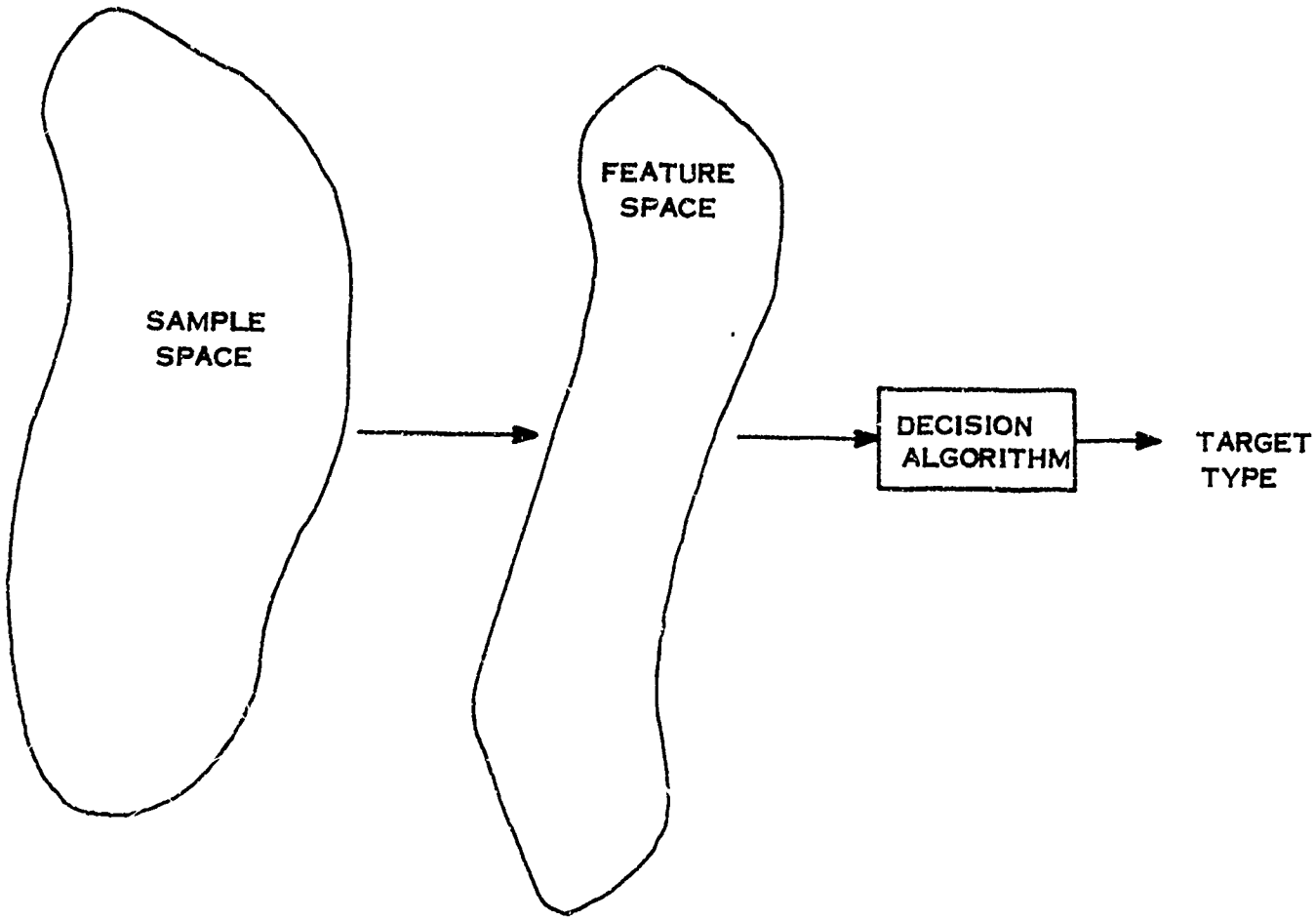

FIGURE 1 THREE-STEP PATTERN RECOGNIZER PROCEDURE

occupying a separate dimension Thus, the measurements of the target are converted into features, forming a single feature vector for each target observed. In one of the approaches considered in this report, 20 alternate dwell samples containing the target were selected to be used as features (the amplitude features set). In addition, 16 other statistical parameters including maximum amplitude, average amplitude, run length, etc., were found for these 20 samples (the statistical features set). These 16 additional quantities, along with the selected 20 target samples, were then treated as forming a 36-vector in feature space (the combined features set). For this example, the dimensionality of the feature space is essentially the same as the sample space mainly due to the limited nature of the study. In order to gain the maximum benefit within the time allowed, features were liberally selected so as not to overlook any possibly significant parameter. Once the significant features are found, the other features can be eliminated, reducing the dimensionality of the feature space required for the decision making process and the complexity of the system. However, the limited scope of the task precluded major effort toward quantitatively identifying the most significant features, or to reducing the number of features to an optimum level

Decision Algorithms

Once these appropriate features have been found, the recognizer uses a decision algorithm which operates on this feature space and identifies the target type by the feature vector found for each unknown target. Basically, the decision algorithm consists of a known partitioning of the feature space into subregions. Previous experience with the algorithm is used to associate each subregion with a target type, and so, when a feature vector for an unknown target falls within a subregion, it is identified with the associated target type. For the angel clutter reduction study, the feature space was partitioned into two subregions, one applicable to angels and the other to aircraft.

Ideally, if angels and aircraft were to separate into two distinct groups, they could be separated by a hyperplane drawn between the two distinct groups, resulting in a simple partitioning of the feature space. The term hyperplane, as used here, is the generalization of a three-dimensional plane to higher dimensional spaces. Since the dimension of the feature spaces used in this study were generally larger than three (the dimensionality of the example considered above was 36, i.e., 20 samples and 16 statistical features), hyperplane techniques for separating target types were necessary. Obviously, illustrations cannot convey the appearance of such high dimensional spaces, so examples will be illustrated in two dimensional spaces where the easy generalization to higher dimensions can be envisioned (a hyperplane in two dimensions is a straight line). Figure 2 illustrates the situation which would occur for two simply separated target types with two features. Here, as in higher dimensions, the decision is made by determining on which side of this hyperplane the known target's feature vector lies.

Unfortunately, it is not always possible to separate target types so easily, as is illustrated in Figure 3. This situation represents the next level of complication, in that the target types are still topologically separable, although now a more complicated hypersurface is required to partition this space. Once the hypersurface is known, however, the decision is still made by noting on which side of the hypersurface the unknown target's feature vector lies. The hypersurface itself may have a rather complicated structure, in general, although for most practical purposes, it may be approximated by the intersection of several hyperplanes. This is, in fact, one of the procedures used in this report.

There is, of course, one more case to consider; that of two target types which are not topologically separable in feature space. This is the case most often realized in practice and is characterized by the groupings of the two target types overlapping to some degree. Figure 4 indicates the case for a moderate degree

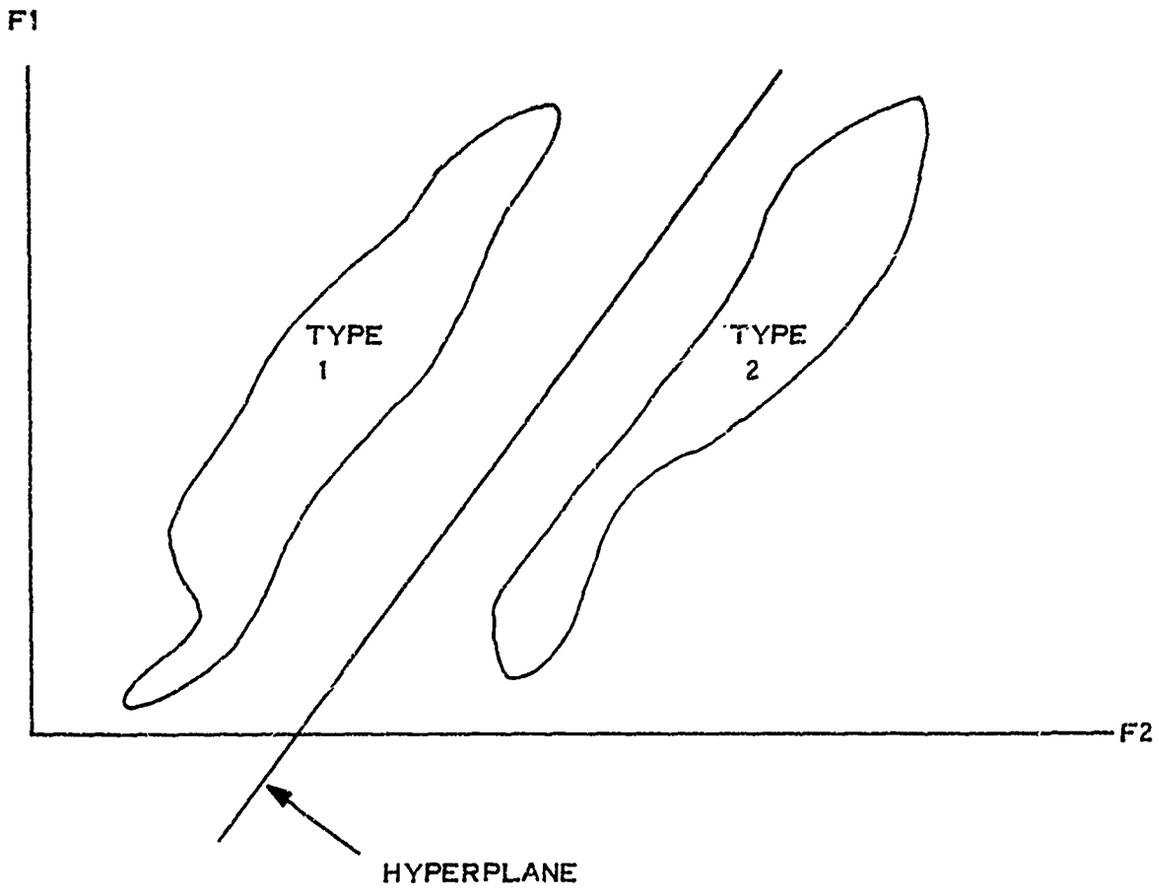

FIGURE 2 HYPERPLANE SEPARATING TWO TARGET CLASSES

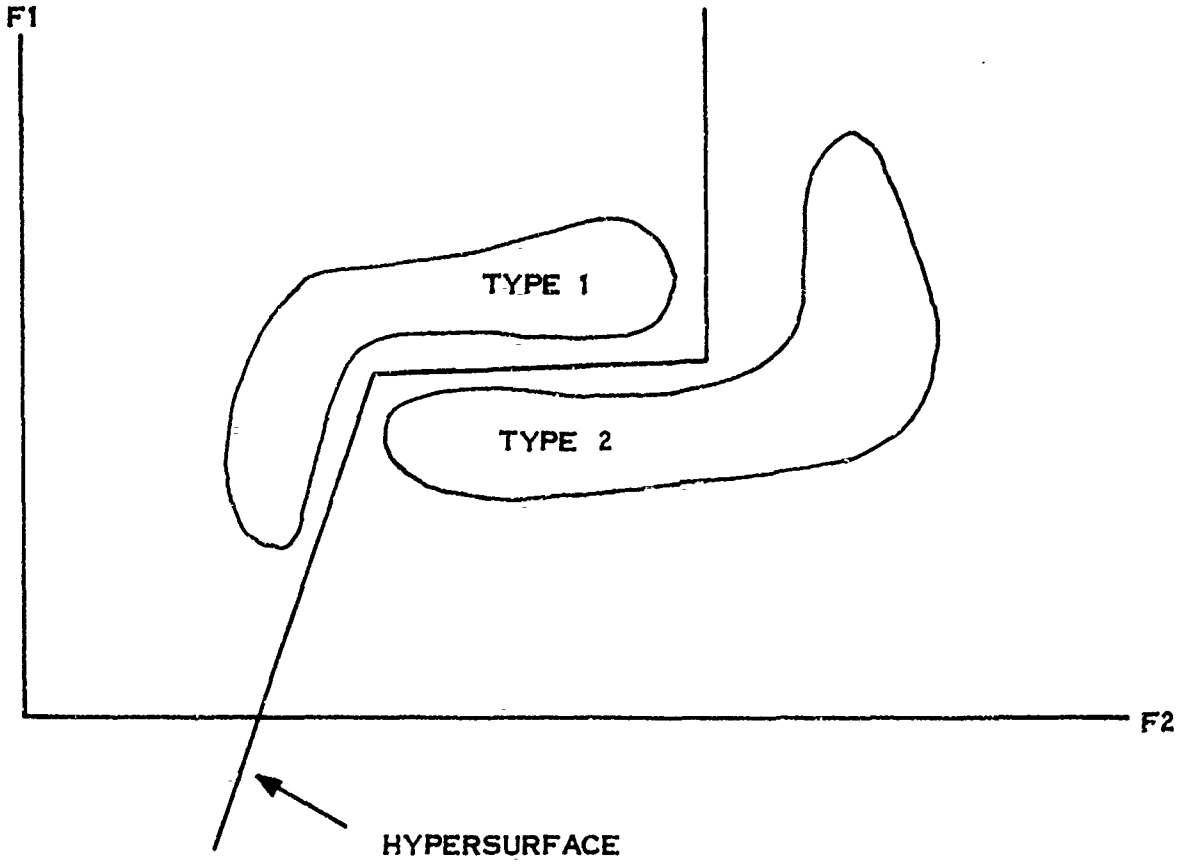

FIGURE 3 HYPERSURFACE SEPARATING TWO TARGET CLASSES

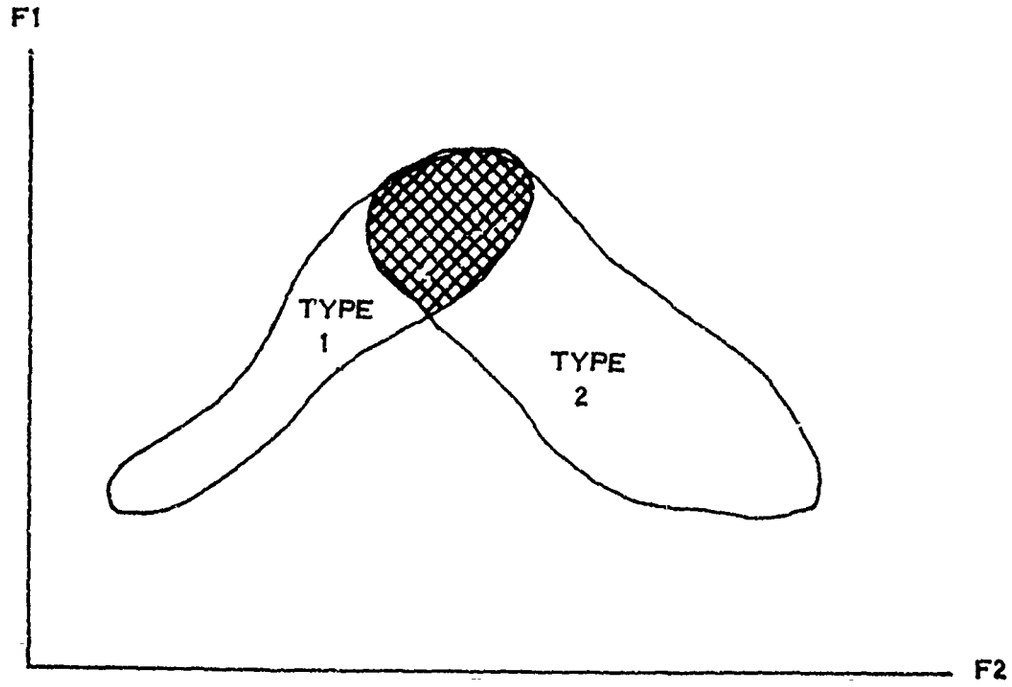

FIGURE 4 OVERLAP OF TARGET CLASSES

of overlap for two target types. Here it is no longer possible to pass a hypersurface between the two target types, so that no completely successful decision making technique can be devised. Hypersurfaces can be found, however, which will either minimize the number of incorrect identifications or use a three-level logic to split targets into either type #1, type #2, or "don't know". This gives at least some information concerning the target. Further identification techniques can then be applied to the "don't know" targets, to complete the process. Occasionally this dilemma may be resolved if another measurement is made, or another feature extracted, adding another dimension to the problem. If the additional feature is chosen properly, the target types may be separated in this higher dimensional space. One is never guaranteed of finding the required feature. (It must exist, however, otherwise the separate target categories would not exist to begin with).

Recognizer Development

Developing a pattern recognizer follows two phases, a learning phase and a testing phase. The learning phase is normally performed off line with a training data set and some learning algorithm which will eventually generate the desired hypersurface. For this report the Widrow-Hoff* technique was used for the learning phase, as the software necessary to implement this technique had already been developed at Bendix. During the testing phase, the hypersurface developed in the learning phase is used by a recognizer (as simulated in a computer) to sort out a new set of targets to verify the proper choice of hypersurface. In the testing phase for the simple case of two regions separated by a single hyperplane, the decision procedure consists of determining on which side of the hyperplane the test target's feature vector lies. Analytically this corresponds to a comparison of the quantity:

*B. Widrow and M. E. Hoff, "Adaptive Switching Circuits", Technical Report #15553-1, Contract NONR-225(24) Standford Electronics Labs, Standford, California, 30 June 1960

$$S = \sum_{i=1}^{n} f_i w_i \qquad (1)$$

to a threshold W_o, where

(f_i) = the feature vector

(w_i) = the hyperplane (weight) vector

Physically, S represents the distance along the hyperplane vector (given by w_i) from the origin of the feature space to the tip of the feature vector (given by f_i). This equation comes from a generalization of the familiar scalar product used in vector analysis. W_o, on the other hand, is the distance of the hyperplane from the origin. If S is greater than W_o, i.e.,

$$S > W_o \qquad (2)$$

then the feature vector is on the far side of the hyperplane; if S is less than W_o, i.e.,

$$S < W_o$$

the feature vector is on the near side of the hyperplane, providing a decision criteria. More complex hypersurfaces proceed in a similar manner, except that now, several thresholds are used, one for each hyperplane used to approximate the hypersurface. Depending on the technique used, all the thresholds need not be implemented for each target.

There is a useful alternative interpretation of equation (1). This interpretation views the components of the hyperplane vector (w_i) as weights. Equation (1) then correlates the weights with the features, weighting features favorable to one target type positive, and the other target type negative. Interestingly, the magnitude of the weight gives the relative effectiveness of the corresponding feature in contributing to the correct target-type identification. Thus these weights can be viewed as a measure of the relative merit of the various features used in the learning phase. A feature corresponding to a low weight

therefore contains little information concerning the identification of the type of target, and would be of little value in practical applications. Heavily weighted features, on the other hand, contain valid information concerning target type and may be considered as distinguishing characteristics of the target. Thus, in addition to providing a systematic approach to utilization of several sources of information to make target identifications, the procedure also yields an evaluation of the relative effectiveness of the information sources.

The object of the Bendix contract was to use the angel data collected by APL, extract appropriate features, and use techniques available at Bendix to select the appropriate hypersurface or hyperplane, to produce the maximum correct-identification rate for angel and aircraft targets. This process of selecting a hyperplane (or hypersurface) is called "training a hyperplane" (or hypersurface). The computer is first given an initial hyperplane, then based on successive iterations through the training set of data, it moves the hyperplane around in the feature space until the maximum number of correct decisions is made. If a perfect separation of target types is not obtained by this hyperplane, successive hyperplanes can be generated, using "don't know" targets from the previous hyperplane, eventually generating a fairly complicated hypersurface. Once this hypersurface is found, it is then used in the pattern recognizer to make all future decisions. Changes in the distribution of the target types are not accounted for, as presumably, the training set was representative of all situations the pattern recognizers will encounter.

Of the techniques discussed, normally one of them will be applicable to almost any type of decision problem. Obviously, the advantage of these techniques is that they can make use of information from several channels at the same time, resulting in increased decision making capabilities over techniques using only one channel. On the other hand, the obvious problems presented by the pattern recognition

technique, is that a correct choice of features must be made in order to allow the simplest separation of target types. In addition, the selection of the appropriate hyperplane or hypersurface, requires fairly sophisticated techniques, particularly, when such large dimensional spaces are used.

In general, the approach can be effective for most problems, provided appropriate features have been selected, the hypersurface has been properly trained, and the training data is representative. The approach, except for feature selection, is systematic, and makes use of all the information available to make decisions, instead of relying on only one or two sources. The results appear quite promising, and should be explored more thoroughly, especially with an eye toward optimizing the features used, and reducing the complexity of the decision-making hardware or software.

APPENDIX D-2

BENDIX PATTERN RECOGNITION STUDY REPORT

Automatic
Aircraft/Angel
Discrimination

January 31, 1973

APL Contract No. 372247

Prepared
For

Johns Hopkins University
Applied Physics Laboratory

Prepared
By

The Bendix Corporation
Communications Division
Baltimore, Maryland 21204

TABLE OF CONTENTS

Automatic Aircraft/Angel Discrimination for Angel Clutter Rejection

I Introduction

This report describes a series of experiments performed at the Bendix Communications Division which applied pattern recognition methodology to the problem of angel radar clutter reduction. Target amplitude versus azimuth data were entered into the Bendix pattern recognition simulation facility to determine:

(1) What level of automatic aircraft/angel discrimination reliability performance may be ultimately feasible and

(2) What level of performance can be expected to be realized within the practical limitations of a modest processor installed at a radar.

Results of these efforts are contained in the next section of this report and are related, as requested, to similar studies reported in JHU/APL reports MSO-F-148 and MSO-F-156.

II Summary of Results

The discrimination experiments conducted extended the techniques previously applied in three areas:

(1) Hyperplane decision rules were trained to make the necessary discrimination by interative algorithms.

(2) Unmodified amplitude data were used as a portion of the input parameter set to the decision rule.

(3) A number of other data statistics were combined with the amplitude data to make the angel/clutter discrimination.

These extensions enabled a hyperplane recognizer to be trained to perform perfect decisions (error free) on the training sample of 130 aircraft and 84 angels. When tested on the entire normally occurring set of 259 aircraft and 168 angels, this recognizer rejected 91% of the angel clutter while maintaining a 96% aircraft acceptance probability. By varying a threshold in this recognizer, aircraft detection probability can be traded-off against angel rejection probability. The combinations of detection and rejection probabilities obtained by this threshold variation are plotted as the highest curve in figure 1. Figure 1 includes curves obtained by APL studies for comparison purposes. Bendix hyperplane decision rules operated on every other dwell amplitude over an interval of 40 dwells for a total of 20 dwell amplitudes. Thus the Bendix curves are best compared to the APL curves generated from 36 dwell data.

The significant performance improvement afforded by hyperplane discrimination is obvious from the curves, which indicate that an operational system could be deployed that rejects between 70 and 80% of the angels without any aircraft loss.

The lower hyperplane performance curve plots the detection and rejection probability combinations for all the aircraft/angel data available. This curve should be regarded as representing the performance that can be expected under the very worst operating conditions. Thirty-three percent of the angels in this data set are labeled as an "anomalous target", treated as a bird but consistently detected as an aircraft. This "anomalous target" is responsible for pulling the lower curve to the left of the upper curve, i.e. for the large loss in angel rejection probability. Also, 61% of the aircraft in this data set are flying tangential to the radar and fading in and out of the MTI notch. The hyperplane threshold setting which produced the 96% detection rate quoted above for normal aircraft only degraded to 90% for such tangential aircraft. Thus the difference in the two Bendix curves in figure 1 is almost entirely due to the "anomalous target".

BENDIX HYPERPLANE DISCRIMINATION PERFORMANCE

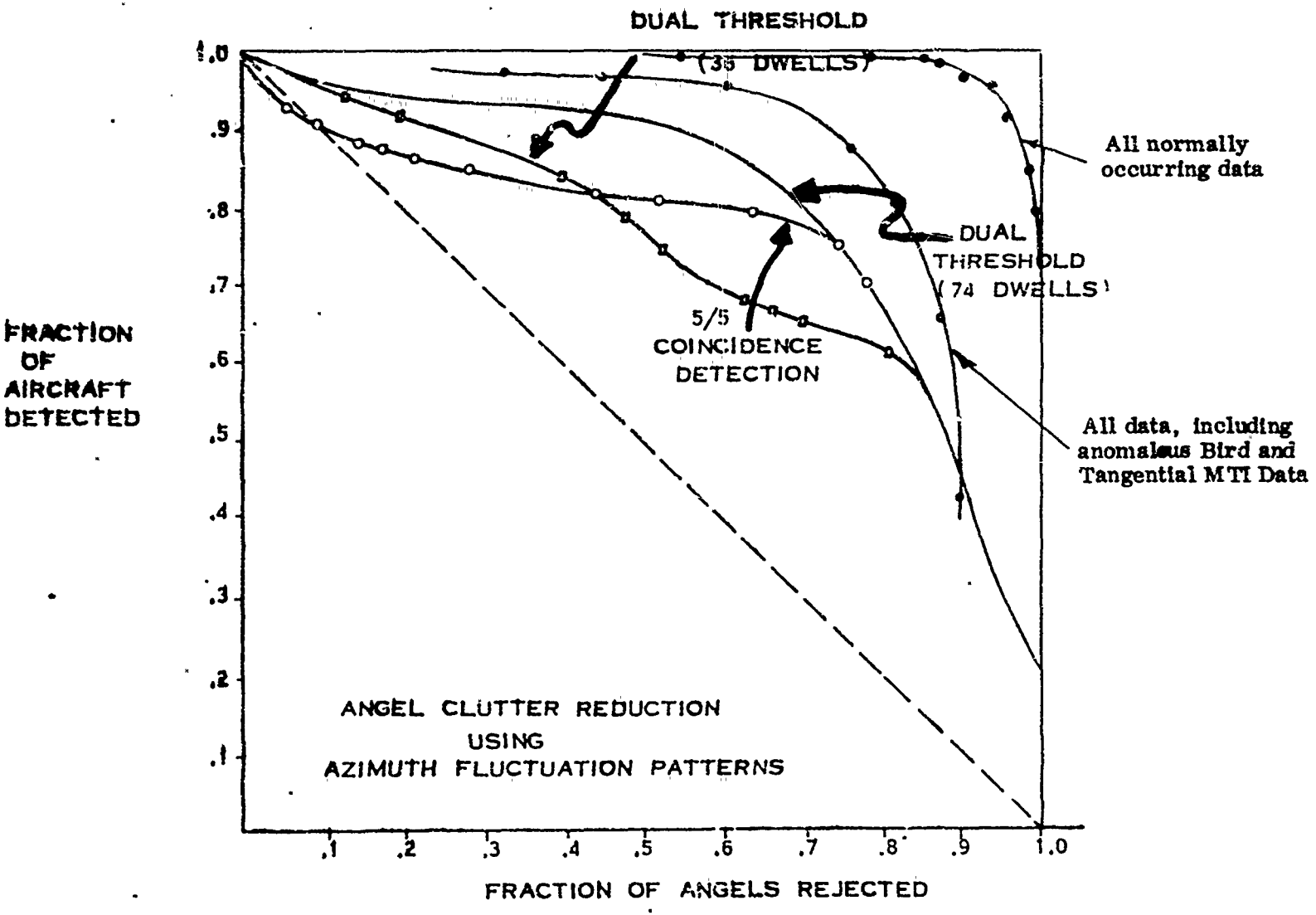

PERFORMANCE OF AZIMUTH PATTERN PROCESSORS

FIGURE I

APL CURVES
TAKEN FROM FIGURE 2.3-3
OF REPORT No. MSO-F-156
Page 2-20

Since it is highly unlikedly that aircraft will fly tangential to the radar 61% of the time, or more importantly that 33% of the time anomalous targets will be present. Bendix hyperplane discrimination performance can be expected to be at or near the upper curve plotted in figure 1.

Fixed target clutter data was also made available to Bendix. Two hyperplane decision rules were trained to separate both aircraft and birds from such fixed target clutter using half of the data. When tested with the entire data base, these decision rules rejected over 90% of the clutter while losing only 2% of the aircraft/birds. This clutter rejection performance is plotted in figure 2. A hyperplane discriminator of this type could be used in conjunction with the angel rejecter to greatly improve PPI legibility.

It should be stressed that all the techniques investigated and/or reported by Bendix are amenable to hardware implementation within the cost constraints of individual radar site deployment.

III Feature Extraction

Bendix was provided with every other dwell amplitude of APL's data base. From this, further selection was made.

1. To the Data Base

In APL's track 3-2, fixed targets (or ground clutter) appear in the data. This data is always excluded from bird/angel recognition problems and is treated as a fixed target in a separate fixed target classifier.

Tracks 16-1 and 16-3 marked "an anomalous target" were not used in training and treated as angels in generalization.

The bulk of APL's aircraft data is without MTI, so tracks 21-1 and 22-1 (with MTI and MTI shut-off in mid run) were not used for training.

CLUTTER REJECTION
GENERALIZATION EXPERIMENT

HYPERPLANES #29 & 32
36 FEATURES UNNORMALIZED

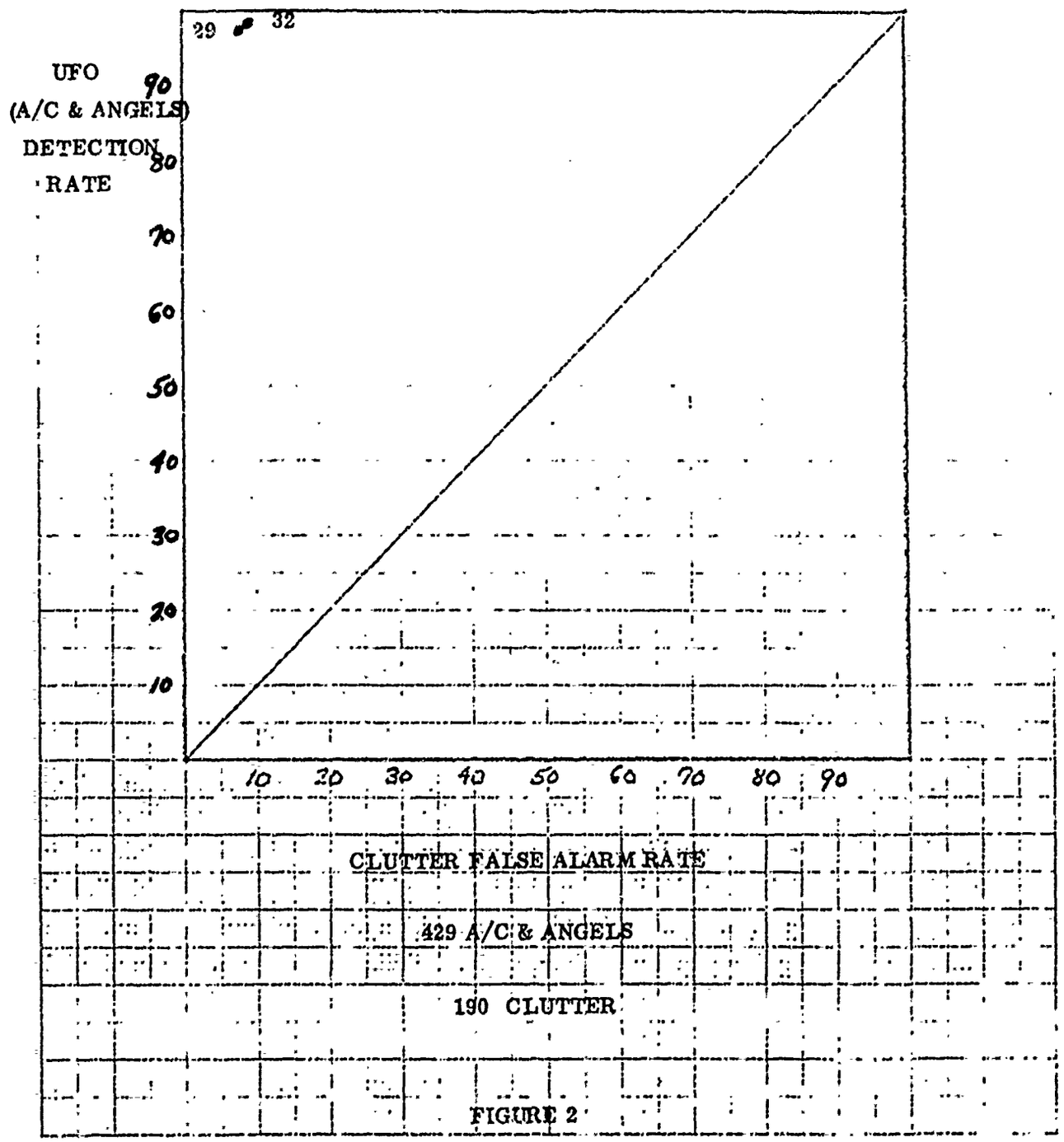

FIGURE 2

2. Dwell Reduction

A threshold of five was compared to each dwell amplitude. Twenty consecutive amplitudes after the first crossing were used as input data. (Twenty dwells are equivalent to forty dwells in the original data.) Only one aircraft target, the 64th run of track 6-2, was lost by this threshold. Inspection revealed that this run does eventually exceed the input threshold level, but too late to take twenty dwells in the available data.

This thresholding has a strobing effect on the data which facilitates the training and operation of a pattern recognizer which operates on waveform amplitude data. Strobing avoids simulation of data propagating through the recognizer during generalization.

3. Extracted Feature Statistics

Sixteen amplitude statistics were generated from the twenty dwells selected by the threshold. These parameters were combined with the twenty dwell amplitudes for a total of thirty six features. The 21st feature is the unbiased estimate of the standard deviation of the first twenty.

The 22nd feature is the maximum amplitude and the 23rd is the average value of the first 20.

Features 24 through 33 were counts derived from amplitude crossings of ten different double threshold settings. Thresholds were set at 10 & 5, 15/5, 15/10, 20/5, 20/10, 20/15, 25/5, 25/10, 25/15 and 25/20. A count was made of decreasing wave form amplitudes as they passed through each threshold. Passage below the upper threshold was counted as a + 1 while passage below the lower was counted as a - 1.

Features 34, 35 and 36 were generated by counting the number of consecutive dwell amplitudes which remained above the thresholds 8, 12 and 16 respectively. Only the first such "run length" was calculated for each scan.

IV A Hyperplane Training Example

In BCD's pattern recognition routines, a set of features can be selected from the 20 amplitude dwells and the 16 extracted statistics. A feature vector is one of the N dimensional vectors generated from N features. In the example diagrammed in figure 3, average vector 1 (AV1) is the average of all aircraft feature vectors without MTI. Area normalization was applied to each 36 dimensional feature vector. Average Vector 2 (AV2) is the average feature vector for area normalized angel data (excluding runs 16-3 and 16-1).

The difference vector is AV1 - AV2, and was amplitude normalized for plotting purposes.

A fourth curve set, "Hyperplane 20", is a representation of weighting values as a recognizer was trained on these data. Since the difference vector was used as a starting point in this training, one of these overlayed curves closely resembles the difference vector plot. In the first training iteration - all data - area normalized - using the difference vector as a hyperplane the recognizer made 67 errors, calling 7 of the 278 aircraft angels and 60 angels of 168, aircraft.

As training proceeded, the total number of errors were reduced and became more balanced between the two classes. With each iteration a hyperplane was plotted and on its movement, speed of convergence etc. further experiments were planned.

The hyperplane decision rules employed by Bendix simply compute the inner product between the input feature vector and the weight vector composed of the N weight parameters. If this inner product crosses a similarly trained threshold, the input feature vector is decided to come from an aircraft. If it does not cross the threshold, the target is rejected as an angel.

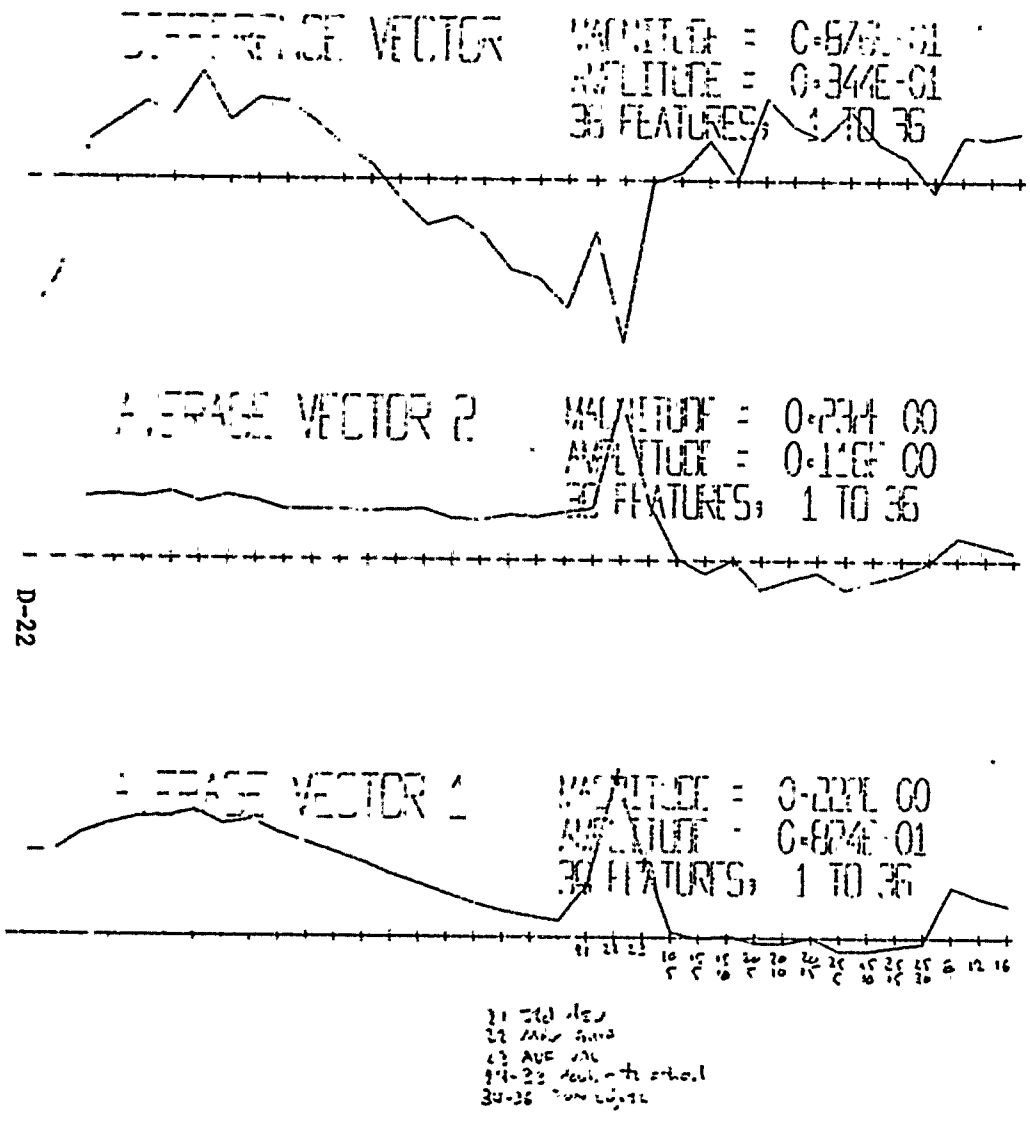
AVERAGE VECTOR 2
AVERAGE VECTOR 1

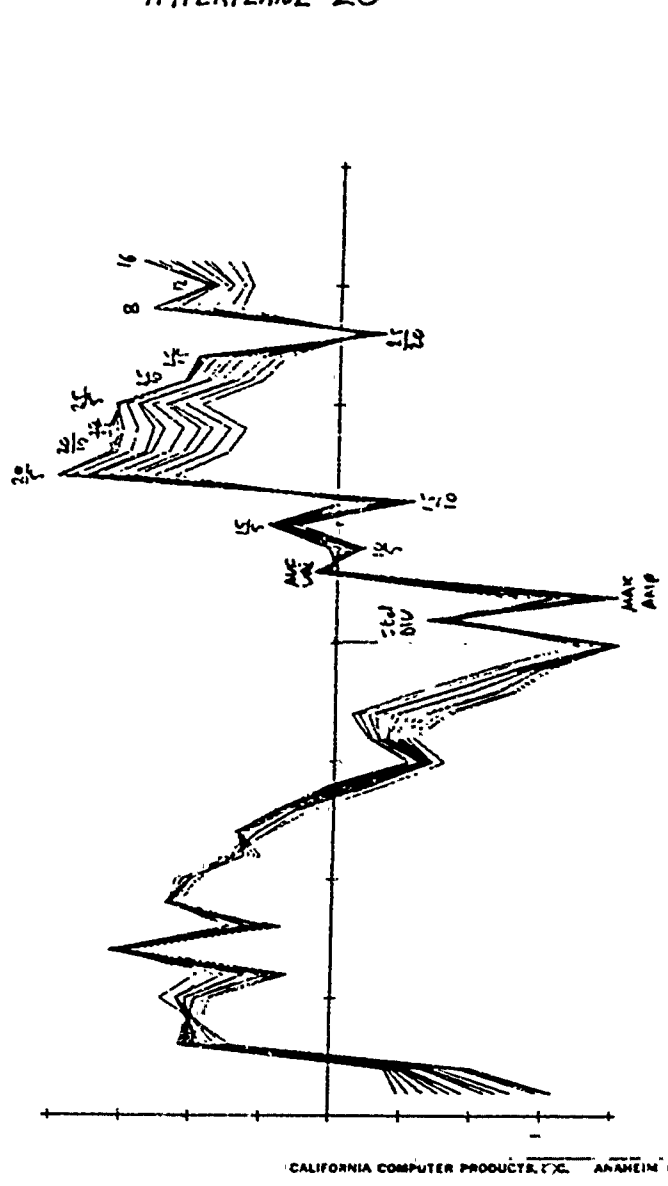
HYPERPLANE 20
CALIFORNIA COMPUTER PRODUCTS, INC. ANAHEIM CALIFORNIA

FIGURE 3

V Discrimination Experiments

A Discrimination based on extracted statistics alone

Angel rejection experiments were conducted using the 16 extracted statistic features alone as input to the hyperplane decision rule. This was done to determine whether dwell amplitude information was needed and to relate hyperplane decision performance to APL results achieved with feature parameters of the same type. It was concluded that extracted statistic information alone is insufficient for reliable angel clutter rejection and that dwell amplitude information must be included.

The following describes the experiments which lead to that conclusion. When a single hyperplane decision rule cannot handle a discrimination problem, other hyperplane decision rules can be added to it to assist it through the following "sequential" structure. Such "sequential" hyperplane structures, since they are nonlinear processors, can handle discrimination problems which are linearly inseparable. The angel clutter rejection problem from Bendix experiments appears to be linearly inseparable, since a sequential structure was necessary to achieve zero errors in a training sample. To create a "sequential" structure, the threshold of the hyperplane is increased and decreased until no errors occur. The two extreme threshold settings which eliminated the errors are termed a double threshold. All those feature vectors which cause hyperplane innerproduct values to lie between the double threshold are difficult cases which that hyperplane cannot discriminate. Therefore, a second hyperplane is trained to discriminate just those feature vectors which proved difficult for the first one. Because the second hyperplane does not have to consider the feature vectors that were successfully handled by the first hyperplane, the "difficult" discrimination problem is "easier" for it. Should the

second hyperplane decision rule also not be able to achieve zero error discrimination without a double threshold, the procedure is concatenated by establishing a double threshold for it and training a third to discriminate its difficult cases. During operation, if the first hyperplane can make a decision, i.e. if both or neither of the double thresholds were crossed, it does. If not, then and only then the subsequent hyperplanes are consulted to resolve the more difficult cases.

Figure 4 documents the training of the first hyperplane using the 16 extracted statistic features. The two plots to the right of the figure depict the gradual changes in the hyperplane weights during each successive training iteration. Since the dimensionality of the feature vector is 16, the weight vector has a dimensionality of 16 and therefore has 16 components. When the weight corresponding to a feature value increases in absolute magnitude, this indicates that the decision rule trainer is finding out that this feature is gaining significance in the overall discrimination problem. On the other hand, when the magnitude of a weight decreases, it can be concluded that the corresponding feature value is not as significant as the other features when used in combination with those features. Note that the 14th weight continually decreases in magnitude, indicating that the 14th, viz. the run length over a threshold setting of 8, could probably be eliminated without effect on the performance of this decision rule. This hyperplane was termed "No. 33". Hyperplane numbers are assigned in the Bendix pattern recognition simulation facility as names, and do not reflect either chronologic events or any other information. Indeed, they rarely are consecutive.

Hyperplane 33 in this case could not achieve zero error operation. Therefore, Hyperplane 36 was trained on its difficult cases, which is documented in figure 5. Hyperplane 36 made errors also. A third level in the sequential logic

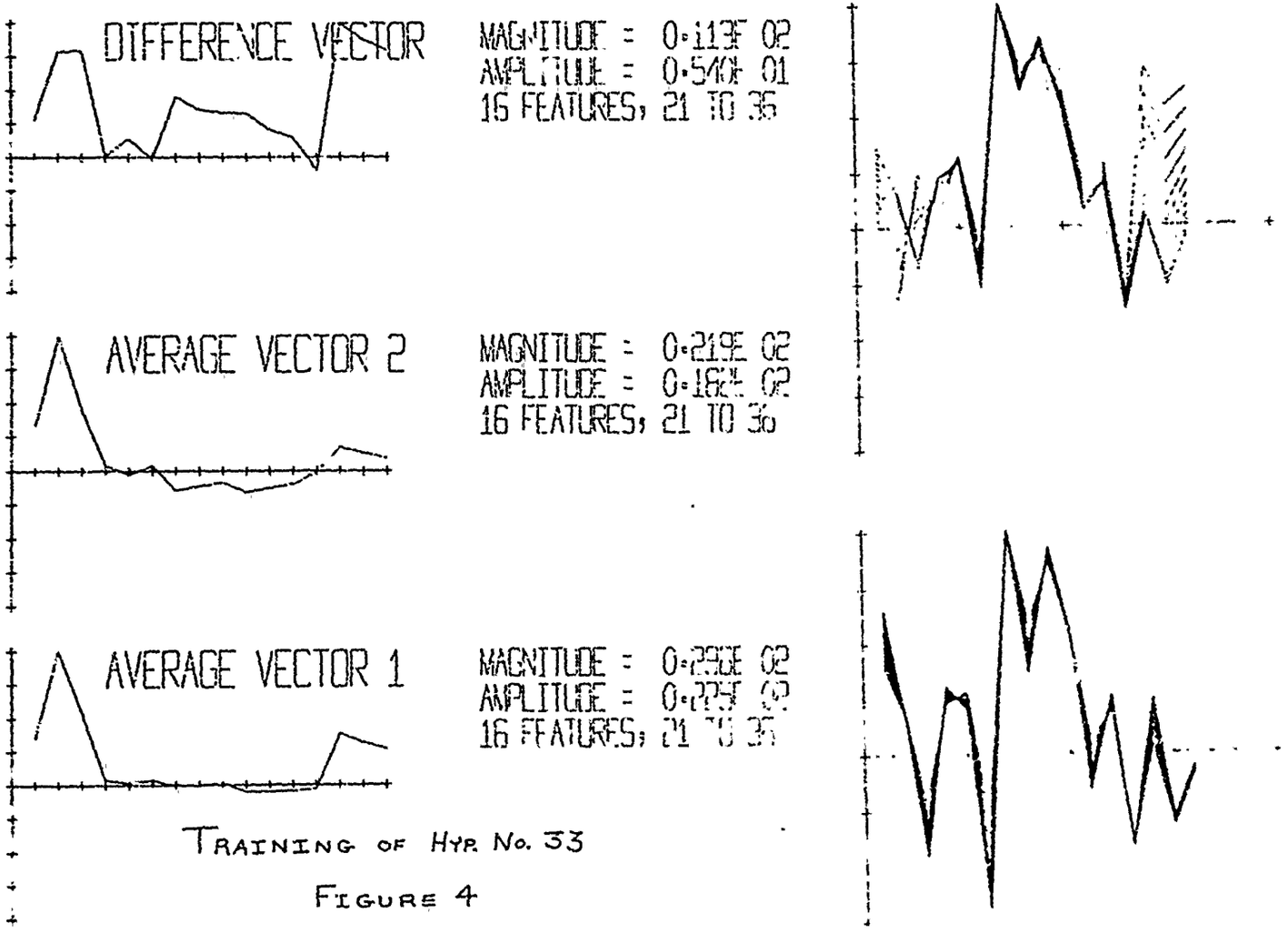

TRAINING OF HYP. No. 33

FIGURE 4

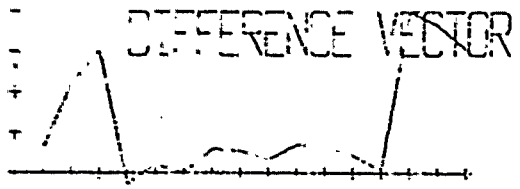

MAGNITUDE = 0·124E 02
AMPLITUDE = 0·657E 01
16 FEATURES, 21 TO 36

MAGNITUDE = 0·215E 02
AMPLITUDE = 0·182E 02
16 FEATURES, 21 TO 36

MAGNITUDE = 0·300E 02
AMPLITUDE = 0·219E 02
16 FEATURES, 21 TO 36

TRAINING OF HYP. No. 36

FIGURE 5

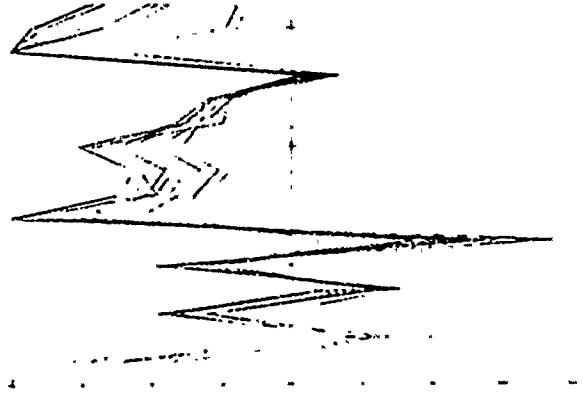

was therefore attempted. However, it was noted in the average vector plots at the beginning of that training, which are plotted in figure 6, that the aircraft and angel average vectors were almost identical both in shape and amplitude. This indicates that the information contained in these 16 features is inadequate for discriminating difficult aircraft and angels. This conclusion was further verified when the attempted training of a third hyperplane ended without significantly increasing the number of feature vectors successfully discriminated.

B Training and generalization of a single hyperplane decision rule with 36 features

The 20 consecutive dwell amplitudes after the first strobe threshold crossing (i.e. amplitude greater than 5) were then added to the 16 extracted statistic features to form a feature vector with a dimensionality of 36. Half of the aircraft feature vectors (130) and half of the angel vectors (84) were picked at random for hyperplane training. Hyperplane No. 22 was trained on this data. Its weights are plotted in figure 7. Note that the 16 extracted statistic features at the end of the feature vector still appear to be more significant than the dwell amplitudes. The training of this hyperplane is documented in figure 8 and 9.

Using the threshold produced by the training algorithm, 17 aircraft and 5 angels were misclassified by Hyperplane 22. Curve A of figure 10 demonstrates how aircraft detection probability and angel rejection probability can be traded-off through threshold variation. One of the points on this curve represents the 17 and 5 errors made by the unmodified threshold.

Without any modification of Hyperplane No. 22, it was tested against 253 aircraft and 168 angels. Curve B of figure 10 plots the probability trade-off curve for this larger data base. Note how closely the knee of this curve approaches

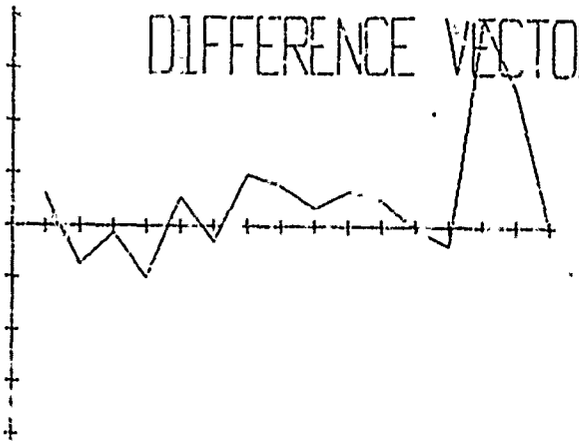

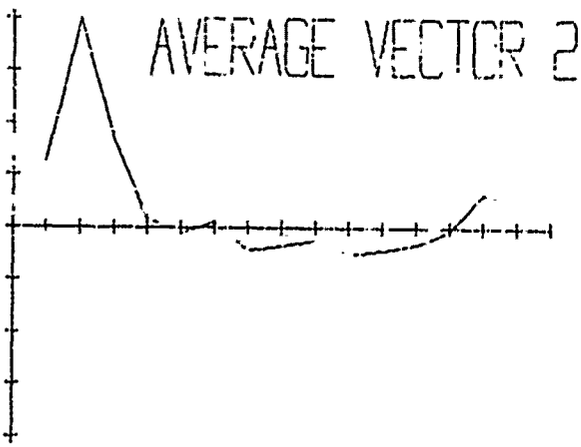

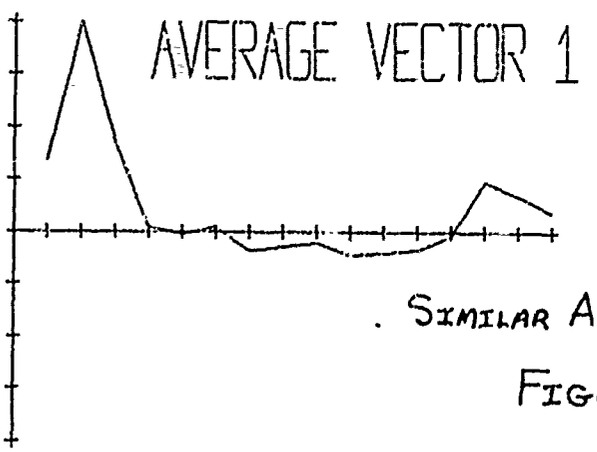

. SIMILAR AVERAGE VECTORS

FIGURE 6

1 36 36 1 2 130 84 1 17 5 22 29

ETA = 0.100E-03

SAM AS 21

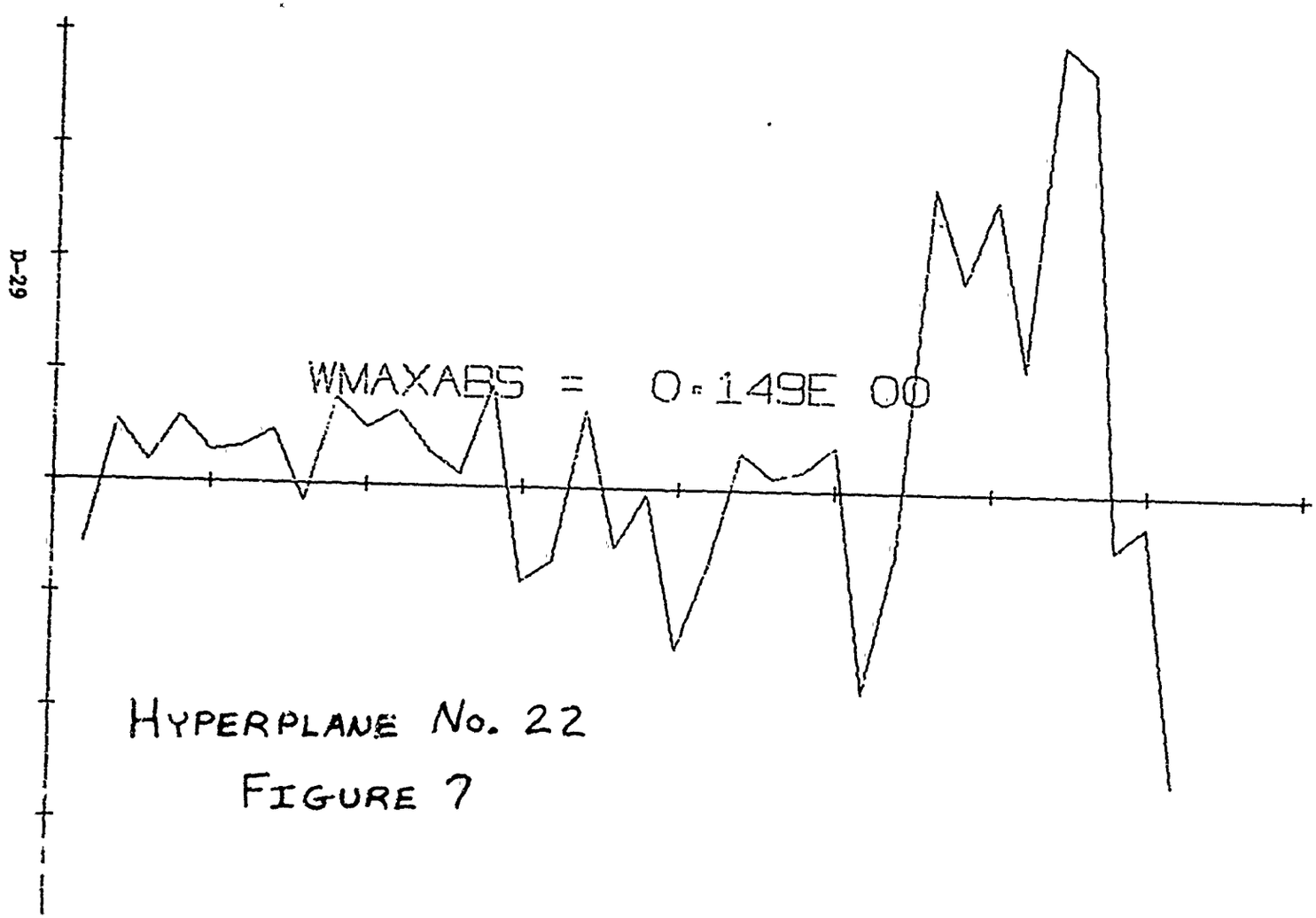

HYPERPLANE No. 22

FIGURE 7

TRAINING OF HYP. No. 22

FIGURE 8

FIGURE 9

CONTINUED TRAINING OF HYP. NO. 22

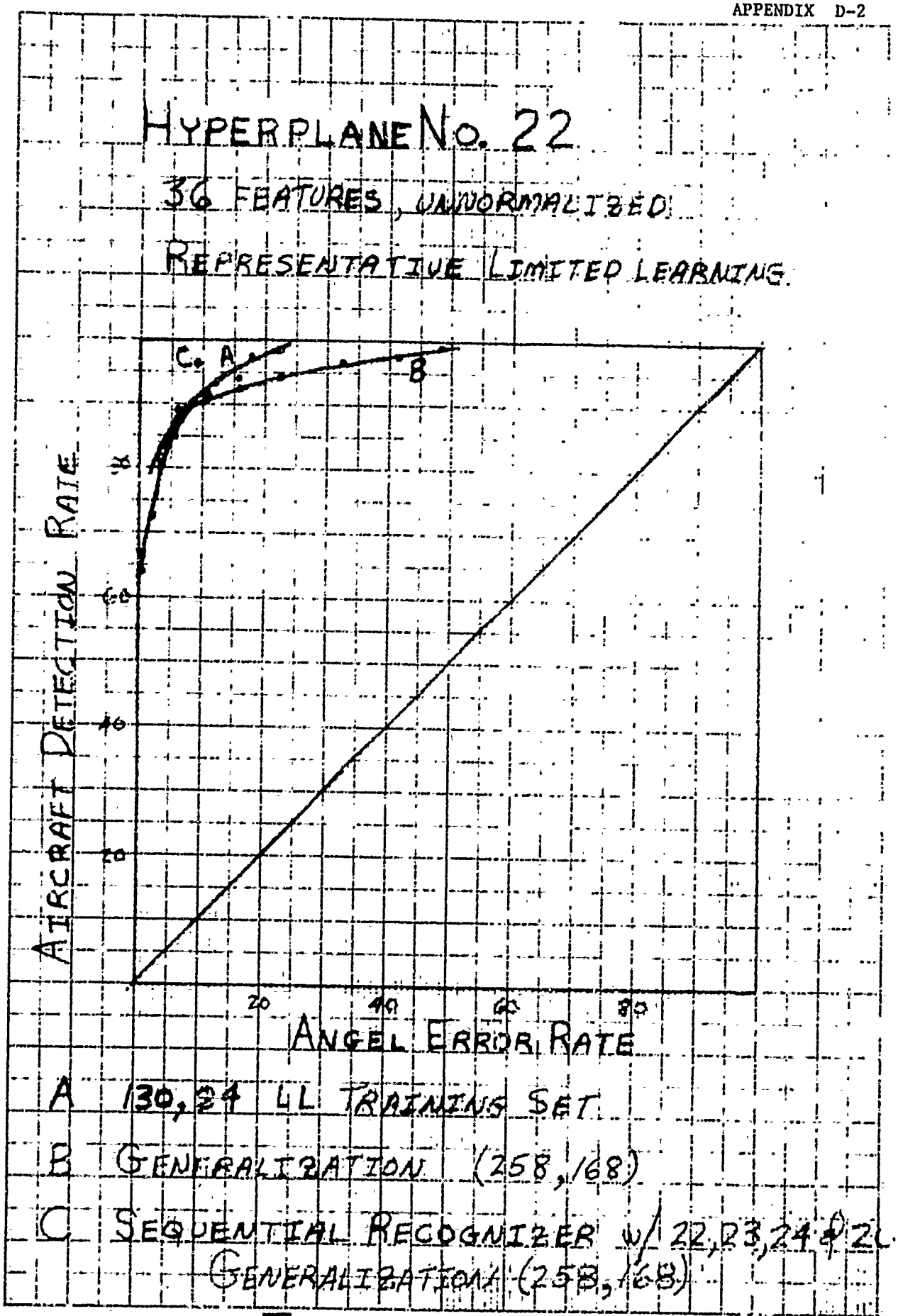
HYPERPLANE No. 22
36 FEATURES, UNNORMALIZED
REPRESENTATIVE LIMITED LEARNING
C
A
B
AIRCRAFT DETECTION RATE
ANGEL ERROR RATE
A 130,24 LL TRAINING SET
B GENERALIZATION (258,168)
C SEQUENTIAL RECOGNIZER W/ 22,23,24 & 2L
GENERALIZATION (258,168)

FIGURE 10

the performance achieved on the training sample alone. This excellent "generalization" of Hyperplane No. 22 guided the construction of a sequential structure based on it and described in the next section. Point C in figure 10 is the generalization of that sequential hyperplane decision rule. It is plotted here simply for reference and to demonstrate that a sequential structure can improve generalization.

Generalization can sometimes be facilitated by training a hyperplane decision rule on "hand selected" data which are very representative of target classes to be discriminated. A training sample of 87 aircraft and 85 angels was so selected. Hyperplane No. 38 plotted in figure 11 was trained on that data base. Note again that the extracted statistic features are still relatively more significant than the dwell amplitudes. The training of this hyperplane is documented in figure 12. The generalization probability trade-off curve of Hyperplane No. 38 is plotted in figure 13. Note through comparison with curve B of figure 10 that the generalization of this hyperplane is inferior to that of No. 22. The knee in this curve is lower and less pronounced. In this case, a selected training sample actually hindered generalization.

Based on these results, a sequential structure was trained using No. 22 as the first hyperplane decision rule.

C Training and generalization of a four hyperplane decision rule with 36 features

Using the same training sample of randomly selected feature vectors, three additional hyperplanes were trained to achieve a sequential structure. These three hyperplanes were numbered 23, 24 and 26 respectively. Their training is

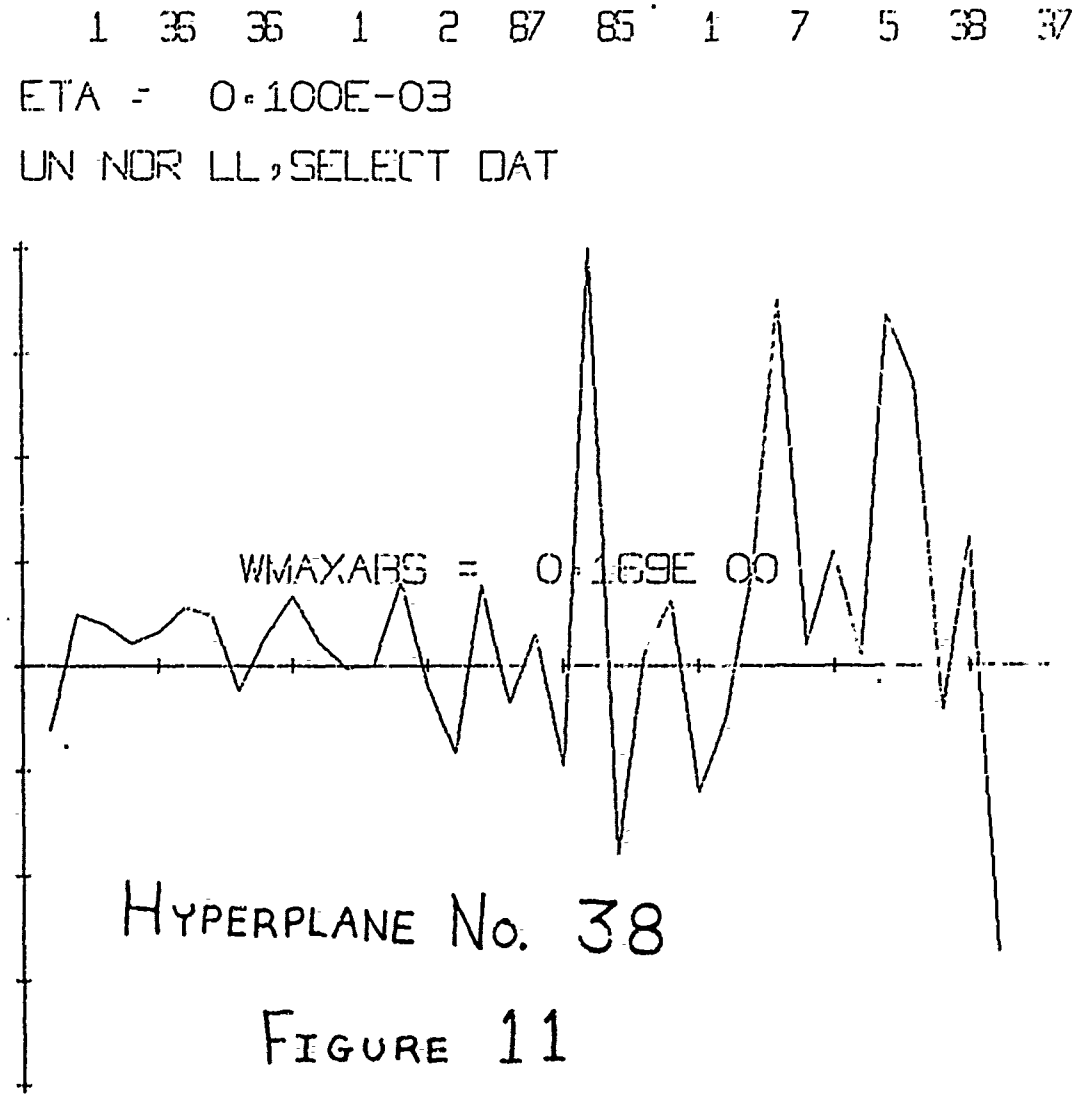

HYPERPLANE No. 38

FIGURE 11

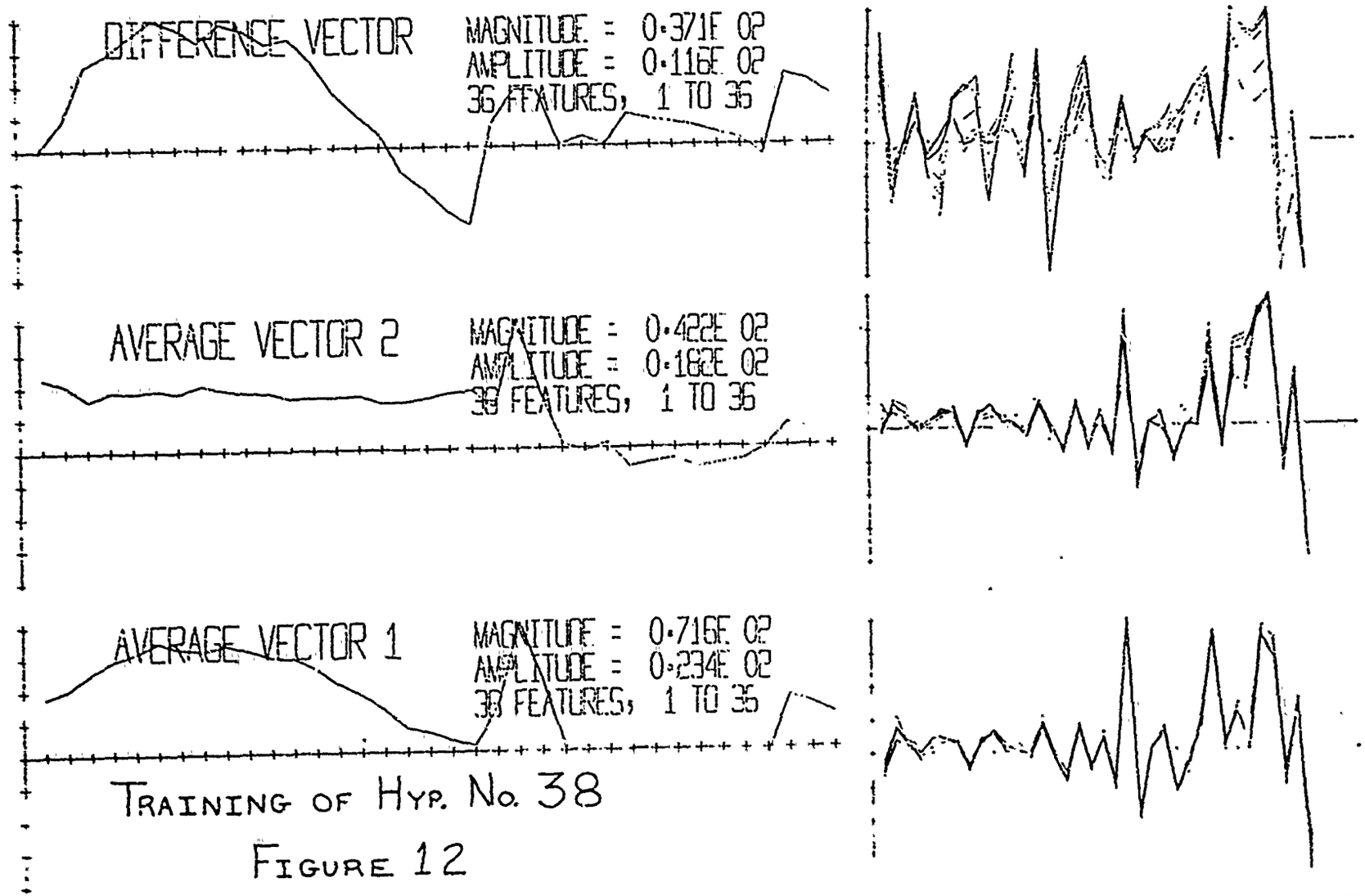

TRAINING OF HYP. NO. 38

FIGURE 12

HYPERPLANE No. 38

36 FEATURES UNNORMALIZED
SELECTED LIMITED LEARNING
GENERALIZATION PERFORMANCE

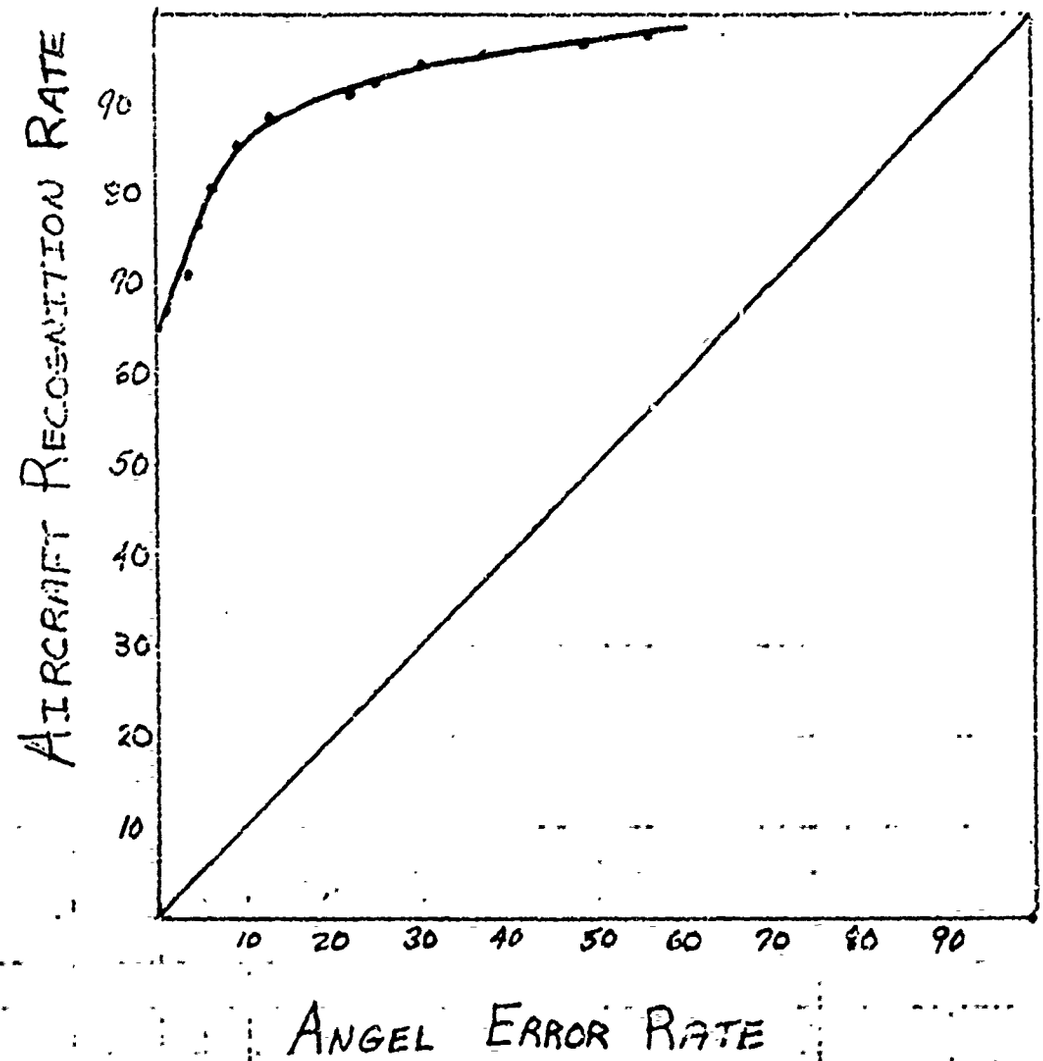

FIGURE 13

documented in figure 14, 15 and 16. Note that the average feature vectors remain distinctive in the 20 dwell amplitude values. This indicates why these higher dimensional feature vectors are more effective in providing sufficient information for the reliable discrimination of "difficult" aircraft and angels.

Figure 17 plots the weight vectors of all four hyperplane decision rules. Note that in the first two hyperplanes in the sequential structure, viz. Nos. 22 and 23, the 16 extracted statistic features are still relatively more significant than the dwell amplitude information. However, in the latter two hyperplanes, Nos. 24 and 26, all 36 features contribute more or less equally to the final discrimination. This result confirms the conclusion that the dwell amplitude information is essential for discrimination of "difficult" aircraft and angels. Reliable angel clutter reduction can only be achieved through inclusion of this type of input data.

The first three hyperplanes, Nos. 22, 23 and 24, all have double thresholds. If an innerproduct value for any of these three decision rules lies between the double thresholds, that hyperplane does not make a decision, but refers the feature vector to the next hyperplane. However, the last hyperplane, No. 26, does not have a double threshold. It is forced to make a decision on all feature vectors which are presented to it. Which hyperplane ultimately makes a decision in a sequential structure like this, can be used to denote the inherent credence in the decision. If the first hyperplane makes the decision, the discrimination can be regarded as firm. On the other hand, if the third or fourth hyperplanes make the discrimination, less credence might be placed in the result. No attempt was made during these efforts to incorporate this type of credence information into the angel rejection problem.

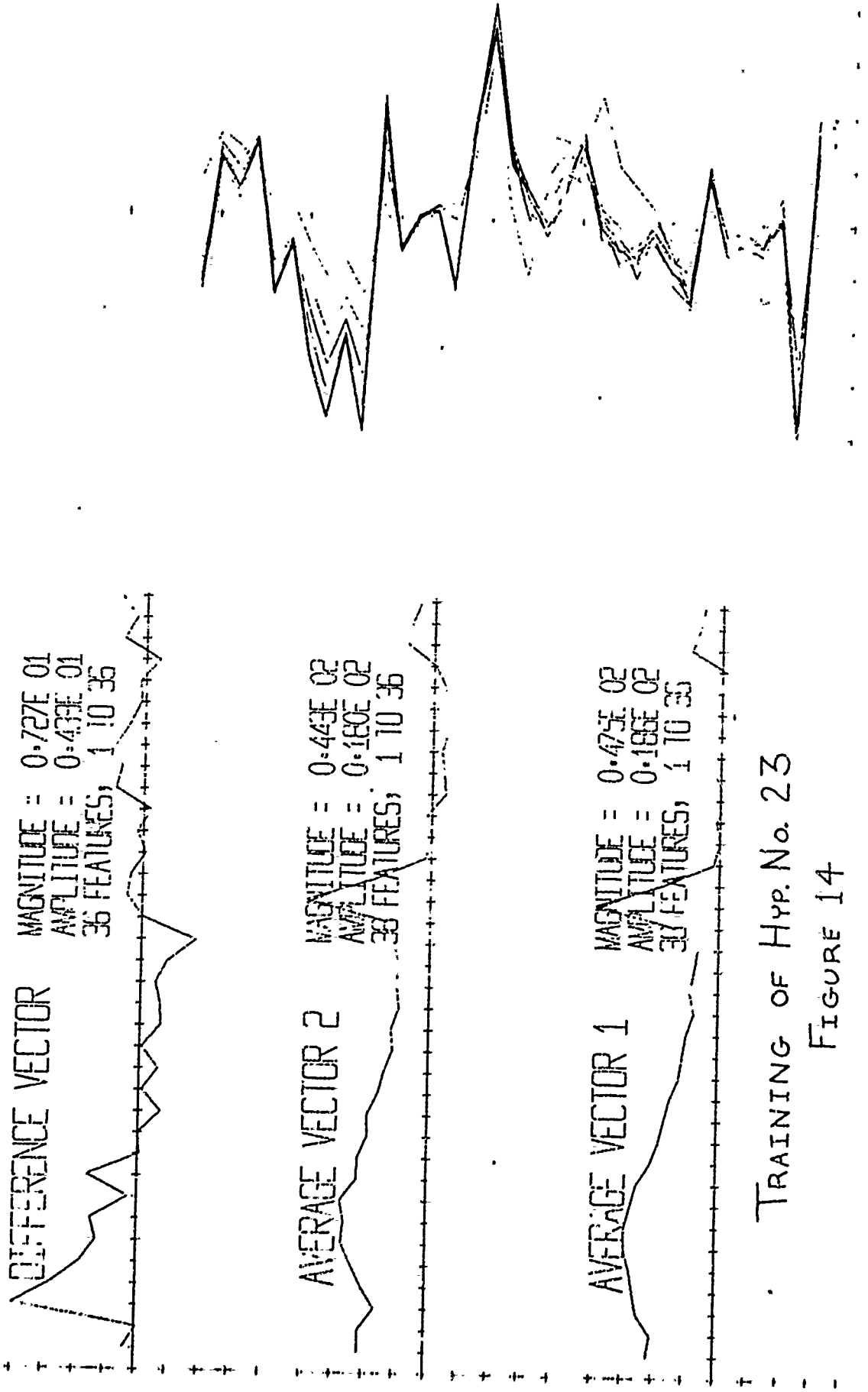

TRAINING OF HYP. NO. 23

FIGURE 14

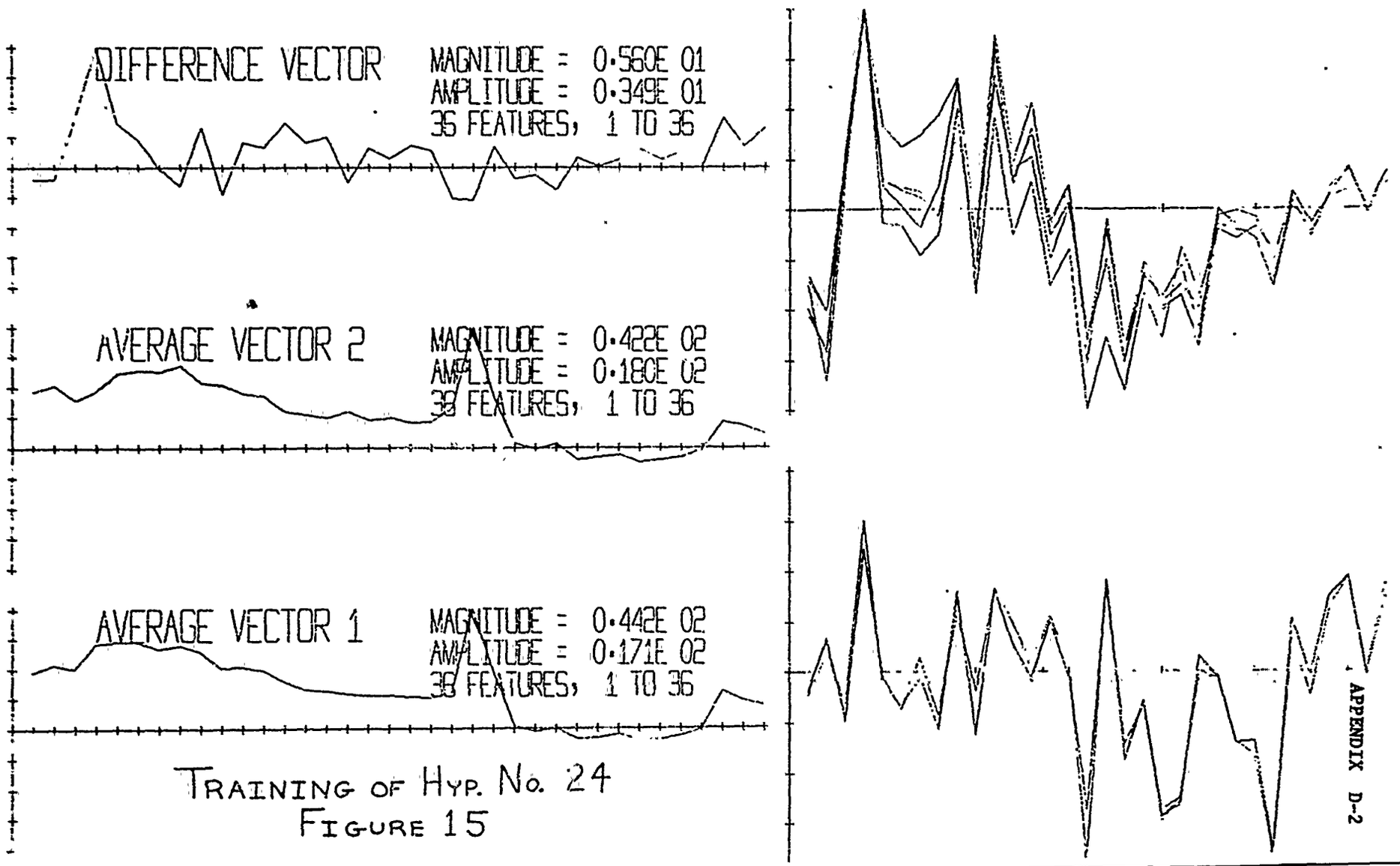

TRAINING OF HYP. No. 24
FIGURE 15

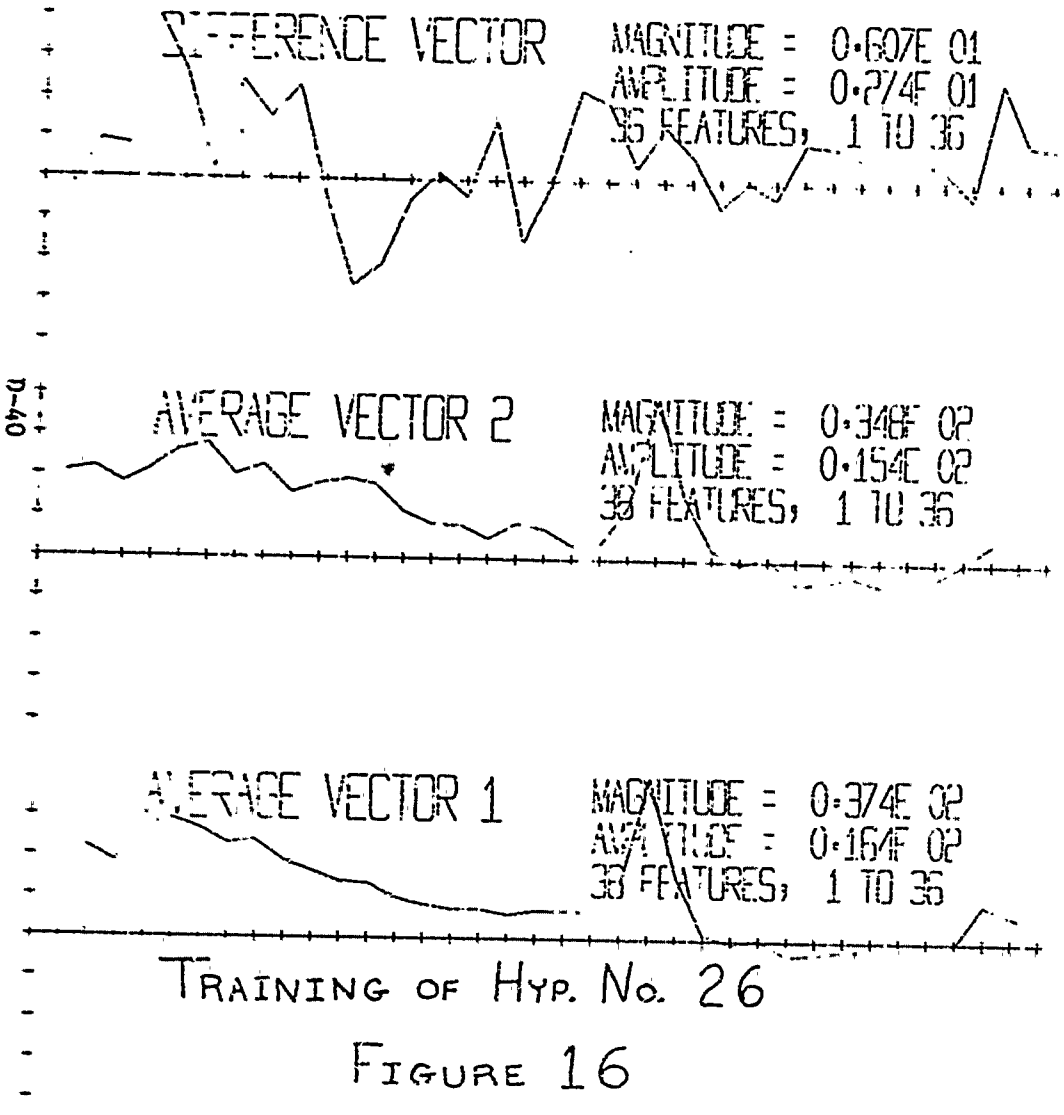

TRAINING OF HYP. NO. 26

FIGURE 16

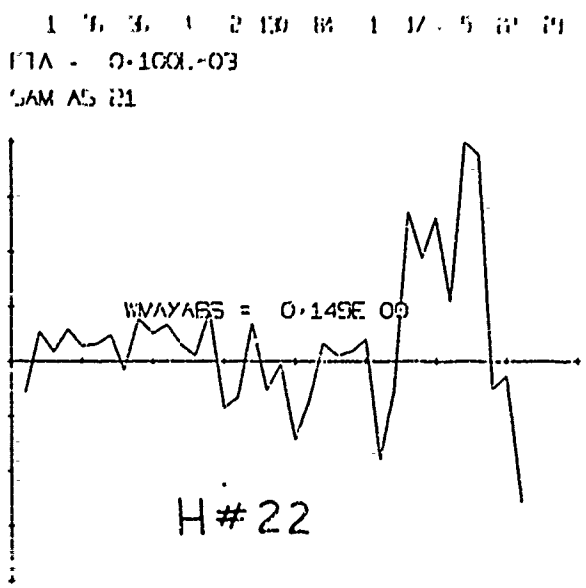

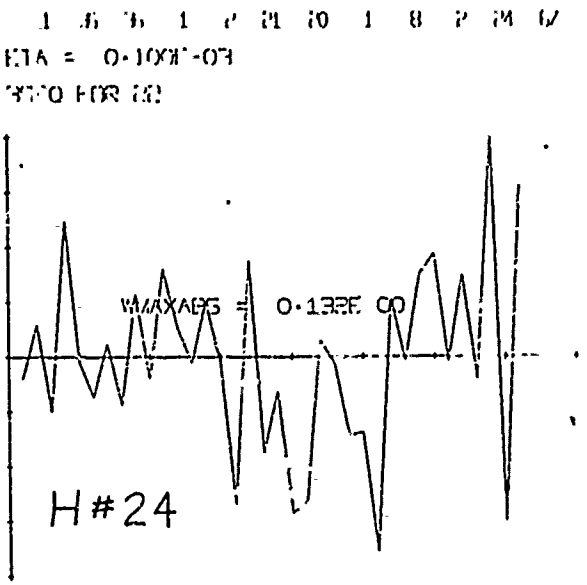

FOUR HYPERPLANES OF SEQUENTIAL RECOGNIZER

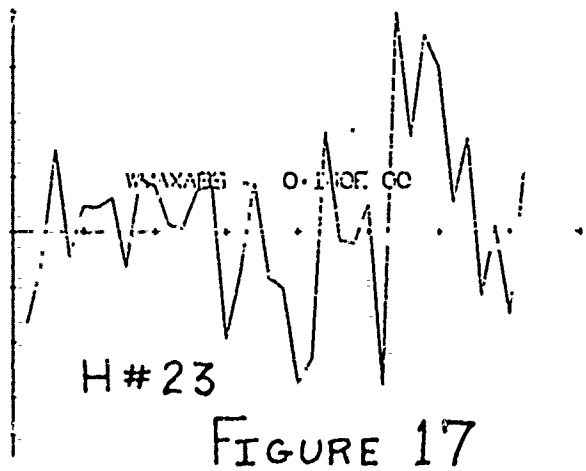

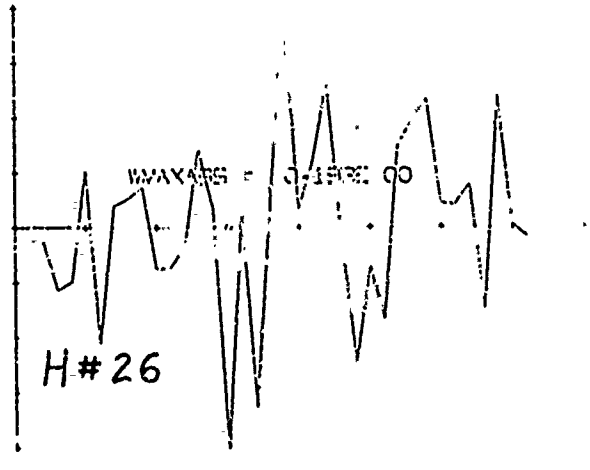

FIGURE 17

Of prime importance is the result that this 4 hyperplane recognizer achieved error free operation on its randomly selected training sample. This perfect performance is plotted as Point A in figure 18. When generalizing to the large sample of 259 aircraft and 168 angels, Curve C resulted. Curve C constitutes a major result of this effort and is discussed in the Summary of Results section of this report. The probability trade-off to generate this curve was performed by shifting the double threshold of Hyperplane No. 22, the first one in the sequential chain. This threshold variation could easily be controlled by a PPI operator to optimize the angel rejection characteristics in the face of varying target and clutter conditions.

Curve C establishes that significant angel rejection is possible with zero aircraft loss. However, improved performance over that given by Curve C could be obtained in deployed systems by implementing a sequential hyperplane decision rule that had the benefit of a large training sample. Training on the full feature vector set was not attempted during this effort.

The sequential decision rule was tested with the "anomalous angel" and "tangential" aircraft feature vectors. Performance against this data is plotted as Point D in figure 18. Note that the "anomalous angel target" was called an aircraft by the hyperplane decision rule over 75% of the time. Combining this difficult data with the normal generalization sample yields the probability trade-off curve labeled E in figure 18. Curves E and C are replotted in figure 1 and discussed in the Summary of Results section of this report.

D Experiments with 20 dwell amplitude features alone

Once reliable angel rejection had been demonstrated using 36 dimensional features, attempts were made to achieve similar levels of performance with feature

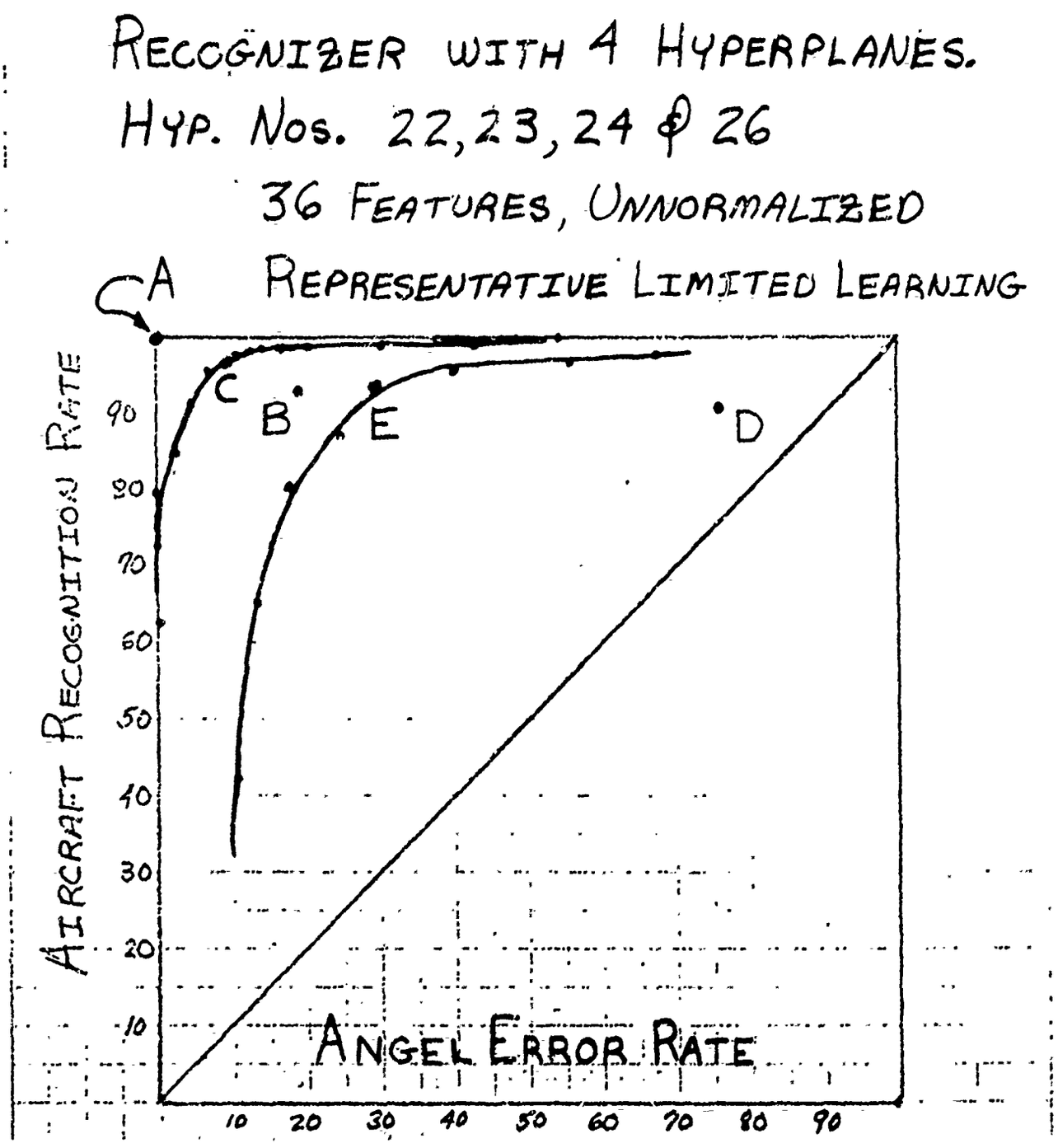

A - Training Sample (130, 84)

B - Generalization Sample (129, 84)

C - A and B Combined (259, 168)

D - Airplanes Tangential to MTI and Anomalous Angels (401, 82)

E - All Aircraft and Angel Data (660, 250)

Figure 18

vectors of reduced dimensionality. Three reasons motivate this approach:

(1) Fewer features require less feature extraction signal processing.

(2) Fewer features permit more efficient hyperplane decision rule training.

(3) Training with 36 dimensional vectors has indicated that some of the features receive insignificant weights during training.

Hyperplane No. 5 plotted in figure 19 was trained on a selection of 167 aircraft and 168 angels using only the 20 dwell amplitudes as features. This training is documented in figure 20. Note that the general shape character of the difference vector has been carried over into the final hyperplane weights. Figure 21 plots the probability trade-off curves for this hyperplane. Curve A for this hyperplane plots the probabilities obtained when tested with the training sample. Comparison with the similar curve for Hyperplane No. 22, Curve A of figure 10, shows that No. 5 has superior performance, viz. a higher and more pronounced knee. This comparison is all the more significant when realizing that No. 5 has a much larger training sample and uses only the 20 amplitude information. This indicates that possibly no statistic feature extraction may be necessary to achieve reliable angel rejection. On the other hand, comparison of the B Curves for these two hyperplanes, which plot the probabilities obtained when tested against all the normally occurring data, shows that the 36 feature hyperplane No. 22, has superior generalization. The final conclusion as to whether or not statistic feature extraction is required can only be answered by the development of a sequential structure based on 20 features similar to that developed for the 36 featured vectors. This report in a later section strongly recommends to pursue that development, since the resolution of this question makes significant impact on the amount of hardware required for on-site implementation.

1 20 20 1 2 167 168 1 45 2 5 32

ETA = 0.100E-03

GOOD DATA; NOT NORM

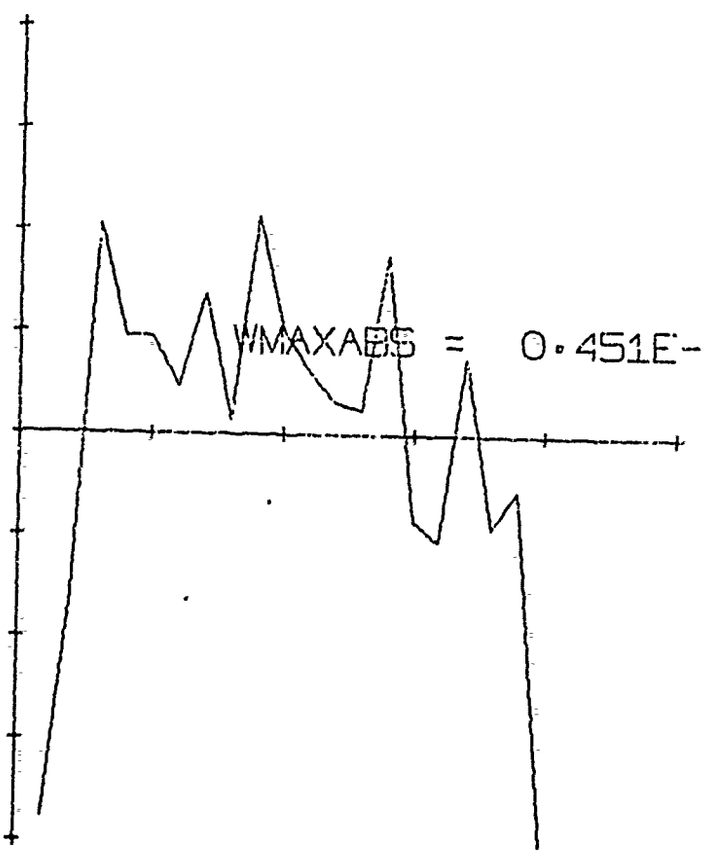

HYPERPLANE No. 5

FIGURE 19

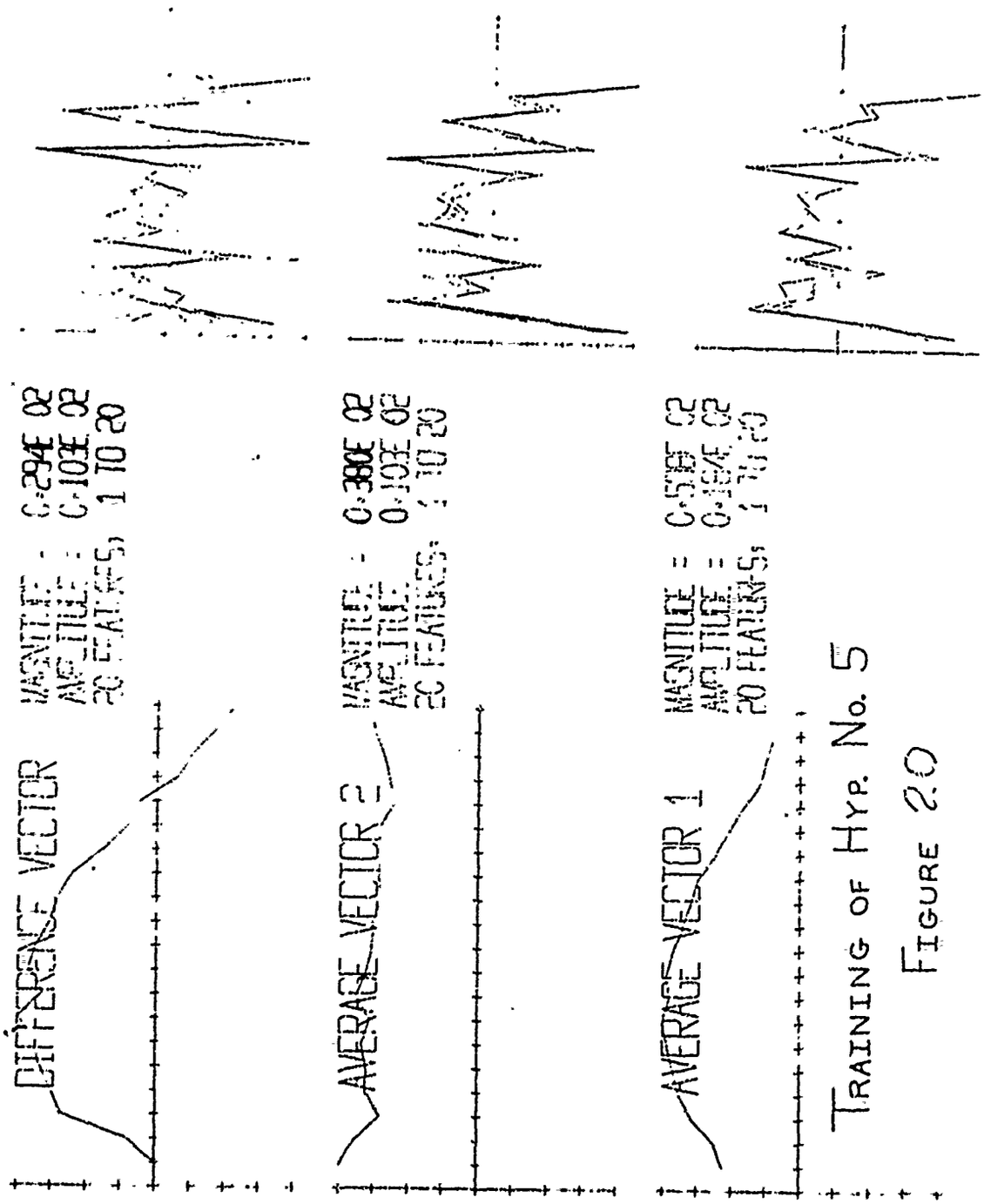

TRAINING OF HYP. No. 5

FIGURE 2.0

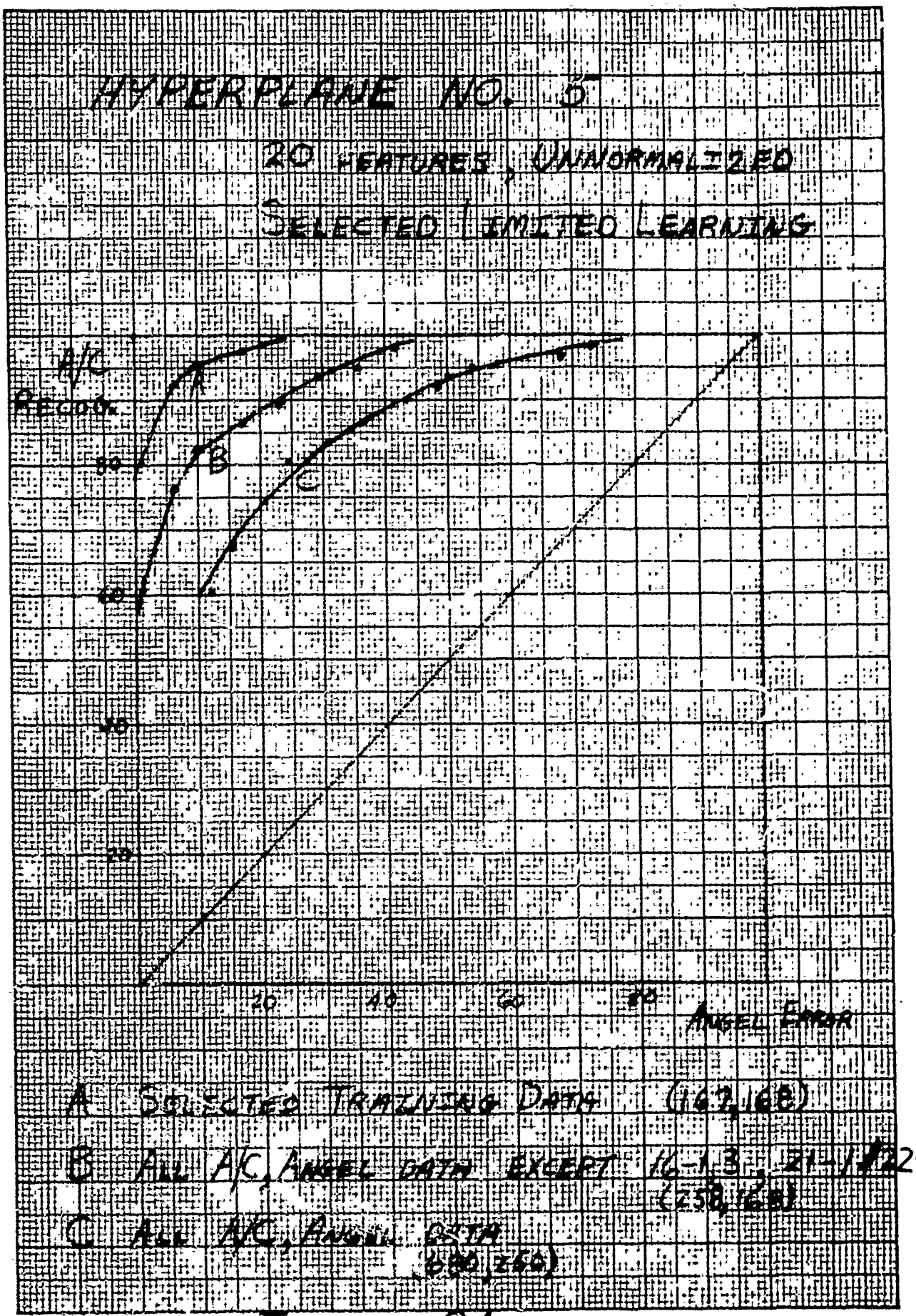
HYPERPLANE NO. 5
20 FEATURES, UNNORMALIZED
SELECTED LIMITED LEARNING
A/C
RECOG.
80
60
40
20
A
B
C
20
40
60
80
ANGEL ERROR
A SELECTED TRAINING DATA (162,162)
B ALL A/C, ANGEL DATA EXCEPT 16-1-3, 21-1-2-1 (258,162)
C ALL A/C, ANGEL DATA (280,260)

FIGURE 21

Curve C of figure 21 documents generalization for all aircraft and angel data available.

Figure 22 plots the weights of Hyperplane No. 37 whichwas trained on the randomly selected training sample. Figure 23 plots the probabilities obtained when this hyperplane is tested with all normally occurring aircraft and angel data. Clearly this performance is inferior to others previously obtained.

E Fixed target (clutter) rejection

Hyperplane decision rules were trained on a randomly selected training sample of fixed target (clutter) and aircraft/angel feature vectors. Hyperplane Nos. 29 and 32 resulted from that training and are plotted in figures 24 and 25. No. 32 was obtained from the same training session as 29, but received more iterations through the training set. This is reflected in the weight plot shapes. No. 29 is smoother and No. 32 had more time to make finer adjustments to its weights. The training of these hyperplanes is documented in figure 26. Note how the weight plot in the right-hand portion of the figure gradually changed from that of No. 29 to that of No. 32.

The excellent generalization properties of these two hyperplanes are plotted and discussed in figure 2 presented in the Summary of Results section. Hyperplane No. 29 had a 97.7% aircraft/angel detection rate and a 92.7% fixed target rejection rate. Comparable percentages for No. 32 are 98.1% and 90.6%.

Figure 27 diagrams the manner in which this fixed target clutter rejection capability could be used in conjunction with an angel rejection function. The serial logic flow conserves signal processing resource in that only target data known to be an angel or an aircraft are presented to the angel rejection decision rule. This serial logic flow is permissible because of the zero-aircraft-loss operation of the strobe threshold and the fixed clutter rejection rule.

1 20 20 1 2 130 84 1 22 15 37 31

ETA = 0.100E-03

UNNORM, BAD LL

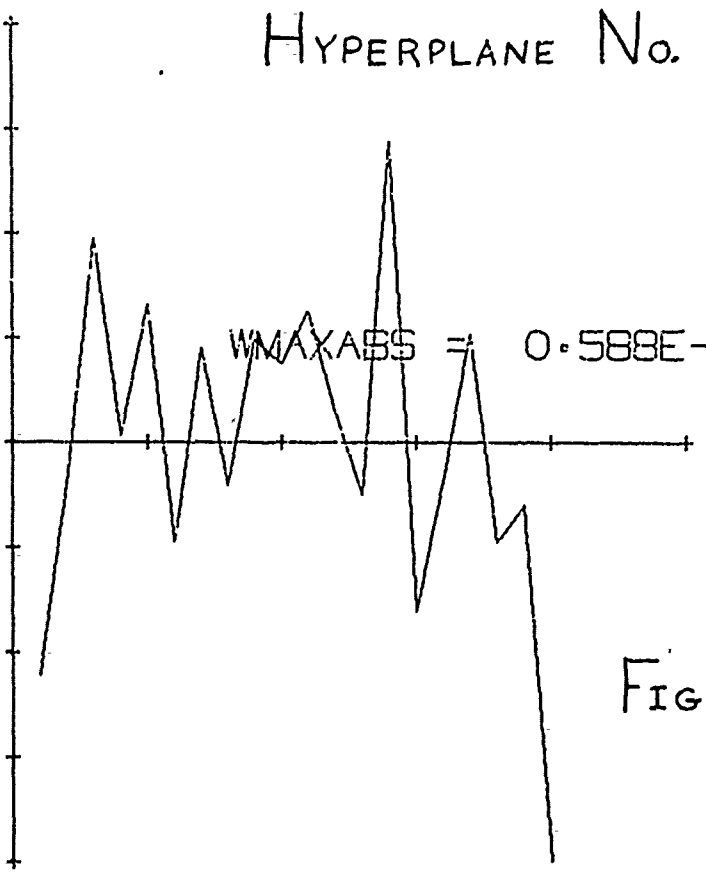

FIGURE 22

HYPERPLANE No. 37

20 FEATURES, UNNORMALIZED

REPRESENTATIVE LIMITED LEARNING

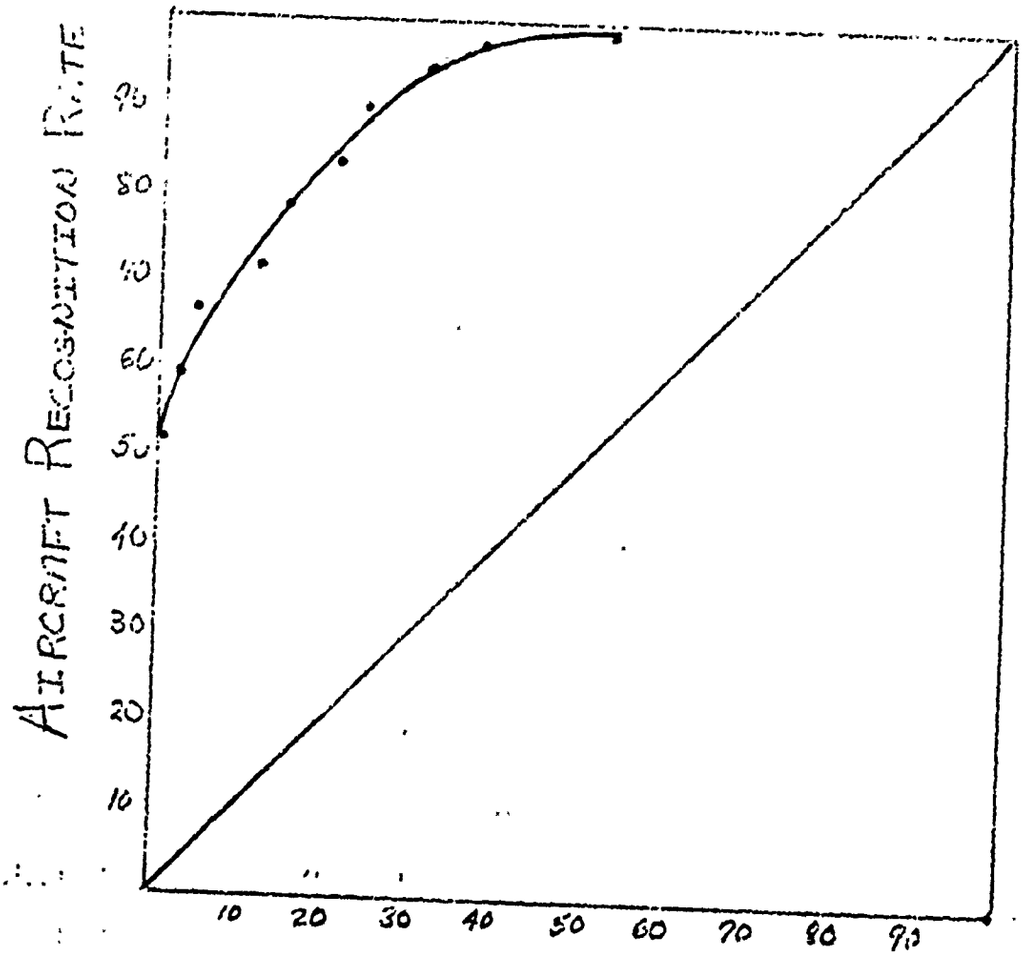

B GENERALIZATION (258,168)

FIGURE 23

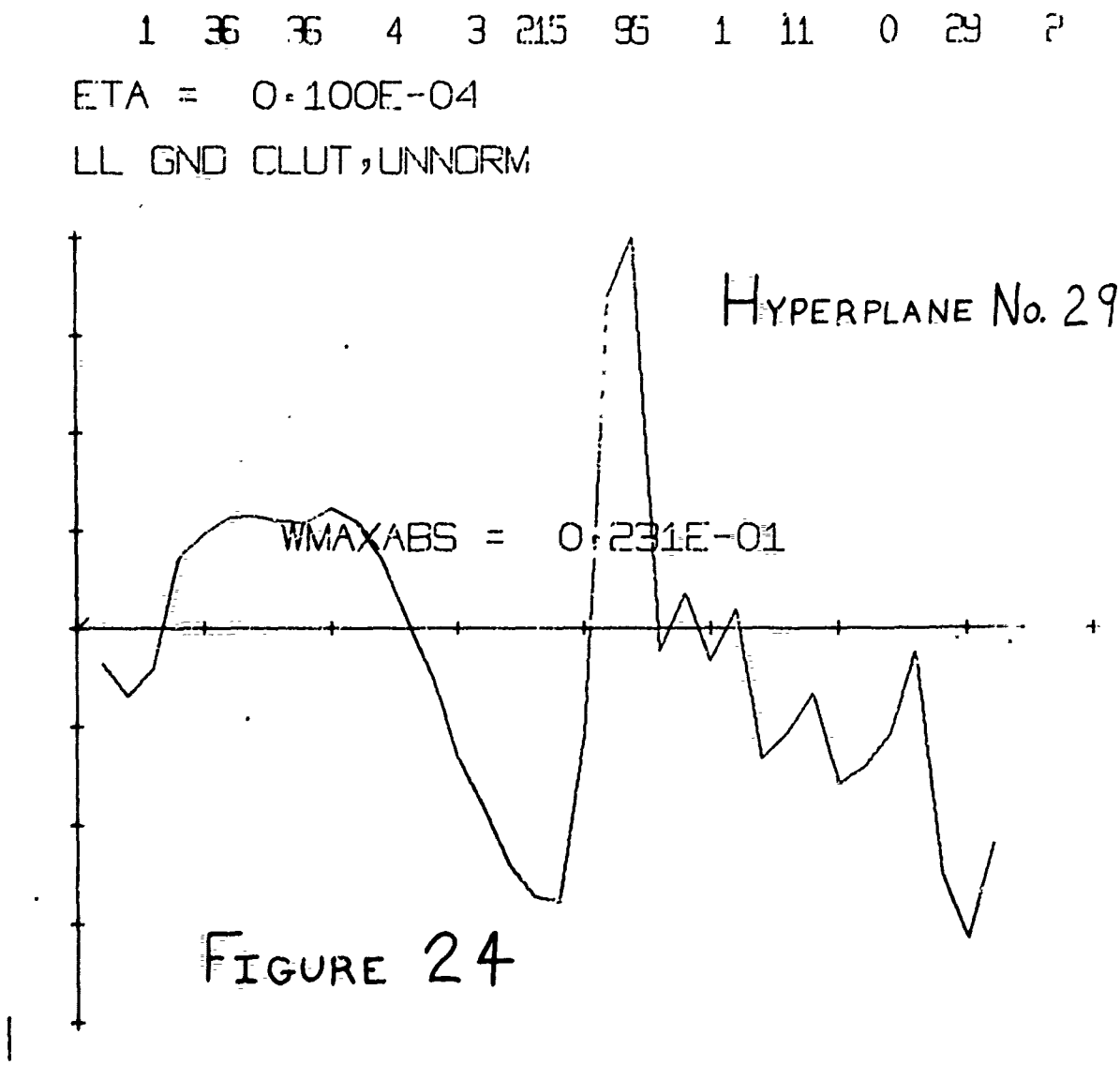
1 36 36 4 3 215 95 1 11 0 29 2
ETA = 0.100E-04
LL GND CLUT, UNNORM
HYPERPLANE No. 29
WMAXABS = 0.231E-01

FIGURE 24

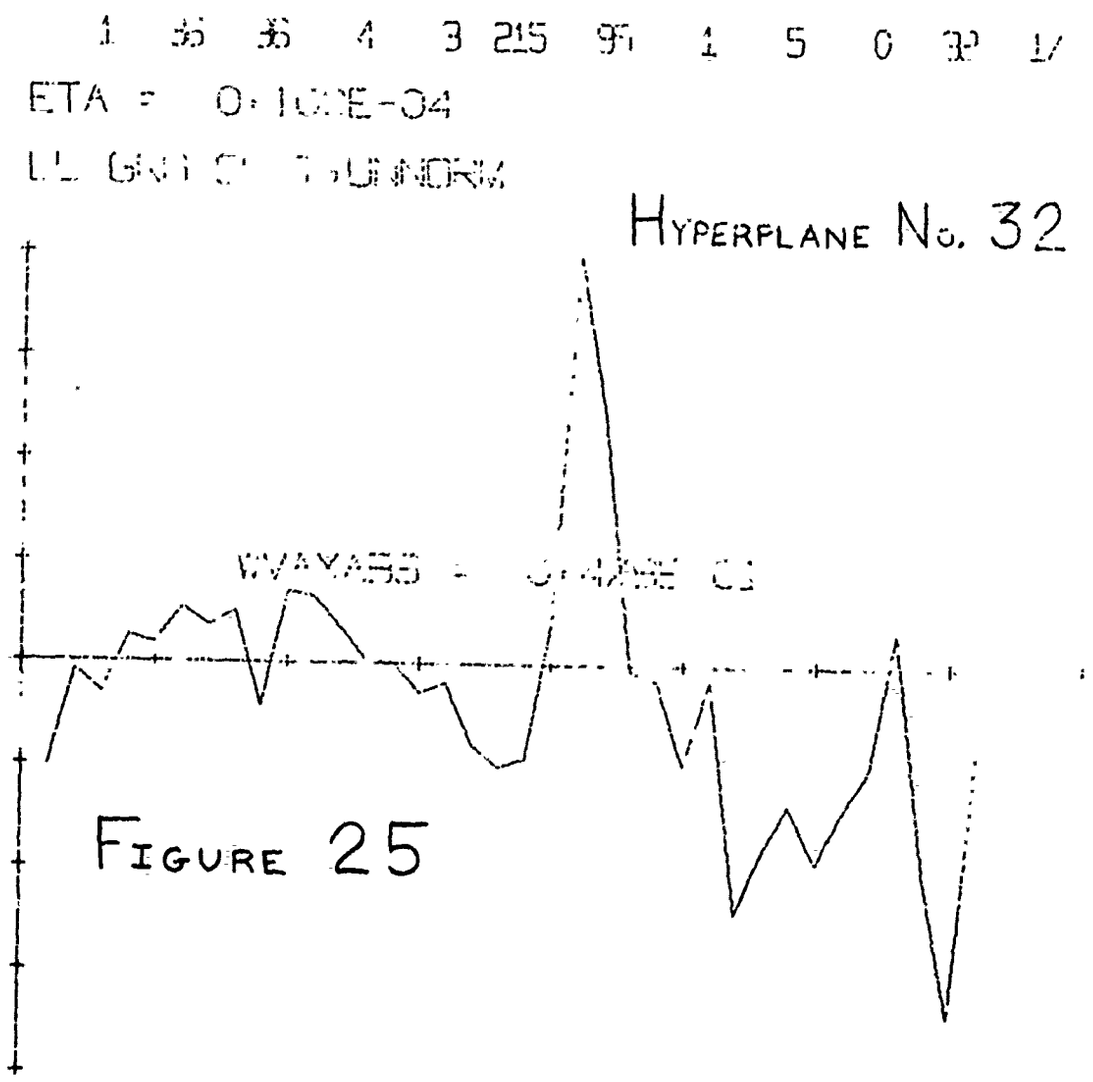

FIGURE 25

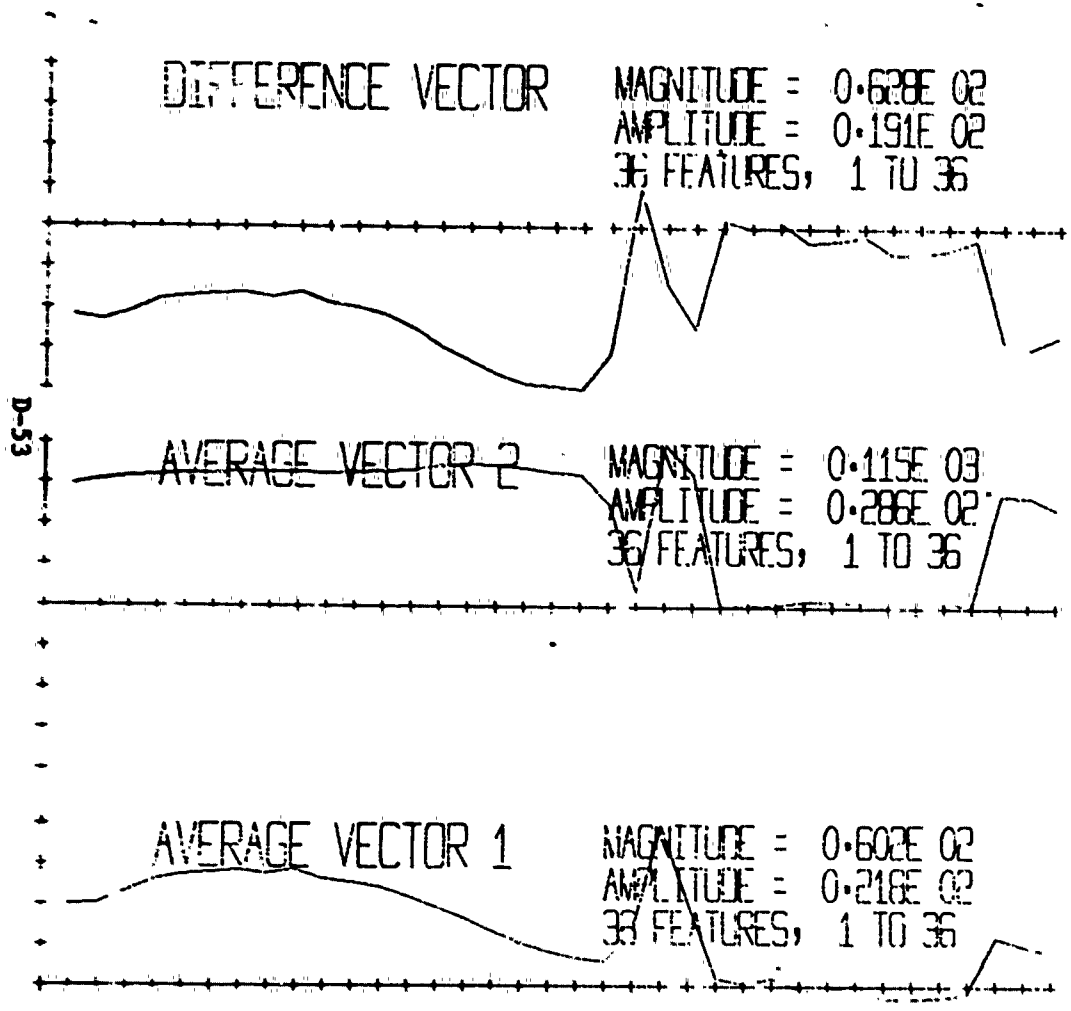

TRAINING OF HYPERPLANES 29 AND 32

FIGURE 26

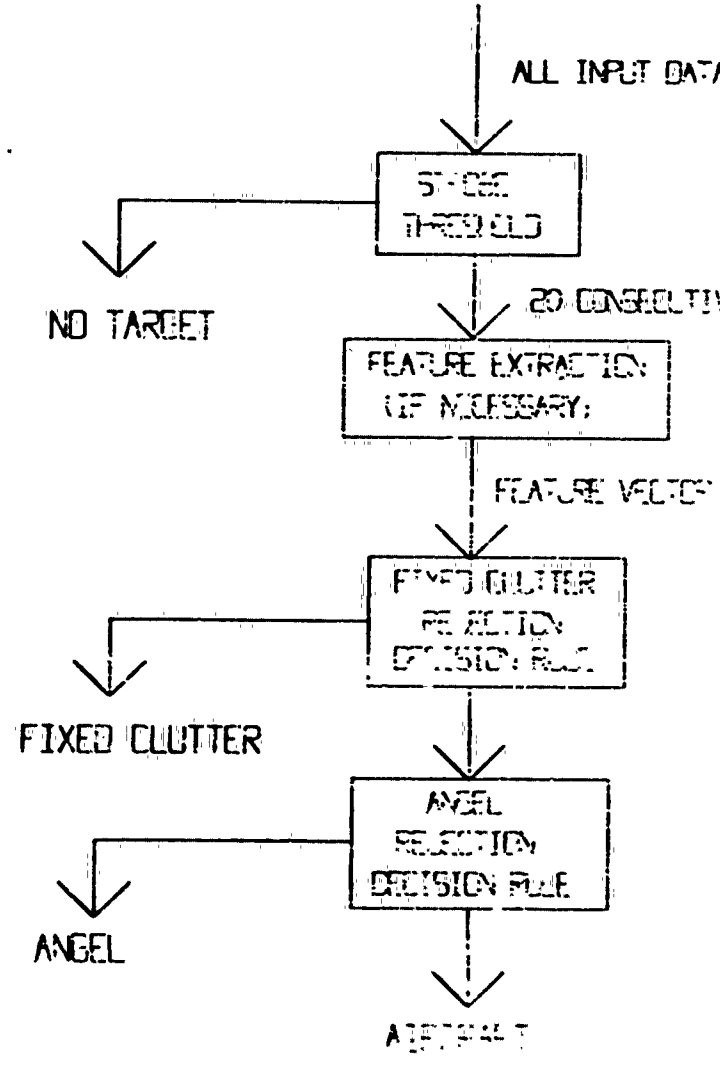

ANGEL REJECTION SYSTEM LOGIC FLOW

FIGURE 27

VI Recommendations

A General Recommendations

The work reported herein establishes that very high levels of angel clutter reduction are possible with zero-aircraft-loss. A recommended implementation is described in the next section of this report which is economically acceptable for on-site deployment.

Therefore, major recommendations can be made at this time:

(1) Continue hyperplane decision rule experimentation to develop a reliable rule trained on a large representative sample of aircraft/angel data using only the 20 dwell amplitudes and as few of the special processors as possible.

(2) Conduct a systems study based on the results of this expermentation and finalize hardware design.

(3) Construct a prototype angel reduction system and install at an active radar site.

(4) Monitor and evaluate site operations.

(5) Finalize system deployment specification.

(6) Produce and deploy angel reduction processor systems to appropriate sites.

Because of its combined in-depth experience in all phases of these required tasks, Bendix Communications Division feels especially qualified to perform them. The integration of decision rule training, systems study, hardware design, radar signal processing, site installation and equipment production capabilities within one contractor's expertise would greatly facilitate action on these recommendations.

B Preliminary Implementation Recommendation

The implementation shown in figure 28 conforms exactly to that simulated on the computer. Thus it is recommended only to the extent that all of the various special processors are needed. Further study will probably show that only a few are truly useful. However, to gain some idea of the worst case cost of an eventual system this maximum system was blocked out and estimates based on it. These budgetary, quantity estimates are under $12,000 for a single channel system and under $23,000 for a dual system.

This system configuration is presented here solely to substantiate the fact that the signal processing developed during the reported work can be implemented within the economic constraints of large scale site deployment.

In developing a proposed hardware realization both minicomputers and special purpose processors were considered. The special purpose circuits won out because of the large number of multiplications required in near real time and because the fixed and parallel nature of the operations required take little advantage of the general purpose, sequential capabilities of a computer.

The major cost centers considered in arriving at quantity budgetary estimates are listed below:

Material

256 Bit Shift Registers
400 Bit Shift Registers
2048 Bit Shift Registers
8 x 20 RAM's
Multipliers
A/D Converter
Square Root ROM
D/A Converters
Miscellaneous Modules

Cabinet
PC Boards
Power Supplies
Miscellaneous Hardware & Cable Set

Assembly & Test

Instruction Books & Documentation

Markup

Single Channel System	$12,000
Dual Channel System	$23,000

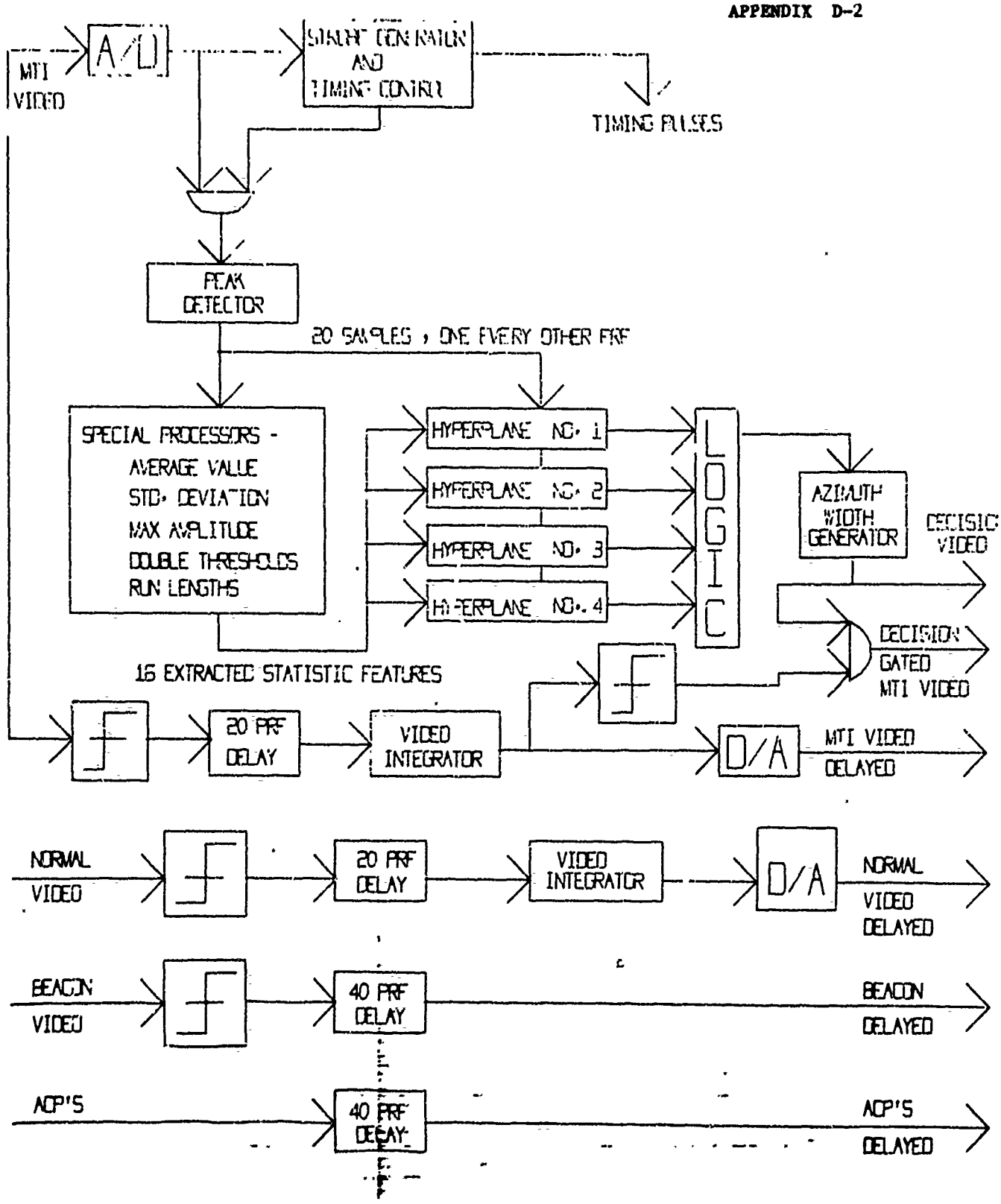

RECOMMENDED IMPLEMENTATION

FIGURE 28

The operation of the system is as follows:

1. MTI Video is converted to 5 bit digital words at a sample rate of 0.4 usec (approximately one half the pulsewidth). All processing is then carried on digitally. When video is mentioned it should be understood as digital video.

2. Whenever the video exceeds a threshold a strobe pulse is generated which places a sampling gate around the range of the strobe. (Typically the gate is 3 range cells (1.2 usec) wide centered on the strobe.) This sampling gate is repeated every other PRF period at the same range for 40 PRF periods.

3. The sampling gate allows video to flow to the peak detector which determines the maximum value in the three contiguous range cells. The output of the peak detector is, therefore, sets of 20 samples taken every other PRF period at each range where a target appears. In this system 256 range cells are considered. This gives a total coverage of 1.2 usec x 256 = 307.2 usec or 24.8 miles.

4. The samples are next processed by the special purpose circuits. These handle the data in real time keeping running sums for each range increment. For example, the average value circuit (figure 29) multiplies each sample by $\frac{1}{20}$ then adds it to the value already recirculating in the shift register memory. In this way $\frac{\Sigma s_i}{N}$ or $\bar{S}$ is available only one multiplication and addition after the last sample. Multiply and add times are typically 300 nanoseconds each. Thus the answer is ready in less than the 1.2 usec range increment.

The other special processor circuits operate in the same general manner with varying degrees of complexity.

5. The 20 amplitude samples are fed to the four recognizers in parallel where they too are processed in real time. Figure 30 shows the amplitude section

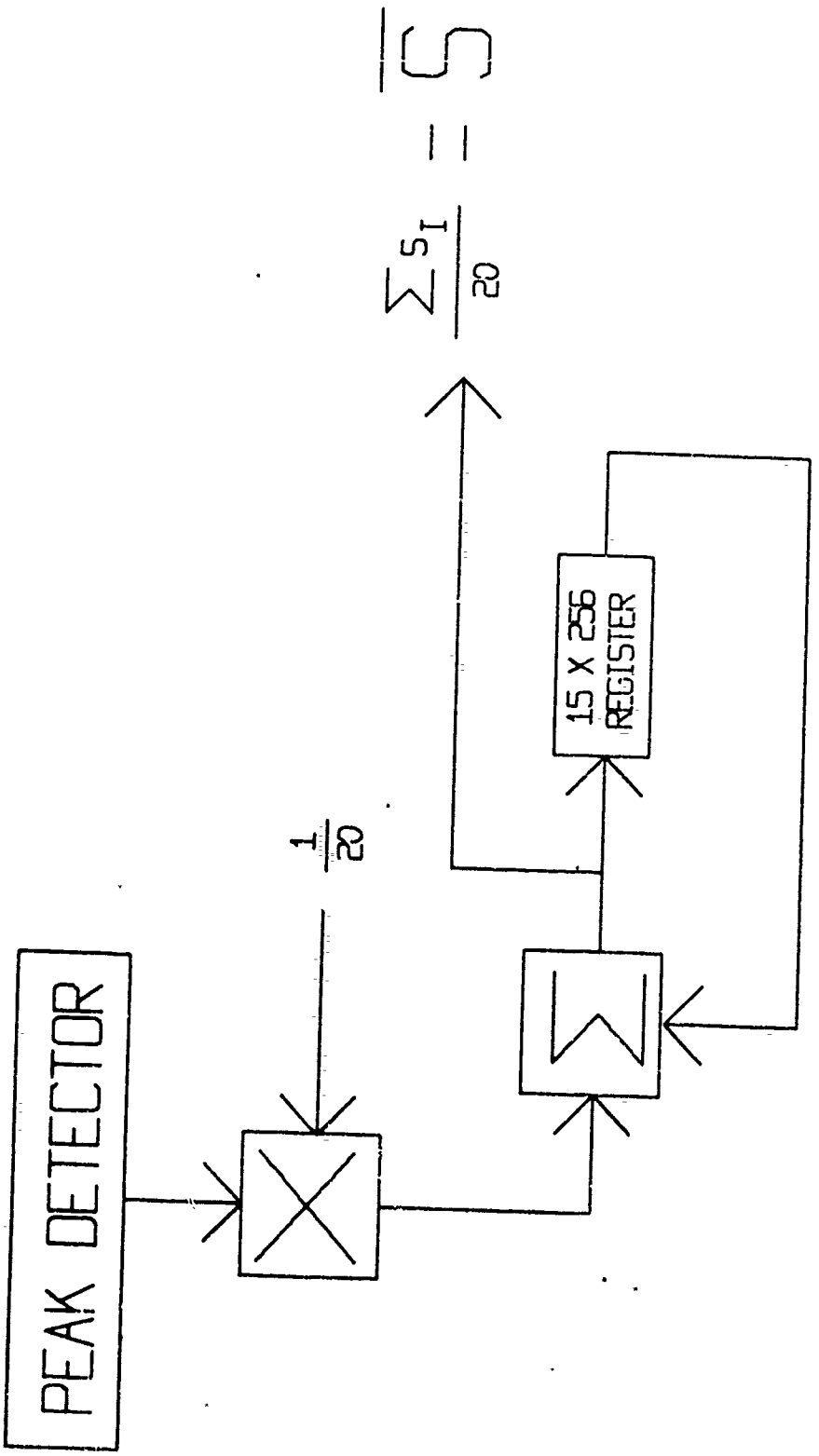

AVERAGE VALUE CIRCUIT

FIGURE 29

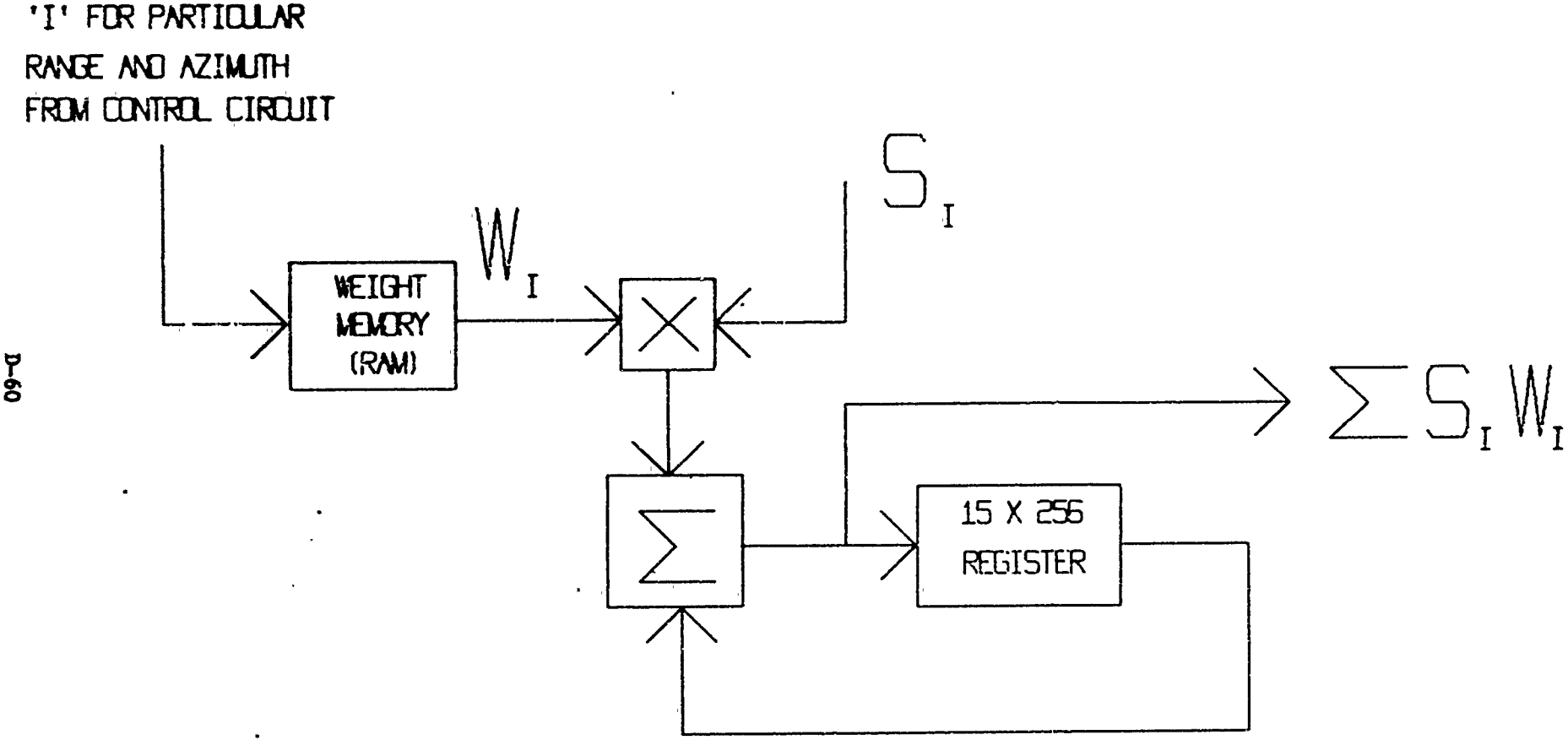

AMPLITUDE SECTION OF HYPERPLANE

FIGURE 30

of a typical recognizer. The weight memories are small, solid state, random access units which operate in 300 nanoseconds. Thus the time required for access, multiply and sum is still under 1.2 usec keeping the process real time.

6. Since the outputs of the special processor for any particular target are not available until after the last sampe (the 20th), they are weighted and added to the amplitude sum during the time beyond the clutter range in the 40th PRF period.

7. With the recognition sums complete, the output of each recognizer is fed to the logic circuit which implements the simple decision tree described previously in the simulation sections. The output of the logic circuit for aircraft is a pulse at the target range.

8. The pulses from the logic circuit are sent to the azimuth width generator which produces pulses at the target range for a number (K) of succeeding PRF periods. This output is called the decision video and when applied to a PPI will show only targets that the recognizer considers to be aircraft. The apparent target azimuth widths can be varied by varying K.

9. Provision is made for generating gated MTI video or MTI video so that by using the PPI mixing circuits various video and background combinations can be obtained.

10. Since the decision making process takes 40 PRF periods all videos and azimuth change pulses must be delayed correspondingly. Videos which are to be integrated (i.e. all primary radar videos) should be delayed less since the integration process also produces a delay.

C Further hyperplane decision rule experimentation

Work can proceed immediately to investigate whether comparable performance can be demonstrated with dwell amplitude information alone without the use of extracted statistic features. If this can be accomplished, significant reductions in signal processing hardware requirements would be possible. This would favorably impact both system cost and reliability/ maintainability considerations.

If satisfactory performance cannot be achieved with dwell amplitude information alone, surely some of the 16 extracted statistic features can be dispensed without noticeable performance degradation. Prime candidates for such deletion from the feature vector are some of the double threshold features and possibly the amplitude standard deviation estimate. Any such reduction in input data requirement would again favorably impact site implementation.

When using dwell amplitude information, it has been demonstrated during this program that area normalization of dwell amplitude feature vectors can significantly improve decision rule performance. Amplitude waveform samples can be efficiently area normalized in hardware implementations. Thus experiments should be conducted which seek to establish the benefits accruing through area normalization.

VII Acknowledgement

The reported work was performed under the direction of The Johns Hopkins University Applied Physics Laboratory, who also supplied the data base.

Special mention is appropriate of the valuable consultation provided by Dr. James T. Miller of the APL technical staff.

APPENDIX E

ANGEL CLUTTER REDUCTION SYSTEM DESIGN DATA

APPENDIX E-1

DESIGN DATA FOR RECEIVER GAIN CONTROL CIRCUITRY

In order to accommodate different density angel situations, different STC attenuation profiles should be provided. Based upon the information presented in Section 4.1.1, the best profile is proportional to R^{-4}; however, the best attenuation level is dependent upon angel altitude. To provide for these variations, the STC generator design provides for the three profiles. It should be emphasized that this circuit approach can be used to generate any desired profile shape. The attenuation profile is maintained in to 2 nmi. Within 2 nmi, constant attenuation is used.

Figure E-1 is a schematic diagram of the STC generator. The remote lines select the appropriate Programmed Read-Only Memory (PROM); they also select the clock frequency. Since the total STC range is different for each curve and since there are 64 range bins in each curve, the clock frequency is a function of the particular curve selected.

The control signals can be easily traced by referring to the Timing Diagram, Figure E-2. The ASR STC trigger is buffered by the input amplifier. The STC trigger is used to reset the address counters and the divide by 14, 12 and 10 counters. One-shots #6 and #7 generate one clock pulse during the radar dead-time and set the address counter to binary "1". The output word of the selected PROM is then decoded by the D/A converter. The analog voltage at the converter output is then at the correct DC level for the start of the sweep. Thus the IF attenuation will be constant out to two nautical miles.

One-shots #3 and #4 along with flip-flop 2 are used to gate the clock into the address counter at a range of two nautical miles. As the counter counts from 1 to 63 the stored

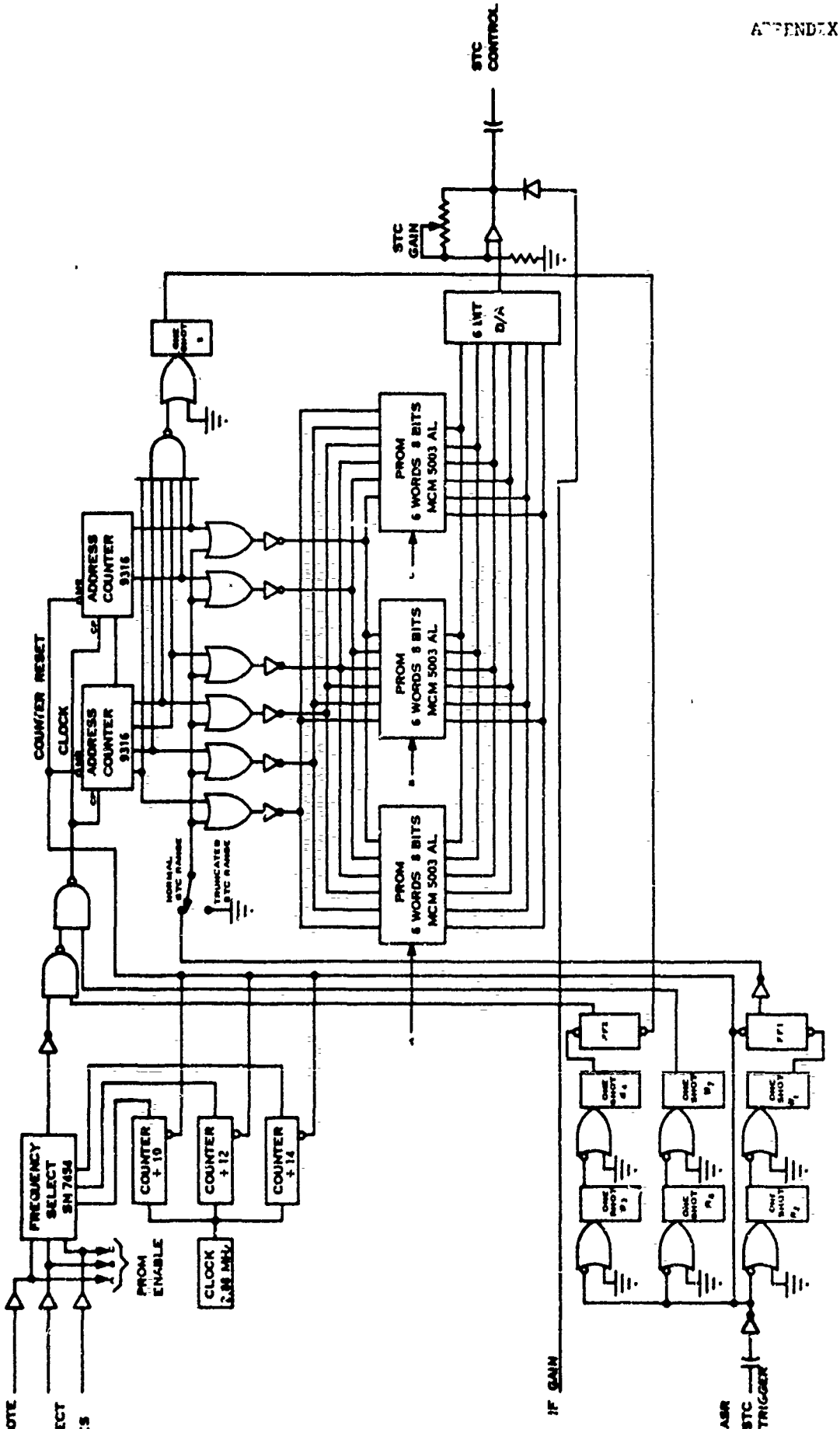

FIGURE E-1 DIGITAL STC SCHEMATIC DIAGRAM

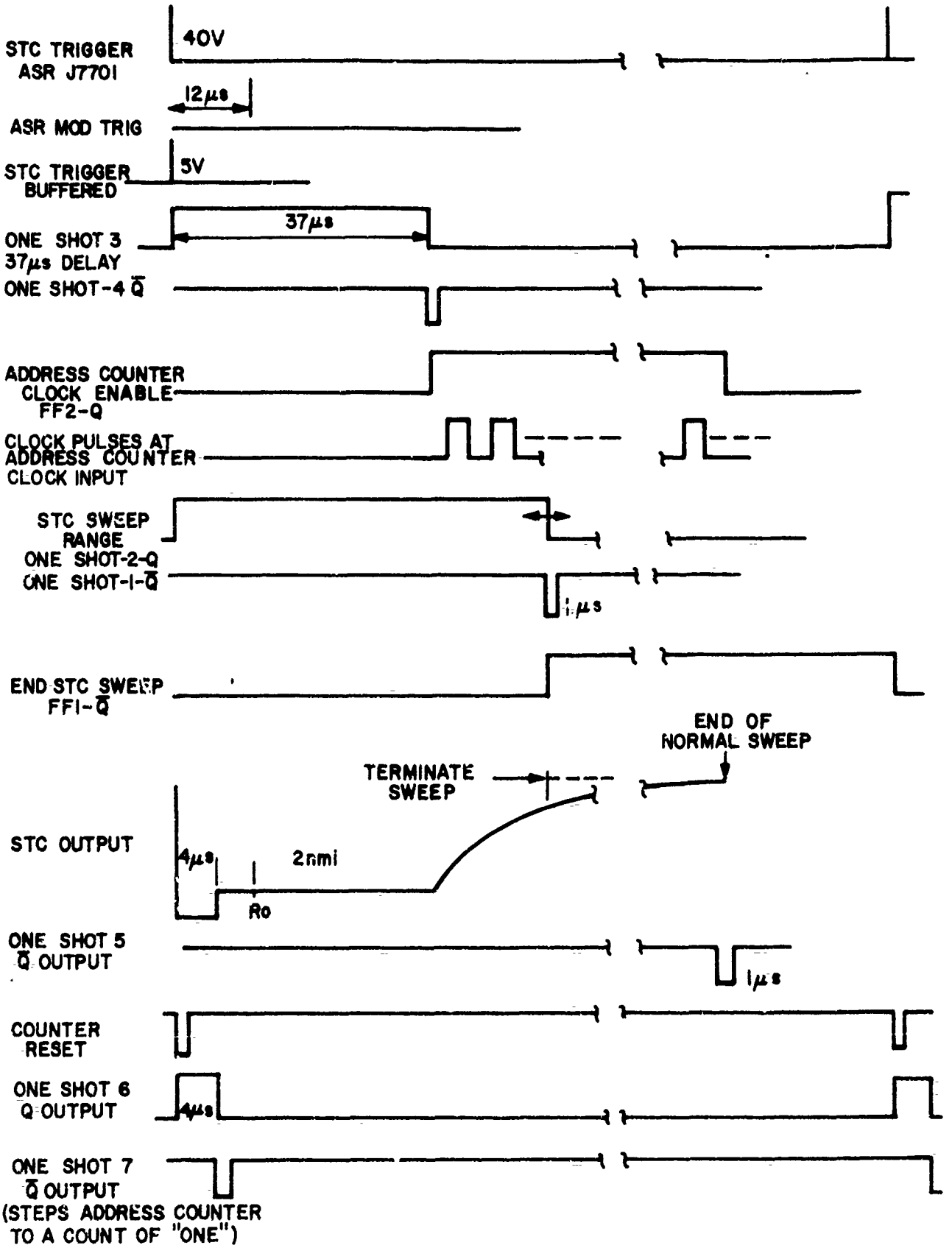

FIGURE E-2 STC TIMING DIAGRAM

words in the PROM which correspond to consecutive amplitude points on the curve are brought out on data lines and converted to an analog voltage by the D/A converter. The operational amplifier following the converter provides for adjustment of the STC sweep amplitude.

When the address reaches "63" the output of the eight-input NAND gate goes to ground which triggers one-shot #5 and its output pulse then clears FF2 thus inhibiting the clock pulses. The contents of the address counters remain at "63" and the output of the D/A converter will be at its maximum value. The next STC trigger will generate a counter reset and the procedure is repeated.

The operation used to terminate the STC sweep at a selected range operates as follows: The control switch is thrown from the "normal sweep" to the "terminate sweep" position. If the sweep is to be terminated at 15 nmi, for example, the potentiometer is adjusted for a delay of 15 nmi x 12.36 μs (delay from Mod Trig to STC Trig = 197 μs).

At a range of 15 nmi the trailing edge of the pulse at one-shot #2-Q output triggers one-shot #1 and a 1 μs pulse is generated which prevents FF1. The ground at the Q output of FF1 is inverted and logic "ones" will be present on address lines. This address places amplitude word number 63 on the PROM output lines, thus causing the output of the D/A converter to reach its maximum amplitude. The address counters are still counting clock pulses until a count of "63" is reached and the eight-input NAND gate generates a clock inhibit via one-shot #5 and FF2.

The next STC trigger clears FF1 and resets all counters and the procedure is then repeated.

APPENDIX E-2

AZIMUTH CORRELATOR DESIGN DATA

A schematic diagram of the Azimuth Correlator is shown in Figure E-3 and E-4. The top row of elements in Figure E-3 is 20 1000-bit shift registers. The outputs are gated to a set of full adders for determining the number of ones at the output of the shift registers. The gates are for range control of n. This sum is then compared with the threshold (m) in the two 4-bit comparators. If the threshold is exceeded, a correlated synthetic video output pulse is indicated. Figure E-4 is a schematic of the control necessary to change the values of n and m at a specified range. The two m values are indicated as m_1 and m_2 and are represented by 5 bits each. When the control line is high one set of 5 is gated to the threshold. When the control line is low, the other set of 5 are used. The operation for n is similar except a decoding matrix is necessary to provide for the proper selection of the gates. With 4 lines for n_1 and n_2, n can be varied from 5 to 20. The timing diagram is included in Figure E-5.

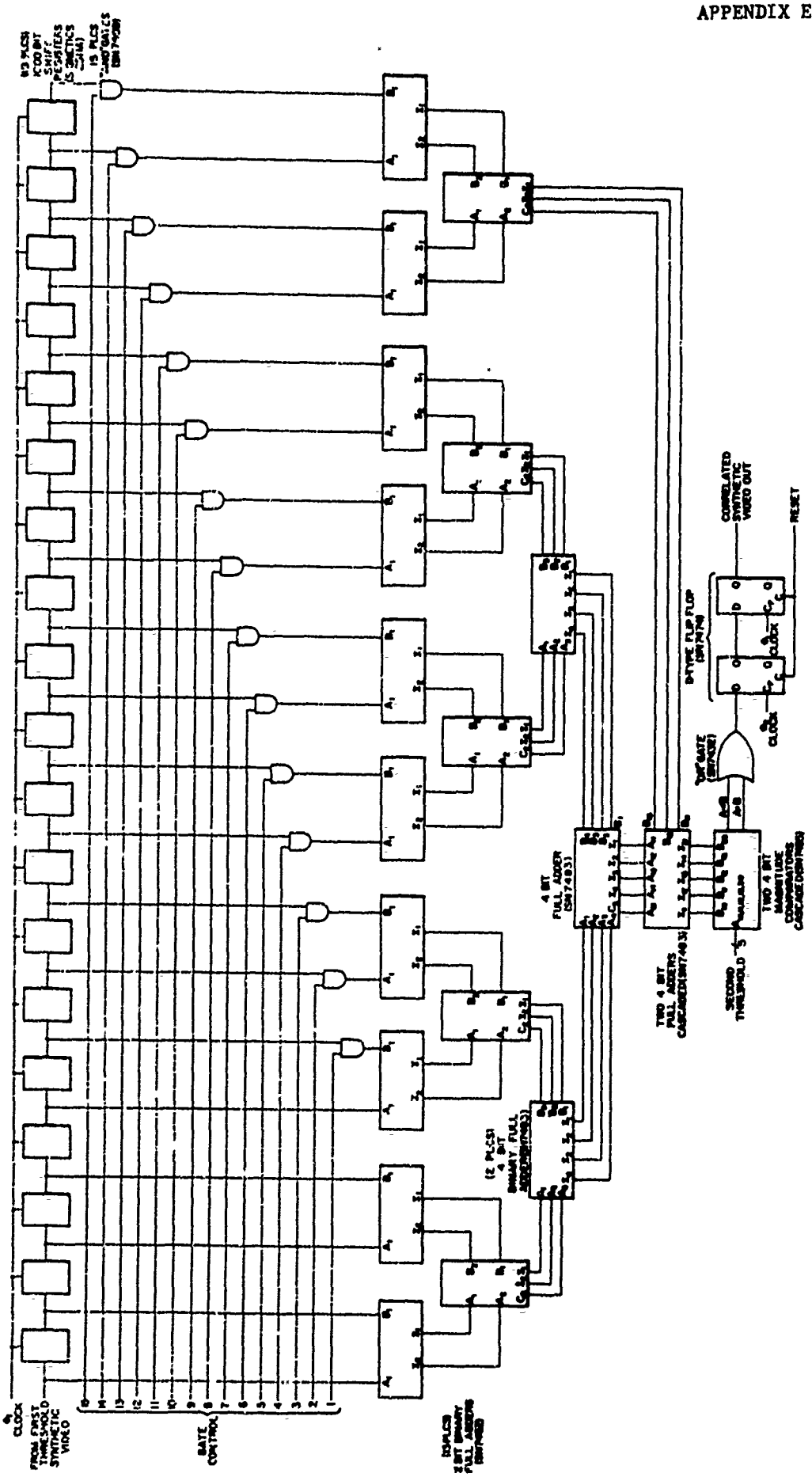

FIGURE E-3 AZIMUTH CORRELATOR DETECTOR SCHEMATIC DIAGRAM (SHEET 1 OF 2)

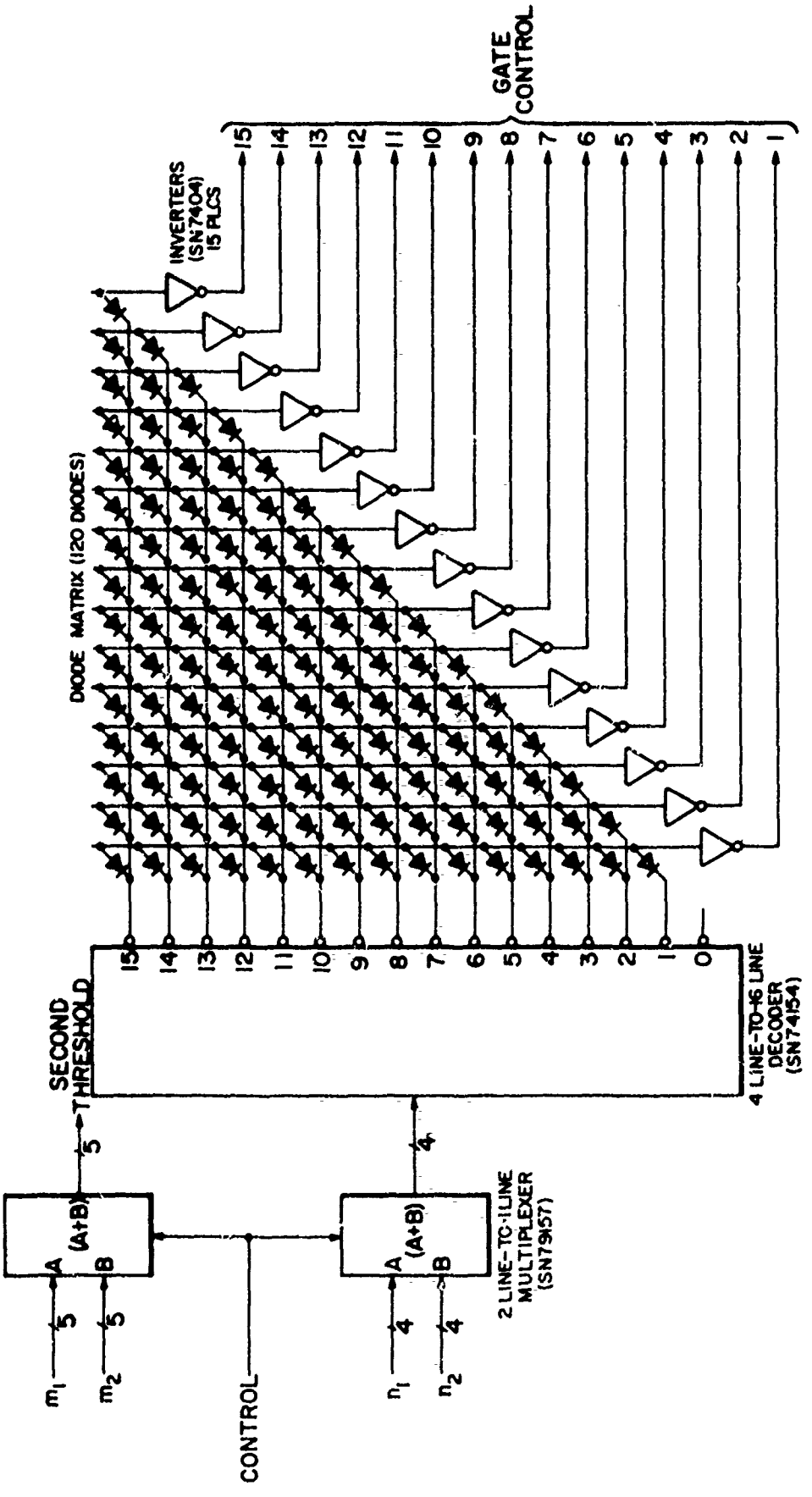

FIGURE E-4 AZIMUTH CORRELATOR DETECTOR SCHEMATIC DIAGRAM

(SHEET 2 or 2)

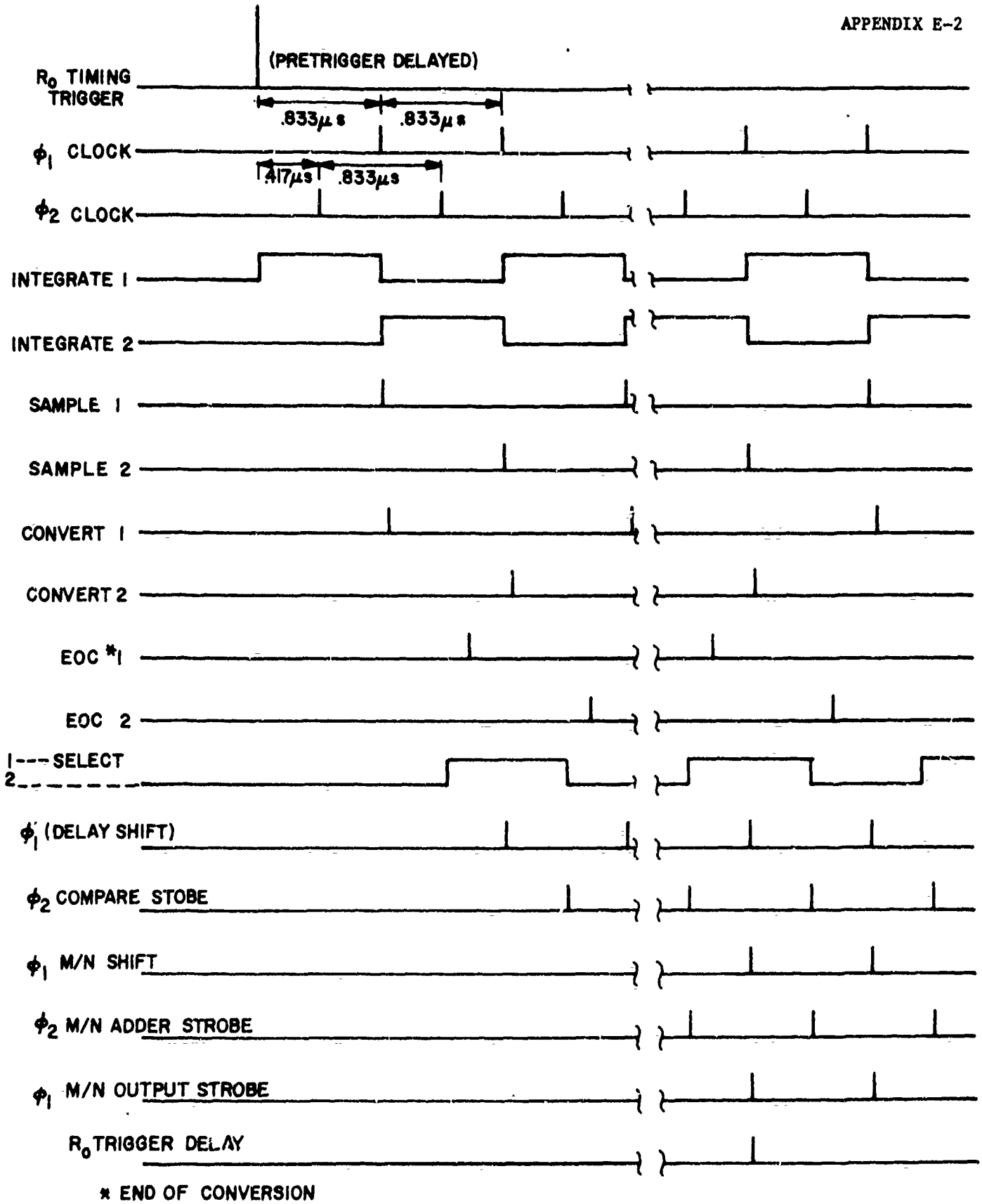

FIGURE E-5 AZIMUTH CORRELATOR AND ADAPTIVE QUANTIZER TIMING DIAGRAM

APPENDIX E-3

ADAPTIVE QUANTIZER DESIGN DATA

An adaptive quantizer is a video signal processor which thresholds each range cell using a threshold which is derived from a sample of the environment surrounding the range cell of interest. The purpose of the adaptive threshold is to maintain a constant or approximately constant false alarm rate in distributed clutter and receiver noise.

An in-depth study of the several forms of adaptive quantizers suitable for use with the ASR radar was conducted under Task I of this contract*. The recommended approach, which is now being used in the Enhanced ARTS Radar Processing Subsystem, is a rank quantizer (Figure E-6), which compares the target with a number of range cells ahead of and behind the target cell. A detection is declared when the target cell exceeds k out of the total number, n, of range cells. The false alarm rate is then independent of the distribution of the input interference (clutter, noise, etc.) and the processor is said to be "distribution free" or "non-parametric", with a false quantization rate given by:

$$P_n = \frac{n + 1 - k}{n + 1}$$

The false quantization rate can also be changed by multiplying the target cell voltage by a constant, K_M, for normal video. (An additive constant K_A, is used for log video.) If K_M is greater

*APL Report MSO-F-183, ARTS Enhancement Support Program Multisensor System Study, 31 January 1973

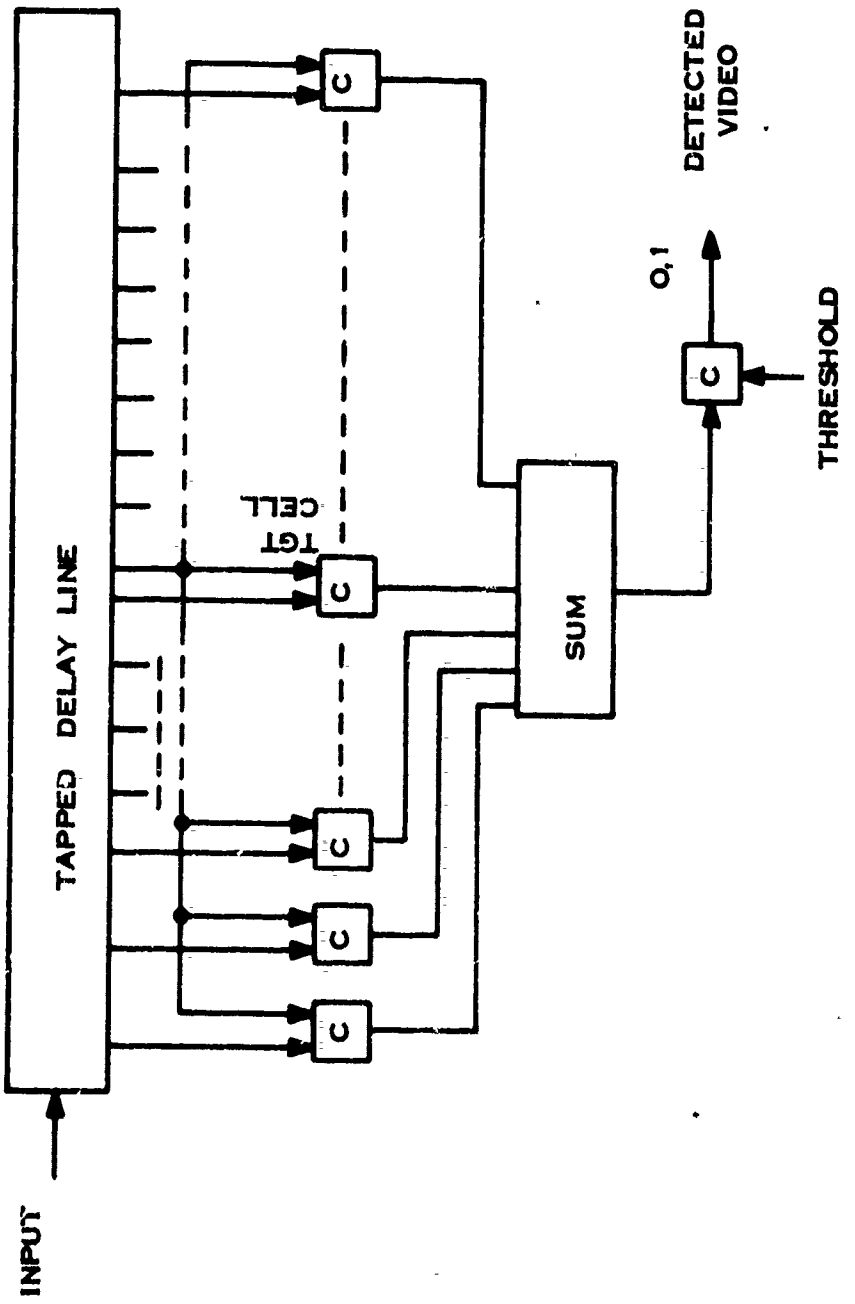

FIGURE E-6 RANK QUANTIZER

than unity, the false quantization rate decreases. Unfortunately, if $K_M \neq 1$ (or $K_A \neq 0$), the processor looses its non-parametricity; the false quantization rate becomes more dependent upon the interference distribution as the target cell modifying constants depart from these values.

Figures E-7 and E-8 are schematics of an Adaptive Rank Quantizer. In Figure E-7 the radar video is integrated, sampled, and A/D converted with two alternating sets of hardware. This is to allow adequate time for the A/D converters to complete the operation. The outputs are multiplexed as a continuous stream of 6 parallel bits. In Figure E-8 the 6 parallel bits are stored in 16 serial hex flip-flops. The outputs of these flip-flops are all compared with the central flip-flop in digital comparators. The outputs of the comparators are summed in full adders to determine the number of cells exceeded by the center cell. This number is then compared with a threshold in another digital comparator to generate the output. The output consists of a single pulse if the threshold is exceeded. The timing diagram is contained in Figure E-5 of Appendix E-2.

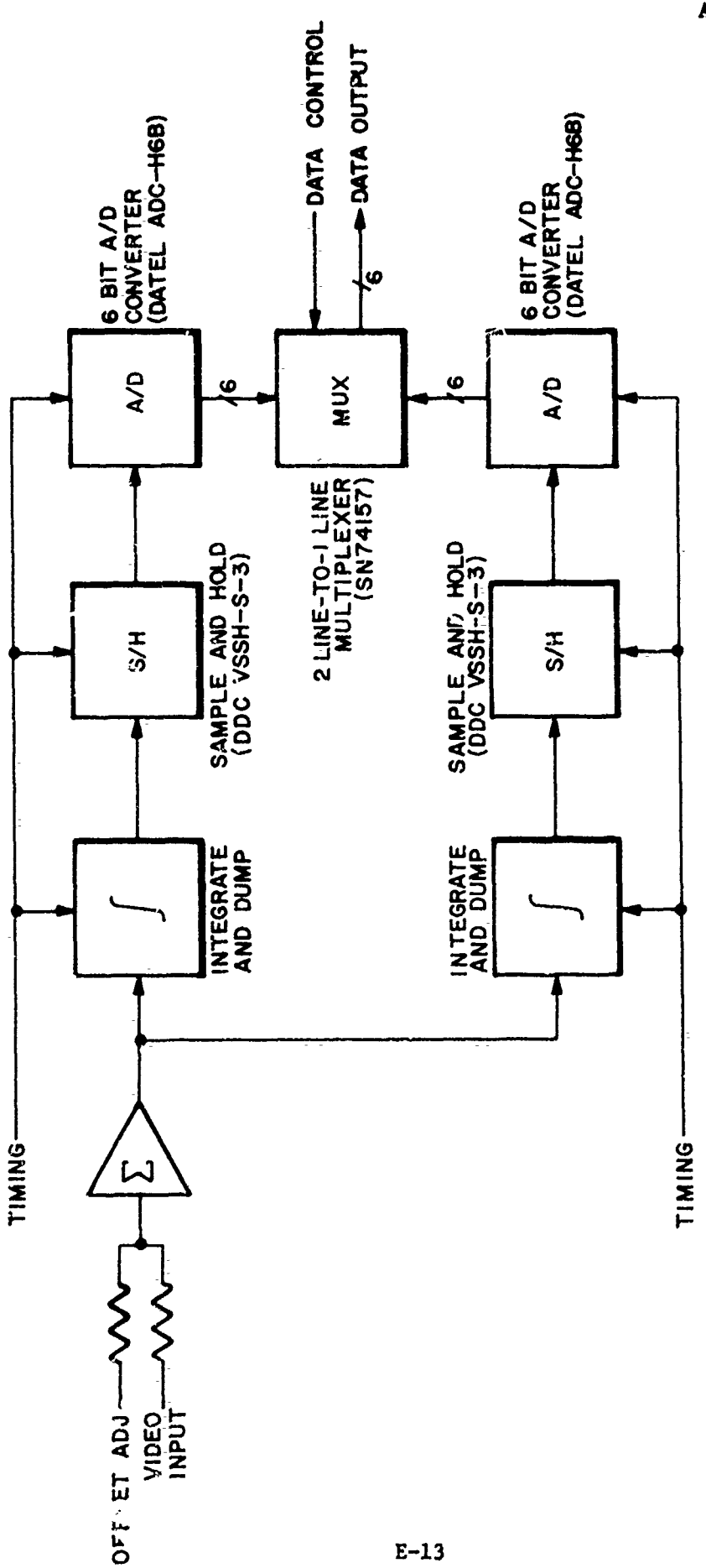

FIGURE E-7 ADAPTIVE QUANTIZER SCHEMATIC DIAGRAM

(SHEET 1 OF 2)

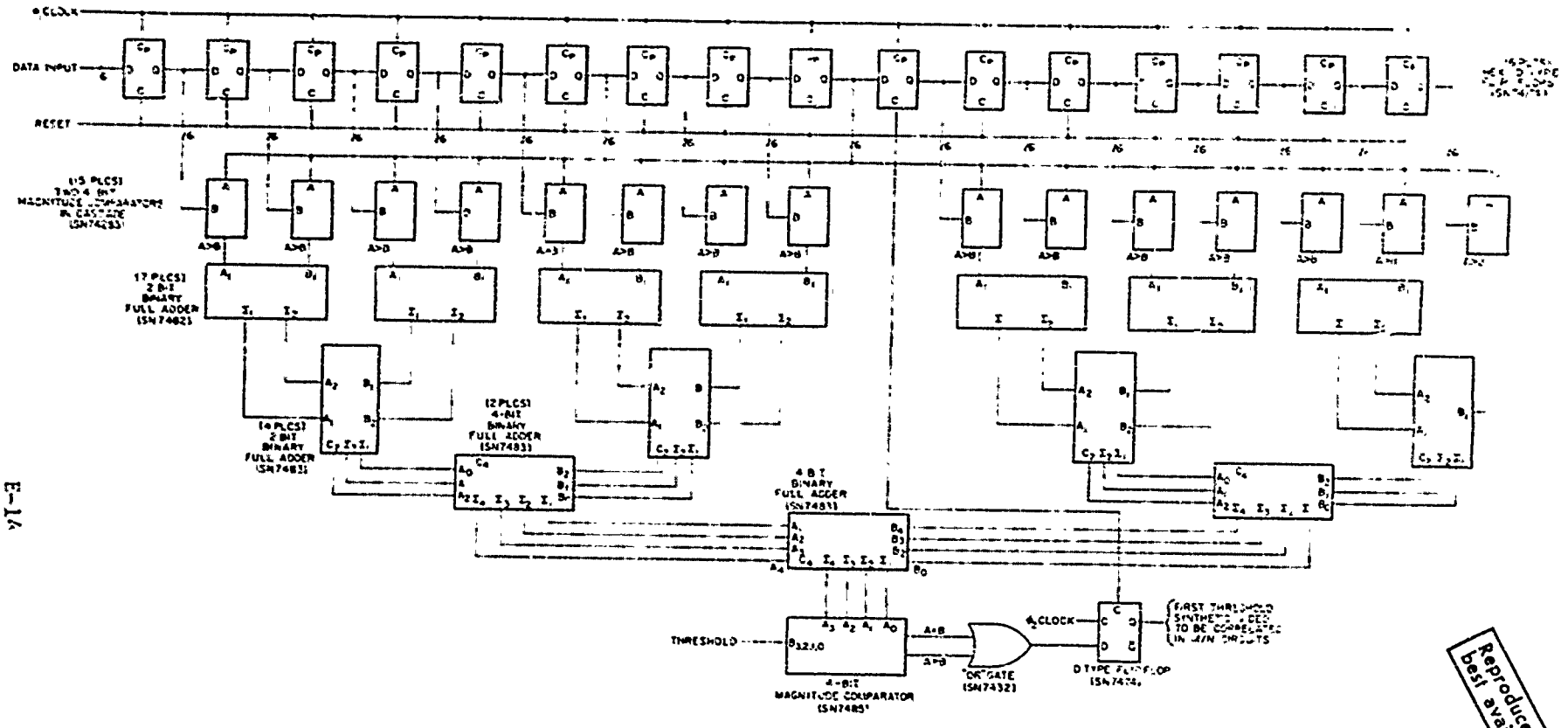

FIGURE E-8 ADAPTIVE QUANTIZER SCHEMATIC DIAGRAM (SHEET 2 OF 2)

APPENDIX E-4

SCAN HISTORY DISPLAY DESIGN DESCRIPTION

The Scan History Display (SHD) is a specialized PPI built to display a maximum of 256 target positions as they appeared during the most recent eight radar scans. The target positions are entered into the SHD from the AN/SYS-1 Target Information Processing System developed by APL for the U.S. Navy. As video processor target detections are correlated in the SYS-1 software, hit centroid positions are generated and transferred to storage in the SHD core memory. For the radars normally used with the SYS-1 system, the target centroids reported to the SHD typically are generated from six ungated hits but may be generated from only one ungated hit. Once the target positions are reported to the SHD they are stored and displayed for eight scans. The eight scan display of target centroids allows a greatly enhanced manual detection and entry capability in adverse clutter environments. True target tracks are easily discriminated against a clutter background by the distinctive trail they produce.

The Scan History Display circuitry is fully documented in an AN/SYS-1 report* which can be made available upon request. Consequently only a general outline of its design will be provided here.

System Block Diagram

The SHD block diagram is shown in Figure E- 9 indicating major functional blocks. There are three computer input functions to the SHD, an x-coordinate word, a y-coordinate word, and a zero bearing mark (Figure E-10). These words are buffered through line

*APL Fleet Systems Report SMS-FS-551, RDS/SHD Scan History Display, August 1972.

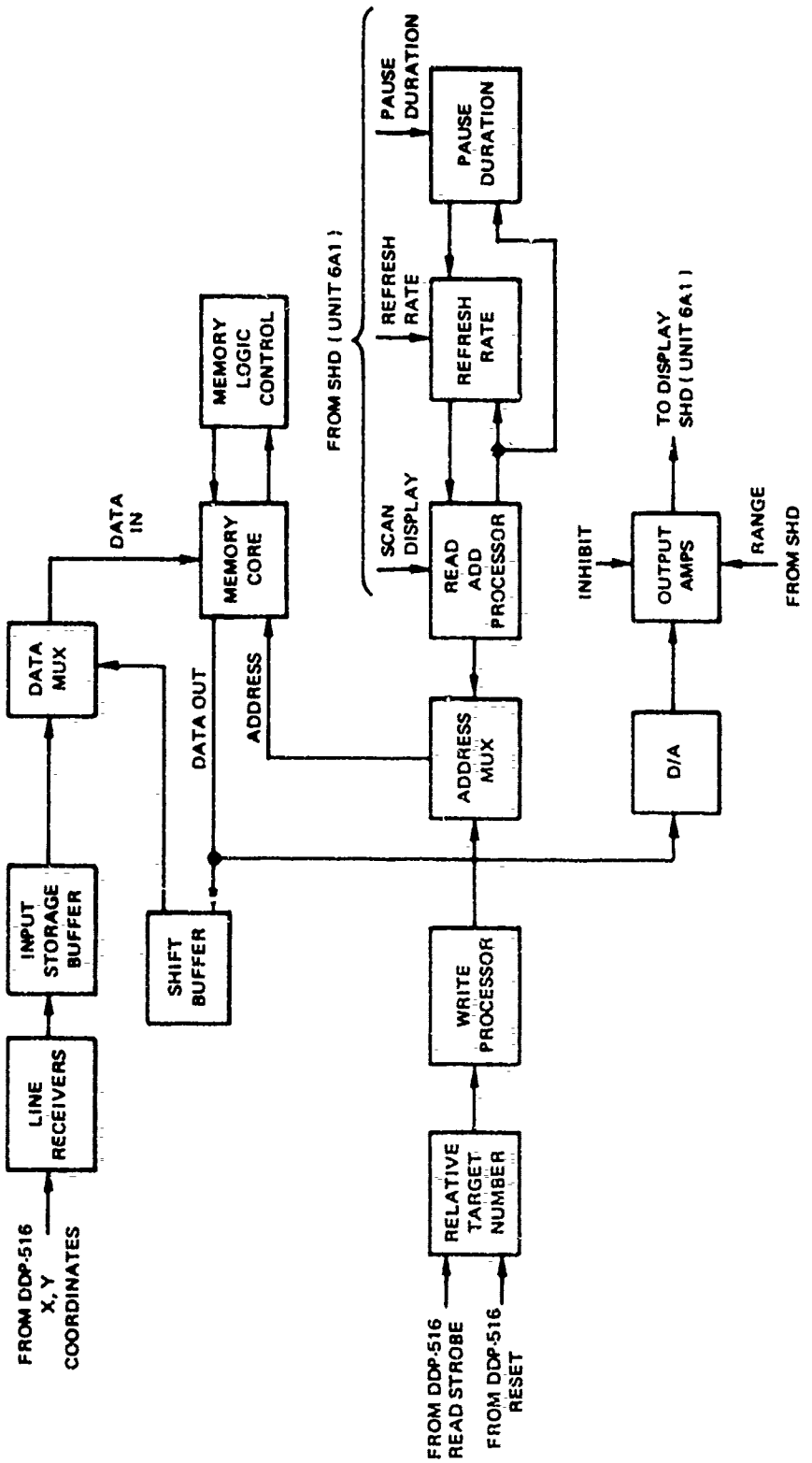

FIGURE E-9 BLOCK DIAGRAM OF SCAN HISTORY DISPLAY ELECTRONICS

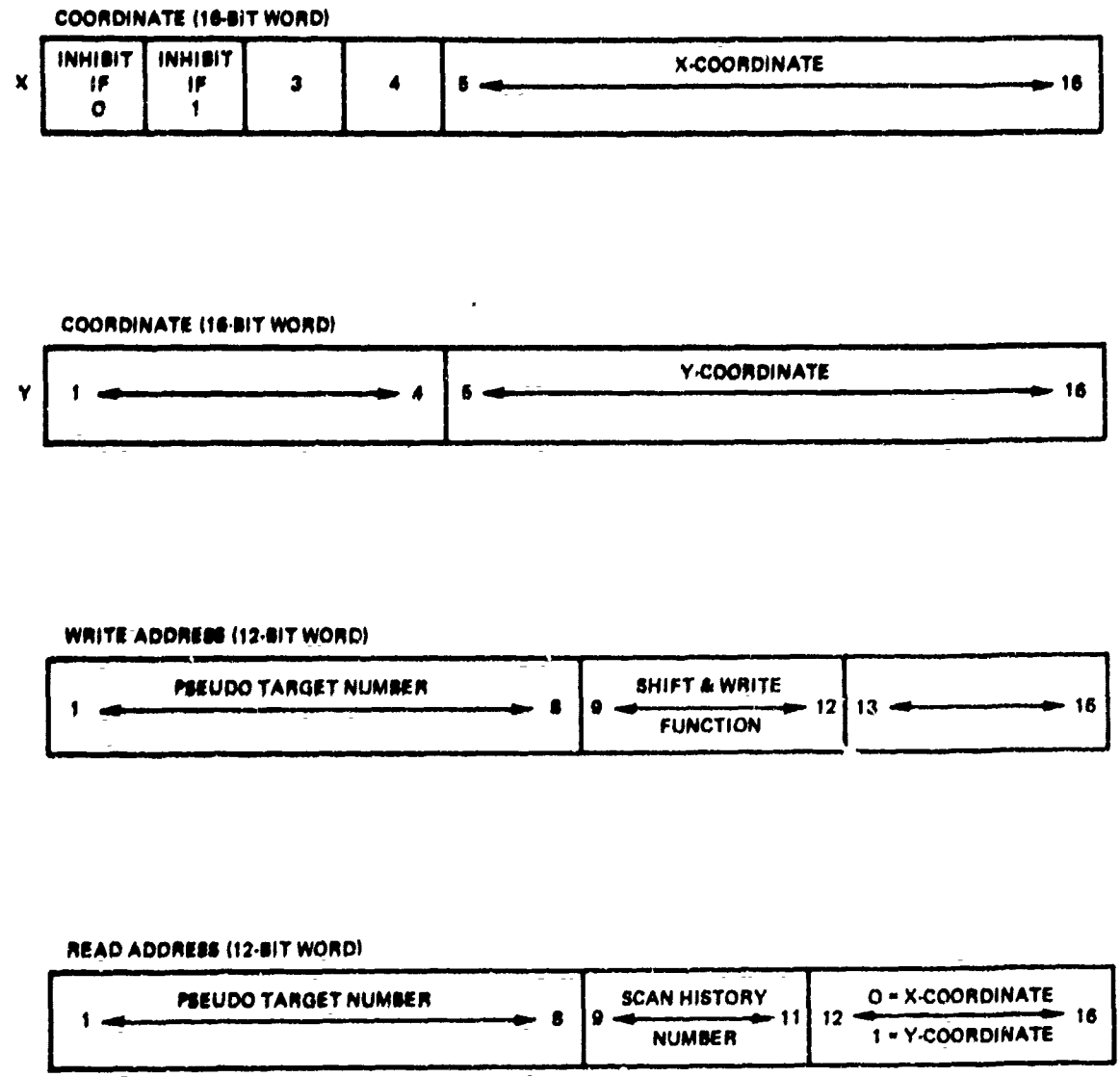

FIGURE E-10 SHD WORD FORMATS

receivers and held in storage buffers until entered into the SHD memory core. Until the SHD has completely processed the input storage buffer contents, which takes from 18 to 30 microseconds, a buffer-ready signal inhibits further computer data transmission. An update target position entered into the storage buffer is given a pseudo target number pertinent only to the current scan. The same target entered in two successive scans will probably have different target numbers. The target number is actually a partial address of where the x-y coordinates are stored in the SHD display memory core. The target number generator is just a counter incremented for each input buffer update and is reset at the zero bearing mark. The target number specifically designates a sixteen word scan block that the input buffer contents will be stored.

The SHD memory is a 4K word by 16 bit magnetic core logically arranged into 256 blocks of 16 words. Each 16-word block is called a scan block. Since each target requires two words, eight scans for 256 targets can be stored. The first word in a scan block corresponds to a position in the current scan, and the last word in the scan block corresponds to a position in the eighth elapsed scan. The two-word sections in a scan block are numbered scan #1 through #8. Each target update is entered into the scan #1 position of a scan block, and all previously stored coordinates in the scan number eight location are dropped. Since each scan block consists of exactly sixteen words, the pseudo target number is actually the eight most significant bits of the 12 bit memory code address word. The lower four bits control a shift and write updating process. Each computer input during a scan is stored in consecutive scan blocks. The target number counter is reset to zero at the radar bearing zero crossing. The counter reset action is actually a process in which the 8 bit counter

is clocked from its state at the time of zero bearing crossing, through roll over to zero. At each interim count, the shift and update process is exercised entering a zero into the scan #1 position of each scan block. During this process, lasting a worst case of 46 milliseconds, the input is inhibited from accepting new data.

Between target updates, stored target coordinates are displayed. There exists a free running address counter selecting consecutive target locations for display. The counter is sectioned into three parts or functions. The upper eight bits address consecutive scan blocks resetting itself every 256 counts. Thus targets are displayed in the same order as they were received. The next lower three bits, (2^1-2^3) address the scan number and are decremented after a variable number of roll-overs of the 8-bit scan block counter. These three bits specify which scan number is displayed for each of the 256 target scan blocks. Inhibiting this counter from decrementing provides the mechanism for continual display of the same scan number. The time duration for display of scan number one of each scan block is an operator entry and sets the time period that the three bit down counter is inhibited from changing from a state of zero. Controlling the counting frequency of this counter is another operator entry and is the refresh rate function. The last bit of the display address is the x-y bit state. A logical zero indicates an x-coordinate is read and a logical one indicates a y-coordinate is read.

After each x-y read cycle, the digital coordinates are D/A converted and displayed. The x-y coordinate fields occupy the lower twelve bits in each word. The upper two bits in the x-coordinate word, serves special functions. No target position is displayed

unless bit number one in the x-coordinate word is set. If a track sense switch is set, only those targets with bit number two in the x-coordinate word set to one will be displayed. The range scale is an operator entry and varies the gain of the output deflection amplifiers.